arXiv:0711.1289v3 [astro-ph] 26 Jun 2008

Deep *Chandra* Monitoring Observations of NGC 3379: Catalog of Source Properties

N. J. Brassington, G. Fabbiano, D.-W. Kim, A. Zezas

Harvard-Smithsonian Center for Astrophysics, 60 Garden Street, Cambridge, MA 02138

nbrassington@head.cfa.harvard.edu

S. Zepf, A. Kundu

Department of Physics and Astronomy, Michigan State University, East Lansing, MI 48824-2320

L. Angelini

Laboratory for X-Ray Astrophysics, NASA Goddard Space Flight Center, Greenbelt, MD 20771

R. L. Davies

Sub-Department of Astrophysics, University of Oxford, Oxford OX1 3RH, UK

J. Gallagher

Department of Astronomy, University of Wisconsin, Madison, WI 53706-1582

V. Kalogera, T. Fragos

Department of Physics and Astronomy, Northwestern University, Evanston, IL 60208

A. R. King

Theoretical Astrophysics Group, University of Leicester, Leicester LE1 7RH, UK

S. Pellegrini

Dipartimento di Astronomia, Universita di Bologna, Via Ranzani 1, 40127 Bologna, Italy

G. Trinchieri

INAF-Osservatorio Astronomico di Brera, Via Brera 28, 20121 Milan, Italy

ABSTRACT

We present the properties of the discrete X-ray sources detected in our monitoring program of the 'typical' elliptical galaxy, NGC 3379, observed with *Chandra* ACIS-S in five separate pointings, resulting in a co-added exposure of 324-ks. From this deep observation, 132 sources have been detected within the region overlapped by all observations, 98 of which lie within the D_{25} ellipse of the galaxy. These 132 sources range in $L_{\rm X}$ from 6×10^{35} erg s^{-1} (with 3σ upper limit $\leq 4\times10^{36}$ erg s^{-1}) to $\sim 2 \times 10^{39}$erg s^{-1}, including one source with $L_{\rm X} > 1 \times 10^{39}$erg s^{-1}, which has been classified as a ULX. From optical data, 10 X-ray sources have been determined to be coincident with a globular cluster, these sources tend to have high X-ray luminosity, with three of these sources exhibiting $L_{\rm X} > 1\times10^{38}$erg s^{-1}. From X-ray source photometry, it has been determined that the majority of the 132 sources that have well constrained colors, have values that are consistent with typical LMXB spectra. Additionally to this, a sub-population of 10 sources has been found to exhibit very hard spectra and it is expected that most of these sources are absorbed background AGN. There are 64 sources in this population that exhibit long-term variability, indicating that they are accreting compact objects. 5 of these sources have been identified as transient candidates, with a further 3 possible transients. Spectral variations have also been identified in the majority of the source population, where a diverse range of variability has been identified, indicating that there are many different source classes located within this galaxy.

Subject headings: galaxies: individual (NGC 3379) — X-rays: galaxies — X-ray: binaries

1. Introduction

Low-mass X-ray binaries (LMXBs) are the only direct fossil evidence of the formation and evolution of binary stars in the old stellar populations of early-type galaxies. First discovered in the Milky Way (see Giacconi 1974), these binaries are composed of a compact accretor, neutron star or black hole, and a late-type stellar donor. The origin and evolution

of Galactic LMXBs has been the subject of much discussion, centered on two main evolution paths (see Grindlay 1984; review by Verbunt & Van den Heuvel 1995): the evolution of primordial binary systems in the stellar field, or formation and evolution in Globular Cluster (GC).

With the advent of *Chandra* (Weisskopf *et al.* 2000), many LMXB populations have been discovered in early-type galaxies (see review Fabbiano 2006), and the same evolutionary themes (field or GC formation and evolution) have again surfaced, supported and stimulated by a considerably larger and growing body of data. These *Chandra* observations have provided important results on the spatial distributions and X-ray luminosity functions of LMXB populations (e.g., Kim & Fabbiano 2004; Gilfanov 2004), on their average spectra, and on their association with GCs (e.g. Angelini *et al.* 2001; Kundu *et al.* 2002; White *et al.* 2002; Sivakoff *et al.* 2006). However, most of the *Chandra* observations of LMXB systems so far consist of fairly shallow individual snapshots for each observed galaxy, with limiting luminosity ($\sim 0.3-8.0$ keV) of a few 10^{37} erg s^{-1}. These data give us information on the high luminosity LMXB sources, but do not cover the typical luminosity range of the well studied LMXB populations of the Galaxy and M31, which extends down a decade towards dimmer luminosities. Moreover, apart from rare exceptions, these observations do not have the time sampling that would permit variability studies and the identification of X-ray transients. Although, from this limited sample of multi-epoch observations with higher limiting luminosities, already a variety of different variability behaviours of LMXBs have been observed (e.g. Irwin 2006; Sivakoff *et al.* 2007). Both multi-epoch observations and low luminosity thresholds are important aspects of the observational characteristics of Galactic LMXBs and are needed for constraining the evolution of these populations (e.g., Piro & Bildsten 2002, Bildsten & Deloye 2004). For these reasons we proposed (and were awarded) a very large program of monitoring observations of nearby elliptical galaxies with *Chandra* ACIS-S3.

NGC3379, in the nearby poor group Leo (D=10.6 Mpc (Tonry *et al.* 2001)) was chosen for this study because is a relatively isolated unperturbed 'typical' elliptical galaxy, with an old stellar population (age of 9.3 Gyr, Terlevich & Forbes 2002) and a poor globular cluster system ($S_{GC} = 1.3 \pm 0.7$, Harris 1991; where $S_{GC} = \mathrm{No.GC} \times 10^{(0.4(M_V+15))}$). These characteristics make NGC3379 ideal for exploring the evolution of LMXB from primordial field binaries.

Observationally, NGC3379 is an ideal target for LMXB population studies, because of its proximity, resulting in a resolution of ~ 30 pc with *Chandra*, and the lack of a prominent hot gaseous halo, demonstrated by a previous short *Chandra* observation (David *et al.* 2005). These characteristics optimize the detection of fainter LMXBs, and minimize source confusion; because of its angular diameter ($D_{25} = 4.6$ arcmin, RC3), NGC3379 is entirely

contained in the ACIS-S3 CCD chip, and is not affected by the degradation of the *Chandra* PSF at large radii.

Here we publish the catalog of LMXBs with their properties resulting from the entire observational campaign of NGC3379 (four observations between January 2006 and January 2007, for a total of $\sim$ 300 ks), which has been recently completed, and including the first 30 ks observation taken in 2001, from the *Chandra* archive. In the companion paper (Fabbiano *et al.* 2007) we summarize our results relative to GC-LMXB associations and discuss their implications for our understanding of LMXB formation.

In addition to these two papers, further highlights from the X-ray binary population of NGC 3379 will be presented in Brassington *et al.* (2008, in prep), where the properties of the transient population of NGC 3379 will be presented. Forthcoming papers will also present: the properties of the ULX, the X-ray luminosity function and the diffuse emission of the galaxy, as well as the properties of the nuclear source and the intensity and spectral variability of the luminous X-ray binary population. Preliminary results from the first *Chandra* observations of our program were reported in Kim *et al.* (2006) and Fabbiano *et al.* (2006).

This paper is organized as follows: §2. details the observational program and describes the data analysis methods and results, including pipeline processing of the data, source detection, astrometry and matching of sources from the different observations, X-ray photometry and overall population results, variability analysis and optical counterpart matching (GC and background objects); §3. is the source catalog, including the results from the individual observations and the co-added data; §4 presents the discussion of the properties of the sources catalog; §5 summarizes the conclusions of this work.

2. Observations and Data Analysis

The five separate *Chandra* observations of NGC 3379 have been carried out over a six year baseline, with the first of these, a 30 ks pointing, being performed in February 2001. This observation has been followed by four deeper pointings, all carried out between January 2006 and January 2007, resulting in a total exposure time of 337-ks.

The initial data processing to correct for the motion of the spacecraft and apply instrument calibration was carried out with the Standard Data Processing (SDP) at the *Chandra* X-ray Center (CXC). The data products were then analysed using the CXC CIAO software suite (v3.4)[1] and HEASOFT (v5.3.1). The data were reprocessed, screened for bad pixels,

[1]http://asc.harvard.edu/ciao

and time filtered to remove periods of high background. Following the methods of Kim *et al.* (2004a), time filtering was done by making a background light curve and then excluding those time intervals beyond a 3σ fluctuation above the mean background count rate, where the mean rate was determined iteratively after excluding the high background intervals. This resulted in a total corrected exposure time of 324-ks, the log of these exposures is presented in Table 1.

From the five individual data sets, a combined observation has been produced. This has been created by using the *merge_all* script[2], where the reprocessed level 2 event files from each observation were reprojected to a given RA and Dec, and then combined, and a combined exposure map was also created. The methods that were applied to correct for the astrometry of the individual observations, used to create the co-added observation, are discussed in §2.2.

From this combined dataset, a 0.3−8.0 keV (from here on referred to as 'full band') *Chandra* image was created and adaptively smoothed using the CIAO task *csmooth*. This uses a smoothing kernel to preserve an approximately constant signal to noise ratio across the image, which was constrained to be between 2.6σ and 4σ. In Figure 1, both the optical image, with the full band X-ray contours overlaid (top), and the 'true color' image of the galaxy system (bottom) are shown. The 'true color' image was created by combining three separate smoothed, and exposure corrected, images in three energy bands; 0.3−0.9 keV, 0.9−2.5 keV and 2.5−8.0 keV, using the same smoothing scale for each image. These energy bands correspond to red, green and blue respectively.

2.1. Source Detection and Count Extraction Regions

Discrete X-ray sources were searched for over each observation (the five single observations and the combined observation) using the CIAO tool *wavdetect*, where the full band, with a significance threshold parameter of 1×10^{-6}, corresponding to roughly one spurious source over one CCD, was searched over. This CIAO tool searches for localized enhancements of the X-ray emission, and does not set any apriori thresholds on the SNR of each source (in contrast to sliding cell algorithms: Freeman *et al.* (2002)). In Kim *et al.* (2004a) simulations were carried out to investigate the number of false detections compared to the expected ∼1 false source per image provided by the threshold significance of 1×10^{-6}. These simulations and results are detailed in §4.4.1 of the paper, where they find that the performance of *wavdetect* is as expected, resulting in ∼1 spurious source per images. These simulations

[2]http://asc.harvard.edu/ciao/ahelp/merge_all.html

cover the values of background (∼0.2 counts/pixel) of our co-added observation. Further to this, these simulations were compared to *Chandra* observations with relatively long exposures (∼100 ks), where 0.3 spurious sources per exposure were detected, fully consistent with the simulation results. A similar approach was also used by Kenter *et al.* (2005).

Following the results of these simulations it is clear that, when setting a detection threshold of 1×10^{-6} in *wavdetect*, only one of the formally identified sources is expected to be a false detection per image and so this prescription has been followed here. We reiterate that using this method does not set any apriori thresholds on the SNR of each source, it is therefore possible to include sources that have a high detection significance but at the same time a low flux significance, or SNR, therefore resulting in sources with poorly constrained flux.

When running *wavdetect* a range of 1, 2, 4, 8, 16 and 32 pixel wavelet scales were selected (where pixel width is $0.49''$), with all other parameters set at the default values. Exposure maps were created for the S3 chip from each observation, at 1.5 keV. The *wavdetect* tool was used in preference to other source detection software, as this detection package can be used within the low counts regime, as it does not require a minimum number of background counts per pixel for the accurate computation of source detection thresholds. Further to this, *wavdetect* also performs better in confused regions, which is the case in the nuclear region of elliptical galaxies (Freeman *et al.* 2002).

Once the X-ray sources had been detected, and their position had been determined by *wavdetect*, counts were extracted from a circular region, centered on the *wavdetect* position, with background counts determined locally, in an annulus surrounding the source, following the prescription of Kim *et al.* (2004a). The extraction radius for each source was chosen to be the 95% encircled energy radius at 1.5 keV (which varies as a function of the off-axis angle[3]), with a minimum of $3''$ near the aim point. Similarly, background counts for each source were estimated from a concentric annulus, with inner and outer radii of two and five times the source radius respectively.

When nearby sources were found within the background region, they were excluded before measuring the background counts. Net count rates were then calculated with the effective exposure (including vignetting) for both the source and background regions. Errors on counts were derived following Gehrels (1986). For cases where sources have fewer than 4 counts, the Gehrels approximation begins to differ to Poissonian errors. However, these error values are still accurate to 1%, and, if anything, provide a more conservative estimate as Gehrels approximation does not account for the smaller error value at the lower limit.

[3]see http://cxc.harvard.edu/cal/Hrma/psf/index.html

When the source extraction regions of nearby regions were found to overlap, to avoid an overestimate of their source count rates, counts were calculated from a pie-sector, excluding the nearby source region, and then rescaled, based on the area ratio of the chosen pie to the full circular region. Once the correction factor was determined, it was applied to correct the counts in all energy bands. For a small number of sources that overlapped with nearby sources in a more complex way (e.g. overlapped with more than 2 sources), instead of correcting the aperture photometry, the source cell determined by *wavdetect* was used to extract the source counts.

From these source counts, fluxes and luminosities were calculated in the 0.3−8.0 keV band, with an energy conversion factor (ECF) corresponding to an assumed power law spectral shape, with $\Gamma = 1.7$ and Galactic $N_{\rm H}$[4] (see Figure 11 for a justification of this assumption). The ECF was calculated with the *arf* (auxiliary response file) and the *rmf* (redistribution matrix file) generated for each source in each observation. For each source, the temporal quantum efficiency variation [5] was accounted for by calculating the ECF in each observation and then taking an exposure-weighted mean ECF. The ECF over the 0.3−8.0 keV band varied by ∼14% between 2001 and 2006, and by only ∼0.3% between the four observations taken in 2006[6]. This procedure was applied to each single observation and to the total co-added exposure.

In the instances where *wavdetect* did not formally identify a source in a single observation, source counts have been extracted from a circle with a 95% encircled energy radius, centered on the position from the co-added observation (or in cases where the source was not formally detected in the co-added observation, the source position from the single observation was used). The definition of background regions and the treatment of overlapping sources are outlined above. From these extracted source counts, a Bayesian approach, developed by Park *et al.* (2006), has been used to provide 68% source intensity upper confidence bounds on the full band counts. These values have then been used to calculate upper limits on the flux and luminosity of these sources.

---

[4] $N_{\rm H}$=2.78×10^{20}cm^2 (from COLDEN: http://cxc.harvard.edu/toolkit/colden.jsp).

[5] See http://cxc.harvard.edu/cal/Acis/Cal_prods/qeDeg/ for the low energy QE degradation.

[6] http://asc.harvard.edu/ciao/why/acisqedeg.html

2.2. Astrometry and Source Correlation

Prior to merging the five exposures into a single co-added observation, the astrometry of the individual pointings were checked, to correct for any systematic shifts in the coordinate systems of the event lists. This was done by selecting the longest single observation, obs-7073, as a point of reference, and then comparing the positions of the twenty brightest point sources, detected in all five separate observations, to the source positions of these 20 sources in each of the individual observations. From these comparisons it was found that the fifth observation, obs-7076, showed a significant declination offset of $0.44''$, compared to values less than $0.2''$ in all other observations. It is believed that this systematic offset is a result of a change in thermal environment, following the procedure to cool the ACA CCD from -15C to -19C, which took place between late Nov-2006 and early Jan-2007[7].

At the time of data processing there were no calibration files to correct for this offset and therefore offsets had to be defined and corrected for individually[8]. This was done by producing a co-added file of the first four individual observations, all of which show offset values of $\leq 0.2''$ in both RA and Dec from the single reference observation. With this co-added observation, the CIAO tool *reproject_aspect* was used calculate offset values for the fifth observation, and from these, produce a new, corrected, aspect solution file, which was used to create a new level 2 event file. This new corrected event file, alongside the four other individual observations, was then combined to produce a co-added observation, using the *merge_all* script, as described in §2. From this co-added file the astrometry was once again checked, a summary of these offset values is given in Table 2, where it can be seen that all five of the individual observations have offsets of $\leq 0.12''$ in both RA and Dec when compared to the corrected, co-added observation.

From the co-added observation only, 164 sources were detected by *wavdetect*. From this list, sources external to the overlapping area covered by the S3 chip in all five individual observations were excluded, reducing this total number to 125 point sources. Using this source list from the co-added observation, sources detected in the individual observations were matched with this combined observation source list, where source correlations were searched for up to a separation of $3''$. In the cases where multiple matches were detected for a source, the closer correlation was selected. From these matches, a histogram of source separations, shown in the left panel of Figure 2, was produced. In this figure it is clear that the peak separation between sources lies $\sim 0.2''$, with the number of correlated sources

[7]http://cxc.harvard.edu/cal/ASPECT/celmon/

[8]Data between these dates have now been reprocessed to correct for this offset, see: http://cxc.harvard.edu/bulletin/bulletin_64.html

dropping at $\sim 1.6''$, and this is therefore the value we set for maximum separation when cross-correlating sources.

Once a cut of $1.6''$ had been applied to the cross-matched source list, the remaining unmatched sources, detected in the separate pointings only, were investigated individually, resulting in further matches being established. These matches correspond to sources with fewer counts, and hence a greater positional uncertainty, leading to larger values of separation. From the list of sources detected in individual observations, seven of these point sources were determined to be well separated from the sources detected in the co-added observation, and were therefore included in the final list of detected sources, increasing the total number of detected sources to 132.

These source correlations were then further investigated by calculating the ratio of the source separation and the combined position uncertainty. Where the position uncertainty at the 95% confidence level has been defined by Kim *et al.* (2007a), as:

$$\mathrm{logPU} = \begin{cases} 0.1145 \times \mathrm{OAA} - 0.4958 \times \mathrm{logC} + 0.1932, & 0.0000 < \mathrm{logC} \leq 2.1393 \\ 0.0968 \times \mathrm{OAA} - 0.2064 \times \mathrm{logC} - 0.4260, & 2.1393 < \mathrm{logC} \leq 3.3000 \end{cases} \quad (1)$$

where the position uncertainty, PU, is in arcseconds, and the off axis angle, OAA, is in arcminutes. Source counts, C, are as extracted by *wavdetect*. Using this ratio of source separation and position uncertainty allows low L_{X} source correlations to be identified. Often these sources, particularly at greater off axis angles, cannot be matched by source separation cuts alone, due to the increasing PSF spread out and asymmetry at larger OAA[9]. Therefore, by using this source separation - PU ratio, the greater position uncertainties in these weak sources can be accounted for, resulting in smaller ratios, and thereby identifying correlations that would otherwise be missed with source separation cuts alone.

In the right panel of Figure 2, a histogram of the ratio of separation and the combined position uncertainty is shown, where sources with a ratio of greater than 1 were investigated individually. In all but two instances it was found that these higher ratio sources lie in the central region of the galaxy, where both source confusion is likely and diffuse gas is present. This emission results in higher background fluctuations, which can lead to the PU of these sources to be underestimated, therefore resulting in a falsely high ratio value. For the two sources that were detected outside the central region, both are too faint (*net counts* $<\sim 100$ counts) to allow their radial profiles to be compared with corresponding model PSF profiles, generated for the position of each source using the CIAO tool *mkpsf*, and have been flagged as possible double sources.

[9]See §5 in Kim *et al.* (2004a) for a full discussion

From this complete list, light curves were produced for sources with *net counts*< 20, which were detected in single observations, to screen for the possibility of false sources by cosmic ray afterglows. None of the 24 sources that were examined exhibited light curves consistent with cosmic ray afterglows, as is expected from the S3 chip (a back-illuminated CCD), due to this problem mostly occurring in the front-illuminated chips. From this screening, the total number of detected point sources remains at 132. These sources are presented in Figure 3, where the unsmoothed full-band image from the co-added dataset, with regions overlaid in white, is shown.

2.3. Hardness Ratios and X-ray colors

Within NGC 3379, the range of net counts for the pointlike sources in the co-added observation is $\sim\ 2-7200$ (with signal-to-noise ratio (SNR) values ranging from 0.5 to 83.7), corresponding to 0.3−8.0 keV luminosities of 6×10^{35} erg s^{-1}(3σ upper limit $\leq 4\times10^{36}$ erg s^{-1}) $-\ 2\ \times10^{39}$erg s^{-1}, when using the energy conversion factor described in §2.1. Most of these sources are too faint for detailed spectral analysis, therefore their hardness ratio and X-ray colors were calculated in order to characterize their spectral properties. The X-ray hardness ratio is defined as HR = (Hc−Sc)/(Hc+Sc), where Sc and Hc are the net counts in the 0.5−2.0 keV and 2.0−8.0 keV band respectively. Following the prescription of Kim *et al.* (2004b), the X-ray colors are defined as C21 = log(S_1/S_2) and C32 = log(S_2/H), where S_1, S_2 and H are the net counts respectively in the energy bands of 0.3−0.9 keV, 0.9−2.5 keV and 2.5−8.0 keV (energy bands and definitions are summarized in Table 3). These counts were corrected for the temporal QE variation, referring them all to the first, recent observing epoch (Jan. 2006, Table 1), and for the effect of the Galactic absorption, using $N_{\rm H}$=2.78×10^{20}cm^2 (from COLDEN: http://cxc.harvard.edu/toolkit/colden.jsp).

By definition, as the X-ray spectra become harder, the HR increases and the X-ray colors decrease. For faint sources with a small number of counts, the formal calculation of the HR and colors often results in unreliable errors, because of negative net counts in one band and an asymmetric Poisson distribution. Therefore a Bayesian approach has been applied to derive the uncertainties associated with the HR and colors. This model was developed by Park *et al.* (2006) and calculates values using a method based on the Bayesian estimation of the 'real' source intensity, which takes into account the Poisson nature of the probability distribution of the source and background counts, as well as the effective area at the position of the source (van Dyk *et al.* 2001), resulting in HR and color values that are more accurate than the classical method, especially in the small-number-of-counts regime (less than 10 counts), where the Poisson distributions become distinctly asymmetric. More

details of this technique and the source and background counts used in the derivation of the HR and color values and the 1σ confidence bounds are provided in Appendix A.

2.4. Source Variability

Due to the monitoring approach that has been used when observing NGC 3379, both long-term and short-term variations have been able to be searched for in the galaxy's LMXB population. Long-term variability was defined by the chi-squared test, where a straight line model was fitted to the luminosities derived for each individual observation, with errors based on the Gehrels approximation (Gehrels 1986). For the cases where sources only had upper limit values of $L_{\rm X}$, the associated error was defined to be the standard deviation of the upper limit from the mode value attained from the Bayesian estimates method, resulting in a conservatively large error, due to the nature of the Poissonian statistics. From these best fit models, sources were determined to be variable if χ^2_ν>1.2, and those with fits with χ^2_ν<1.2 were defined as non-variable sources. For sources that were only detected in the co-added observation, long-term variability was not searched for. This long-term behaviour will be further investigated in a forthcoming paper, where full Poissonian error treatment will be applied to sources with very low observed counts.

In addition to the chi-squared test variability criterion, transient candidates (TC), sources that either appear or disappear, or are only detected for a limited amount of 'contiguous' time during the observations, were searched for. Typically, sources are defined to be TCs if the ratio between the 'on-state', the peak $L_{\rm X}$ luminosity, and the 'off-state', the lower $L_{\rm X}$ luminosity or non-detection upper limit, is greater than a certain value (usually between $5-10$; e.g. Williams *et al.* (2008)). However, such a criterion can overestimate the number of transient candidates, when the 'on-state' X-ray luminosity is poorly constrained. To address this, the Bayesian model developed by Park *et al.* (2006) was used to derive the uncertainties associated with the ratio between 'on-state' and 'off-state'. In this model, source and background counts from both the peak $L_{\rm X}$ luminosity and the non-detection observations were used to estimate the ratio, where the differences in both the exposure and ECF values were also accounted for. From this Bayesian approach a value of peak $L_{\rm X}$/non-detection upper limit was calculated, along with a lower bound value of this ratio. This lower bound value was then used to determine the transient nature of the source, where a ratio of greater than 10 indicated a TC and sources with a ratio between 5 and 10 were labeled as possible transient candidates (PTC). This transient behavior was only searched for in sources that were only detected for a limited amount of 'contiguous' time during the observations and were determined to be variable using the chi-squared test.

Further to these four long-term variability classifications, the variation of the source luminosity between each observation was also investigated, by comparing the significance (in σ) of the change in luminosity between exposures, where the significance has been estimated by:

$$sign = \frac{|L_{\rm X1} - L_{\rm X2}|}{\sqrt{(\sigma_1^2 + \sigma_2^2)}}, \tag{2}$$

where σ_n is the error value of the luminosity from that individual observation, based on the Gehrels approximation, or, where upper limits have been used, the standard deviation of the estimated luminosity.

Short-term variations in each source were investigated when *net counts* > 20 in a single observation. In these instances, the variability was identified by using the Kolmogorov-Smirnov test (K-S test), where sources with variability values >90% confidence were labeled as possible variable sources and sources with values >99% confidence were defined as variable sources. This short-term variability was also quantified by using the Bayesian blocks method (BB) (Scargle 1998; Scargle *et al.* 2008, in prep). This method searches for abrupt changes in the source intensity during an observation, and therefore is very efficient for detecting bursts or state changes. Because it is based on the Poisson likelihood it can be used on the unbinned lightcurves of sources with very few counts. The implementation of the method used in this analysis is the same as in the ChaMP pipeline (see §3.3.2 in Kim *et al.* 2004a). This assumes a prior of $\gamma = 4.0$ which *roughly* translates to a significance level of $\sim$ 99% for each detected block (however see Scargle *et al.* (2008, in prep)[10], for a caveat on this interpretation of the value of the prior).

2.5. Radial Profile

From the complete source list from the co-added observation a radial distribution of LMXBs has been created, using annuli centered on the nucleus of the galaxy (source 81). This profile has been compared to a multi-Gaussian expansion model of the I-band optical data (Cappellari *et al.* 2006), which is assumed to follow the stellar mass of the galaxy (Gilfanov 2004). This X-ray source density profile is presented in Figure 6, where the optical profile has been normalized to the X-ray data by way of a χ^2 fit. Also indicated in this figure is the D_{25} ellipse and the number of background sources, which has been estimated from the hard-band $ChaMP + CDF\ logN - logS$ relation (Kim *et al.* 2007b), where $\sim$36 sources are expected to be objects not associated with NGC 3379. From this figure it can be

[10]see also http://space.mit.edu/CXC/analysis/SITAR/functions.html

seen that the X-ray profile follows the optical surface density profile at larger radii, with the flattening in the central region (r$\leq$10″) a consequence of source confusion. This indicates that the number and spatial distribution of LMXBs follows that of their parent population, the old stellar population.

2.6. Optical Counterparts

The globular cluster system of NGC 3379, observed with WFPC2, on-board *HST*, is reported in Kundu & Whitmore (2001), where images in both the V and I bands have been analyzed. In addition to this GC system identified in the *HST* data, background objects have also been classified (Kundu, A. 2007, private communication). These have been identified as objects that were well resolved in the *HST* images and were clearly more extended than any known globular cluster. Further to this, these background objects often had other features, such as visible disks, indicative of a galaxy rather than a globular cluster. In addition to the *HST* data, radial velocities and $B-R$ values of spectroscopically confirmed GCs within this galaxy have been reported in Bergond *et al.* (2006), Puzia et al. (2004), and Pierce *et al.* (2006). With further BVR photometry information, provided by images obtained with the Mosaic detector on the Kitt Peak 4-m telescope (Rhode & Zepf, 2004).

Right ascension and declination corrections have been applied to the astrometry of these data-sets, relative to the co-added *Chandra* observation. These offsets were calculated and corrected for using the methods described in §2.2, where correlations between the X-ray and optical sources were made, and systematic offsets in RA and Dec were removed. In the case of the Rhode & Zepf (2004) data, only two correlations were found between the X-ray and optical sources, therefore the corrected *HST* data were used to make these offset adjustments.

After correcting the astrometry of the optical data, correlations up to an offset of 3″ with the X-ray sources, were searched for. When multiple matches were found, the closer matching object was selected. In the left panel of Figure 4, a histogram of these matches is shown, where it can be seen that, due to the poor statistics, it is not clear where the separation cut off should be made. Initially, this was set to 1″, and sources between 1″ and 3″ were defined as 'excluded matches'. This cut off value was then tested by comparing these correlations with the ratio of the separation divided by the combined position uncertainty from the co-added X-ray point sources (the definition of this is given in equation 1) and the uncertainty in the astrometry in the optical data, which has been conservatively set at 0.2″.

These ratios are shown in the right panel in Figure 4, where a histogram of all optical-X-ray correlations is presented, with a shaded histogram of the background correlations only,

overlaid. From this figure, it is shown that the correlated sources with a separation-position uncertainty ratio of greater than 2 are background objects. Both of these objects have separations >0.9″, and, from both of the histograms presented in Figure 4, the separation value cut off was redefined to be 0.6″. This results in 14 X-ray-optical correlations, 4 of which have been classified as background objects, leaving 10 GC-X-ray source correlations, one of which lies external to the *HST* FOV, although this source has been detected in two separate studies (Bergond *et al.*, 2006; Rhode & Zepf, 2004). The optical properties of these GC-LMXB sources, and the 'excluded matches' are shown in Tables 11 and 12 respectively (Full descriptions of these tables are given in §3).

In order to estimate the chance coincidence probability of the sources within the *HST* FOV, the same method as in Zezas *et al.* (2002) was followed, where the positions of the globular clusters were randomized by adding a random shift between 0.6″and 30″, and for each new fake dataset the cross-correlation was performed using the same search radius as for the observed list of globular clusters. The limits of the shifts were chosen so that the new positions did not fall within the search radius and that they follow the general spatial distribution of the globular clusters. 500 such simulations were performed, resulting in 0.35±0.59 associations expected by chance. If the cross-correlation radius is increased to 1″, the chance associations rises to 0.5±1.1. Increasing this radius to 3″ results in 8.4±14.2 associations expected by chance, which compares well with the nine 'excluded matches' that have been found within this radius.

The 10 GC-X-ray correlations that have been found in NGC 3379 are shown in Figure 5, where an X-ray image with confirmed GCs is shown. In this figure the GCs are indicated by white 'X' marks and the corresponding X-ray sources are indicated by box regions. The 'excluded matches' are indicated by diamond regions and X-ray sources with no matches are shown as circular regions. X-ray luminosities are also indicated in this image, where sources with $L_{\rm X}\geq 1\times10^{38}$erg s^{-1} are shown in yellow, sources with $1\times10^{38}\geq L_{\rm X}\geq 1\times10^{37}$erg s^{-1} are shown in red and sources with $L_{\rm X}\leq 1\times10^{37}$erg s^{-1} are indicated in cyan.

3. Source Catalog and Variability Atlas

Table 4 presents the properties of the master list of the 132 X-ray sources detected within NGC 3379, from the co-added observation of 324-ks. This table has been divided into two sections, where the first part presents all sources with SNR>3 in at least one observation, and the second part lists all sources with SNR<3. In this table column (1) gives the source number used through out this series of papers, column (2) gives the IAU name (following the convention "CXOU Jhhmmss.s+/−ddmmss"), columns (3) and (4) give the R.A. and Dec. of

the source aperture, columns (5) and (6) give the radius and the position uncertainty (*PU*) of the source (both in arcseconds), column (7) gives the SNR, column (8) gives the log value of the co-added luminosity in the 0.3−8.0 keV energy band (for sources with SNR<3, 3σ upper limit values are also presented in brackets). For sources detected in a single observation only, 1σ upper limit from the co-added observation are shown, with 3σ upper limit values from the detected observation presented in brackets. Column (9) provides information about the long-term variability of the source, indicating if the source is non-variable (N), variable (V), a transient candidate (TC) or a possible transient (PTC). In all other cases the source was only detected in the combined observation, providing insufficient information to investigate long-term variability. In columns (10) and (11) the short-term variability of the source is indicated from both Bayesian block analysis (BB) and the Kolmogorov-Smirnov test (K-S), where 'V' indicates that the source is variable in at least one observation and 'N' indicates that is has been found to be non-variable in all five observations. In the K-S column, sources have also been labeled as possible variable sources (P) (see §2.4 for further information). In all other cases there were insufficient counts to investigate the short-term variability. In column (12) the optical associations with the X-ray source are indicated, where 'GC' indicates that the associated optical sources has been confirmed as a globular cluster, and 'BG' indicates that the sources has been classified as a background object. 'corr' denotes matches that have been defined as correlations, and 'exmt' denotes the 'excluded matches', between $0.6''$ and $3''$ in separation. Sources with a 'none' label were inside the field of view of the *HST* observation, but have no optical counterpart, and sources denoted with an 'X' were within the *HST* FOV, but were also within $5''$ of the nucleus, and were therefore not considered for optical associations. All other sources were external to the *HST* FOV. Column (13) gives the distance from the galactic center (in arcseconds), where values in bold type face indicate sources that lie within the D_{25} ellipse. Column (14) provides source flag information, indicating sources that have been detected in a single observation only (X), overlapping sources (O1 for single overlaps and O2 for more complicated cases), possible background objects (BKG?) (see §4.2 for details of this classification) and possible double sources (double?).

In this table, the 132 sources presented are the complete list detected by *wavdetect*, for which we estimate that ∼1 source is a spurious detection (see §2.1). Since this catalog of X-ray sources is intended to be as complete a study as possible, all detected sources are included in the complete list, although for sources with SNR<3 source parameters such as flux, hardness ratio and color values are not as well constrained as sources with higher flux significance. We have therefore separated the table into two sections, where the first part presents sources with SNR >3 in at least one observation and well constrained properties, and the second part lists the sources with low SNR values.

Table 5 presents the detailed source parameters from the co-added observation; column (1) gives the source number, columns (2)−(8) give the net counts, in each of the 7 energy bands (see Table 3 for definitions of these bands), column (9) indicates the hardness ratio, columns (10) and (11) show the color-color values and column (12) gives the log value of the luminosity in the 0.3−8.0 keV energy band. Where sources were not detected in the co-added observation, upper limits for net broad band counts and $L_{\rm X}$ are given.

Tables 6−10 present the source parameters, measured for each observation, where columns (1)−(11) provide the same information presented in Table 5, but further provided in this table is source variability information, where columns (12)−(14) present results of Bayesian block analysis (BB), the Kolmogorov-Smirnov test (K-S) and the significance of the change in $L_{\rm X}$ between the previous observation and the current observation respectively. Column (15) indicates the log value of the luminosity in the 0.3−8.0 keV energy band.

Table 11 presents the optical properties of the counterparts found from the optical data of NGC 3379, where 10 GCs and 4 background objects have been found to be coincident with X-ray sources. Table 12 summarizes the results for the 'excluded matches' sources. In both tables column (1) gives the X-ray source number, column (2) the V band magnitude, column (3) the I band magnitude, column (4) $V-I$ colors, column (5) $B-V$ colors, column (6) $V-R$ colors, column (7) $B-R$ colors, column (8) gives the radial velocity, column (9) the separation between the X-ray source and the GC, column (10) the ratio between separation and the combined position error and column (11) gives a references to where the GC information comes from; 1. Bergond *et al.* 2006, 2. Puzia *et al.* 2004, 3. Pierce et al. 2006, 4. Kundu & Whitmore (2001), confirmed GCs, 5. Kundu & Whitmore (2001), background objects, 6. Rhode & Zepf, 2004. The horizontal line in both tables separates the confirmed GCs (top section of table) from the background objects (bottom section of table).

Figure 7 presents the intensity and spectral variability of each of the 132 X-ray sources, over all five pointings, where the temporal properties of each point source are shown in four separate panels. In the top panel the long-term light curve of each source is presented, with errorbars indicating the 1σ uncertainty in the intensity of the source, with upper limit values provided for sources that were not detected in a single observation. The second panel shows the hardness ratio variation of each source, and panels three and four, show the temporal properties of C21 and C32 respectively. In all four panels, the co-added values are also indicated, by a horizontal dashed green line. In instances where the source was not detected in the co-added observation, a blue line indicates the upper limit of the source luminosity.

Figure 8 presents the $L_{\rm X}$-HR plots for sources with measured hardness ratios in at least two observations. Each point shows the X-ray luminosity and hardness ratio value of a source during each pointing, as well as the values derived from the co-added observation. Each point

is labeled and color coded, where magenta, green, blue, red and cyan indicate observations 1−5 respectively, and black represents the co-added observation value. Similarly, Figure 9 presents the color-color values for sources with measured color-color values in at least two observations, where again individual observations are labeled and color coded (following the same color scheme as in Figure 8), with the co-added observation indicated in black.

4. Discussion

4.1. X-ray Source Population

In the previous sections the data analysis methods, used to determine the properties of the X-ray binary population of NGC 3379, have been presented. From the five individual *Chandra* pointings, taken between February 2001 and January 2007, a co-added observation, totaling an exposure time of 324-ks, has been produced. From this deep observation of the galaxy, 132 X-ray point sources have been detected in the region overlapped by all of the individual pointings, with 98 of these sources residing within the D_{25} ellipse of the system. These 132 sources are presented in Figure 3 where a raw, full band image from the co-added observation, with the overlap region and D_{25} ellipse overlaid, is presented in the main image, with source regions also indicated. The smaller images present the central region of the galaxy, where the dense population of sources can be more clearly seen. Of these 132 sources, based on the hard-band $ChaMP + CDF\ logN - logS$ relation (Kim *et al.* 2007b), ∼36 sources detected in the co-added observation are expected to be objects not associated with NGC 3379. Within the D_{25} ellipse of the galaxy it is expected that ∼17 of these sources are background objects. In Figure 6 the number of expected background objects is indicated in the X-ray source number density profile of the galaxy.

The X-ray luminosity of the sources detected within NGC 3379 ranges from 6×10^{35} erg s^{-1} (with 3σ upper limit $\leq 4\times 10^{36}$ erg s^{-1}) up to 2×10^{39}erg s^{-1}, where the brightest source, 70, is the only ULX detected within this system. The properties of this source from the first two observations have been reported in Fabbiano *et al.* (2006), and the full analysis of the five individual pointings of the ULX will be presented in the forthcoming paper, Angelini *et al.* (2008, in prep). The $L_{\rm X}$ distribution of all of the detected X-ray sources within NGC 3379 is shown in Figure 10, where the GC associations are also indicated.

In this figure the main histogram presents the calculated $L_{\rm X}$ values from all sources (with 1σ upper limits from the co-added observation provided for sources only detected in a single observation). The bottom left histogram presents these same sources, but for those with SNR<3, 3σ upper limits are shown), these upper limit values are then presented separately

in the bottom right histogram. From the main figure it can bee seen that the GC-LMXB sources appear to predominantly lie at the high X-ray luminosity end of this distribution. The properties of these 10 GC-LMXB sources and their implications for the understanding of LMXB evolution in galaxies are presented and discussed in detail in the companion paper Fabbiano *et al.* (2007). Also from this figure it can be seen that the majority of sources detected from this observation lie in the luminosity range of 5×10^{36}erg s^{-1}–5×10^{37}erg s^{-1}, with a mode luminosity of $\sim 6 \times 10^{36}$erg s^{-1} and with source incompleteness beginning to affect the source distribution $\sim 5 \times 10^{36}$erg s^{-1}. From the histogram including 3σ upper limit values, this mode value rises to $1{\times}10^{37}$erg s^{-1}, with source incompleteness beginning to affect the source distribution $\sim 8 \times 10^{36}$erg s^{-1}.

In the forthcoming paper Kim *et al.* (2008, in prep), the X-ray luminosity function (XLF) of NGC 3379 will be investigated, and a correction to allow for source incompleteness will be applied. Some preliminary results, investigating the XLF of NGC 3379, have been reported in Kim *et al.* (2006), where sources, down to a 90% completeness limit of $L_{\rm X}$=$1{\times}10^{37}$erg s^{-1}, from the first two observations, have been detected. From the even greater sensitivity afforded to us by combining the five separate pointings, we can investigate the XLF down to the X-ray luminosity range of normal Galactic LMXBs. Previously, this has only been possible for the nearby radio galaxy Centaurus A (NGC 512), where the XLF has been measured down to $\sim 2 \times 10^{36}$erg s^{-1} (Kraft *et al.* 2001; Voss & Gilfanov 2006). With our greater sensitivity we can compare our results to these studies, allowing us to investigate the shape of the low luminosity LMXB XLF, although it should be noted that NGC 3379 is a much more 'normal' galaxy than Centaurus A.

In addition the X-ray point sources that have been presented in this catalog, the optical sources within NGC 3379 have also been identified. These were detected in a WFPC2 *HST* observation, where 70 confirmed globular clusters have been identified. From these 70 sources, 9 GC-LMXB, with separations $< 0.6''$, have been detected, with one further GC-LMXB connection, found external to the *HST* FOV.

GC-LMXB associations within this galaxy were previously reported by Kundu, Maccarone & Zepf (2007), where correlations between the same WFPC2 data used here, and the archival *Chandra* observation, were used to search for associations. This archival observation is much shorter than the deep dataset presented here, providing a typical source detection threshold of $\sim 1 - 2 \times 10^{37}$erg s^{-1}. Even so, from their work 7 GC-LMXB sources were detected. From our study we also detect 7 correlations in this individual observation, however, due to the better astrometry we have from our deep observation, used to correct the offsets in the *HST* data, we detect one different optical match to Kundu, Maccarone & Zepf (2007), with their additional source determined to be an 'excluded match' in this work.

4.2. X-ray Colors

In Figure 11 the LMXB population color-color diagram, based on the photometry of the co-added observation, is presented. In the top panel color-color values are plotted, with the sources divided into luminosity bins, with symbols of each bin indicated by the labeling in the panel. In the bottom panel, the errorbars for each of these points are plotted. Also in this figure source variability is indicated, where variable sources are plotted in blue, non-variable sources are shown in green and sources with undetermined variability are indicated in cyan. Additionally, in both of the panels a grid has been overlaid to indicate the predicted locations of the sources at redshift z=0 for different spectra, described by a power law with various photon indices ($0\leq \Gamma_{ph} \leq 4$, from top to bottom.) and absorption column densities ($10^{20} \leq N_{\rm H} \leq 10^{22}$ cm^2, from right to left). In Figure 12 the $L_{\rm X}$-HR, $L_{\rm X}$-C21 and $L_{\rm X}$-C32 population plots are presented, where variability is again indicated by color, with variable sources shown in blue, non-variable sources are plotted in green and sources with undetermined variability are shown in cyan.

From the color-color diagram, presented in Figure 11, it can be seen that most of the well defined colors lie within the area of a typical LMXB spectrum of $\Gamma = 1.5 - 2.0$, with no intrinsic absorption (e.g. Irwin, Athey & Bregman, 2003; Fabbiano 2006). However, there also appears to be a population of sources that have much harder spectra, again with either no intrinsic absorption, or sources with a possible soft excess, albeit with colors that are not as well defined. This sub-population can also be seen in the $L_{\rm X}$-HR population plot presented in the top panel of Figure 12, where a significant number of sources have higher hardness ratios than one would expect from LMXB sources.

This sub-population was investigated by identifying sources with HR values >0.2, resulting in a selection of 10 sources, 4 of which lie within the D_{25} ellipse of the galaxy. The HR and color-color values of these objects are presented in Figure 13, where red values indicate sources that lie within the D_{25} ellipse and black points show those that lie outside of this region. Alongside these plots, an image indicating the spatial distribution of these objects is also presented. These plots indicate that these hard sources have similar C21 values to the majority of the LMXB population but have lower C32 values, indicating that these sources not only have large hardness ratios but also exhibit spectral hardness in their color values.

Because many of these objects have $L_{\rm X} \leq 10^{37}$erg s^{-1}, the sources were stacked to ensure that these harder values are not a consequence of the low counts in the individual sources. From this stacked photometry, a C21 value of -0.53 (-0.61−-0.41) and C32 value of -0.23 (-0.28−-0.18) was derived, with a hardness ratio of 0.41 (0.36−0.46). These values indicate that these sources are truly hard objects and, from looking at their spatial distribution (bottom right panel in Figure 13), it is clear that they are located throughout the galaxy,

which suggests that, coupled with their HR and color values, most of these sources are likely to be objects not associated with NGC 3379, possibly absorbed background AGN. This result is consistent with the number of sources that are expected to be background objects (36) from the hard-band $ChaMP + CDF\ logN - logS$ relation.

However, if we compare the color-color plot in Figure 13 to the one presented in Figure 11, it can be seen that some of the harder sources, with no intrinsic absorption (or a soft excess component) from the whole population plot are not selected with the HR >0.2 cut that has been imposed. From the $L_{\rm X}$-HR population plot in Figure 12 it is clear that there is continuum of HR values for the sources within NGC 3379, rather than a distinct separation of different classes. We therefore impose a lower HR value cut of 0, in an attempt to further identify the population of hard sources within the galaxy, identified in Figure 11.

Extending this cut down to HR>0 increases the sub-population of harder sources to 17, all of which exhibit colors indicating that they are sources with hard spectra and no intrinsic absorption. However, 5 of these extra sources lie within the D_{25} ellipse, with only 2 external to this region. This centrally concentrated distribution of objects indicates that it is likely that some of these additional sources are associated with the galaxy, and are not AGN. Such an affect is unsurprising, as it is not unusual for different classes of sources to have regions of overlap in color-color diagrams (Prestwich *et al.* 2003). As a consequence of this confusion, we use the HR>0.2 cut to identify 10 sources that are likely to be absorbed background AGN, but also note that there are a further seven sources within this galaxy that, whilst exhibiting lower HR values, also exhibit spectral hardness in their color values. We suggest here that, due to their centrally concentrated distribution, it is likely that these sources are associated with NGC 3379, although, we do not rule out the possibility that some of these objects could be background AGN.

4.3. Source Variability

A characteristic of compact accretion sources such as LMXBs is variability, and, as a result of the monitoring nature of the observing campaign, we have been able to search for this variability, in both the long-term regime, and also over short-term baselines, where changes over hours and days have been identified. One of the specific aims of our monitoring campaign has been to identity transient candidate sources as it has been suggested that field LMXBs are expected to be transients (Piro & Bildsten 2002; King 2002) and low luminosity ultracompact binaries in GCs are also expected to be transient in nature (Bildsten & Deloye 2004). In the forthcoming paper Brassington *et al.* (2008, in prep) we investigate the sub-population of transient candidates that has been discovered in NGC 3379.

Our data represent the most complete variability study for an extragalactic LMXB population (see Fabbiano 2006; Xu *et al.* 2005), investigating both long and short term behaviour. In the case of the long-term variability, sources have been separated into four different classifications; non-variable and variable sources, and also transient candidates (TC) or possible transients candidates (PTC). These two latter definitions have been applied to sources that either appear or disappear, or are only detected for a limited amount of 'contiguous' time during the observations, with a lower bound ratio of greater than 10 between the 'on-state' and the 'off-state', for TCs, or a lower bound ratio between 5 and 10 for the PTCs (see §2.4 for a full discussion of this definition).

The 11 sources that were investigated for transient behavior are presented in Table 13, where both the ratio and lower bound ratio, calculated from Bayesian modeling, are presented, along with each source's variability classification. From this table is can be seen that many of these sources appear to be strong TCs from their ratio alone, but when allowing for the uncertainties from their source and background counts, they can only be classified as variable sources. Including the uncertainties when determining TCs is particularly important when dealing with sources with low SNR values, as is the case here for a number of sources in this catalog.

Out of the 132 sources, 56, 42% of the sources within NGC 3379, have been defined as variable sources. A further 5 sources are TCs, and 3 are PTCs, with 44 sources found to be non-varying in intensity over the five observations. The remaining 24 sources have insufficient data to investigate their long-term variability. These, alongside the number of sources exhibiting short-term variability, are summarized in Table 14, where these two variability parameters have been cross-correlated, to indicate the number of sources exhibiting both long and short-term variations, although, the majority of these sources do not have sufficient counts in each observation to determine their short-term variability. The numbers within this table indicate the number of sources from the whole observation and the numbers in brackets represent the sources within the D_{25} ellipse.

From this table it can be seen that, for the sources with a defined short-term variability measure, both long-term variable and non-variable sources have a variety of short-term behavior. For the transient candidates, both classes have few sources with determined short-term variability, but, for all sources that do have short-term measures, all have been found to also exhibit short-term variability. Also, as an additional point, nearly all of the TCs, and PTCs found within NGC 3379 reside within the D_{25} ellipse of the galaxy, with only one confirmed TC, 128, external to this region, indicating that they are likely LMXBs associated with NGC 3379.

In addition to the $L_{\rm X}$ variability, spectral variations have also been investigated. These

are presented in Figures 8 and 9, where $L_{\rm X}$-HR and color-color plots for each source are shown. From these figures it is clear that the majority of sources within NGC 3379 are variable, and that their distribution follows the total source distribution. There is a variety of different spectral variations within this population, similar to spectral variability behaviour discussed in McClintock & Remillard (2006), with a significant number of sources emitting harder spectra as $L_{\rm X}$ increases (e.g sources 25 and 99). Conversely, sources exhibiting spectral softening with increasing $L_{\rm X}$ are also present within the galaxy (e.g sources 81 and 119), as well as sources that show little to no spectral variation with increasing luminosity (e.g. sources 86 and 121), and sources that show no discernible pattern at all (e.g. sources 62 and 98). A more detailed discussion of the spectral variability of the X-ray sources presented in this catalog will be the subject of a forthcoming paper.

5. Conclusions

We have presented a source catalog and variability atlas resulting from our monitoring deep observations of the nearby elliptical NGC 3379 with *Chandra* ACIS-S. Our results can be summarized as follows:

- 132 X-ray point sources have been detected within NGC 3379, ranging in luminosity from 6×10^{35}erg s^{-1} (with 3σ upper limit $\leq 4\times10^{36}$ erg s^{-1}) to $\sim 2\ \times 10^{39}$erg s^{-1}, with 98 of these sources residing within the D_{25} ellipse of the galaxy.
- Only one ULX has been identified within this galaxy, with a galactocentric radius of $6.7''$, and a peak luminosity of $L_{\rm X}\sim 3\times10^{39}$erg s^{-1}.
- Ten globular clusters have been identified to be coincident with X-ray sources, all of which lie within the D_{25} ellipse of the galaxy. These GC-LMXB associations tend to have high X-ray luminosities, with three of these sources exhibiting $L_{\rm X}> \ 1\times 10^{38}$erg s^{-1}.
- From source photometry, it has been determined that the majority of source with well constrained colors have values that are consistent with a typical LMXB spectrum of $\Gamma = 1.5 - 2.0$, with no intrinsic absorption.
- A sub-population of 10 sources has been found to exhibit very hard spectra. These objects are distributed uniformly in the sky and it is expected that most of these sources are absorbed background AGN.

- 64 sources, 48% of the X-ray source population, have been found to exhibit some type of long-term variability, which clearly identifies them as accreting compact objects. 5 of these variable sources have been identified as transient candidates, with a further 3 identified as possible transients.

- Spectral variability analysis has revealed that the sources within NGC 3379 exhibit a range of variability patterns, where both high/soft−low/hard and low/soft−high/hard spectral transitions have been observed, as well as sources that vary in luminosity, but exhibit no spectral variation, indicating that there are many different source classes within this galaxy.

In addition to this catalog paper, our companion paper Fabbiano *et al.* (2007) discusses the dearth of low-luminosity GC-LMXBs within this galaxy. Further highlights from the X-ray binary population of NGC 3379 will also be presented in Brassington *et al.* (2008, in prep), where the properties of the transient population of NGC 3379 will be presented.

Forthcoming papers will also present: the properties of the ULX, the X-ray luminosity function and the diffuse emission of the galaxy, as well as the properties of the nuclear source and the intensity and spectral variability of the luminous X-ray binary population. The results from this deep observation will then be compared to the X-ray source catalog of the old, GC rich elliptical galaxies NGC 4278, which has also recently been the subject of a deep *Chandra* observation.

A. Bayesian Estimations of Source Upper-Limits and HR Values

In order to obtain accurate estimates of the source intensities and their hardness ratios we use a method based on the Bayesian estimation of the true source intensity in the presence of background, and effective area variations (Park *et al.* 2006). This method is based on the posterior predictive probability distribution of the source intensity, given the number of observed counts (source plus background), and an estimate of the local background (van Dyk *et al.* 2001). The advantage of this method is that it takes into account the Poisson nature of the source *and* the background, allowing a more accurate decomposition of the net source intensity. This is particularly important for sources very close to the detection limit: in these cases the classical method (e.g. assuming Gaussian errors, or even the simplified version of the Gehrels approximation) may give zero or negative counts. However, our method overcomes these problems and can provide the full probability distribution of the source intensities. The raw source and background counts (divided by the background to

source area ratio), used to determine the HR and color values from Bayesian estimations, are presented in Table 15.

For sources very close to the detection limit we can obtain the mode of the distribution which, although lower than the average background, might well be above zero. In those cases we can also estimate the upper 68% quantile of the distribution, which would correspond to the 68% confidence level on the source intensity (a similar method, which however does not model the Poisson probability distribution of the background counts, is presented in Kraft *et al.* 1991). In Figure 14 we present the posterior probability distributions for hypothetical sources with 10 observed counts and estimated background of 6, 8, and 10 counts. None of these cases is a formal 'detection' (i.e. flux intensity at least 3σ above the background) in the classical method[11], however, from these distributions we can recover the source intensity, and even in the most extreme case (10 background counts) we can estimate the upper confidence bound on the source intensity.

We thank the CXC DS and SDS teams for their efforts in reducing the data and developing the software used for the reduction (SDP) and analysis (CIAO). We would also like to thank the anonymous referee for helpful comments which have improved this paper. This work was supported by *Chandra* G0 grant G06-7079A (PI:Fabbiano) and subcontract G06-7079B (PI:Kalogera). We acknowledge partial support from NASA contract NAS8-39073(CXC). A. Zezas acknowledges support from NASA LTSA grant NAG5-13056. S. Pellegrini acknowledges partial financial support from the Italian Space Agency ASI (Agenzia Spaziale Italiana) through grant ASI-INAF I/023/05/0.

REFERENCES

Angelini, L., Loewenstein, M. & Mushotzky, R. F. 2001, ApJ, 557, L35

Bergond, G., Zephf, S. E., Romanowsky, A. J., Sharples, R. M., & Rhodes, K. L. 2006, A&A, 448, 155

Bildsten, L. & Deloye, C. J. 2004, ApJ, 607, L119

Cappellari, M., *et al.* 2006, MNRAS, 366, 1126

[11]We note however that significance of the source flux has a different meaning from the significance of the detection which strongly depends on the detection process; a more detailed description of these nuanced terms will be presented in van Dyk *et al.* (2008, in prep).

David, L. P., Jones, C., Forman, W., & Murray, S. S. 2005, ApJ, 635, 1053

Fabbiano, G. 2006, ARAA, 44, 323

Fabbiano, G., *et al.* 2006, ApJ, 650, 879

Fabbiano, G., *et al.* 2007, astro-ph/0710.5126

Freeman, P. E., Kashyap, V., Rosner, R. & Lamb D. Q., 2002, ApJS, 138, 185

Gehrels, N. 1986, ApJ, 303, 336

Giacconi, R. 1974, in X-ray Astronomy, eds. R. Giacconi & H. Gursky, p.155, Dordrecht: Reidel

Gilfanov, M. 2004, MNRAS, 349, 146

Grindlay, J. E. 1984, Adv. Space Res., 3, 19

Harris, W. E. 1991, ARAA, 29, 543

Irwin, J., Athey, A. & Bregman, J. 2003, ApJ, 393, 134

Irwin, J. 2006, MNRAS, 371, 1903

Kenter, A., *et al.* 2005, ApJS, 161, 9

Kim, D.-W. & Fabbiano, G. 2004, ApJ, 611, 846

Kim, D.-W., Cameron, R. A., Drake, J. J., *et al.* 2004a, ApJS, 150, 19

Kim, D.-W., Wilkes, B., Green, P., *et al.* 2004b, ApJ, 600, 59

Kim, D.-W., *et al.* 2006, ApJ, 652, 1090

Kim, M., *et al.* 2007a, ApJS, 169, 401

Kim, M., *et al.* 2007b, ApJ, 659, 29

King, A. R. 2002, MNRAS, 335, L13

Kraft, R. P., *et al.* 2001, ApJ, 560, 675

Kundu, A., Maccarone, T. J. & Zepf, S. E. 2002, ApJ, 574, L5

Kundu, A., Whitmore, B. C. 2001, ApJ, 121, 2950

McClintock, J. E., & Remillard, R. A. 2006, in Compact Stellar X-Ray Sources, ed. W. H. G. Lewin & M. van der Klis (Cambridge: Cambridge Univ. Press), in press

Park, T., Kashyap, V., Siemiginowska, A., van Dyk, D., Zezas, A., Heinke, C., Wargelin, B. 2006, ApJ, 652, 610

Pierce, M., *et al.* 2006, MNRAS, 366, 1253

Piro, A. L. & Bildsten, L. 2002, ApJ, 571, L103

Prestwich, A. H., Irwin, J. A., Kilgard, R. E., Krauss, M. I., Zezas, A., Primini, F., Kaaret, P. & Boroson, B., 2003, ApJ, 595, 719

Puzia, T. H., *et al.* 2004, A&A, 415, 123

Rhode, K.L., Zepf, S.E. 2004, AJ, 127, 302

Scargle, J.D. 1998, ApJ, 504, 405

Sivakoff, G. R., Jordán, A., Juett, A. M., Sarazin, C. L., & Irwin, J. A., 2007, astro-ph/0712.3052

Sivakoff, G. R., *et al.* 2006, ApJ, 660, 1246

Terlevich, A. I. & Forbes, D. A. 2002, MNRAS, 330, 547

Tonry J., *et al.* 2001, ApJ, 546, 681

van Dyk, D., *et al.* 2001, ApJ, 548, 224

Verbunt, F. & van den Heuvel, E. P. J. 1995, in X-ray Binaries, eds. Lewin, W. H. G., van Paradijs, J., van den Heuvel, E. P. J., Cambridge, UK: CUP, p.457

Voss, R. & Gilfanov, M. 2006, A&A, 447, 71

Weisskopf, M. C., Tananbaum, H. D., Van Speybroeck, L. P. & O'Dell, S. L. 2000, Proc. SPIE, 4012, 2

White, R. E. III, Sarazin, C. L. & Kulkarni, S. R. 2002, ApJ, 571, L23

Williams, B. F., *et al.* 2008, astro-ph/0802.3724

Xu, Y., Xu, H., Zhang, Z., Kundu, A., Wang, Y. & Wu, X.-P., 2005, 631, 809

Zezas, A, Fabbiano, G., Rots, A. H., Murray, S. S. 2002, ApJ, 577, 710

This preprint was prepared with the AAS LaTeX macros v5.2.

Table 1. Observation Log

Obs. Num.	OBSID	Date	Exposure (sec)	Cleaned Exposure (sec)
1	1587	2001-02-13	31519.0	28951.9
2	7073	2006-01-23	84099.0	80347.1
3	7074	2006-04-09	69066.2	66696.6
4	7075	2006-07-03	83110.1	79555.7
5	7076	2007-01-10	69249.5	68657.1
Total	-	-	337043.8	324208.4

Table 2. Average Right Ascension and Declination offsets of the twenty brightest sources, detected in all five observations, from the source position defined in the co-added observation.

Offset	Obs 1587	Obs 7073	Obs 7074	Obs 7075	Original Obs 7076	Corrected Obs 7076
Four co-added observation						
RA offset	-0.100	-0.110	0.091	0.042	-0.025	-0.009
DEC offset	-0.102	0.105	-0.133	-0.014	0.573	-0.008
Separation	0.196	0.168	0.181	0.100	0.598	0.151
Five co-added observation						
RA offset	-0.106	-0.114	0.082	0.036	-	-0.039
DEC offset	-0.081	0.114	-0.118	-0.007	-	-0.015
Separation	0.181	0.178	0.186	0.124	-	0.129

Table 3. Definition of Energy Bands and X-ray Colors

Band	Definition
Broad (B)	0.3−8 keV
Soft (S)	0.3−2.5 keV
Hard (H)	2.5−8 keV
Soft 1 (S_1)	0.3−0.9 keV
Soft 2 (S_2)	0.9−2.5 keV
Conventional Broad (Bc)	0.5−8 keV
Conventional Soft (Sc)	0.5−2 keV
Conventional Hard (Hc)	2−8 keV
Hardness Ratio HR	(Hc−Sc)/(Hc+Sc)
X-ray Color C21	$-log(S_2) + log(S_1) = log(S_1/S_2)$
X-ray Color C32	$-log(H) + log(S_2) = log(S_2/H)$

Table 4. Master Source List

Masterid	CXOU Name	RA (J2000)	Dec (J2000)	Radius (″)	PU (″)	SNR	Log L_X(0.3−8.0 keV) (erg s^{-1})	Variability LT	BB	K-S	Opt Corr	DG (″)	Flag
(1)	(2)	(3)	(4)	(5)	(6)	(7)	(8)	(9)	(10)	(11)	(12)	(13)	(14)
1	J104806.4+123621	10:48:06.4	+12:36:21.0	3.13	0.54	5.8	37.3	V	-	-	-	261.1	-
2	J104806.2+123534	10:48:06.2	+12:35:34.3	3.10	0.68	4.2	37.1	V	-	-	-	246.3	-
3	J104805.5+123423	10:48:05.5	+12:34:22.7	3.29	1.09	3.5	37.0	-	-	-	-	235.5	-
7	J104803.0+123438	10:48:03.0	+12:34:37.8	3.00	0.68	4.4	37.1	V	-	-	-	197.5	-
8	J104801.9+123607	10:48:01.9	+12:36:07.2	3.00	0.72	3.1	36.9	-	-	-	-	194.6	-
9	J104801.7+123145	10:48:01.7	+12:31:44.8	4.42	0.27	30.0	38.5	V	N	N	-	259.4	-
10	J104801.4+123426	10:48:01.4	+12:34:26.4	3.00	1.28	3.4	36.9	-	-	-	-	175.5	BKG?
11	J104801.3+123526	10:48:01.3	+12:35:26.4	3.00	0.23	11.2	37.7	N	-	-	-	174.0	-
12	J104801.0+123434	10:48:01.0	+12:34:34.4	3.00	0.61	3.9	37.0	-	-	-	-	167.7	-
13	J104800.5+123645	10:48:00.5	+12:36:44.5	3.00	0.47	4.5	37.1	N	-	-	-	194.2	-
14	J104759.9+123116	10:47:59.9	+12:31:16.4	4.78	0.95	3.7	37.1	-	-	-	-	264.7	-
16	J104758.4+123459	10:47:58.4	+12:34:59.4	3.00	0.32	7.0	37.4	V	-	-	-	**129.4**	-
17	J104758.1+123326	10:47:58.1	+12:33:26.0	3.00	0.45	6.4	37.3	N	-	-	-	152.0	-
18	J104757.5+123136	10:47:57.5	+12:31:35.6	4.11	0.36	11.9	37.8	V	-	-	-	229.6	-
21	J104756.5+123121	10:47:56.5	+12:31:20.8	4.26	0.49	9.1	37.6	V	-	-	-	235.6	BKG?
23	J104755.7+123142	10:47:55.7	+12:31:41.5	3.91	0.72	4.5	37.2	N	-	-	-	212.1	BKG?
25	J104754.5+123531	10:47:54.5	+12:35:30.9	3.00	0.16	10.7	37.8	TC	-	-	BGexmt	**80.6**	O1
27	J104754.2+123223	10:47:54.2	+12:32:22.9	3.22	0.24	21.4	38.2	V	-	-	-	165.4	-
28	J104754.2+123529	10:47:54.2	+12:35:29.4	3.00	0.20	7.5	37.5	N	-	-	GCexmt	**76.3**	O1
29	J104754.1+123556	10:47:54.1	+12:35:56.2	3.00	0.21	7.1	37.4	N	-	-	BGexmt	**90.7**	-
30	J104753.7+123543	10:47:53.7	+12:35:43.2	3.00	0.15	11.5	37.7	N	V	P	none	**77.9**	-
32	J104753.6+123525	10:47:53.6	+12:35:25.2	3.00	0.36	3.7	37.0	N	-	-	none	**66.8**	-
33	J104753.6+123300	10:47:53.6	+12:33:00.2	3.00	0.86	3.1	36.9	N	-	-	-	**127.7**	-
35	J104753.3+123319	10:47:53.3	+12:33:18.5	3.00	0.55	3.7	37.0	N	-	-	-	**109.9**	-
37	J104753.0+123530	10:47:53.0	+12:35:29.7	3.00	0.24	6.3	37.3	V	-	-	none	**61.0**	-
39	J104752.8+123604	10:47:52.8	+12:36:03.7	3.00	0.31	3.3	36.9	N	-	-	none	**84.6**	-
40	J104752.8+123452	10:47:52.8	+12:34:52.4	3.00	0.41	3.3	36.9	V	-	-	GCexmt	**47.0**	-
41	J104752.8+123509	10:47:52.8	+12:35:08.5	3.00	0.12	25.3	38.3	V	N	N	GCcorr	**48.9**	-
42	J104752.7+123338	10:47:52.7	+12:33:38.0	3.00	0.14	40.5	38.7	V	N	N	GCcorr	**88.1**	-
44	J104752.4+123418	10:47:52.4	+12:34:17.7	3.00	0.39	4.1	37.1	V	-	-	BGexmt	**54.7**	-
45	J104752.3+123524	10:47:52.3	+12:35:24.2	3.00	0.30	4.4	37.1	V	-	-	BGexmt	**50.3**	-
47	J104751.8+123508	10:47:51.8	+12:35:07.8	3.00	0.14	12.6	37.9	N	V	N	none	**35.5**	O1
48	J104751.7+123518	10:47:51.7	+12:35:17.8	3.00	0.38	3.1	37.0	N	-	-	none	**39.4**	O1

Table 4—Continued

Masterid	CXOU Name	RA (J2000)	Dec (J2000)	Radius (″)	PU (″)	SNR	Log L_X(0.3−8.0 keV) (erg s^{-1})	Variability LT	BB	K-S	Opt Corr	DG (″)	Flag
(1)	(2)	(3)	(4)	(5)	(6)	(7)	(8)	(9)	(10)	(11)	(12)	(13)	(14)
50	J104751.6+123536	10:47:51.6	+12:35:35.9	3.00	0.27	5.2	37.2	PTC	-	-	GCcorr	**51.1**	-
52	J104751.2+123410	10:47:51.2	+12:34:10.0	3.00	0.34	4.5	37.2	V	-	-	none	**49.7**	O1
53	J104751.2+123458	10:47:51.2	+12:34:58.3	3.00	0.17	10.4	37.7	V	-	-	BGexmt	**23.5**	-
54	J104751.1+123445	10:47:51.1	+12:34:44.9	3.00	0.34	4.2	37.1	N	-	-	BGexmt	**23.6**	-
55	J104751.1+123549	10:47:51.1	+12:35:49.1	3.00	0.13	13.9	37.9	V	-	-	GCcorr	**59.4**	-
56	J104751.0+123439	10:47:51.0	+12:34:39.0	3.00	0.37	3.5	37.0	N	-	-	BGexmt	**25.4**	-
58	J104750.9+123408	10:47:50.9	+12:34:08.3	3.00	0.35	5.3	37.3	N	-	-	GCexmt	**49.6**	O1
59	J104750.8+123507	10:47:50.8	+12:35:07.2	3.00	0.23	6.2	37.3	V	-	V	BGexmt	**22.0**	-
60	J104750.5+123450	10:47:50.5	+12:34:50.3	3.00	0.18	10.5	37.7	N	-	-	none	**14.2**	-
62	J104750.5+123437	10:47:50.5	+12:34:37.0	3.00	0.18	9.0	37.7	V	-	P	GCcorr	**21.2**	O1
63	J104750.5+123210	10:47:50.5	+12:32:09.6	3.38	0.83	3.2	36.9	V	-	-	-	164.7	-
64	J104750.4+123527	10:47:50.4	+12:35:26.5	3.00	0.15	12.5	37.8	V	-	-	none	**34.7**	-
66	J104750.3+123507	10:47:50.3	+12:35:06.6	3.00	0.16	10.8	37.7	N	-	P	GCcorr	**16.8**	-
67	J104750.2+123455	10:47:50.2	+12:34:55.3	3.00	0.12	30.2	38.5	N	N	N	GCcorr	**8.9**	O2
68	J104750.1+123500	10:47:50.1	+12:34:59.5	3.00	0.26	7.1	37.3	-	-	-	BGcorr	**9.7**	O2
70	J104750.0+123457	10:47:50.0	+12:34:56.9	3.00	0.08	83.7	39.3	V	V	V	GCexmt	**6.7**	O2
71	J104750.0+123452	10:47:50.0	+12:34:52.3	3.00	0.23	7.9	37.4	-	-	-	GCexmt	**5.8**	O2
72	J104750.0+123445	10:47:50.0	+12:34:44.7	3.00	0.32	8.3	37.5	N	-	P	BGexmt	**10.6**	double?
74	J104749.8+123455	10:47:49.8	+12:34:55.0	3.00	0.11	32.4	38.6	V	N	P	X	**3.2**	O2
75	J104749.8+123452	10:47:49.8	+12:34:52.0	3.00	0.14	16.9	38.1	V	-	-	X	**3.2**	O2
77	J104749.7+123458	10:47:49.7	+12:34:57.9	3.00	0.14	18.4	38.1	V	N	N	X	**4.2**	O2
78	J104749.6+123452	10:47:49.6	+12:34:51.5	3.00	0.17	11.8	37.7	V	-	-	X	**2.4**	O2
80	J104749.6+123502	10:47:49.6	+12:35:02.3	3.00	0.24	7.2	37.4	N	-	-	none	**8.5**	-
81	J104749.6+123454	10:47:49.6	+12:34:53.9	3.00	0.12	27.8	38.4	V	N	N	X	**0.0**	O2
82	J104749.5+123500	10:47:49.5	+12:34:59.9	3.00	0.13	24.2	38.3	V	N	N	none	**6.2**	O2
83	J104749.4+123459	10:47:49.4	+12:34:59.3	3.00	0.17	11.7	37.7	N	-	-	none	**6.3**	O2
84	J104749.2+123432	10:47:49.2	+12:34:32.0	3.00	0.34	6.1	37.2	V	-	-	none	**22.4**	O2
85	J104749.2+123431	10:47:49.2	+12:34:31.1	3.00	0.48	4.2	36.9	PTC	-	-	BGcorr	**23.6**	O2
86	J104749.1+123449	10:47:49.1	+12:34:48.8	3.00	0.11	44.3	38.8	V	N	P	none	**8.7**	-
87	J104749.1+123456	10:47:49.1	+12:34:55.8	3.00	0.16	12.6	37.8	N	N	N	none	**7.6**	O2
88	J104748.9+123515	10:47:48.9	+12:35:14.7	3.00	0.20	8.8	37.5	V	-	-	-	**23.0**	-
89	J104748.9+123459	10:47:48.9	+12:34:59.1	3.00	0.23	6.9	37.5	TC	-	-	BGexmt	**11.9**	O1
90	J104748.7+123547	10:47:48.7	+12:35:46.7	3.00	0.13	18.0	38.1	N	N	P	-	**54.3**	-

Table 4—Continued

Masterid	CXOU Name	RA (J2000)	Dec (J2000)	Radius (″)	PU (″)	SNR	Log L_X(0.3−8.0 keV) (erg s^{-1})	Variability LT	BB	K-S	Opt Corr	DG (″)	Flag
(1)	(2)	(3)	(4)	(5)	(6)	(7)	(8)	(9)	(10)	(11)	(12)	(13)	(14)
92	J104748.5+123233	10:47:48.5	+12:32:32.8	3.08	0.67	3.1	36.9	V	-	-	-	**141.9**	-
93	J104748.5+123501	10:47:48.5	+12:35:01.0	3.00	0.18	9.7	37.6	V	-	-	BGexmt	**18.1**	-
94	J104748.0+123446	10:47:48.0	+12:34:45.7	3.00	0.29	7.1	37.4	TC	V	V	-	**24.8**	double?
95	J104747.8+123505	10:47:47.8	+12:35:04.7	3.00	0.26	7.0	37.4	V	-	-	-	**28.1**	-
96	J104747.7+123453	10:47:47.7	+12:34:53.3	3.00	0.33	5.2	37.2	V	-	-	-	**27.9**	-
98	J104747.6+123715	10:47:47.6	+12:37:15.2	3.00	0.23	8.7	37.5	V	-	-	-	144.4	-
99	J104747.3+123416	10:47:47.3	+12:34:15.9	3.00	0.20	11.9	37.8	V	-	-	none	**50.9**	-
100	J104747.2+123500	10:47:47.2	+12:34:59.8	3.00	0.26	6.7	37.4	TC	-	-	-	**35.2**	-
101	J104747.1+123506	10:47:47.1	+12:35:05.5	3.00	0.31	5.9	37.3	N	-	-	-	**38.5**	BKG?
102	J104747.0+123439	10:47:47.0	+12:34:38.7	3.00	0.13	35.9	38.6	V	N	N	-	**41.4**	-
103	J104746.8+123427	10:47:46.8	+12:34:27.4	3.00	0.15	24.0	38.3	V	N	P	-	**48.4**	O2
104	J104746.6+123345	10:47:46.6	+12:33:45.1	3.00	0.58	3.5	37.0	V	-	-	-	**81.3**	-
105	J104746.6+123431	10:47:46.6	+12:34:30.8	3.00	0.49	4.0	37.1	V	-	-	-	**50.1**	O1
106	J104746.5+123424	10:47:46.5	+12:34:23.5	3.00	0.19	13.7	37.9	V	-	-	-	**54.0**	O1
108	J104746.4+123440	10:47:46.4	+12:34:40.0	3.00	0.56	3.4	36.9	-	-	-	-	**48.9**	-
109	J104745.8+123322	10:47:45.8	+12:33:22.0	3.00	0.49	5.0	37.2	V	-	-	-	**107.5**	BKG?
110	J104745.8+123222	10:47:45.8	+12:32:22.2	3.41	0.42	8.7	37.5	N	-	-	-	161.7	-
111	J104745.7+123527	10:47:45.7	+12:35:27.3	3.00	0.37	4.4	37.1	N	-	-	-	**66.3**	-
112	J104745.4+123352	10:47:45.4	+12:33:51.9	3.00	0.46	4.8	37.1	N	-	-	-	**87.0**	-
113	J104744.2+123418	10:47:44.2	+12:34:17.6	3.00	0.51	3.7	37.0	N	-	-	-	**86.9**	-
114	J104744.0+123401	10:47:44.0	+12:34:00.5	3.00	0.46	4.5	37.1	V	-	-	-	**98.1**	-
115	J104743.6+123411	10:47:43.6	+12:34:10.8	3.00	0.74	2.3	36.7	PTC	-	-	-	**97.2**	-
116	J104743.4+123249	10:47:43.4	+12:32:48.8	3.27	0.32	10.0	37.6	V	-	-	-	**154**.1	-
119	J104741.9+123331	10:47:41.9	+12:33:31.1	3.00	0.29	10.0	37.6	N	-	-	GCcorr	**139.9**	-
120	J104741.8+123745	10:47:41.8	+12:37:45.0	3.00	0.19	24.0	38.3	V	V	V	-	205.3	-
121	J104741.0+123505	10:47:41.0	+12:35:04.6	3.00	0.22	14.5	37.9	V	N	N	-	**126.7**	-
122	J104740.8+123538	10:47:40.8	+12:35:37.8	3.00	2.01	4.0	37.0	-	-	-	-	**135.7**	-
125	J104739.7+123258	10:47:39.7	+12:32:57.8	3.66	0.34	10.5	37.7	N	-	-	-	185.1	-
126	J104738.9+123731	10:47:38.9	+12:37:31.1	3.00	0.90	3.0	36.9	-	-	-	-	221.5	BKG?
127	J104738.4+123340	10:47:38.4	+12:33:40.0	3.46	0.70	3.9	37.0	V	-	-	-	180.0	-
128	J104738.2+123308	10:47:38.2	+12:33:07.6	3.80	0.27	22.3	38.3	TC	V	V	-	197.7	-
129	J104738.0+123721	10:47:38.0	+12:37:20.8	3.02	0.56	5.1	37.2	N	-	-	-	224.3	-
130	J104737.4+123651	10:47:37.4	+12:36:51.0	3.02	0.29	10.5	37.7	V	-	-	-	213.8	-

Table 4—Continued

Masterid	CXOU Name	RA (J2000)	Dec (J2000)	Radius (″)	PU (″)	SNR	Log L_X(0.3−8.0 keV) (erg s^{-1})	Variability LT	BB	K-S	Opt Corr	DG (″)	Flag
(1)	(2)	(3)	(4)	(5)	(6)	(7)	(8)	(9)	(10)	(11)	(12)	(13)	(14)
131	J104735.3+123349	10:47:35.3	+12:33:48.5	3.96	0.48	8.6	37.6	V	-	-	-	219.1	-
132	J104733.3+123446	10:47:33.3	+12:34:45.6	4.03	0.37	10.3	37.7	N	-	-	-	238.7	-
Master Source List for sources with SNR<3													
4	J104804.3+123344	10:48:04.3	+12:33:43.9	3.35	2.77	0.5	35.8 ($\leq$ 36.6)	-	-	-	-	225.8	BKG?
5	J104804.0+123502	10:48:04.0	+12:35:01.7	3.00	1.73	1.3	36.2 ($\leq$ 36.7)	-	-	-	-	211.3	BKG?
6	J104803.1+123310	10:48:03.1	+12:33:09.8	3.00	-	-	$\leq$ 36.6 ($\leq$ 37.4)	N	-	-	-	223.0	X
15	J104758.7+123635	10:47:58.7	+12:36:35.0	3.00	0.69	2.6	36.8 ($\leq$ 37.1)	-	-	-	-	167.9	-
19	J104757.5+123348	10:47:57.5	+12:33:48.1	3.00	-	-	$\leq$ 36.2 ($\leq$ 37.3)	N	-	-	-	**132.7**	X
20	J104757.3+123529	10:47:57.3	+12:35:29.1	3.00	0.61	2.6	36.8 ($\leq$ 37.1)	-	-	-	-	**118.9**	-
22	J104756.3+123206	10:47:56.3	+12:32:05.8	3.62	-	-	$\leq$ 36.9 ($\leq$ 37.7)	N	-	-	-	194.9	X
24	J104754.9+123530	10:47:54.9	+12:35:30.2	3.00	0.49	2.7	36.8 ($\leq$ 37.2)	V	-	-	none	**85.7**	-
26	J104754.4+123242	10:47:54.4	+12:32:41.7	3.00	0.84	2.5	36.8 ($\leq$ 37.1)	-	-	-	-	150.0	-
31	J104753.7+123443	10:47:53.7	+12:34:43.4	3.00	0.72	2.4	36.8 ($\leq$ 37.1)	-	-	-	BGcorr	**60.7**	BKG?
34	J104753.5+123506	10:47:53.5	+12:35:05.9	3.00	0.49	1.2	36.4 ($\leq$ 37.0)	-	-	-	GCexmt	**58.9**	-
36	J104753.2+123500	10:47:53.2	+12:34:59.7	3.00	0.43	2.8	36.8 ($\leq$ 37.2)	V	-	-	none	**53.1**	-
38	J104752.9+123326	10:47:52.9	+12:33:25.9	3.00	0.72	1.7	36.6 ($\leq$ 37.0)	N	-	-	-	**100.5**	-
43	J104752.5+123518	10:47:52.5	+12:35:17.6	3.00	0.48	1.9	36.7 ($\leq$ 37.1)	-	-	-	BGcorr	**48.7**	-
46	J104751.9+123504	10:47:51.9	+12:35:04.1	3.00	0.44	2.1	36.8 ($\leq$ 37.2)	-	-	-	GCexmt	**35.2**	O1
49	J104751.6+123523	10:47:51.6	+12:35:22.5	3.00	0.40	1.5	36.6 ($\leq$ 37.1)	N	-	-	GCexmt	**41.5**	O1
51	J104751.3+123511	10:47:51.3	+12:35:10.8	3.00	0.34	2.8	36.9 ($\leq$ 37.2)	N	-	-	GCexmt	**29.7**	-
57	J104750.9+123458	10:47:50.9	+12:34:58.1	3.00	-	-	$\leq$ 37.0 ($\leq$ 37.7)	V	-	-	none	**20.3**	X
61	J104750.5+123423	10:47:50.5	+12:34:23.1	3.00	0.65	1.5	36.5 ($\leq$ 37.0)	N	-	-	GCcorr	**33.4**	-
65	J104750.4+123434	10:47:50.4	+12:34:33.8	3.00	0.52	1.6	36.7 ($\leq$ 37.2)	-	-	-	BGexmt	**23.0**	O1
69	J104750.1+123514	10:47:50.1	+12:35:13.6	3.00	0.45	2.6	36.8 ($\leq$ 37.2)	-	-	-	BGexmt	**20.9**	-
73	J104749.9+123448	10:47:49.9	+12:34:47.9	3.00	-	-	$\leq$ 36.7 ($\leq$ 37.9)	V	-	-	none	**7.3**	X
76	J104749.7+123440	10:47:49.7	+12:34:40.4	3.00	-	-	$\leq$ 36.6 ($\leq$ 37.8)	N	-	-	GCexmt	**13.5**	X
79	J104749.6+123411	10:47:49.6	+12:34:10.5	3.00	0.97	0.8	36.2 ($\leq$ 36.9)	N	-	-	GCcorr	**43.4**	-
91	J104748.6+123430	10:47:48.6	+12:34:29.5	3.00	0.63	0.7	36.2 ($\leq$ 36.9)	V	-	-	none	**28.2**	-
97	J104747.7+123433	10:47:47.7	+12:34:33.2	3.00	0.62	2.6	36.8 ($\leq$ 37.1)	-	-	-	-	**34.9**	-
107	J104746.5+123626	10:47:46.5	+12:36:26.3	3.00	-	-	$\leq$ 36.2 ($\leq$ 37.4)	N	-	-	-	**103.1**	X
117	J104743.3+123448	10:47:43.3	+12:34:47.6	3.00	0.71	1.7	36.7 ($\leq$ 37.0)	N	-	-	-	**91.7**	-

Table 4—Continued

Masterid	CXOU Name	RA (J2000)	Dec (J2000)	Radius (″)	PU (″)	SNR	Log L_X(0.3−8.0 keV) (erg s^{-1})	Variability LT	BB	K-S	Opt Corr	DG (″)	Flag
(1)	(2)	(3)	(4)	(5)	(6)	(7)	(8)	(9)	(10)	(11)	(12)	(13)	(14)
118	J104742.2+123539	10:47:42.2	+12:35:39.3	3.00	0.68	2.1	36.7 ($\leq$ 37.1)	V	-	-	-	**117.9**	-
123	J104740.8+123446	10:47:40.8	+12:34:46.2	3.00	0.76	2.8	36.8 ($\leq$ 37.1)	-	-	-	-	**129.5**	-
124	J104739.9+123457	10:47:39.9	+12:34:57.4	3.00	1.20	2.4	36.8 ($\leq$ 37.1)	-	-	-	-	**141.7**	BKG?

Note. — Table has been divided into two parts. The first part lists all sources with SNR >3, in at least one observation. The second section lists the remaining sources, that have SNR <3 in all observations. Col. (1): source number, col. (2): IAU name (following the convention "CXOU Jhhmmss.s+/−ddmmss"), cols. (3) and (4): right ascension and declination, col. (5): source extraction radius in arcseconds, col. (6): position uncertainty (from section 2.2, equation 1), col. (7): signal-to-noise ratio, col. (8): log L_X (0.3−8.0 keV) assuming D=10.6 Mpc (for the sources with SNR<3, 3σ upper limits are also quoted in brackets). For sources only detected in a single observation, 1σ upper limits from the co-added observation are quoted (with 3σ upper limits from the detected observatioin presented in brackets), col. (9): long-term source variability - (N) indicates non-variable sources, (V) indicates variable sources, (TC) transient candidates, (PTC) possible transients, cols. (10) and (11): short-term variability, where (BB) indicates Bayesian block analysis and (K-S) indicates the Kolmogorov-Smirnov test, in both columns symbols indicate - (N) non-variable in all observations, (V) variable in at least one observation, (P) possible variability in at least one observation, col. (12): optical associations - 'GC' indicates that the optical source is a confirmed globular cluster, 'BG' indicates that optical source is a background objects. 'corr' denotes matches that have been defined as correlations, and 'exmt' denotes matches between 0.6″ and 3″ in separation. 'none' indicates sources inside the field of view of the *HST* observation, but have no optical counterpart, 'X' indicates sources within the *HST* FOV, but also within 5″ of the nucleus. All other sources are external to the *HST* FOV. Col. (13): distance from the galactic center (in arcseconds), where values in bold type face indicate sources that lie within the D_{25} ellipse. Col. (14): flag information - (X) sources detected in a single observation only, O1 and O2 overlapping sources (single and complicated cases respectively), (BKG?) possible background objects and (double?) possible double sources.

Table 5. Source counts, hardness ratios and color-color values: Coadded Observation

MID	Net Counts							HR	C21	C32	Log L_X
	B-band	S1-band	S2-band	S-band	H-band	Sc-band	Hc-band				(0.3−8.0 keV)
(1)	(2)	(3)	(4)	(5)	(6)	(7)	(8)	(9)	(10)	(11)	(12)
1	58.9±10.2	14.2±5.6	36.4±7.5	50.6±8.9	8.3±5.6	45.7±8.3	11.9±6.1	$-0.65^{+0.13}_{-0.14}$	$-0.31^{+0.18}_{-0.15}$	$0.65^{+0.34}_{-0.24}$	37.3
2	36.2±8.7	1.5±3.6	23.0±6.5	24.5±7.0	11.7±5.8	24.8±6.6	13.4±6.1	$-0.39^{+0.19}_{-0.20}$	$-0.97^{+0.53}_{-0.63}$	$0.30^{+0.26}_{-0.17}$	37.1
3	28.9±8.3	7.3±4.7	15.1±5.7	22.4±6.9	6.5±5.3	16.5±5.9	9.1±5.8	$-0.39^{+0.27}_{-0.30}$	$-0.22^{+0.28}_{-0.28}$	$0.43^{+0.40}_{-0.40}$	37.0
4	1.8±3.6	-0.1±2.3	-0.1±2.3	-0.2±2.7	2.0±3.2	0.8±2.7	1.7±3.2	$0.20^{+0.80}_{-0.18}$	$0.08^{+1.07}_{-1.07}$	$-0.38^{+0.76}_{-1.07}$	35.8
5	4.6±3.6	-0.3±1.9	2.6±2.9	2.3±2.9	2.3±2.9	1.6±2.7	3.2±3.2	$0.29^{+0.50}_{-0.40}$	$-0.69^{+0.69}_{-0.99}$	$0.08^{+0.48}_{-0.46}$	36.2
6	≤10.6	-	-	-	-	-	-	-	-	-	≤36.6
7	38.7±8.8	7.0±4.6	23.9±6.5	30.8±7.5	7.8±5.3	23.1±6.5	14.5±6.2	$-0.31^{+0.21}_{-0.19}$	$-0.39^{+0.21}_{-0.30}$	$0.44^{+0.39}_{-0.21}$	37.1
8	24.7±8.0	8.6±4.7	15.4±5.7	24.0±6.9	0.7±4.7	17.2±5.9	3.0±5.2	$-0.78^{+0.14}_{-0.22}$	$-0.13^{+0.21}_{-0.25}$	$0.75^{+0.86}_{-0.43}$	36.9
9	997.6±33.2	271.4±17.8	567.3±25.0	838.7±30.3	159.0±14.4	725.7±28.1	224.4±16.7	$-0.58^{+0.02}_{-0.03}$	$-0.23^{+0.04}_{-0.02}$	$0.59^{+0.03}_{-0.05}$	38.5
10	27.9±8.1	1.5±3.8	3.5±4.1	5.0±5.1	22.9±6.8	1.7±4.0	25.6±7.1	$0.90^{+0.10}_{-0.10}$	$-0.11^{+0.75}_{-0.94}$	$-0.66^{+0.33}_{-0.56}$	36.9
11	165.6±14.7	43.3±8.0	95.8±11.1	139.2±13.3	26.4±7.1	123.9±12.5	35.7±8.0	$-0.60^{+0.07}_{-0.07}$	$-0.23^{+0.07}_{-0.09}$	$0.58^{+0.12}_{-0.10}$	37.7
12	32.8±8.4	8.2±4.7	18.2±6.0	26.4±7.1	6.4±5.1	20.0±6.2	11.0±5.8	$-0.38^{+0.25}_{-0.21}$	$-0.24^{+0.22}_{-0.25}$	$0.53^{+0.34}_{-0.40}$	37.0
13	40.2±8.9	-0.4±3.2	20.6±6.2	20.1±6.5	20.1±6.5	18.2±6.0	23.6±7.0	$0.05^{+0.20}_{-0.17}$	$-1.00^{+0.43}_{-0.95}$	$0.03^{+0.18}_{-0.14}$	37.1
14	38.4±10.4	5.0±5.2	17.6±6.5	22.7±7.8	15.8±7.3	16.0±6.4	22.0±8.0	$0.08^{+0.24}_{-0.24}$	$-0.38^{+0.34}_{-0.51}$	$0.10^{+0.23}_{-0.27}$	37.1
15	18.7±7.3	5.9±4.3	6.5±4.6	12.4±5.8	6.3±5.1	11.1±5.2	5.7±5.2	$-0.45^{+0.18}_{-0.55}$	$0.03^{+0.42}_{-0.37}$	$0.08^{+0.47}_{-0.50}$	36.8
16	76.8±11.0	22.9±6.4	34.2±7.4	57.1±9.3	19.7±6.6	52.1±8.7	19.8±6.8	$-0.51^{+0.12}_{-0.13}$	$-0.06^{+0.11}_{-0.15}$	$0.25^{+0.17}_{-0.13}$	37.4
17	66.9±10.4	13.8±5.3	33.4±7.2	47.2±8.5	19.7±6.6	40.8±7.8	23.7±7.1	$-0.34^{+0.14}_{-0.13}$	$-0.27^{+0.16}_{-0.16}$	$0.23^{+0.20}_{-0.10}$	37.3
18	195.7±16.4	14.3±6.0	121.9±12.5	136.2±13.5	59.5±9.9	111.3±12.1	80.9±11.2	$-0.23^{+0.07}_{-0.08}$	$-0.81^{+0.13}_{-0.19}$	$0.35^{+0.07}_{-0.09}$	37.8
19	≤5.5	-	-	-	-	-	-	-	-	-	≤36.2
20	19.8±7.6	7.2±4.6	9.8±5.0	17.0±6.3	2.8±5.0	13.3±5.4	2.1±5.1	$-0.78^{+0.15}_{-0.22}$	$-0.03^{+0.29}_{-0.31}$	$0.42^{+0.75}_{-0.45}$	36.8
21	127.2±14.0	0.1±4.3	51.8±8.9	51.9±9.5	75.3±10.8	35.7±7.8	94.6±11.9	$0.39^{+0.10}_{-0.10}$	$-1.32^{+0.51}_{-0.79}$	$-0.13^{+0.09}_{-0.08}$	37.6
22	≤23.4	-	-	-	-	-	-	-	-	-	≤36.9
23	44.9±10.1	4.6±4.7	9.7±5.3	14.3±6.6	30.6±8.1	11.5±5.7	31.7±8.3	$0.42^{+0.20}_{-0.19}$	$-0.18^{+0.44}_{-0.54}$	$-0.42^{+0.19}_{-0.28}$	37.2
24	21.0±7.7	2.7±4.0	7.9±4.7	10.6±5.7	10.4±5.8	8.7±5.0	12.2±6.1	$0.09^{+0.34}_{-0.32}$	$-0.23^{+0.45}_{-0.70}$	$-0.07^{+0.31}_{-0.35}$	36.8
25	195.3±18.3	62.1±9.2	118.3±12.2	180.3±14.8	14.5±6.1	163.5±14.1	17.9±6.5	$-0.83^{+0.05}_{-0.06}$	$-0.16^{+0.06}_{-0.08}$	$0.91^{+0.20}_{-0.13}$	37.8
26	18.5±7.4	5.4±4.1	10.3±5.1	15.7±6.1	2.8±4.8	16.2±5.8	1.6±4.8	$-0.88^{+0.14}_{-0.12}$	$-0.16^{+0.32}_{-0.35}$	$0.43^{+0.72}_{-0.43}$	36.8
27	525.7±24.5	195.3±15.2	250.2±17.1	445.5±22.4	80.2±10.7	381.7±20.8	100.2±11.8	$-0.63^{+0.03}_{-0.04}$	$0.00^{+0.03}_{-0.05}$	$0.52^{+0.07}_{-0.05}$	38.2
28	109.9±14.6	12.8±5.3	68.1±9.6	80.9±10.6	29.0±7.4	75.1±10.1	33.4±7.8	$-0.45^{+0.10}_{-0.09}$	$-0.63^{+0.16}_{-0.15}$	$0.38^{+0.14}_{-0.08}$	37.5
29	78.9±11.0	20.9±6.1	45.2±8.1	66.1±9.7	12.7±6.0	58.2±9.0	15.6±6.4	$-0.63^{+0.11}_{-0.11}$	$-0.22^{+0.13}_{-0.12}$	$0.59^{+0.19}_{-0.19}$	37.4
30	171.9±15.0	46.3±8.2	107.5±11.7	153.8±13.8	18.1±6.5	129.6±12.7	35.6±8.0	$-0.62^{+0.07}_{-0.06}$	$-0.26^{+0.07}_{-0.09}$	$0.79^{+0.16}_{-0.12}$	37.7
31	18.7±7.8	2.4±4.0	7.2±4.8	9.6±5.8	9.1±5.8	6.1±4.8	11.3±6.2	$0.26^{+0.40}_{-0.40}$	$-0.28^{+0.58}_{-0.72}$	$-0.02^{+0.39}_{-0.43}$	36.8
32	32.6±8.8	14.9±5.7	22.8±6.5	37.7±8.2	-5.0±4.0	38.1±7.9	-3.4±4.4	$-0.99^{+0.03}_{-0.01}$	$-0.05^{+0.14}_{-0.21}$	$1.31^{+1.00}_{-0.48}$	37.0
33	24.7±7.9	7.1±4.4	11.7±5.3	18.7±6.5	5.9±5.2	13.1±5.6	8.6±5.7	$-0.33^{+0.34}_{-0.31}$	$-0.08^{+0.24}_{-0.32}$	$0.33^{+0.45}_{-0.41}$	36.9

Table 5—Continued

MID				Net Counts				HR	C21	C32	Log L_X
	B-band	S1-band	S2-band	S-band	H-band	Sc-band	Hc-band				(0.3−8.0 keV)
(1)	(2)	(3)	(4)	(5)	(6)	(7)	(8)	(9)	(10)	(11)	(12)
34	8.9±7.2	3.0±4.3	6.1±4.7	9.1±5.9	-0.2±4.7	8.6±5.3	0.5±5.0	$-0.72^{+0.23}_{-0.28}$	$-0.11^{+0.57}_{-0.75}$	$0.43^{+0.99}_{-0.62}$	36.4
35	31.1±8.4	13.5±5.3	13.7±5.4	27.2±7.1	3.9±5.1	25.1±6.6	5.5±5.4	$-0.74^{+0.11}_{-0.26}$	$0.07^{+0.22}_{-0.18}$	$0.49^{+0.65}_{-0.37}$	37.0
36	22.5±8.2	14.5±5.8	7.6±4.8	22.1±7.1	0.4±4.7	16.9±6.3	0.2±4.8	$-0.92^{+0.12}_{-0.08}$	$0.35^{+0.32}_{-0.24}$	$0.48^{+0.91}_{-0.53}$	36.8
37	66.2±10.5	18.0±6.0	33.7±7.4	51.7±9.1	14.5±6.1	41.5±8.1	23.5±7.0	$-0.35^{+0.14}_{-0.13}$	$-0.14^{+0.11}_{-0.18}$	$0.38^{+0.20}_{-0.16}$	37.3
38	11.8±7.1	-0.2±3.4	14.4±5.6	14.1±6.1	-2.4±4.3	9.5±5.1	0.9±5.0	$-0.74^{+0.19}_{-0.26}$	$-0.84^{+0.46}_{-0.92}$	$0.99^{+0.84}_{-0.53}$	36.6
39	26.6±8.1	14.6±5.6	9.3±5.0	23.9±7.0	2.6±4.8	19.7±6.3	3.4±5.1	$-0.78^{+0.12}_{-0.22}$	$0.27^{+0.24}_{-0.22}$	$0.40^{+0.75}_{-0.45}$	36.9
40	28.3±8.5	4.4±4.6	17.3±6.0	21.7±7.1	6.5±5.3	20.6±6.5	7.2±5.6	$-0.59^{+0.24}_{-0.29}$	$-0.46^{+0.39}_{-0.46}$	$0.45^{+0.43}_{-0.34}$	36.9
41	718.7±28.4	261.3±17.4	362.0±20.3	623.3±26.3	95.3±11.4	525.1±24.2	131.0±13.1	$-0.65^{+0.03}_{-0.03}$	$-0.04^{+0.03}_{-0.04}$	$0.62^{+0.04}_{-0.06}$	38.3
42	1741.8±43.0	350.2±19.9	1051.5±33.5	1401.7±38.6	340.1±19.8	1207.0±35.8	482.3±23.3	$-0.49^{+0.02}_{-0.02}$	$-0.39^{+0.04}_{-0.01}$	$0.53^{+0.02}_{-0.04}$	38.7
43	14.9±7.7	1.1±4.0	6.5±4.8	7.6±5.8	7.2±5.6	6.2±5.1	8.9±5.9	$0.09^{+0.50}_{-0.50}$	$-0.33^{+0.61}_{-0.91}$	$-0.02^{+0.52}_{-0.51}$	36.7
44	37.0±8.9	14.9±5.7	15.6±5.8	30.4±7.6	6.5±5.3	21.1±6.5	9.4±5.8	$-0.48^{+0.25}_{-0.24}$	$0.06^{+0.22}_{-0.16}$	$0.43^{+0.37}_{-0.42}$	37.1
45	41.8±9.4	7.6±5.0	24.6±6.7	32.2±7.9	9.7±5.8	32.5±7.5	9.3±5.9	$-0.63^{+0.18}_{-0.20}$	$-0.43^{+0.30}_{-0.24}$	$0.45^{+0.28}_{-0.26}$	37.1
46	20.4±9.8	10.5±5.3	9.2±5.2	19.7±7.0	1.0±4.8	15.6±6.2	0.3±5.0	$-0.86^{+0.13}_{-0.14}$	$0.20^{+0.24}_{-0.33}$	$0.77^{+0.59}_{-0.79}$	36.8
47	278.0±22.0	79.3±10.3	142.4±13.3	221.7±16.4	55.9±9.3	186.9±15.1	76.5±10.5	$-0.48^{+0.06}_{-0.06}$	$-0.17^{+0.08}_{-0.04}$	$0.43^{+0.08}_{-0.07}$	37.9
48	31.0±9.9	2.5±4.3	25.1±6.8	27.6±7.6	3.9±5.0	28.4±7.3	5.2±5.3	$-0.78^{+0.10}_{-0.22}$	$-0.72^{+0.38}_{-0.69}$	$0.72^{+0.63}_{-0.36}$	37.0
49	12.8±8.4	6.5±4.7	1.4±4.1	7.9±5.8	6.2±5.3	6.7±5.1	4.6±5.3	$-0.32^{+0.30}_{-0.68}$	$0.43^{+0.92}_{-0.54}$	$-0.32^{+0.65}_{-0.98}$	36.6
50	49.5±9.5	8.6±4.8	28.3±6.9	37.0±8.0	12.5±5.8	22.8±6.5	23.6±6.9	$-0.06^{+0.16}_{-0.19}$	$-0.37^{+0.18}_{-0.26}$	$0.36^{+0.22}_{-0.16}$	37.2
51	23.7±8.5	12.9±5.7	10.9±5.8	23.7±7.6	-0.1±4.4	19.4±6.8	1.7±5.0	$-0.85^{+0.12}_{-0.15}$	$0.10^{+0.34}_{-0.21}$	$0.70^{+0.92}_{-0.52}$	36.9
52	52.1±11.6	12.3±5.4	32.4±7.3	44.7±8.7	8.3±5.6	36.2±7.8	12.3±6.1	$-0.57^{+0.17}_{-0.16}$	$-0.34^{+0.22}_{-0.14}$	$0.59^{+0.34}_{-0.25}$	37.2
53	152.9±14.7	53.9±9.0	77.6±10.5	131.5±13.4	21.4±6.8	114.8±12.4	30.0±7.7	$-0.63^{+0.07}_{-0.08}$	$-0.05^{+0.08}_{-0.09}$	$0.57^{+0.16}_{-0.11}$	37.7
54	41.7±9.8	22.2±6.7	15.6±6.3	37.9±8.7	3.8±5.1	32.1±7.9	4.7±5.5	$-0.81^{+0.08}_{-0.19}$	$0.23^{+0.22}_{-0.16}$	$0.46^{+0.67}_{-0.35}$	37.1
55	240.0±17.2	80.1±10.2	144.7±13.3	224.8±16.4	15.2±6.2	186.8±15.0	34.9±7.9	$-0.72^{+0.05}_{-0.05}$	$-0.17^{+0.08}_{-0.04}$	$0.97^{+0.18}_{-0.12}$	37.9
56	31.0±9.0	3.8±4.6	25.9±7.1	29.7±8.0	1.3±4.7	27.4±7.4	3.3±5.2	$-0.84^{+0.10}_{-0.16}$	$-0.62^{+0.33}_{-0.59}$	$0.91^{+0.81}_{-0.40}$	37.0
57	≤31.5	-	-	-	-	-	-	-	-	-	≤37.0
58	64.7±12.2	20.2±6.3	34.2±7.4	54.4±9.2	10.5±5.7	52.4±8.8	11.3±5.9	$-0.70^{+0.13}_{-0.12}$	$-0.16^{+0.18}_{-0.10}$	$0.50^{+0.27}_{-0.18}$	37.3
59	72.2±11.6	16.3±6.3	43.1±8.5	59.4±10.2	12.9±6.2	49.9±9.3	17.0±6.7	$-0.56^{+0.15}_{-0.13}$	$-0.33^{+0.18}_{-0.15}$	$0.60^{+0.16}_{-0.25}$	37.3
60	159.9±15.2	41.0±8.3	90.2±11.2	131.3±13.5	28.7±7.6	105.2±12.1	48.9±9.1	$-0.43^{+0.08}_{-0.08}$	$-0.24^{+0.09}_{-0.09}$	$0.53^{+0.12}_{-0.10}$	37.7
61	11.3±7.3	2.5±4.3	4.3±4.6	6.8±5.8	4.5±5.1	3.3±4.8	5.3±5.3	$0.16^{+0.48}_{-0.32}$	$-0.05^{+0.74}_{-0.86}$	$-0.04^{+0.84}_{-0.65}$	36.5
62	169.8±18.9	30.3±7.4	104.4±11.7	134.8±13.4	35.3±8.1	117.1±12.4	45.0±8.9	$-0.50^{+0.07}_{-0.08}$	$-0.44^{+0.10}_{-0.10}$	$0.50^{+0.11}_{-0.09}$	37.7
63	27.7±8.6	4.6±4.4	17.7±6.0	22.2±7.0	5.5±5.7	17.3±6.1	10.0±6.3	$-0.38^{+0.33}_{-0.27}$	$-0.40^{+0.30}_{-0.49}$	$0.46^{+0.56}_{-0.32}$	36.9
64	201.2±16.1	47.4±8.4	104.6±11.6	152.0±13.9	49.2±8.7	128.5±12.8	64.8±9.8	$-0.40^{+0.07}_{-0.07}$	$-0.23^{+0.07}_{-0.09}$	$0.36^{+0.09}_{-0.08}$	37.8
65	16.3±10.2	6.8±5.1	6.5±5.1	13.3±6.7	2.1±5.1	11.4±6.0	3.0±5.5	$-0.67^{+0.21}_{-0.33}$	$-0.04^{+0.74}_{-0.31}$	$0.36^{+0.93}_{-0.70}$	36.7
66	164.5±15.3	30.4±7.5	96.1±11.5	126.5±13.3	38.0±8.1	111.4±12.4	51.2±9.1	$-0.43^{+0.08}_{-0.08}$	$-0.40^{+0.11}_{-0.10}$	$0.44^{+0.09}_{-0.10}$	37.7

Table 5—Continued

MID				Net Counts				HR	C21	C32	Log L_X
	B-band	S1-band	S2-band	S-band	H-band	Sc-band	Hc-band				(0.3−8.0 keV)
(1)	(2)	(3)	(4)	(5)	(6)	(7)	(8)	(9)	(10)	(11)	(12)
67	1008.9±33.4	200.1±15.6	582.3±25.4	782.4±29.4	226.5±16.4	670.1±27.3	311.6±19.0	$-0.43^{+0.03}_{-0.03}$	$-0.37^{+0.04}_{-0.03}$	$0.44^{+0.04}_{-0.03}$	38.5
68	71.8±10.2	16.3±5.6	39.8±7.7	56.1±9.0	15.7±5.4	55.0±8.9	17.1±5.7	$-0.58^{+0.10}_{-0.10}$	$-0.27^{+0.12}_{-0.16}$	$0.43^{+0.15}_{-0.14}$	37.3
69	21.4±8.4	2.4±4.6	7.1±5.2	9.5±6.5	11.9±5.9	9.5±6.0	14.2±6.3	$0.14^{+0.34}_{-0.38}$	$-0.19^{+0.63}_{-0.84}$	$-0.16^{+0.33}_{-0.42}$	36.8
70	7222.3±86.3	1819.2±43.8	4124.5±65.4	5943.7±78.3	1278.6±36.9	5131.2±72.8	1777.0±43.3	$-0.54^{+0.01}_{-0.01}$	$-0.26^{+0.02}_{-0.01}$	$0.54^{+0.01}_{-0.01}$	39.3
71	91.5±11.6	34.8±7.5	46.2±8.4	81.0±10.8	10.4±5.0	71.9±10.2	10.0±5.1	$-0.79^{+0.07}_{-0.09}$	$-0.03^{+0.11}_{-0.10}$	$0.65^{+0.20}_{-0.16}$	37.4
72	111.0±13.4	39.5±8.3	53.1±9.2	92.6±11.9	18.4±6.7	68.9±10.4	29.8±7.9	$-0.46^{+0.10}_{-0.11}$	$-0.05^{+0.13}_{-0.08}$	$0.45^{+0.19}_{-0.12}$	37.5
73	≤18.1	-	-	-	-	-	-	-	-	-	≤36.7
74	1165.4±35.9	356.5±20.4	653.1±27.0	1009.6±33.4	155.8±13.9	874.5±31.1	228.7±16.6	$-0.63^{+0.02}_{-0.03}$	$-0.17^{+0.04}_{-0.02}$	$0.66^{+0.03}_{-0.05}$	38.6
75	373.6±22.1	159.9±14.6	187.2±15.6	347.2±20.9	26.5±7.4	317.2±19.8	36.2±8.3	$-0.82^{+0.03}_{-0.04}$	$0.03^{+0.05}_{-0.05}$	$0.86^{+0.13}_{-0.09}$	38.1
76	≤12.5	-	-	-	-	-	-	-	-	-	≤36.6
77	414.4±22.5	109.3±12.3	224.3±16.5	333.6±20.1	80.7±10.4	295.9±18.9	101.8±11.6	$-0.54^{+0.03}_{-0.05}$	$-0.21^{+0.05}_{-0.05}$	$0.49^{+0.05}_{-0.07}$	38.1
78	174.9±14.8	45.5±8.2	92.5±10.9	138.0±13.2	36.9±7.5	118.3±12.3	49.3±8.4	$-0.47^{+0.06}_{-0.07}$	$-0.20^{+0.08}_{-0.08}$	$0.43^{+0.10}_{-0.08}$	37.7
79	5.1±6.5	-0.2±3.4	5.0±4.6	4.9±5.2	0.2±4.4	7.6±5.1	0.1±4.6	$-0.79^{+0.22}_{-0.21}$	$-0.38^{+0.61}_{-1.07}$	$0.35^{+1.02}_{-0.67}$	36.2
80	77.9±10.8	15.1±5.6	51.0±8.7	66.1±9.9	11.8±5.1	56.9±9.2	18.1±5.9	$-0.57^{+0.10}_{-0.11}$	$-0.41^{+0.13}_{-0.17}$	$0.66^{+0.17}_{-0.15}$	37.4
81	858.2±30.9	293.5±18.5	459.7±22.7	753.2±28.9	105.0±11.7	666.0±27.2	139.6±13.3	$-0.70^{+0.03}_{-0.02}$	$-0.10^{+0.04}_{-0.03}$	$0.67^{+0.05}_{-0.05}$	38.4
82	661.8±27.4	157.1±14.0	361.5±20.3	518.6±24.3	143.2±13.3	450.5±22.7	188.1±15.0	$-0.47^{+0.03}_{-0.04}$	$-0.26^{+0.04}_{-0.04}$	$0.43^{+0.05}_{-0.04}$	38.3
83	177.3±15.2	51.4±8.7	102.3±11.6	153.7±14.0	23.6±6.5	130.1±13.0	39.7±7.8	$-0.58^{+0.06}_{-0.07}$	$-0.19^{+0.07}_{-0.08}$	$0.67^{+0.11}_{-0.11}$	37.7
84	55.0±9.0	13.5±5.1	35.8±7.2	49.3±8.4	5.7±4.1	42.8±7.8	8.2±4.6	$-0.72^{+0.10}_{-0.12}$	$-0.36^{+0.20}_{-0.10}$	$0.79^{+0.30}_{-0.22}$	37.2
85	27.7±6.6	7.0±4.0	15.0±5.1	22.0±6.0	5.7±3.8	18.6±5.6	6.5±4.0	$-0.54^{+0.16}_{-0.19}$	$-0.21^{+0.18}_{-0.22}$	$0.43^{+0.24}_{-0.22}$	36.9
86	2114.3±47.7	466.8±23.2	1199.0±35.9	1665.7±42.3	448.6±22.6	1413.5±39.0	631.8±26.5	$-0.45^{+0.02}_{-0.01}$	$-0.31^{+0.02}_{-0.02}$	$0.46^{+0.02}_{-0.02}$	38.8
87	213.6±17.0	60.3±9.7	120.1±12.5	180.5±15.4	33.1±7.6	161.1±14.5	46.6±8.6	$-0.60^{+0.06}_{-0.06}$	$-0.20^{+0.08}_{-0.07}$	$0.59^{+0.10}_{-0.09}$	37.8
88	115.8±13.1	29.9±7.2	79.7±10.5	109.6±12.3	6.2±5.3	97.4±11.5	16.1±6.5	$-0.76^{+0.08}_{-0.08}$	$-0.32^{+0.10}_{-0.10}$	$1.13^{+0.43}_{-0.30}$	37.5
89	101.8±14.7	18.8±6.6	53.8±9.1	72.6±10.8	28.8±7.6	58.4±9.7	34.7±8.2	$-0.33^{+0.12}_{-0.11}$	$-0.36^{+0.15}_{-0.15}$	$0.26^{+0.16}_{-0.08}$	37.5
90	377.8±21.0	77.8±10.2	217.5±16.0	295.3±18.5	82.5±10.7	252.1±17.1	108.2±12.0	$-0.46^{+0.04}_{-0.05}$	$-0.32^{+0.03}_{-0.08}$	$0.46^{+0.06}_{-0.06}$	38.1
91	5.1±6.9	4.2±4.6	4.2±4.6	8.4±6.0	-3.3±4.1	8.6±5.4	-3.2±4.4	$-0.90^{+0.15}_{-0.10}$	$0.11^{+0.69}_{-0.73}$	$0.53^{+1.07}_{-0.76}$	36.2
92	25.6±8.2	8.1±4.8	12.6±5.3	20.7±6.7	5.0±5.3	14.7±5.8	7.0±5.7	$-0.50^{+0.31}_{-0.34}$	$-0.03^{+0.21}_{-0.33}$	$0.49^{+0.44}_{-0.54}$	36.9
93	138.4±14.3	34.2±7.8	73.3±10.2	107.5±12.4	30.9±7.7	94.1±11.5	38.0±8.3	$-0.49^{+0.09}_{-0.08}$	$-0.23^{+0.11}_{-0.10}$	$0.38^{+0.14}_{-0.08}$	37.6
94	83.6±11.8	37.9±7.8	44.1±8.3	82.0±11.0	1.6±5.0	72.2±10.2	2.7±5.3	$-0.95^{+0.04}_{-0.05}$	$0.02^{+0.12}_{-0.09}$	$1.08^{+0.83}_{-0.36}$	37.4
95	81.6±11.7	18.0±6.2	52.2±8.9	70.1±10.4	11.4±6.0	58.8±9.5	15.7±6.6	$-0.64^{+0.13}_{-0.11}$	$-0.37^{+0.15}_{-0.14}$	$0.66^{+0.24}_{-0.20}$	37.4
96	53.2±10.2	24.4±6.7	24.3±6.7	48.7±9.1	4.5±5.3	37.7±8.0	7.7±5.9	$-0.74^{+0.16}_{-0.18}$	$0.09^{+0.15}_{-0.14}$	$0.77^{+0.47}_{-0.43}$	37.2
97	20.3±7.9	2.7±4.1	14.8±5.8	17.5±6.6	2.8±5.0	15.8±6.1	4.0±5.3	$-0.68^{+0.14}_{-0.32}$	$-0.42^{+0.32}_{-0.73}$	$0.67^{+0.66}_{-0.50}$	36.8
98	107.0±12.3	28.2±6.7	54.8±8.8	83.0±10.6	24.1±6.9	64.5±9.4	35.6±7.9	$-0.36^{+0.10}_{-0.11}$	$-0.17^{+0.09}_{-0.12}$	$0.37^{+0.14}_{-0.10}$	37.5
99	185.1±15.5	42.0±8.0	117.4±12.2	159.5±14.1	25.7±7.1	137.7±13.1	39.2±8.3	$-0.61^{+0.06}_{-0.07}$	$-0.34^{+0.08}_{-0.08}$	$0.69^{+0.11}_{-0.12}$	37.8

Table 5—Continued

MID				Net Counts				HR	C21	C32	Log L_X
	B-band	S1-band	S2-band	S-band	H-band	Sc-band	Hc-band				(0.3−8.0 keV)
(1)	(2)	(3)	(4)	(5)	(6)	(7)	(8)	(9)	(10)	(11)	(12)
100	75.6±11.3	81.1±10.4	-1.0±3.8	80.0±10.8	-4.5±4.0	50.2±8.8	-6.6±4.0	$-1.00^{+0.01}_{-0.00}$	$1.85^{+0.82}_{-0.54}$	$0.20^{+1.08}_{-1.18}$	37.4
101	61.3±10.4	0.3±3.8	19.3±6.3	19.6±6.9	41.6±8.3	9.2±5.4	54.2±9.2	$0.69^{+0.15}_{-0.14}$	$-0.98^{+0.61}_{-0.70}$	$-0.33^{+0.16}_{-0.12}$	37.3
102	1389.0±38.7	556.7±24.7	655.5±26.8	1212.2±36.0	176.8±14.8	1001.0±32.8	246.8±17.2	$-0.65^{+0.02}_{-0.02}$	$0.03^{+0.02}_{-0.03}$	$0.60^{+0.04}_{-0.04}$	38.6
103	636.9±26.6	149.2±13.4	362.9±20.2	512.1±23.8	124.8±12.5	444.6±22.2	166.9±14.3	$-0.51^{+0.03}_{-0.04}$	$-0.30^{+0.06}_{-0.02}$	$0.49^{+0.05}_{-0.04}$	38.3
104	29.3±8.3	2.4±4.0	14.4±5.6	16.8±6.4	12.5±6.0	12.2±5.4	15.9±6.5	$0.05^{+0.25}_{-0.26}$	$-0.54^{+0.42}_{-0.66}$	$0.11^{+0.22}_{-0.24}$	37.0
105	40.4±10.2	7.3±4.8	27.8±7.0	35.1±8.1	5.7±5.3	32.7±7.5	9.3±5.9	$-0.64^{+0.19}_{-0.19}$	$-0.45^{+0.25}_{-0.29}$	$0.78^{+0.36}_{-0.42}$	37.1
106	261.1±19.0	85.8±10.6	162.6±14.0	248.4±17.1	13.2±6.1	218.9±16.1	25.9±7.3	$-0.82^{+0.04}_{-0.04}$	$-0.18^{+0.07}_{-0.05}$	$1.09^{+0.21}_{-0.14}$	37.9
107	≤5.5	-	-	-	-	-	-	-	-	-	≤36.2
108	28.9±8.6	2.7±4.1	17.7±6.1	20.4±6.9	8.5±5.7	19.8±6.5	9.7±6.0	$-0.44^{+0.27}_{-0.26}$	$-0.60^{+0.40}_{-0.63}$	$0.40^{+0.28}_{-0.36}$	36.9
109	46.5±9.4	0.1±3.4	20.4±6.2	20.6±6.6	25.9±7.1	15.0±5.8	32.5±7.8	$0.31^{+0.16}_{-0.19}$	$-1.16^{+0.70}_{-0.63}$	$-0.08^{+0.16}_{-0.15}$	37.2
110	113.9±13.0	16.4±6.0	58.8±9.2	75.3±10.5	38.6±8.3	61.1±9.4	47.3±9.1	$-0.20^{+0.10}_{-0.11}$	$-0.45^{+0.15}_{-0.14}$	$0.22^{+0.09}_{-0.11}$	37.5
111	39.8±9.1	6.6±4.7	18.2±6.0	24.9±7.1	14.9±6.3	19.6±6.3	18.5±6.7	$-0.11^{+0.19}_{-0.22}$	$-0.32^{+0.28}_{-0.31}$	$0.09^{+0.21}_{-0.18}$	37.1
112	44.2±9.2	12.4±5.2	26.3±6.6	38.7±8.0	5.5±5.2	37.0±7.6	4.2±5.2	$-0.85^{+0.07}_{-0.15}$	$-0.28^{+0.25}_{-0.10}$	$0.65^{+0.48}_{-0.32}$	37.1
113	32.0±8.5	12.7±5.3	14.1±5.6	26.9±7.2	5.1±5.2	21.8±6.5	7.6±5.7	$-0.59^{+0.22}_{-0.28}$	$-0.01^{+0.26}_{-0.15}$	$0.39^{+0.55}_{-0.35}$	37.0
114	41.4±9.1	16.5±5.8	24.1±6.5	40.6±8.3	0.8±4.6	33.6±7.5	2.4±5.0	$-0.90^{+0.07}_{-0.10}$	$-0.09^{+0.19}_{-0.13}$	$1.02^{+0.78}_{-0.49}$	37.1
115	17.2±7.6	5.7±4.6	7.7±4.8	13.4±6.2	3.8±5.0	13.9±5.8	4.4±5.2	$-0.63^{+0.16}_{-0.37}$	$-0.04^{+0.45}_{-0.41}$	$0.32^{+0.63}_{-0.58}$	36.7
116	140.2±14.0	52.7±8.7	86.7±10.7	139.4±13.4	0.8±4.8	126.1±12.6	7.4±5.9	$-0.92^{+0.03}_{-0.08}$	$-0.11^{+0.08}_{-0.08}$	$1.43^{+0.90}_{-0.35}$	37.6
117	12.0±6.9	8.3±4.7	6.4±4.4	14.7±6.0	-2.7±4.1	12.1±5.3	-2.8±4.3	$-0.94^{+0.09}_{-0.06}$	$0.19^{+0.35}_{-0.32}$	$0.69^{+0.91}_{-0.61}$	36.6
118	15.4±7.3	1.1±3.8	10.0±5.1	11.1±5.9	4.4±5.0	11.4±5.4	5.0±5.2	$-0.53^{+0.19}_{-0.47}$	$-0.53^{+0.52}_{-0.78}$	$0.38^{+0.57}_{-0.47}$	36.7
119	136.9±13.6	42.4±7.8	72.0±9.9	114.4±12.2	22.5±6.9	93.2±11.0	34.2±7.9	$-0.52^{+0.08}_{-0.09}$	$-0.10^{+0.07}_{-0.11}$	$0.53^{+0.12}_{-0.13}$	37.6
120	643.2±26.8	373.2±20.5	257.9±17.3	631.0±26.4	12.2±5.8	570.1±25.0	11.1±5.9	$-0.97^{+0.02}_{-0.01}$	$0.26^{+0.04}_{-0.03}$	$1.31^{+0.22}_{-0.14}$	38.3
121	258.4±17.8	80.3±10.3	120.4±12.3	200.7±15.6	57.7±9.3	165.6±14.1	75.2±10.4	$-0.44^{+0.06}_{-0.06}$	$-0.05^{+0.04}_{-0.09}$	$0.36^{+0.07}_{-0.08}$	37.9
122	34.9±8.7	5.2±4.4	22.0±6.4	27.2±7.3	7.7±5.3	21.8±6.5	12.1±6.0	$-0.38^{+0.23}_{-0.21}$	$-0.44^{+0.25}_{-0.43}$	$0.37^{+0.43}_{-0.20}$	37.0
123	21.1±7.6	1.2±3.6	16.3±5.8	17.5±6.4	3.5±4.8	12.3±5.4	8.3±5.6	$-0.33^{+0.34}_{-0.35}$	$-0.69^{+0.38}_{-0.76}$	$0.56^{+0.65}_{-0.37}$	36.8
124	18.0±7.5	3.2±4.1	7.0±4.6	10.1±5.7	7.9±5.6	6.6±4.7	12.7±6.2	$0.27^{+0.35}_{-0.35}$	$-0.16^{+0.49}_{-0.66}$	$-0.06^{+0.45}_{-0.40}$	36.8
125	153.6±14.6	28.9±7.0	82.9±10.6	111.8±12.3	41.8±8.5	88.7±10.9	59.2±9.7	$-0.27^{+0.08}_{-0.09}$	$-0.35^{+0.10}_{-0.10}$	$0.33^{+0.09}_{-0.09}$	37.7
126	23.3±7.7	2.8±3.8	7.4±4.7	10.2±5.6	13.1±5.9	5.6±4.4	15.5±6.3	$0.45^{+0.29}_{-0.31}$	$-0.21^{+0.45}_{-0.70}$	$-0.20^{+0.29}_{-0.32}$	36.9
127	35.5±9.1	13.0±5.4	16.2±5.9	29.2±7.5	6.3±5.7	25.0±6.8	7.4±6.0	$-0.65^{+0.11}_{-0.35}$	$-0.03^{+0.23}_{-0.16}$	$0.48^{+0.44}_{-0.40}$	37.0
128	567.7±25.5	120.3±12.3	272.8±17.8	393.1±21.2	174.6±14.8	325.5±19.3	214.6±16.3	$-0.28^{+0.04}_{-0.04}$	$-0.27^{+0.07}_{-0.03}$	$0.23^{+0.04}_{-0.05}$	38.3
129	48.0±9.3	5.0±4.1	32.2±7.2	37.2±7.9	10.8±5.7	30.9±7.1	17.7±6.5	$-0.35^{+0.15}_{-0.17}$	$-0.65^{+0.25}_{-0.36}$	$0.50^{+0.22}_{-0.22}$	37.2
130	146.7±14.0	44.4±8.1	81.5±10.4	125.9±12.7	20.8±6.7	106.7±11.7	29.4±7.5	$-0.62^{+0.07}_{-0.08}$	$-0.15^{+0.08}_{-0.09}$	$0.63^{+0.14}_{-0.12}$	37.7
131	114.4±13.3	35.7±7.6	52.3±8.9	88.0±11.2	26.4±7.8	75.6±10.3	33.8±8.5	$-0.45^{+0.10}_{-0.10}$	$-0.06^{+0.10}_{-0.10}$	$0.32^{+0.15}_{-0.11}$	37.6
132	152.9±14.8	35.2±7.6	91.1±11.0	126.3±13.0	26.6±7.8	112.7±12.1	34.7±8.5	$-0.58^{+0.08}_{-0.08}$	$-0.30^{+0.09}_{-0.10}$	$0.55^{+0.14}_{-0.11}$	37.7

Table 5—Continued

MID	Net Counts							HR	C21	C32	Log L_X
	B-band	S1-band	S2-band	S-band	H-band	Sc-band	Hc-band				(0.3−8.0 keV)
(1)	(2)	(3)	(4)	(5)	(6)	(7)	(8)	(9)	(10)	(11)	(12)

Note. — Col. (1): Master ID, cols. (2)−(8): net counts, in each of the 7 energy bands (see Table 3 for definitions of these bands), col. (9): hardness ratio, cols. (10) and (11) color values, col. (12): log L_X (0.3−8.0 keV). Upper limit L_X values are at the 68% confidence level.

Table 6. Source counts, hardness ratios, color-color values and variability: Observation 1

MID	Net Counts							HR	C21	C32	Variability			Log L_X
	B-band	S1-band	S2-band	S-band	H-band	Sc-band	Hc-band				BB	k-S	signif.	(erg s^{-1})
(1)	(2)	(3)	(4)	(5)	(6)	(7)	(8)	(9)	(10)	(11)	(12)	(13)	(14)	(15)
1	8.3±4.3	2.6±2.9	4.7±3.4	7.3±4.0	0.9±2.7	6.6±3.8	1.9±2.9	$-0.66^{+0.17}_{-0.23}$	$-0.13^{+0.32}_{-0.41}$	$0.53^{+0.69}_{-0.53}$	-	-	-	37.5
2	≤1.3	-	-	-	-	-	-	-	-	-	-	-	-	≤36.7
3	≤3.0	-	-	-	-	-	-	-	-	-	-	-	-	≤37.0
4	≤2.7	-	-	-	-	-	-	-	-	-	-	-	-	≤37.0
5	≤0.5	-	-	-	-	-	-	-	-	-	-	-	-	≤36.2
6	≤2.1	-	-	-	-	-	-	-	-	-	-	-	-	≤36.9
7	14.9±5.1	4.7±3.4	8.6±4.1	13.3±4.8	1.6±2.7	12.4±4.7	2.6±2.9	$-0.68^{+0.16}_{-0.22}$	$-0.21^{+0.24}_{-0.27}$	$0.64^{+0.46}_{-0.37}$	-	-	-	37.7
8	≤3.3	-	-	-	-	-	-	-	-	-	-	-	-	≤37.0
9	92.3±10.8	41.9±7.6	35.4±7.1	77.3±9.9	15.0±5.2	62.0±9.0	17.0±5.4	$-0.58^{+0.08}_{-0.10}$	$0.10^{+0.09}_{-0.11}$	$0.39^{+0.13}_{-0.15}$	N	N	-	38.5
10	≤5.4	-	-	-	-	-	-	-	-	-	-	-	-	≤37.2
11	18.4±5.6	6.6±3.8	9.4±4.3	16.0±5.2	2.4±2.9	16.3±5.2	2.2±2.9	$-0.79^{+0.09}_{-0.17}$	$-0.13^{+0.21}_{-0.22}$	$0.54^{+0.37}_{-0.33}$	-	-	-	37.8
12	≤2.2	-	-	-	-	-	-	-	-	-	-	-	-	≤36.8
13	3.6±3.4	-0.5±1.9	2.6±2.9	2.1±2.9	1.5±2.7	2.6±2.9	1.3±2.7	$-0.38^{+0.27}_{-0.41}$	$-0.76^{+0.68}_{-1.00}$	$0.16^{+0.59}_{-0.51}$	-	-	-	37.0
14	≤1.4	-	-	-	-	-	-	-	-	-	-	-	-	≤36.7
15	≤5.7	-	-	-	-	-	-	-	-	-	-	-	-	≤37.2
16	≤2.6	-	-	-	-	-	-	-	-	-	-	-	-	≤36.9
17	≤8.1	-	-	-	-	-	-	-	-	-	-	-	-	≤37.4
18	≤10.9	-	-	-	-	-	-	-	-	-	-	-	-	≤37.6
19	≤0.9	-	-	-	-	-	-	-	-	-	-	-	-	≤36.5
20	≤6.6	-	-	-	-	-	-	-	-	-	-	-	-	≤37.3
21	≤7.9	-	-	-	-	-	-	-	-	-	-	-	-	≤37.4
22	≤1.2	-	-	-	-	-	-	-	-	-	-	-	-	≤36.6
23	≤8.4	-	-	-	-	-	-	-	-	-	-	-	-	≤37.5
24	7.1±4.0	1.7±2.7	3.8±3.2	5.5±3.6	1.6±2.7	3.7±3.2	2.6±2.9	$-0.21^{+0.39}_{-0.42}$	$-0.29^{+0.40}_{-0.49}$	$0.32^{+0.54}_{-0.43}$	-	-	-	37.3
25	≤3.2	-	-	-	-	-	-	-	-	-	-	-	-	≤37.0
26	≤1.9	-	-	-	-	-	-	-	-	-	-	-	-	≤36.8
27	21.6±6.0	7.3±4.0	11.2±4.6	18.5±5.6	3.1±3.2	17.1±5.3	3.9±3.4	$-0.65^{+0.17}_{-0.19}$	$-0.19^{+0.22}_{-0.21}$	$0.51^{+0.35}_{-0.30}$	N	N	-	37.8
28	8.9±4.3	2.7±2.9	3.7±3.2	6.4±3.8	2.5±2.9	5.6±3.6	2.4±2.9	$-0.43^{+0.31}_{-0.35}$	$-0.13^{+0.34}_{-0.38}$	$0.16^{+0.43}_{-0.37}$	-	-	-	37.4
29	8.1±4.3	1.5±2.7	5.6±3.6	7.1±4.0	1.1±2.7	5.4±3.6	0.9±2.7	$-0.77^{+0.19}_{-0.23}$	$-0.48^{+0.40}_{-0.57}$	$0.54^{+0.69}_{-0.46}$	-	-	-	37.4
30	26.7±6.4	9.5±4.3	14.8±5.0	24.2±6.1	2.5±2.9	20.5±5.7	4.4±3.4	$-0.65^{+0.13}_{-0.17}$	$-0.19^{+0.16}_{-0.19}$	$0.70^{+0.37}_{-0.27}$	V	N	-	37.9
31	≤0.8	-	-	-	-	-	-	-	-	-	-	-	-	≤36.4
32	≤3.1	-	-	-	-	-	-	-	-	-	-	-	-	≤37.0
33	≤5.9	-	-	-	-	-	-	-	-	-	-	-	-	≤37.3

Table 6—Continued

MID	Net Counts							HR	C21	C32	Variability			Log L_X
	B-band	S1-band	S2-band	S-band	H-band	Sc-band	Hc-band				BB	k-S	signif.	(erg s^{-1})
(1)	(2)	(3)	(4)	(5)	(6)	(7)	(8)	(9)	(10)	(11)	(12)	(13)	(14)	(15)
34	≤1.9	-	-	-	-	-	-	-	-	-	-	-	-	≤36.8
35	≤7.9	-	-	-	-	-	-	-	-	-	-	-	-	≤37.4
36	≤1.3	-	-	-	-	-	-	-	-	-	-	-	-	≤36.6
37	≤7.7	-	-	-	-	-	-	-	-	-	-	-	-	≤37.4
38	≤1.3	-	-	-	-	-	-	-	-	-	-	-	-	≤36.6
39	≤2.6	-	-	-	-	-	-	-	-	-	-	-	-	≤36.9
40	≤1.2	-	-	-	-	-	-	-	-	-	-	-	-	≤36.6
41	77.5±10.0	33.2±6.9	33.3±6.9	66.5±9.3	11.0±4.6	52.9±8.4	16.0±5.2	$-0.54^{+0.09}_{-0.12}$	$0.02^{+0.08}_{-0.14}$	$0.49^{+0.14}_{-0.17}$	N	N	-	38.4
42	170.4±14.1	52.6±8.3	97.7±10.9	150.3±13.3	20.0±5.7	130.6±12.5	27.9±6.5	$-0.65^{+0.05}_{-0.07}$	$-0.28^{+0.08}_{-0.07}$	$0.69^{+0.11}_{-0.11}$	N	N	-	38.7
43	≤3.6	-	-	-	-	-	-	-	-	-	-	-	-	≤37.0
44	12.6±4.9	5.6±3.6	5.7±3.6	11.2±4.6	1.3±2.7	6.5±3.8	3.2±3.2	$-0.36^{+0.31}_{-0.33}$	$-0.03^{+0.27}_{-0.24}$	$0.51^{+0.59}_{-0.43}$	-	-	-	37.6
45	≤1.7	-	-	-	-	-	-	-	-	-	-	-	-	≤36.7
46	≤0.8	-	-	-	-	-	-	-	-	-	-	-	-	≤36.4
47	23.9±6.2	6.1±3.8	13.3±4.8	19.4±5.7	4.5±3.4	17.7±5.4	5.5±3.6	$-0.53^{+0.16}_{-0.20}$	$-0.32^{+0.21}_{-0.22}$	$0.46^{+0.24}_{-0.25}$	N	N	-	37.9
48	≤1.4	-	-	-	-	-	-	-	-	-	-	-	-	≤36.6
49	≤1.3	-	-	-	-	-	-	-	-	-	-	-	-	≤36.6
50	≤0.8	-	-	-	-	-	-	-	-	-	-	-	-	≤36.4
51	5.5±4.0	3.9±3.4	2.2±2.9	6.1±4.0	-0.6±1.9	3.6±3.4	0.4±2.3	$-0.77^{+0.22}_{-0.23}$	$0.19^{+0.53}_{-0.43}$	$0.69^{+1.14}_{-0.69}$	-	-	-	37.2
52	20.8±7.3	4.4±3.6	13.2±5.0	17.7±5.7	2.1±3.4	18.8±5.7	2.8±3.6	$-0.83^{+0.10}_{-0.07}$	$-0.32^{+0.24}_{-0.32}$	$0.70^{+0.64}_{-0.38}$	N	N	-	37.5
53	14.3±5.2	7.6±4.1	7.2±4.0	14.8±5.2	-0.5±1.9	10.3±4.6	0.4±2.3	$-0.93^{+0.08}_{-0.07}$	$0.00^{+0.24}_{-0.24}$	$1.22^{+0.92}_{-0.61}$	-	-	-	37.6
54	8.4±4.4	4.6±3.6	4.2±3.4	8.9±4.4	-0.5±1.9	7.2±4.1	-0.5±1.9	$-0.98^{+0.06}_{-0.02}$	$0.03^{+0.35}_{-0.35}$	$0.99^{+1.00}_{-0.61}$	-	-	-	37.4
55	13.2±5.0	7.7±4.0	6.4±3.8	14.1±5.0	-1.0±1.9	14.3±5.0	-1.0±1.9	$-0.99^{+0.03}_{-0.01}$	$0.05^{+0.24}_{-0.21}$	$1.15^{+0.99}_{-0.54}$	-	-	-	37.6
56	≤6.6	-	-	-	-	-	-	-	-	-	-	-	-	≤37.3
57	≤4.5	-	-	-	-	-	-	-	-	-	-	-	-	≤37.1
58	≤3.5	-	-	-	-	-	-	-	-	-	-	-	-	≤37.0
59	≤2.4	-	-	-	-	-	-	-	-	-	-	-	-	≤36.9
60	22.3±6.2	4.2±3.6	12.7±4.8	16.9±5.6	5.4±3.6	14.4±5.2	8.3±4.1	$-0.28^{+0.20}_{-0.22}$	$-0.46^{+0.27}_{-0.32}$	$0.35^{+0.24}_{-0.22}$	-	-	-	37.8
61	5.8±4.0	2.1±2.9	2.3±2.9	4.4±3.6	1.4±2.7	2.9±3.2	1.4±2.7	$-0.38^{+0.27}_{-0.42}$	$-0.03^{+0.57}_{-0.59}$	$0.16^{+0.67}_{-0.59}$	-	-	-	37.2
62	15.9±5.5	2.8±3.2	8.0±4.1	10.8±4.7	5.2±3.6	9.1±4.4	6.2±3.8	$-0.20^{+0.26}_{-0.28}$	$-0.40^{+0.32}_{-0.46}$	$0.19^{+0.24}_{-0.27}$	-	-	-	37.7
63	≤6.9	-	-	-	-	-	-	-	-	-	-	-	-	≤37.3
64	15.9±5.3	4.2±3.4	7.2±4.0	11.5±4.7	4.4±3.4	8.7±4.3	7.4±4.0	$-0.09^{+0.25}_{-0.26}$	$-0.21^{+0.26}_{-0.30}$	$0.21^{+0.27}_{-0.26}$	-	-	-	37.7
65	≤3.6	-	-	-	-	-	-	-	-	-	-	-	-	≤37.0
66	16.3±5.6	4.2±3.6	9.9±4.4	14.1±5.2	2.2±2.9	13.7±5.1	2.2±2.9	$-0.76^{+0.10}_{-0.20}$	$-0.35^{+0.30}_{-0.32}$	$0.59^{+0.46}_{-0.35}$	-	-	-	37.7

Table 6—Continued

MID				Net Counts				HR	C21	C32	Variability			Log L_X
	B-band	S1-band	S2-band	S-band	H-band	Sc-band	Hc-band				BB	k-S	signif.	(erg s^{-1})
(1)	(2)	(3)	(4)	(5)	(6)	(7)	(8)	(9)	(10)	(11)	(12)	(13)	(14)	(15)
67	95.4±11.1	21.8±6.1	51.4±8.4	73.2±9.9	19.8±5.7	61.4±9.2	31.4±6.8	$-0.34^{+0.09}_{-0.10}$	$-0.35^{+0.10}_{-0.12}$	$0.40^{+0.15}_{-0.08}$	N	N	-	38.5
68	≤9.0	-	-	-	-	-	-	-	-	-	-	-	-	≤37.4
69	≤3.8	-	-	-	-	-	-	-	-	-	-	-	-	≤37.1
70	711.4±27.9	254.5±17.2	392.7±21.0	647.3±26.7	58.9±8.9	543.6±24.5	103.2±11.4	$-0.69^{+0.03}_{-0.02}$	$-0.20^{+0.04}_{-0.03}$	$0.83^{+0.05}_{-0.07}$	N	V	-	39.3
71	≤16.3	-	-	-	-	-	-	-	-	-	-	-	-	≤37.7
72	≤12.2	-	-	-	-	-	-	-	-	-	-	-	-	≤37.6
73	8.3±5.7	-0.6±3.5	9.3±4.8	8.7±5.4	-0.4±2.4	6.8±4.9	2.4±3.2	$-0.51^{+0.23}_{-0.35}$	$-0.76^{+0.45}_{-0.92}$	$0.99^{+1.00}_{-0.46}$	-	-	-	37.4
74	55.8±9.0	13.0±5.5	29.2±7.0	42.3±8.4	5.2±4.0	38.7±8.0	8.7±4.6	$-0.62^{+0.10}_{-0.12}$	$-0.31^{+0.16}_{-0.12}$	$0.67^{+0.20}_{-0.20}$	N	P	-	38.2
75	≤38.2	-	-	-	-	-	-	-	-	-	-	-	-	≤38.1
76	6.7±4.3	6.4±4.0	0.9±2.7	7.4±4.3	-0.6±1.9	0.9±2.9	-0.9±1.9	$-0.68^{+0.27}_{-0.32}$	$0.59^{+0.78}_{-0.48}$	$0.46^{+1.14}_{-0.92}$	-	-	-	37.3
77	25.5±6.7	7.8±5.1	2.7±4.3	10.5±6.2	2.3±3.4	10.2±5.8	2.6±3.6	$-0.58^{+0.16}_{-0.20}$	$0.21^{+0.22}_{-0.21}$	$0.24^{+0.32}_{-0.27}$	N	N	-	37.9
78	≤23.3	-	-	-	-	-	-	-	-	-	-	-	-	≤37.8
79	≤0.7	-	-	-	-	-	-	-	-	-	-	-	-	≤36.3
80	≤5.2	-	-	-	-	-	-	-	-	-	-	-	-	≤37.2
81	106.4±11.5	36.9±7.3	62.0±9.0	98.9±11.2	6.2±3.8	86.8±10.5	9.8±4.4	$-0.80^{+0.06}_{-0.06}$	$-0.21^{+0.08}_{-0.10}$	$1.00^{+0.15}_{-0.22}$	N	N	-	38.5
82	87.8±8.9	24.1±6.4	48.0±8.4	72.1±10.1	12.7±5.0	63.4±9.4	16.8±5.6	$-0.59^{+0.10}_{-0.10}$	$-0.30^{+0.12}_{-0.12}$	$0.57^{+0.16}_{-0.14}$	N	N	-	38.4
83	≤19.2	-	-	-	-	-	-	-	-	-	-	-	-	≤37.8
84	≤1.2	-	-	-	-	-	-	-	-	-	-	-	-	≤36.6
85	≤0.5	-	-	-	-	-	-	-	-	-	-	-	-	≤36.2
86	195.7±15.2	57.2±8.7	101.8±11.2	159.1±13.8	36.6±7.2	128.7±12.5	58.4±8.7	$-0.39^{+0.07}_{-0.07}$	$-0.24^{+0.06}_{-0.08}$	$0.46^{+0.07}_{-0.10}$	N	N	-	38.8
87	29.1±7.1	12.3±4.9	12.4±5.0	24.7±6.5	4.5±3.6	20.5±6.0	4.8±3.8	$-0.65^{+0.18}_{-0.19}$	$-0.01^{+0.19}_{-0.20}$	$0.40^{+0.32}_{-0.27}$	N	N	-	37.9
88	11.3±4.9	5.1±3.6	7.2±4.0	12.4±4.8	-1.1±1.9	10.8±4.6	-1.3±1.9	$-0.99^{+0.04}_{-0.01}$	$-0.13^{+0.24}_{-0.30}$	$1.22^{+0.92}_{-0.61}$	-	-	-	37.5
89	≤1.9	-	-	-	-	-	-	-	-	-	-	-	-	≤36.8
90	47.7±8.1	13.7±4.8	23.6±6.0	37.3±7.2	10.4±4.4	34.4±7.0	11.2±4.6	$-0.52^{+0.12}_{-0.13}$	$-0.23^{+0.13}_{-0.16}$	$0.36^{+0.16}_{-0.16}$	N	N	-	38.2
91	12.9±5.0	4.4±3.4	8.2±4.1	12.6±4.8	0.3±2.3	11.9±4.7	1.1±2.7	$-0.87^{+0.10}_{-0.13}$	$-0.24^{+0.24}_{-0.30}$	$0.92^{+0.84}_{-0.46}$	-	-	-	37.6
92	12.3±4.9	6.6±3.8	2.4±2.9	9.0±4.3	3.3±3.2	6.3±3.8	3.3±3.2	$-0.34^{+0.31}_{-0.34}$	$0.38^{+0.40}_{-0.35}$	$-0.11^{+0.43}_{-0.45}$	-	-	-	37.6
93	13.3±5.1	3.1±3.2	6.2±3.8	9.3±4.4	4.0±3.4	6.7±4.0	5.9±3.8	$-0.08^{+0.30}_{-0.31}$	$-0.27^{+0.32}_{-0.37}$	$0.19^{+0.32}_{-0.30}$	-	-	-	37.6
94	58.3±8.9	24.3±6.1	32.3±6.8	56.6±8.7	1.7±2.9	51.0±8.3	2.6±3.2	$-0.92^{+0.04}_{-0.06}$	$-0.14^{+0.13}_{-0.11}$	$1.16^{+0.58}_{-0.35}$	V	V	-	38.2
95	≤3.7	-	-	-	-	-	-	-	-	-	-	-	-	≤37.0
96	6.5±4.1	1.2±2.7	3.3±3.2	4.5±3.6	2.1±2.9	4.0±3.4	2.0±2.9	$-0.41^{+0.28}_{-0.44}$	$-0.32^{+0.53}_{-0.70}$	$0.16^{+0.56}_{-0.48}$	-	-	-	37.3
97	≤7.0	-	-	-	-	-	-	-	-	-	-	-	-	≤37.3
98	21.8±5.9	8.8±4.1	8.7±4.1	17.5±5.3	4.4±3.4	9.7±4.3	6.3±3.8	$-0.22^{+0.23}_{-0.26}$	$0.00^{+0.19}_{-0.21}$	$0.29^{+0.27}_{-0.26}$	N	N	-	37.8
99	18.8±5.7	7.3±4.0	9.2±4.3	16.5±5.3	2.2±2.9	14.9±5.1	3.2±3.2	$-0.66^{+0.17}_{-0.21}$	$-0.11^{+0.22}_{-0.21}$	$0.54^{+0.45}_{-0.33}$	-	-	-	37.8

Table 6—Continued

MID				Net Counts				HR	C21	C32	Variability			Log L_X
	B-band	S1-band	S2-band	S-band	H-band	Sc-band	Hc-band				BB	k-S	signif.	(erg s^{-1})
(1)	(2)	(3)	(4)	(5)	(6)	(7)	(8)	(9)	(10)	(11)	(12)	(13)	(14)	(15)
100	≤3.4	-	-	-	-	-	-	-	-	-	-	-	-	≤37.0
101	≤9.2	-	-	-	-	-	-	-	-	-	-	-	-	≤37.4
102	165.5±14.0	81.5±10.1	71.0±9.5	152.6±13.4	12.9±4.8	123.0±12.2	17.7±5.4	$-0.75^{+0.05}_{-0.06}$	$0.07^{+0.05}_{-0.09}$	$0.73^{+0.14}_{-0.13}$	N	N	-	38.7
103	75.1±10.6	14.6±5.0	44.4±7.8	59.0±8.8	16.1±5.2	52.2±8.3	18.9±5.6	$-0.48^{+0.10}_{-0.11}$	$-0.52^{+0.17}_{-0.10}$	$0.43^{+0.16}_{-0.10}$	N	N	-	38.4
104	≤2.2	-	-	-	-	-	-	-	-	-	-	-	-	≤36.8
105	≤2.9	-	-	-	-	-	-	-	-	-	-	-	-	≤36.9
106	22.2±6.5	8.3±4.1	14.4±5.0	22.8±6.0	-0.8±1.9	20.1±5.7	0.1±2.3	$-0.98^{+0.04}_{-0.02}$	$-0.24^{+0.19}_{-0.19}$	$1.45^{+1.00}_{-0.53}$	-	-	-	37.8
107	≤0.8	-	-	-	-	-	-	-	-	-	-	-	-	≤36.4
108	≤6.5	-	-	-	-	-	-	-	-	-	-	-	-	≤37.3
109	≤5.3	-	-	-	-	-	-	-	-	-	-	-	-	≤37.2
110	10.7±4.7	1.2±2.7	6.6±3.8	7.8±4.1	2.9±3.2	6.1±3.8	3.8±3.4	$-0.26^{+0.34}_{-0.35}$	$-0.59^{+0.43}_{-0.64}$	$0.32^{+0.40}_{-0.35}$	-	-	-	37.5
111	6.1±4.0	1.4±2.7	1.4±2.7	2.9±3.2	3.2±3.2	2.2±2.9	3.0±3.2	$0.14^{+0.52}_{-0.47}$	$0.00^{+0.70}_{-0.72}$	$-0.24^{+0.51}_{-0.62}$	-	-	-	37.3
112	11.6±4.7	4.5±3.4	4.7±3.4	9.2±4.3	2.4±2.9	8.5±4.1	2.3±2.9	$-0.61^{+0.21}_{-0.28}$	$-0.03^{+0.30}_{-0.29}$	$0.24^{+0.43}_{-0.35}$	-	-	-	37.6
113	≤2.9	-	-	-	-	-	-	-	-	-	-	-	-	≤37.0
114	6.4±4.0	6.7±3.8	0.6±2.3	7.3±4.0	-0.9±1.9	2.4±2.9	-0.9±1.9	$-0.88^{+0.18}_{-0.12}$	$0.76^{+0.69}_{-0.45}$	$0.38^{+1.07}_{-0.99}$	-	-	-	37.3
115	18.3±5.6	8.5±4.1	8.4±4.1	16.9±5.3	1.4±2.7	14.3±5.0	3.2±3.2	$-0.65^{+0.17}_{-0.21}$	$0.00^{+0.21}_{-0.21}$	$0.64^{+0.57}_{-0.40}$	-	-	-	37.7
116	≤7.1	-	-	-	-	-	-	-	-	-	-	-	-	≤37.3
117	≤0.5	-	-	-	-	-	-	-	-	-	-	-	-	≤36.2
118	≤6.0	-	-	-	-	-	-	-	-	-	-	-	-	≤37.3
119	10.6±4.6	3.7±3.2	2.6±2.9	6.3±3.8	4.3±3.4	3.4±3.2	6.2±3.8	$0.28^{+0.34}_{-0.31}$	$0.13^{+0.41}_{-0.37}$	$-0.19^{+0.38}_{-0.40}$	-	-	-	37.5
120	168.7±14.1	99.7±11.0	63.4±9.0	163.2±13.8	5.6±3.6	138.4±12.8	5.4±3.6	$-0.93^{+0.03}_{-0.03}$	$0.19^{+0.08}_{-0.06}$	$1.07^{+0.16}_{-0.23}$	V	V	-	38.7
121	26.4±6.4	8.7±4.1	12.2±4.7	20.9±5.8	5.5±3.6	16.2±5.2	8.4±4.1	$-0.33^{+0.18}_{-0.20}$	$-0.13^{+0.18}_{-0.19}$	$0.32^{+0.24}_{-0.21}$	N	N	-	37.9
122	≤3.7	-	-	-	-	-	-	-	-	-	-	-	-	≤37.1
123	≤2.4	-	-	-	-	-	-	-	-	-	-	-	-	≤36.9
124	≤2.1	-	-	-	-	-	-	-	-	-	-	-	-	≤36.8
125	17.1±5.5	5.7±3.6	7.5±4.0	13.1±4.8	4.0±3.4	10.5±4.4	4.8±3.6	$-0.40^{+0.24}_{-0.26}$	$-0.11^{+0.24}_{-0.24}$	$0.24^{+0.32}_{-0.27}$	-	-	-	37.7
126	≤1.7	-	-	-	-	-	-	-	-	-	-	-	-	≤36.7
127	≤7.5	-	-	-	-	-	-	-	-	-	-	-	-	≤37.4
128	≤0.7	-	-	-	-	-	-	-	-	-	-	-	-	≤36.4
129	10.8±4.6	1.6±2.7	7.7±4.0	9.3±4.3	1.5±2.7	7.8±4.0	2.3±2.9	$-0.60^{+0.22}_{-0.28}$	$-0.54^{+0.38}_{-0.48}$	$0.62^{+0.53}_{-0.38}$	-	-	-	37.6
130	11.4±4.7	4.8±3.4	6.5±3.8	11.2±4.6	0.2±2.3	9.5±4.3	1.1±2.7	$-0.86^{+0.12}_{-0.14}$	$-0.08^{+0.27}_{-0.27}$	$0.84^{+0.92}_{-0.46}$	-	-	-	37.6
131	≤7.9	-	-	-	-	-	-	-	-	-	-	-	-	≤37.4
132	11.7±4.7	2.6±2.9	4.6±3.4	7.2±4.0	4.5±3.4	7.5±4.0	4.4±3.4	$-0.36^{+0.24}_{-0.29}$	$-0.05^{+0.34}_{-0.41}$	$0.05^{+0.30}_{-0.29}$	-	-	-	37.8

Table 6—Continued

MID	Net Counts							HR	C21	C32	Variability			Log L_X
	B-band	S1-band	S2-band	S-band	H-band	Sc-band	Hc-band				BB	k-S	signif.	(erg s^{-1})
(1)	(2)	(3)	(4)	(5)	(6)	(7)	(8)	(9)	(10)	(11)	(12)	(13)	(14)	(15)

Note. — Col. (1): Master ID, cols. (2)−(8): net counts, in each of the 7 energy bands (see Table 3 for definitions of these bands), col. (9): hardness ratio, cols. (10) and (11) color values, errors are given as 1σ, cols. (12) and (13): short-term variability, where (BB) indicate Bayesian block analysis and (K-S) indicates the Kolmogorov-Smirnov test, in both columns symbols indicate - (N) non-variable in all observations, (V) variable in at least one observation, (P) possible variability in at least one observation, col. (14): the significance of the change in L_X between the previous observation and the current observation respectively (equation 2), col. (15): log L_X (0.3−8.0 keV). Upper limit values of net B and L_X are at the 68% confidence level.

Table 7. Source counts, hardness ratios, color-color values and variability: Observation 2

MID	Net Counts							HR	C21	C32	Variability			Log L_X
	B-band	S1-band	S2-band	S-band	H-band	Sc-band	Hc-band				BB	k-S	signif.	(erg s^{-1})
(1)	(2)	(3)	(4)	(5)	(6)	(7)	(8)	(9)	(10)	(11)	(12)	(13)	(14)	(15)
1	≤16.6	-	-	-	-	-	-	-	-	-	-	-	0.3	≤37.4
2	≤2.2	-	-	-	-	-	-	-	-	-	-	-	0.3	≤36.5
3	≤9.9	-	-	-	-	-	-	-	-	-	-	-	0.3	≤37.1
4	≤1.0	-	-	-	-	-	-	-	-	-	-	-	0.9	≤36.1
5	≤1.4	-	-	-	-	-	-	-	-	-	-	-	0.1	≤36.3
6	3.7±4.3	2.4±3.2	2.4±3.2	4.8±4.0	-1.0±2.7	1.3±2.9	0.4±3.2	$-0.27^{+0.17}_{-0.73}$	$0.16^{+0.67}_{-0.64}$	$0.46^{+1.14}_{-0.69}$	-	-	0.2	36.7
7	≤4.7	-	-	-	-	-	-	-	-	-	-	-	2.4	≤36.8
8	≤10.6	-	-	-	-	-	-	-	-	-	-	-	0.3	≤37.1
9	269.4±17.9	67.4±9.5	153.2±13.6	220.5±16.1	48.9±8.5	193.1±15.1	65.8±9.6	$-0.56^{+0.04}_{-0.06}$	$-0.18^{+0.05}_{-0.07}$	$0.52^{+0.08}_{-0.07}$	N	N	1.7	38.6
10	≤8.8	-	-	-	-	-	-	-	-	-	-	-	0.6	≤37.1
11	40.4±7.9	7.8±4.1	23.3±6.1	31.1±6.9	9.3±4.6	26.1±6.4	12.9±5.1	$-0.41^{+0.15}_{-0.15}$	$-0.35^{+0.19}_{-0.19}$	$0.40^{+0.22}_{-0.16}$	N	N	0.3	37.7
12	≤6.5	-	-	-	-	-	-	-	-	-	-	-	0.2	≤36.9
13	≤10.0	-	-	-	-	-	-	-	-	-	-	-	0.1	≤37.1
14	≤17.8	-	-	-	-	-	-	-	-	-	-	-	2.3	≤37.4
15	≤1.3	-	-	-	-	-	-	-	-	-	-	-	1.9	≤36.2
16	26.2±6.7	2.3±3.2	12.7±4.8	15.0±5.3	11.2±4.8	15.2±5.2	10.8±4.8	$-0.25^{+0.20}_{-0.21}$	$-0.54^{+0.35}_{-0.51}$	$0.09^{+0.20}_{-0.20}$	N	N	2.3	37.6
17	18.1±5.9	4.1±3.4	8.8±4.3	13.0±5.0	5.2±4.0	10.9±4.6	6.9±4.3	$-0.31^{+0.25}_{-0.26}$	$-0.19^{+0.27}_{-0.29}$	$0.24^{+0.32}_{-0.29}$	-	-	0.2	37.4
18	21.2±6.8	1.0±3.2	11.0±4.7	12.0±5.2	9.2±5.0	9.3±4.6	10.7±5.2	$-0.02^{+0.28}_{-0.27}$	$-0.66^{+0.49}_{-0.76}$	$0.11^{+0.24}_{-0.25}$	N	N	0.6	37.4
19	≤2.3	-	-	-	-	-	-	-	-	-	-	-	0.0	≤36.5
20	≤6.7	-	-	-	-	-	-	-	-	-	-	-	1.3	≤36.9
21	24.8±7.2	-0.7±2.9	9.5±4.6	8.8±5.0	16.0±5.8	6.4±4.1	19.1±6.2	$0.45^{+0.23}_{-0.22}$	$-0.87^{+0.60}_{-0.86}$	$-0.18^{+0.19}_{-0.22}$	N	N	0.5	37.5
22	≤2.4	-	-	-	-	-	-	-	-	-	-	-	0.1	≤36.5
23	≤12.8	-	-	-	-	-	-	-	-	-	-	-	1.0	≤37.2
24	≤11.8	-	-	-	-	-	-	-	-	-	-	-	0.4	≤37.2
25	≤0.6	-	-	-	-	-	-	-	-	-	-	-	2.0	≤35.9
26	≤2.3	-	-	-	-	-	-	-	-	-	-	-	0.5	≤36.5
27	276.5±17.9	112.8±11.7	128.4±12.4	241.2±16.6	35.3±7.3	206.2±15.4	46.8±8.2	$-0.67^{+0.04}_{-0.05}$	$0.04^{+0.06}_{-0.05}$	$0.58^{+0.09}_{-0.08}$	N	N	9.7	38.6
28	32.4±7.3	3.3±3.4	21.0±5.9	24.4±6.4	8.1±4.4	21.5±6.0	10.7±4.8	$-0.41^{+0.17}_{-0.18}$	$-0.62^{+0.27}_{-0.40}$	$0.43^{+0.21}_{-0.19}$	N	N	1.0	37.6
29	15.2±5.6	5.1±3.6	8.8±4.3	13.9±5.1	1.3±3.2	12.5±4.8	2.1±3.4	$-0.82^{+0.12}_{-0.18}$	$-0.11^{+0.24}_{-0.27}$	$0.64^{+0.75}_{-0.43}$	-	-	0.4	37.3
30	37.0±7.6	9.7±4.4	22.4±6.0	32.1±7.0	4.9±4.0	22.1±6.0	11.6±5.0	$-0.38^{+0.16}_{-0.18}$	$-0.24^{+0.16}_{-0.19}$	$0.64^{+0.35}_{-0.24}$	N	N	1.7	37.7
31	≤8.8	-	-	-	-	-	-	-	-	-	-	-	1.5	≤37.0
32	9.5±5.1	6.4±4.0	4.0±3.6	10.4±4.8	-0.9±2.7	10.8±4.7	-1.2±2.7	$-0.97^{+0.06}_{-0.03}$	$0.27^{+0.40}_{-0.32}$	$0.69^{+0.99}_{-0.61}$	-	-	0.3	37.1
33	≤6.1	-	-	-	-	-	-	-	-	-	-	-	0.9	≤36.9

Table 7—Continued

MID	Net Counts							HR	C21	C32	Variability			Log L_X
	B-band	S1-band	S2-band	S-band	H-band	Sc-band	Hc-band				BB	k-S	signif.	(erg s^{-1})
(1)	(2)	(3)	(4)	(5)	(6)	(7)	(8)	(9)	(10)	(11)	(12)	(13)	(14)	(15)
34	≤4.1	-	-	-	-	-	-	-	-	-	-	-	0.1	≤36.7
35	≤4.2	-	-	-	-	-	-	-	-	-	-	-	1.7	≤36.8
36	≤1.3	-	-	-	-	-	-	-	-	-	-	-	0.6	≤36.2
37	12.8±5.5	3.1±3.4	7.1±4.1	10.1±4.8	2.6±3.4	9.0±4.6	4.5±3.8	$-0.44^{+0.30}_{-0.30}$	$-0.21^{+0.37}_{-0.46}$	$0.38^{+0.56}_{-0.38}$	-	-	0.6	37.2
38	7.6±4.7	1.9±2.9	5.9±3.8	7.8±4.3	-0.1±2.9	5.9±3.8	0.7±3.2	$-0.81^{+0.19}_{-0.19}$	$-0.29^{+0.42}_{-0.54}$	$0.69^{+0.84}_{-0.54}$	-	-	0.9	37.1
39	10.2±5.1	3.5±3.4	4.1±3.6	7.6±4.4	2.6±3.4	4.8±3.8	2.2±3.4	$-0.53^{+0.24}_{-0.47}$	$0.05^{+0.43}_{-0.45}$	$0.19^{+0.61}_{-0.51}$	-	-	0.5	37.1
40	≤10.2	-	-	-	-	-	-	-	-	-	-	-	1.3	≤37.1
41	146.0±13.5	58.9±8.9	66.6±9.4	125.5±12.4	20.6±6.0	113.1±11.8	26.0±6.5	$-0.67^{+0.06}_{-0.07}$	$0.03^{+0.10}_{-0.06}$	$0.54^{+0.12}_{-0.11}$	N	N	1.5	38.3
42	457.8±22.5	65.9±9.2	290.9±18.1	356.8±20.0	100.9±11.2	309.8±18.7	140.6±13.0	$-0.43^{+0.04}_{-0.05}$	$-0.53^{+0.05}_{-0.07}$	$0.48^{+0.05}_{-0.05}$	N	N	2.3	38.8
43	≤3.1	-	-	-	-	-	-	-	-	-	-	-	0.6	≤36.6
44	5.7±4.6	3.5±3.4	2.3±3.2	5.8±4.1	-0.1±2.9	3.5±3.6	0.6±3.2	$-0.64^{+0.28}_{-0.36}$	$0.24^{+0.65}_{-0.51}$	$0.31^{+1.07}_{-0.69}$	-	-	2.0	36.9
45	≤12.0	-	-	-	-	-	-	-	-	-	-	-	1.3	≤37.2
46	≤14.0	-	-	-	-	-	-	-	-	-	-	-	2.7	≤37.2
47	62.9±9.5	15.9±5.3	32.2±7.0	48.1±8.3	14.8±5.3	40.5±7.7	20.3±6.0	$-0.40^{+0.12}_{-0.13}$	$-0.18^{+0.14}_{-0.15}$	$0.35^{+0.17}_{-0.12}$	N	N	0.3	37.9
48	≤11.8	-	-	-	-	-	-	-	-	-	-	-	1.5	≤37.2
49	≤3.8	-	-	-	-	-	-	-	-	-	-	-	0.1	≤36.7
50	44.1±8.1	6.4±4.0	27.2±6.5	33.6±7.1	10.5±4.7	24.6±6.3	19.2±5.8	$-0.20^{+0.15}_{-0.16}$	$-0.48^{+0.19}_{-0.22}$	$0.43^{+0.18}_{-0.16}$	N	N	5.1	37.8
51	≤4.0	-	-	-	-	-	-	-	-	-	-	-	0.9	≤36.7
52	≤2.1	-	-	-	-	-	-	-	-	-	-	-	2.5	≤36.4
53	47.7±8.7	14.8±5.3	18.1±5.8	33.0±7.4	14.7±5.3	29.9±7.0	17.1±5.7	$-0.34^{+0.13}_{-0.16}$	$-0.01^{+0.21}_{-0.13}$	$0.10^{+0.21}_{-0.13}$	N	N	0.8	37.8
54	≤4.1	-	-	-	-	-	-	-	-	-	-	-	1.4	≤36.7
55	76.7±10.2	19.7±5.7	53.1±8.5	72.9±9.8	3.8±3.8	62.8±9.1	10.3±4.8	$-0.76^{+0.08}_{-0.08}$	$-0.30^{+0.10}_{-0.13}$	$1.11^{+0.41}_{-0.28}$	N	N	2.7	38.0
56	5.4±4.9	-1.7±2.3	9.5±4.6	7.7±4.7	-2.4±2.3	7.3±4.4	-1.7±2.7	$-0.95^{+0.09}_{-0.05}$	$-1.07^{+0.54}_{-0.92}$	$1.22^{+0.92}_{-0.61}$	-	-	1.2	36.8
57	≤30.1	-	-	-	-	-	-	-	-	-	-	-	2.6	≤37.6
58	9.7±5.1	1.3±2.9	7.3±4.1	8.6±4.6	1.0±3.2	9.1±4.4	1.6±3.4	$-0.80^{+0.16}_{-0.20}$	$-0.46^{+0.46}_{-0.69}$	$0.59^{+0.80}_{-0.46}$	-	-	0.1	37.1
59	17.7±6.4	2.7±3.4	12.0±5.1	14.7±5.7	3.0±3.8	12.0±5.2	4.5±4.1	$-0.58^{+0.25}_{-0.26}$	$-0.46^{+0.38}_{-0.51}$	$0.54^{+0.56}_{-0.38}$	-	-	1.4	37.3
60	34.2±7.8	10.3±4.8	18.4±5.8	28.6±7.1	5.5±4.1	20.2±6.2	10.2±4.8	$-0.40^{+0.18}_{-0.20}$	$-0.13^{+0.18}_{-0.19}$	$0.51^{+0.32}_{-0.24}$	N	N	1.2	37.6
61	≤2.4	-	-	-	-	-	-	-	-	-	-	-	1.2	≤36.5
62	34.6±7.7	5.8±4.0	26.4±6.5	32.2±7.1	2.4±3.6	28.3±6.7	5.0±4.1	$-0.77^{+0.13}_{-0.14}$	$-0.51^{+0.22}_{-0.27}$	$0.94^{+0.62}_{-0.35}$	N	N	0.3	37.6
63	≤3.1	-	-	-	-	-	-	-	-	-	-	-	1.7	≤36.6
64	36.8±7.6	13.1±5.0	16.2±5.3	29.3±6.8	7.5±4.3	24.9±6.3	9.1±4.6	$-0.53^{+0.15}_{-0.17}$	$0.01^{+0.17}_{-0.17}$	$0.35^{+0.24}_{-0.19}$	N	N	0.1	37.7
65	≤2.9	-	-	-	-	-	-	-	-	-	-	-	1.2	≤36.6
66	43.6±8.4	8.2±4.4	27.5±6.7	35.8±7.6	7.8±4.4	32.2±7.2	9.2±4.7	$-0.62^{+0.14}_{-0.14}$	$-0.40^{+0.19}_{-0.22}$	$0.56^{+0.22}_{-0.18}$	N	P	0.3	37.7

Table 7—Continued

MID				Net Counts				HR	C21	C32	Variability			Log L_X
	B-band	S1-band	S2-band	S-band	H-band	Sc-band	Hc-band				BB	k-S	signif.	(erg s^{-1})
(1)	(2)	(3)	(4)	(5)	(6)	(7)	(8)	(9)	(10)	(11)	(12)	(13)	(14)	(15)
67	239.5±16.9	45.4±8.1	138.4±13.1	183.8±15.0	52.4±8.5	152.9±13.8	76.1±10.0	$-0.40^{+0.05}_{-0.07}$	$-0.35^{+0.05}_{-0.10}$	$0.45^{+0.08}_{-0.06}$	N	N	0.3	38.5
68	≤19.8	-	-	-	-	-	-	-	-	-	-	-	0.2	≤37.4
69	≤2.5	-	-	-	-	-	-	-	-	-	-	-	0.7	≤36.5
70	2432.8±50.5	466.8±22.8	1379.8±38.3	1846.7±44.2	579.1±25.2	1593.0±41.1	764.9±28.8	$-0.42^{+0.02}_{-0.02}$	$-0.37^{+0.03}_{-0.02}$	$0.41^{+0.02}_{-0.02}$	V	V	8.4	39.5
71	≤26.3	-	-	-	-	-	-	-	-	-	-	-	1.1	≤37.5
72	30.7±7.4	15.2±5.3	14.7±5.3	29.9±7.1	0.9±3.2	23.2±6.4	4.2±4.0	$-0.78^{+0.13}_{-0.15}$	$0.10^{+0.21}_{-0.14}$	$1.06^{+0.67}_{-0.59}$	N	P	0.1	37.6
73	≤28.7	-	-	-	-	-	-	-	-	-	-	-	0.6	≤37.6
74	181.1±14.8	62.9±9.3	84.4±10.7	147.3±13.7	24.8±6.5	122.4±12.6	36.6±7.6	$-0.59^{+0.06}_{-0.06}$	$-0.03^{+0.08}_{-0.07}$	$0.54^{+0.11}_{-0.09}$	N	N	1.7	38.4
75	89.1±10.9	39.3±7.7	43.1±8.2	82.4±10.8	-0.3±3.0	72.4±10.1	5.2±4.2	$-0.86^{+0.06}_{-0.06}$	$0.02^{+0.13}_{-0.06}$	$1.34^{+0.71}_{-0.36}$	N	N	0.2	38.0
76	≤1.3	-	-	-	-	-	-	-	-	-	-	-	1.4	≤36.2
77	111.1±12.2	27.5±6.8	54.0±9.0	81.5±10.9	23.0±6.3	77.4±10.6	25.2±6.6	$-0.56^{+0.07}_{-0.09}$	$-0.15^{+0.08}_{-0.13}$	$0.38^{+0.14}_{-0.09}$	N	N	2.4	38.1
78	48.2±8.2	10.2±4.6	19.0±5.7	29.2±6.8	16.7±5.3	23.8±6.3	21.4±5.9	$-0.14^{+0.14}_{-0.15}$	$-0.10^{+0.12}_{-0.22}$	$0.09^{+0.15}_{-0.14}$	N	N	0.6	37.8
79	≤1.7	-	-	-	-	-	-	-	-	-	-	-	0.0	≤36.3
80	≤11.6	-	-	-	-	-	-	-	-	-	-	-	0.1	≤37.2
81	206.9±15.7	69.3±9.6	109.1±11.7	178.4±14.7	25.7±6.5	159.9±14.0	33.1±7.1	$-0.70^{+0.05}_{-0.05}$	$-0.12^{+0.10}_{-0.03}$	$0.64^{+0.11}_{-0.08}$	N	N	1.6	38.4
82	166.9±14.2	37.5±7.4	85.2±10.5	122.7±12.4	42.3±7.8	109.2±11.8	49.0±8.3	$-0.45^{+0.07}_{-0.07}$	$-0.22^{+0.07}_{-0.10}$	$0.34^{+0.09}_{-0.08}$	N	N	1.8	38.3
83	45.7±8.2	15.9±5.3	22.3±6.2	38.2±7.7	4.2±3.8	34.9±7.4	5.8±4.1	$-0.72^{+0.10}_{-0.12}$	$-0.05^{+0.16}_{-0.13}$	$0.61^{+0.30}_{-0.19}$	N	N	0.1	37.8
84	3.9±4.5	-1.0±2.3	5.7±4.0	4.8±4.1	-0.8±2.7	3.9±3.8	-0.3±2.9	$-0.78^{+0.24}_{-0.22}$	$-0.76^{+0.53}_{-1.00}$	$0.84^{+0.92}_{-0.61}$	-	-	0.2	36.7
85	≤0.5	-	-	-	-	-	-	-	-	-	-	-	0.5	≤35.8
86	572.9±25.3	118.9±12.2	334.0±19.4	452.9±22.6	119.9±12.1	389.6±21.0	165.0±14.0	$-0.47^{+0.04}_{-0.04}$	$-0.33^{+0.04}_{-0.06}$	$0.48^{+0.04}_{-0.05}$	N	P	2.2	38.9
87	50.0±9.9	10.0±5.2	31.2±7.2	41.2±8.4	7.7±4.6	37.9±8.0	9.2±4.9	$-0.67^{+0.13}_{-0.13}$	$-0.38^{+0.21}_{-0.21}$	$0.61^{+0.26}_{-0.22}$	N	N	1.0	37.8
88	44.3±8.3	7.0±4.1	31.4±6.9	38.5±7.6	5.8±4.1	31.6±7.0	12.3±5.1	$-0.51^{+0.14}_{-0.13}$	$-0.51^{+0.19}_{-0.21}$	$0.72^{+0.27}_{-0.21}$	N	N	1.2	37.7
89	≤1.9	-	-	-	-	-	-	-	-	-	-	-	0.5	≤36.4
90	81.7±10.4	18.6±5.6	45.6±7.9	64.2±9.2	17.5±5.6	57.0±8.7	20.2±5.9	$-0.54^{+0.10}_{-0.10}$	$-0.29^{+0.15}_{-0.10}$	$0.44^{+0.13}_{-0.12}$	N	N	1.8	38.0
91	≤1.4	-	-	-	-	-	-	-	-	-	-	-	2.4	≤36.3
92	≤9.1	-	-	-	-	-	-	-	-	-	-	-	1.7	≤37.1
93	49.1±8.8	11.1±4.8	29.7±6.8	40.8±7.9	8.4±4.6	37.2±7.5	10.8±5.0	$-0.61^{+0.12}_{-0.14}$	$-0.31^{+0.17}_{-0.17}$	$0.56^{+0.22}_{-0.18}$	N	N	1.1	37.8
94	7.5±5.0	6.1±4.0	4.6±3.8	10.6±5.0	-3.1±1.9	7.8±4.4	-2.7±2.3	$-0.97^{+0.06}_{-0.03}$	$0.21^{+0.38}_{-0.34}$	$0.99^{+1.07}_{-0.61}$	-	-	6.1	37.0
95	16.8±6.0	6.5±4.0	8.5±4.4	15.0±5.4	1.8±3.4	12.2±5.0	2.1±3.6	$-0.81^{+0.13}_{-0.19}$	$0.00^{+0.24}_{-0.27}$	$0.54^{+0.72}_{-0.41}$	-	-	0.7	37.3
96	≤10.2	-	-	-	-	-	-	-	-	-	-	-	0.5	≤37.1
97	≤4.1	-	-	-	-	-	-	-	-	-	-	-	1.5	≤36.7
98	35.0±7.4	10.2±4.4	16.6±5.3	26.8±6.5	8.2±4.4	23.4±6.1	10.9±4.8	$-0.44^{+0.16}_{-0.17}$	$-0.11^{+0.19}_{-0.16}$	$0.32^{+0.22}_{-0.19}$	N	N	1.1	37.6
99	70.0±9.8	14.6±5.1	41.5±7.6	56.0±8.7	14.0±5.2	48.1±8.1	19.5±5.9	$-0.48^{+0.10}_{-0.12}$	$-0.30^{+0.10}_{-0.17}$	$0.51^{+0.13}_{-0.16}$	N	N	1.5	37.9

Table 7—Continued

MID	Net Counts							HR	C21	C32	Variability			Log L_X
	B-band	S1-band	S2-band	S-band	H-band	Sc-band	Hc-band				BB	k-S	signif.	(erg s^{-1})
(1)	(2)	(3)	(4)	(5)	(6)	(7)	(8)	(9)	(10)	(11)	(12)	(13)	(14)	(15)
100	54.8±8.9	57.2±8.7	-1.1±2.3	56.1±8.8	-1.3±2.7	38.5±7.5	-1.9±2.7	$-1.00^{+0.02}_{-0.00}$	$1.99^{+0.91}_{-0.54}$	$-0.08^{+1.15}_{-1.14}$	N	N	3.9	37.8
101	17.8±6.0	0.3±2.7	4.5±3.6	4.8±4.0	13.0±5.1	1.8±3.2	16.8±5.6	$0.84^{+0.16}_{-0.12}$	$-0.46^{+0.54}_{-0.92}$	$-0.38^{+0.25}_{-0.32}$	-	-	0.4	37.3
102	459.4±22.6	191.9±14.9	208.7±15.6	400.6±21.1	58.8±8.9	330.6±19.3	83.2±10.4	$-0.65^{+0.04}_{-0.03}$	$0.07^{+0.04}_{-0.04}$	$0.60^{+0.04}_{-0.09}$	N	N	1.4	38.8
103	131.3±12.6	36.0±7.1	69.0±9.4	105.1±11.4	24.9±6.3	93.6±10.8	30.7±6.8	$-0.56^{+0.07}_{-0.07}$	$-0.16^{+0.09}_{-0.09}$	$0.45^{+0.11}_{-0.09}$	N	N	1.8	38.2
104	12.9±5.4	2.8±3.2	1.8±2.9	4.6±3.8	8.3±4.4	2.4±3.2	9.0±4.6	$0.60^{+0.30}_{-0.18}$	$0.24^{+0.67}_{-0.59}$	$-0.51^{+0.40}_{-0.56}$	-	-	1.1	37.3
105	6.0±5.1	0.0±2.3	5.3±3.8	5.3±4.0	0.9±3.2	4.0±3.6	2.5±3.6	$-0.38^{+0.27}_{-0.38}$	$-0.69^{+0.54}_{-0.91}$	$0.48^{+0.83}_{-0.51}$	-	-	0.1	36.9
106	107.9±12.5	34.9±7.1	69.4±9.5	104.3±11.4	3.5±3.8	95.3±10.9	8.0±4.6	$-0.87^{+0.05}_{-0.06}$	$-0.18^{+0.09}_{-0.10}$	$1.25^{+0.45}_{-0.31}$	N	N	2.7	38.1
107	6.0±4.5	2.2±2.9	3.7±3.4	5.9±4.0	0.1±2.9	4.7±3.6	0.8±3.2	$-0.76^{+0.23}_{-0.24}$	$-0.08^{+0.48}_{-0.54}$	$0.46^{+0.99}_{-0.54}$	-	-	0.8	36.9
108	≤4.0	-	-	-	-	-	-	-	-	-	-	-	1.4	≤36.7
109	≤6.0	-	-	-	-	-	-	-	-	-	-	-	0.8	≤36.9
110	20.3±6.5	3.2±3.4	10.6±4.7	13.8±5.3	6.5±4.4	10.3±4.7	7.8±4.7	$-0.23^{+0.29}_{-0.29}$	$-0.35^{+0.32}_{-0.43}$	$0.21^{+0.33}_{-0.26}$	N	N	0.4	37.4
111	8.5±4.9	3.7±3.4	4.0±3.4	7.6±4.3	0.9±3.2	4.5±3.6	1.7±3.4	$-0.60^{+0.26}_{-0.40}$	$0.08^{+0.40}_{-0.40}$	$0.38^{+0.85}_{-0.54}$	-	-	0.6	37.0
112	≤8.5	-	-	-	-	-	-	-	-	-	-	-	1.6	≤37.1
113	11.3±5.2	1.8±2.9	8.1±4.3	10.0±4.7	1.3±3.2	7.0±4.1	4.8±4.0	$-0.30^{+0.36}_{-0.35}$	$-0.43^{+0.40}_{-0.56}$	$0.59^{+0.75}_{-0.43}$	-	-	0.5	37.2
114	21.3±6.3	4.8±3.6	13.4±5.0	18.2±5.7	3.2±3.6	16.2±5.3	4.7±4.0	$-0.64^{+0.20}_{-0.21}$	$-0.29^{+0.21}_{-0.30}$	$0.59^{+0.46}_{-0.35}$	N	N	0.4	37.5
115	≤1.0	-	-	-	-	-	-	-	-	-	-	-	3.2	≤36.1
116	26.4±6.8	7.5±4.1	15.2±5.2	22.8±6.2	3.6±3.8	23.4±6.1	2.9±3.8	$-0.86^{+0.08}_{-0.14}$	$-0.19^{+0.19}_{-0.21}$	$0.59^{+0.46}_{-0.32}$	N	N	1.0	37.5
117	≤0.9	-	-	-	-	-	-	-	-	-	-	-	0.2	≤36.1
118	5.9±4.5	0.7±2.7	4.8±3.6	5.5±4.0	0.3±2.9	6.6±4.0	0.0±2.9	$-0.89^{+0.14}_{-0.11}$	$-0.38^{+0.46}_{-0.84}$	$0.53^{+0.92}_{-0.45}$	-	-	1.3	36.9
119	36.4±7.6	11.2±4.6	17.5±5.4	28.7±6.6	7.7±4.4	22.5±6.0	10.4±4.8	$-0.44^{+0.16}_{-0.18}$	$-0.08^{+0.17}_{-0.16}$	$0.38^{+0.21}_{-0.22}$	N	N	0.8	37.7
120	109.9±11.7	68.1±9.4	40.0±7.5	108.1±11.5	1.9±3.2	99.8±11.1	1.6±3.2	$-0.98^{+0.02}_{-0.02}$	$0.35^{+0.11}_{-0.07}$	$1.28^{+0.54}_{-0.42}$	N	N	8.2	38.2
121	71.8±9.8	19.1±5.6	32.8±6.9	51.8±8.4	20.0±5.8	45.3±7.9	22.8±6.1	$-0.41^{+0.10}_{-0.11}$	$-0.10^{+0.11}_{-0.15}$	$0.25^{+0.14}_{-0.12}$	N	N	0.4	38.0
122	≤10.9	-	-	-	-	-	-	-	-	-	-	-	0.4	≤37.1
123	≤6.3	-	-	-	-	-	-	-	-	-	-	-	0.1	≤36.9
124	≤1.5	-	-	-	-	-	-	-	-	-	-	-	0.7	≤36.3
125	39.5±7.9	7.7±4.1	27.4±6.5	35.1±7.3	4.4±4.0	29.4±6.7	9.8±4.8	$-0.57^{+0.15}_{-0.15}$	$-0.43^{+0.19}_{-0.19}$	$0.78^{+0.37}_{-0.27}$	N	N	0.2	37.7
126	≤2.6	-	-	-	-	-	-	-	-	-	-	-	0.3	≤36.6
127	≤14.6	-	-	-	-	-	-	-	-	-	-	-	0.4	≤37.3
128	548.3±24.6	113.1±11.8	264.0±17.3	377.1±20.5	171.2±14.3	315.8±18.9	209.6±15.7	$-0.28^{+0.04}_{-0.04}$	$-0.27^{+0.08}_{-0.02}$	$0.22^{+0.05}_{-0.04}$	V	V	22.2	38.9
129	15.8±5.6	1.4±2.7	8.5±4.3	9.9±4.6	5.9±4.0	7.4±4.1	8.7±4.4	$-0.06^{+0.28}_{-0.28}$	$-0.46^{+0.41}_{-0.56}$	$0.19^{+0.29}_{-0.24}$	-	-	0.8	37.4
130	42.4±7.9	10.3±4.4	23.0±6.0	33.3±7.0	9.2±4.6	29.9±6.6	9.8±4.7	$-0.60^{+0.12}_{-0.14}$	$-0.13^{+0.13}_{-0.19}$	$0.43^{+0.21}_{-0.16}$	N	N	1.1	37.8
131	43.2±8.3	11.4±4.7	20.0±5.8	31.4±7.0	11.9±5.2	27.0±6.5	15.2±5.7	$-0.38^{+0.15}_{-0.15}$	$-0.06^{+0.14}_{-0.20}$	$0.23^{+0.22}_{-0.15}$	N	N	2.0	37.8
132	34.7±7.6	9.4±4.4	18.9±5.7	28.3±6.7	6.4±4.3	24.5±6.3	7.9±4.6	$-0.63^{+0.14}_{-0.16}$	$-0.05^{+0.18}_{-0.16}$	$0.51^{+0.27}_{-0.22}$	N	N	0.1	37.8

Table 7—Continued

MID	Net Counts							HR	C21	C32	Variability			Log L_X
	B-band	S1-band	S2-band	S-band	H-band	Sc-band	Hc-band				BB	k-S	signif.	(erg s^{-1})
(1)	(2)	(3)	(4)	(5)	(6)	(7)	(8)	(9)	(10)	(11)	(12)	(13)	(14)	(15)

Note. — Col. (1): Master ID, cols. (2)−(8): net counts, in each of the 7 energy bands (see Table 3 for definitions of these bands), col. (9): hardness ratio, cols. (10) and (11) color values, errors are given as 1σ, cols. (12) and (13): short-term variability, where (BB) indicate Bayesian block analysis and (K-S) indicates the Kolmogorov-Smirnov test, in both columns symbols indicate - (N) non-variable in all observations, (V) variable in at least one observation, (P) possible variability in at least one observation, col. (14): the significance of the change in L_X between the previous observation and the current observation respectively (equation 2), col. (15): log L_X (0.3−8.0 keV). Upper limit values of net B and L_X are at the 68% confidence level.

Table 8. Source counts, hardness ratios, color-color values and variability: Observation 3

MID	Net Counts							HR	C21	C32	Variability			Log L_X
	B-band	S1-band	S2-band	S-band	H-band	Sc-band	Hc-band				BB	k-S	signif.	(erg s^{-1})
(1)	(2)	(3)	(4)	(5)	(6)	(7)	(8)	(9)	(10)	(11)	(12)	(13)	(14)	(15)
1	≤2.7	-	-	-	-	-	-	-	-	-	-	-	2.6	≤36.6
2	≤16.2	-	-	-	-	-	-	-	-	-	-	-	3.1	≤37.4
3	≤4.3	-	-	-	-	-	-	-	-	-	-	-	0.5	≤36.9
4	≤1.1	-	-	-	-	-	-	-	-	-	-	-	0.3	≤36.3
5	≤0.6	-	-	-	-	-	-	-	-	-	-	-	0.4	≤36.0
6	≤1.1	-	-	-	-	-	-	-	-	-	-	-	0.5	≤36.3
7	≤10.9	-	-	-	-	-	-	-	-	-	-	-	1.5	≤37.3
8	≤8.6	-	-	-	-	-	-	-	-	-	-	-	0.0	≤37.1
9	39.2±5.1	11.7±4.6	21.5±5.8	33.2±6.9	7.0±4.0	32.4±6.8	5.9±3.8	$-0.78^{+0.08}_{-0.10}$	$0.03^{+0.15}_{-0.16}$	$0.54^{+0.21}_{-0.16}$	N	N	7.1	38.2
10	≤2.8	-	-	-	-	-	-	-	-	-	-	-	1.1	≤36.6
11	35.0±7.4	10.9±4.6	17.7±5.4	28.6±6.6	6.4±4.1	27.5±6.5	6.1±4.1	$-0.70^{+0.14}_{-0.14}$	$-0.09^{+0.17}_{-0.18}$	$0.46^{+0.24}_{-0.22}$	N	N	0.3	37.7
12	≤12.9	-	-	-	-	-	-	-	-	-	-	-	1.7	≤37.3
13	≤7.8	-	-	-	-	-	-	-	-	-	-	-	0.1	≤37.1
14	≤2.2	-	-	-	-	-	-	-	-	-	-	-	2.4	≤36.6
15	≤5.3	-	-	-	-	-	-	-	-	-	-	-	1.8	≤36.9
16	17.2±5.7	4.1±3.4	10.3±4.4	14.4±5.1	2.8±3.4	13.0±4.8	3.6±3.6	$-0.67^{+0.19}_{-0.22}$	$-0.27^{+0.27}_{-0.29}$	$0.51^{+0.51}_{-0.32}$	-	-	0.7	37.4
17	14.7±5.5	1.3±2.7	12.0±4.7	13.3±5.0	1.4±3.2	12.9±4.8	2.2±3.4	$-0.81^{+0.11}_{-0.19}$	$-0.70^{+0.41}_{-0.59}$	$0.75^{+0.73}_{-0.40}$	-	-	0.0	37.4
18	53.0±8.6	1.1±2.7	34.2±7.0	35.3±7.1	17.7±5.6	29.9±6.6	23.5±6.2	$-0.24^{+0.12}_{-0.15}$	$-1.10^{+0.38}_{-0.67}$	$0.33^{+0.15}_{-0.12}$	N	N	3.6	37.9
19	2.6±3.8	1.4±2.7	1.8±2.9	3.2±3.4	-0.6±2.7	3.8±3.4	-0.8±2.7	$-0.86^{+0.19}_{-0.14}$	$0.03^{+0.72}_{-0.75}$	$0.38^{+1.07}_{-0.76}$	-	-	0.2	36.6
20	≤1.0	-	-	-	-	-	-	-	-	-	-	-	1.8	≤36.2
21	29.8±6.8	0.4±2.3	14.2±5.0	14.5±5.1	15.3±5.2	9.3±4.3	20.9±5.9	$0.28^{+0.19}_{-0.18}$	$-0.97^{+0.49}_{-0.81}$	$0.01^{+0.18}_{-0.16}$	N	N	1.1	37.7
22	≤1.6	-	-	-	-	-	-	-	-	-	-	-	0.2	≤36.4
23	≤12.2	-	-	-	-	-	-	-	-	-	-	-	0.3	≤37.3
24	≤1.4	-	-	-	-	-	-	-	-	-	-	-	2.3	≤36.3
25	174.9±16.7	53.1±8.4	103.3±11.3	156.5±13.6	18.9±5.7	139.1±12.9	25.6±6.4	$-0.73^{+0.04}_{-0.06}$	$-0.16^{+0.05}_{-0.10}$	$0.76^{+0.13}_{-0.10}$	N	N	10.4	38.4
26	≤5.7	-	-	-	-	-	-	-	-	-	-	-	1.5	≤36.9
27	137.3±13.0	42.1±7.6	69.5±9.5	111.6±11.7	25.7±6.4	91.4±10.7	33.2±7.1	$-0.53^{+0.06}_{-0.08}$	$-0.08^{+0.07}_{-0.11}$	$0.46^{+0.12}_{-0.08}$	N	N	4.7	38.3
28	22.4±7.4	2.1±2.9	12.3±4.8	14.3±5.2	7.6±4.3	15.1±5.2	7.1±4.3	$-0.43^{+0.21}_{-0.23}$	$-0.56^{+0.35}_{-0.49}$	$0.21^{+0.25}_{-0.21}$	N	N	0.5	37.5
29	15.0±5.5	3.0±3.2	7.1±4.0	10.0±4.6	5.0±3.8	9.8±4.4	5.8±4.0	$-0.34^{+0.26}_{-0.27}$	$-0.21^{+0.32}_{-0.41}$	$0.16^{+0.32}_{-0.29}$	-	-	0.5	37.4
30	36.2±7.4	9.3±4.3	26.1±6.3	35.5±7.1	0.7±2.9	33.0±6.9	3.6±3.6	$-0.85^{+0.08}_{-0.11}$	$-0.32^{+0.16}_{-0.16}$	$1.22^{+0.77}_{-0.46}$	N	P	1.3	37.8
31	≤2.1	-	-	-	-	-	-	-	-	-	-	-	1.3	≤36.5
32	≤11.1	-	-	-	-	-	-	-	-	-	-	-	0.5	≤37.2
33	≤8.0	-	-	-	-	-	-	-	-	-	-	-	0.5	≤37.1

Table 8—Continued

MID	Net Counts							HR	C21	C32	Variability			Log L_X
	B-band	S1-band	S2-band	S-band	H-band	Sc-band	Hc-band				BB	k-S	signif.	(erg s^{-1})
(1)	(2)	(3)	(4)	(5)	(6)	(7)	(8)	(9)	(10)	(11)	(12)	(13)	(14)	(15)
34	≤4.8	-	-	-	-	-	-	-	-	-	-	-	0.2	≤36.9
35	10.9±5.1	2.1±2.9	4.4±3.6	6.5±4.1	4.4±3.8	5.5±3.8	4.8±4.0	$-0.21^{+0.40}_{-0.37}$	$-0.16^{+0.45}_{-0.54}$	$0.03^{+0.43}_{-0.41}$	-	-	1.0	37.2
36	≤10.3	-	-	-	-	-	-	-	-	-	-	-	2.4	≤37.2
37	18.1±5.9	3.1±3.2	11.2±4.7	14.2±5.2	3.9±3.6	10.9±4.7	6.6±4.1	$-0.32^{+0.24}_{-0.26}$	$-0.40^{+0.29}_{-0.38}$	$0.43^{+0.37}_{-0.30}$	-	-	1.0	37.4
38	≤4.0	-	-	-	-	-	-	-	-	-	-	-	0.6	≤36.8
39	8.7±4.7	5.9±3.8	1.0±2.7	6.9±4.1	1.8±3.2	5.8±3.8	2.7±3.4	$-0.51^{+0.25}_{-0.33}$	$0.69^{+0.69}_{-0.46}$	$-0.15^{+0.84}_{-0.84}$	-	-	0.1	37.1
40	≤2.4	-	-	-	-	-	-	-	-	-	-	-	1.3	≤36.6
41	143.6±13.2	53.5±8.5	63.8±9.1	117.3±12.0	26.4±6.5	99.1±11.1	30.1±6.8	$-0.59^{+0.06}_{-0.08}$	$0.04^{+0.07}_{-0.09}$	$0.41^{+0.11}_{-0.09}$	N	N	1.4	38.3
42	269.0±17.6	64.2±9.1	164.8±13.9	229.0±16.2	40.0±7.6	195.0±15.0	60.5±9.0	$-0.58^{+0.04}_{-0.06}$	$-0.28^{+0.04}_{-0.09}$	$0.67^{+0.06}_{-0.10}$	N	N	5.9	38.6
43	≤2.4	-	-	-	-	-	-	-	-	-	-	-	0.0	≤36.6
44	≤1.9	-	-	-	-	-	-	-	-	-	-	-	0.7	≤36.4
45	≤2.9	-	-	-	-	-	-	-	-	-	-	-	1.5	≤36.6
46	≤2.1	-	-	-	-	-	-	-	-	-	-	-	2.4	≤36.5
47	43.6±8.1	12.4±4.8	20.1±5.8	32.5±7.1	11.1±4.8	28.4±6.6	12.8±5.1	$-0.44^{+0.14}_{-0.15}$	$-0.10^{+0.17}_{-0.16}$	$0.28^{+0.19}_{-0.17}$	N	N	0.7	37.8
48	≤2.9	-	-	-	-	-	-	-	-	-	-	-	1.5	≤36.6
49	9.1±5.0	0.7±2.7	0.9±2.9	1.6±3.4	7.5±4.3	1.9±3.2	6.9±4.3	$0.60^{+0.40}_{-0.22}$	$0.00^{+0.99}_{-0.92}$	$-0.61^{+0.46}_{-0.77}$	-	-	1.0	37.1
50	≤3.8	-	-	-	-	-	-	-	-	-	-	-	4.3	≤36.8
51	≤5.8	-	-	-	-	-	-	-	-	-	-	-	0.4	≤36.9
52	23.3±7.6	2.4±3.2	13.8±5.0	16.3±5.4	6.9±4.1	11.2±4.7	10.7±4.7	$-0.10^{+0.22}_{-0.24}$	$-0.56^{+0.35}_{-0.49}$	$0.32^{+0.24}_{-0.21}$	N	N	2.8	37.5
53	43.1±8.2	15.1±5.2	23.6±6.2	38.7±7.6	4.4±3.8	33.8±7.1	6.1±4.1	$-0.74^{+0.11}_{-0.13}$	$-0.06^{+0.14}_{-0.17}$	$0.73^{+0.32}_{-0.29}$	N	N	0.3	37.8
54	7.4±4.7	4.6±3.6	4.1±3.6	8.7±4.6	-1.2±2.3	7.8±4.3	-0.7±2.7	$-0.94^{+0.09}_{-0.06}$	$0.16^{+0.40}_{-0.37}$	$0.76^{+1.07}_{-0.61}$	-	-	0.7	37.0
55	50.0±8.4	18.4±5.4	28.7±6.5	47.2±8.1	2.8±3.4	38.8±7.4	8.5±4.4	$-0.68^{+0.10}_{-0.12}$	$-0.07^{+0.13}_{-0.13}$	$0.95^{+0.47}_{-0.33}$	N	N	1.1	37.9
56	9.0±5.0	1.5±2.9	4.0±3.6	5.5±4.1	3.5±3.6	5.5±4.0	4.1±3.8	$-0.26^{+0.39}_{-0.42}$	$-0.19^{+0.54}_{-0.75}$	$0.08^{+0.51}_{-0.48}$	-	-	0.7	37.1
57	≤33.1	-	-	-	-	-	-	-	-	-	-	-	1.0	≤37.7
58	10.2±6.0	-0.7±2.3	6.2±3.8	5.5±4.0	4.9±3.8	6.5±4.0	4.8±3.8	$-0.25^{+0.34}_{-0.34}$	$-0.76^{+0.45}_{-1.00}$	$0.13^{+0.33}_{-0.29}$	-	-	0.3	37.2
59	9.2±5.4	2.6±3.4	7.9±4.4	10.5±5.1	-1.3±2.7	9.0±4.7	0.2±3.2	$-0.90^{+0.12}_{-0.10}$	$-0.29^{+0.40}_{-0.57}$	$0.99^{+0.92}_{-0.53}$	-	-	0.7	37.1
60	30.9±7.4	11.0±4.7	14.9±5.3	26.0±6.6	4.9±4.0	24.3±6.4	5.5±4.1	$-0.70^{+0.16}_{-0.16}$	$-0.02^{+0.19}_{-0.19}$	$0.48^{+0.35}_{-0.27}$	N	N	0.3	37.7
61	≤3.1	-	-	-	-	-	-	-	-	-	-	-	0.3	≤36.7
62	50.4±8.6	11.1±4.7	28.0±6.5	39.0±7.6	11.4±4.8	33.7±7.1	14.7±5.3	$-0.46^{+0.12}_{-0.14}$	$-0.28^{+0.16}_{-0.16}$	$0.41^{+0.18}_{-0.15}$	N	N	2.0	37.9
63	≤10.9	-	-	-	-	-	-	-	-	-	-	-	1.7	≤37.2
64	44.7±8.1	6.8±4.0	27.1±6.5	33.9±7.1	10.8±4.7	27.8±6.5	16.4±5.4	$-0.33^{+0.14}_{-0.15}$	$-0.46^{+0.17}_{-0.21}$	$0.42^{+0.17}_{-0.16}$	N	N	1.4	37.8
65	≤5.6	-	-	-	-	-	-	-	-	-	-	-	0.9	≤36.9
66	30.7±7.3	3.8±3.6	17.9±5.7	21.7±6.3	9.1±4.6	18.9±5.9	12.5±5.1	$-0.27^{+0.17}_{-0.20}$	$-0.51^{+0.27}_{-0.38}$	$0.32^{+0.22}_{-0.19}$	N	N	0.5	37.7

Table 8—Continued

MID	Net Counts							HR	C21	C32	Variability			Log L_X
	B-band	S1-band	S2-band	S-band	H-band	Sc-band	Hc-band				BB	k-S	signif.	(erg s^{-1})
(1)	(2)	(3)	(4)	(5)	(6)	(7)	(8)	(9)	(10)	(11)	(12)	(13)	(14)	(15)
67	219.0±16.1	39.3±7.5	126.3±12.5	165.5±14.2	51.6±8.4	137.5±13.0	69.1±9.5	$-0.40^{+0.05}_{-0.07}$	$-0.37^{+0.06}_{-0.10}$	$0.41^{+0.09}_{-0.05}$	N	N	1.0	38.5
68	≤19.8	-	-	-	-	-	-	-	-	-	-	-	0.5	≤37.5
69	≤4.3	-	-	-	-	-	-	-	-	-	-	-	0.5	≤36.8
70	1516.4±40.1	364.4±20.3	870.4±30.7	1234.8±36.4	275.7±17.8	1068.1±33.9	379.8±20.7	$-0.53^{+0.02}_{-0.03}$	$-0.28^{+0.04}_{-0.02}$	$0.54^{+0.02}_{-0.04}$	V	V	8.6	39.4
71	≤28.3	-	-	-	-	-	-	-	-	-	-	-	0.9	≤37.6
72	31.4±7.4	8.6±4.4	12.0±5.0	20.6±6.2	10.8±4.8	12.0±5.1	14.2±5.3	$0.01^{+0.21}_{-0.24}$	$-0.03^{+0.22}_{-0.21}$	$0.08^{+0.21}_{-0.21}$	N	N	0.6	37.7
73	≤24.2	-	-	-	-	-	-	-	-	-	-	-	0.1	≤37.6
74	147.5±13.7	33.0±7.4	83.9±10.7	116.9±12.6	23.0±6.3	101.6±11.7	30.6±7.1	$-0.58^{+0.06}_{-0.07}$	$-0.28^{+0.10}_{-0.08}$	$0.59^{+0.11}_{-0.10}$	N	N	0.1	38.3
75	58.3±9.4	24.6±6.7	23.2±6.5	47.8±8.8	5.6±4.0	46.0±8.4	5.4±4.2	$-0.80^{+0.08}_{-0.10}$	$0.13^{+0.14}_{-0.12}$	$0.58^{+0.26}_{-0.18}$	N	N	1.2	37.9
76	≤1.7	-	-	-	-	-	-	-	-	-	-	-	0.3	≤36.4
77	90.0±11.2	16.7±6.0	54.0±9.0	70.7±10.4	12.2±5.1	59.8±9.6	18.2±5.9	$-0.58^{+0.08}_{-0.09}$	$-0.35^{+0.12}_{-0.13}$	$0.68^{+0.12}_{-0.17}$	N	N	0.1	38.1
78	≤22.9	-	-	-	-	-	-	-	-	-	-	-	2.1	≤37.5
79	≤1.0	-	-	-	-	-	-	-	-	-	-	-	0.2	≤36.2
80	≤15.0	-	-	-	-	-	-	-	-	-	-	-	0.9	≤37.4
81	148.3±13.5	46.1±8.1	79.6±10.2	125.7±12.5	20.9±5.9	107.0±11.6	30.4±6.8	$-0.61^{+0.06}_{-0.07}$	$-0.10^{+0.06}_{-0.10}$	$0.59^{+0.13}_{-0.09}$	N	N	1.3	38.3
82	93.1±10.9	21.5±6.0	53.9±8.6	75.4±10.1	14.7±5.1	61.6±9.2	23.4±6.1	$-0.51^{+0.08}_{-0.10}$	$-0.25^{+0.09}_{-0.13}$	$0.60^{+0.12}_{-0.14}$	N	N	2.8	38.1
83	26.9±6.6	6.3±4.0	15.6±5.3	21.9±6.2	3.0±3.2	18.7±5.8	5.5±3.8	$-0.58^{+0.14}_{-0.18}$	$-0.24^{+0.19}_{-0.22}$	$0.67^{+0.32}_{-0.24}$	N	N	1.2	37.6
84	≤14.2	-	-	-	-	-	-	-	-	-	-	-	2.2	≤37.3
85	38.4±7.7	11.4±4.7	16.5±5.3	27.9±6.6	10.4±4.7	25.2±6.3	11.0±4.8	$-0.46^{+0.15}_{-0.16}$	$-0.04^{+0.16}_{-0.18}$	$0.22^{+0.19}_{-0.18}$	N	N	4.9	37.8
86	371.4±20.6	83.1±10.4	188.7±14.9	271.8±17.7	99.7±11.1	240.9±16.7	121.1±12.2	$-0.40^{+0.05}_{-0.05}$	$-0.24^{+0.06}_{-0.06}$	$0.30^{+0.06}_{-0.04}$	N	N	3.6	38.7
87	43.5±9.1	8.4±4.6	29.4±6.8	37.8±7.8	6.8±4.2	27.5±6.9	14.4±5.3	$-0.39^{+0.14}_{-0.17}$	$-0.40^{+0.19}_{-0.24}$	$0.64^{+0.25}_{-0.18}$	N	N	0.2	37.8
88	18.8±6.1	3.2±3.4	14.3±5.1	17.5±5.7	1.4±3.2	15.4±5.3	4.1±3.8	$-0.67^{+0.19}_{-0.21}$	$-0.48^{+0.32}_{-0.41}$	$0.83^{+0.73}_{-0.40}$	-	-	1.9	37.5
89	≤1.1	-	-	-	-	-	-	-	-	-	-	-	0.2	≤36.2
90	83.5±10.4	13.6±5.0	54.0±8.5	67.6±9.4	15.9±5.3	55.7±8.6	23.8±6.2	$-0.46^{+0.09}_{-0.11}$	$-0.46^{+0.11}_{-0.16}$	$0.56^{+0.14}_{-0.12}$	N	P	1.0	38.1
91	≤1.4	-	-	-	-	-	-	-	-	-	-	-	0.1	≤36.3
92	≤3.3	-	-	-	-	-	-	-	-	-	-	-	0.9	≤36.7
93	14.3±5.7	2.4±3.4	8.7±4.3	11.0±5.0	3.2±3.6	11.1±4.8	3.1±3.6	$-0.68^{+0.14}_{-0.22}$	$-0.35^{+0.38}_{-0.59}$	$0.40^{+0.49}_{-0.35}$	-	-	2.9	37.3
94	5.4±4.6	4.8±3.8	1.0±2.9	5.8±4.3	-0.5±2.7	4.1±3.8	-0.9±2.7	$-0.86^{+0.19}_{-0.14}$	$0.54^{+0.83}_{-0.54}$	$0.23^{+1.15}_{-0.92}$	-	-	0.1	36.9
95	10.4±5.3	2.6±3.4	6.6±4.0	9.2±4.7	1.2±3.2	8.2±4.4	1.9±3.4	$-0.75^{+0.18}_{-0.25}$	$-0.21^{+0.40}_{-0.57}$	$0.54^{+0.77}_{-0.46}$	-	-	0.5	37.2
96	≤3.1	-	-	-	-	-	-	-	-	-	-	-	1.1	≤36.7
97	≤10.1	-	-	-	-	-	-	-	-	-	-	-	1.3	≤37.2
98	16.8±5.7	5.0±3.6	9.9±4.4	14.9±5.2	1.9±3.2	13.9±5.0	3.4±3.6	$-0.70^{+0.18}_{-0.20}$	$-0.16^{+0.24}_{-0.27}$	$0.62^{+0.61}_{-0.41}$	-	-	1.4	37.4
99	19.6±6.1	2.5±3.2	14.7±5.1	17.1±5.6	2.5±3.4	16.2±5.3	2.3±3.4	$-0.84^{+0.10}_{-0.16}$	$-0.56^{+0.32}_{-0.49}$	$0.70^{+0.56}_{-0.35}$	-	-	3.7	37.5

Table 8—Continued

MID	Net Counts							HR	C21	C32	Variability			Log L_X
	B-band	S1-band	S2-band	S-band	H-band	Sc-band	Hc-band				BB	k-S	signif.	(erg s^{-1})
(1)	(2)	(3)	(4)	(5)	(6)	(7)	(8)	(9)	(10)	(11)	(12)	(13)	(14)	(15)
100	19.5±6.1	22.5±6.0	-0.3±2.3	22.2±6.1	-2.7±1.9	10.1±4.6	-3.1±1.9	$-0.99^{+0.04}_{-0.01}$	$1.53^{+0.92}_{-0.46}$	$0.23^{+1.22}_{-1.07}$	-	-	2.7	37.5
101	6.7±4.6	-0.6±2.3	0.7±2.7	0.1±2.9	6.6±4.1	-1.1±2.3	7.4±4.3	$0.94^{+0.06}_{-0.10}$	$-0.15^{+0.99}_{-1.07}$	$-0.61^{+0.46}_{-0.84}$	-	-	1.2	37.0
102	332.5±19.5	144.0±13.1	144.3±13.2	288.3±18.1	44.1±7.9	236.7±16.5	61.5±9.1	$-0.64^{+0.05}_{-0.04}$	$0.10^{+0.06}_{-0.04}$	$0.53^{+0.09}_{-0.06}$	N	N	1.9	38.7
103	127.1±13.4	35.4±7.1	77.7±10.0	113.1±11.9	14.7±5.2	93.1±10.8	28.5±6.6	$-0.59^{+0.07}_{-0.08}$	$-0.22^{+0.08}_{-0.10}$	$0.77^{+0.12}_{-0.14}$	N	P	1.3	38.3
104	≤7.8	-	-	-	-	-	-	-	-	-	-	-	0.8	≤37.1
105	≤16.7	-	-	-	-	-	-	-	-	-	-	-	2.0	≤37.4
106	51.1±9.2	19.7±5.7	28.8±6.6	48.4±8.3	1.5±3.2	41.5±7.7	6.2±4.1	$-0.78^{+0.10}_{-0.11}$	$-0.06^{+0.15}_{-0.11}$	$1.13^{+0.69}_{-0.40}$	N	N	2.6	37.9
107	≤2.1	-	-	-	-	-	-	-	-	-	-	-	0.7	≤36.5
108	≤11.3	-	-	-	-	-	-	-	-	-	-	-	1.6	≤37.2
109	21.7±6.1	0.2±2.3	12.0±4.7	12.2±4.8	9.5±4.4	7.7±4.1	13.4±5.0	$0.19^{+0.23}_{-0.23}$	$-0.99^{+0.46}_{-0.84}$	$0.13^{+0.19}_{-0.18}$	N	N	2.1	37.5
110	20.9±6.1	4.0±3.4	9.6±4.4	13.6±5.1	7.3±4.1	11.5±4.7	9.9±4.6	$-0.16^{+0.23}_{-0.23}$	$-0.24^{+0.27}_{-0.32}$	$0.13^{+0.25}_{-0.21}$	N	N	0.5	37.5
111	≤13.5	-	-	-	-	-	-	-	-	-	-	-	1.1	≤37.3
112	9.1±4.7	1.5±2.7	6.1±3.8	7.6±4.1	1.5±3.2	8.1±4.1	1.3±3.2	$-0.82^{+0.16}_{-0.18}$	$-0.40^{+0.43}_{-0.54}$	$0.48^{+0.70}_{-0.45}$	-	-	0.3	37.1
113	7.7±4.6	4.0±3.4	0.9±2.7	4.9±3.8	2.7±3.4	4.8±3.6	2.4±3.4	$-0.51^{+0.23}_{-0.29}$	$0.53^{+0.77}_{-0.53}$	$-0.23^{+0.69}_{-0.92}$	-	-	0.3	37.1
114	8.1±4.6	2.2±2.9	7.1±4.0	9.3±4.4	-1.2±2.3	9.1±4.3	-0.5±2.7	$-0.95^{+0.08}_{-0.05}$	$-0.32^{+0.35}_{-0.46}$	$0.99^{+1.00}_{-0.46}$	-	-	1.5	37.1
115	≤1.0	-	-	-	-	-	-	-	-	-	-	-	0.1	≤36.2
116	18.4±5.8	10.2±4.4	8.9±4.3	19.1±5.7	-0.7±2.3	17.0±5.3	-0.2±2.7	$-0.98^{+0.05}_{-0.02}$	$0.16^{+0.22}_{-0.19}$	$1.07^{+0.92}_{-0.54}$	-	-	0.5	37.4
117	10.7±5.0	5.2±3.6	1.9±2.9	7.2±4.1	3.6±3.6	4.1±3.4	4.2±3.8	$-0.11^{+0.45}_{-0.41}$	$0.46^{+0.56}_{-0.41}$	$-0.19^{+0.59}_{-0.64}$	-	-	2.0	37.2
118	≤2.2	-	-	-	-	-	-	-	-	-	-	-	0.6	≤36.5
119	26.3±6.6	5.4±3.6	16.9±5.3	22.3±6.0	4.0±3.6	19.8±5.7	6.7±4.1	$-0.56^{+0.17}_{-0.18}$	$-0.38^{+0.22}_{-0.21}$	$0.62^{+0.35}_{-0.27}$	N	N	0.5	37.6
120	102.1±11.5	57.2±8.7	41.2±7.6	98.4±11.1	3.7±3.8	92.9±10.8	3.2±3.8	$-0.95^{+0.02}_{-0.05}$	$0.26^{+0.10}_{-0.08}$	$1.03^{+0.40}_{-0.33}$	N	N	0.8	38.2
121	63.9±9.3	18.5±5.6	30.2±6.6	48.7±8.2	15.2±5.2	41.2±7.5	19.0±5.7	$-0.44^{+0.11}_{-0.12}$	$-0.13^{+0.18}_{-0.08}$	$0.33^{+0.14}_{-0.15}$	N	N	0.4	38.0
122	≤8.6	-	-	-	-	-	-	-	-	-	-	-	0.1	≤37.1
123	≤7.2	-	-	-	-	-	-	-	-	-	-	-	0.5	≤37.0
124	≤5.1	-	-	-	-	-	-	-	-	-	-	-	0.7	≤36.9
125	23.8±6.3	2.1±2.9	15.2±5.1	17.3±5.4	6.6±4.0	14.8±5.1	9.4±4.4	$-0.29^{+0.19}_{-0.21}$	$-0.64^{+0.32}_{-0.49}$	$0.38^{+0.21}_{-0.22}$	N	N	0.5	37.8
126	≤9.6	-	-	-	-	-	-	-	-	-	-	-	1.8	≤37.2
127	≤12.3	-	-	-	-	-	-	-	-	-	-	-	0.0	≤37.3
128	9.1±4.4	5.7±3.6	2.4±2.9	8.1±4.1	1.0±2.7	4.6±3.4	1.8±2.9	$-0.58^{+0.21}_{-0.24}$	$0.43^{+0.43}_{-0.35}$	$0.23^{+0.76}_{-0.61}$	-	-	20.1	37.4
129	≤13.1	-	-	-	-	-	-	-	-	-	-	-	0.1	≤37.3
130	37.8±7.6	11.4±4.7	21.8±5.9	33.2±7.1	4.5±3.8	32.5±6.9	5.3±4.0	$-0.78^{+0.11}_{-0.12}$	$-0.11^{+0.15}_{-0.18}$	$0.67^{+0.32}_{-0.24}$	N	N	0.1	37.8
131	31.9±7.1	6.0±3.8	15.0±5.1	21.0±5.9	10.8±4.7	18.1±5.4	13.5±5.1	$-0.22^{+0.17}_{-0.19}$	$-0.27^{+0.22}_{-0.21}$	$0.16^{+0.18}_{-0.18}$	N	N	0.6	37.7
132	44.9±8.1	8.8±4.3	27.2±6.4	36.0±7.2	8.9±4.4	30.9±6.7	11.8±4.8	$-0.52^{+0.12}_{-0.14}$	$-0.32^{+0.16}_{-0.19}$	$0.51^{+0.16}_{-0.19}$	N	N	0.7	37.9

Table 8—Continued

MID	Net Counts							HR	C21	C32	Variability			Log L_X
	B-band	S1-band	S2-band	S-band	H-band	Sc-band	Hc-band				BB	k-S	signif.	(erg s^{-1})
(1)	(2)	(3)	(4)	(5)	(6)	(7)	(8)	(9)	(10)	(11)	(12)	(13)	(14)	(15)

Note. — Col. (1): Master ID, cols. (2)−(8): net counts, in each of the 7 energy bands (see Table 3 for definitions of these bands), col. (9): hardness ratio, cols. (10) and (11) color values, errors are given as 1σ, cols. (12) and (13): short-term variability, where (BB) indicate Bayesian block analysis and (K-S) indicates the Kolmogorov-Smirnov test, in both columns symbols indicate - (N) non-variable in all observations, (V) variable in at least one observation, (P) possible variability in at least one observation, col. (14): the significance of the change in L_X between the previous observation and the current observation respectively (equation 2), col. (15): log L_X (0.3−8.0 keV). Upper limit values of net B and L_X are at the 68% confidence level.

Table 9. Source counts, hardness ratios, color-color values and variability: Observation 4

MID	Net Counts							HR	C21	C32	Variability			Log L_X
	B-band	S1-band	S2-band	S-band	H-band	Sc-band	Hc-band				BB	k-S	signif.	(erg s^{-1})
(1)	(2)	(3)	(4)	(5)	(6)	(7)	(8)	(9)	(10)	(11)	(12)	(13)	(14)	(15)
1	24.3±7.2	7.7±4.3	13.3±5.2	21.0±6.3	3.3±4.3	16.0±5.6	5.5±4.7	$-0.65^{+0.21}_{-0.21}$	$-0.03^{+0.22}_{-0.24}$	$0.54^{+0.61}_{-0.35}$	N	N	2.7	37.6
2	≤16.1	-	-	-	-	-	-	-	-	-	-	-	0.3	≤37.4
3	≤10.8	-	-	-	-	-	-	-	-	-	-	-	0.8	≤37.2
4	≤0.8	-	-	-	-	-	-	-	-	-	-	-	0.3	≤36.1
5	≤2.4	-	-	-	-	-	-	-	-	-	-	-	0.7	≤36.6
6	≤2.5	-	-	-	-	-	-	-	-	-	-	-	0.4	≤36.6
7	≤8.3	-	-	-	-	-	-	-	-	-	-	-	0.9	≤37.1
8	≤0.7	-	-	-	-	-	-	-	-	-	-	-	2.1	≤36.0
9	244.4±16.8	56.1±8.6	147.9±13.2	204.0±15.4	40.3±7.6	172.8±14.2	62.0±9.1	$-0.59^{+0.04}_{-0.05}$	$-0.14^{+0.05}_{-0.08}$	$0.64^{+0.08}_{-0.08}$	N	N	7.0	38.6
10	≤17.1	-	-	-	-	-	-	-	-	-	-	-	2.4	≤37.4
11	36.1±7.6	7.7±4.1	24.5±6.2	32.2±7.0	3.9±3.8	26.0±6.4	7.4±4.4	$-0.62^{+0.14}_{-0.17}$	$-0.35^{+0.16}_{-0.21}$	$0.78^{+0.40}_{-0.30}$	N	N	0.4	37.7
12	≤9.2	-	-	-	-	-	-	-	-	-	-	-	1.0	≤37.1
13	14.5±5.8	0.6±2.7	7.0±4.1	7.6±4.4	6.9±4.4	7.7±4.3	7.3±4.6	$-0.13^{+0.33}_{-0.32}$	$-0.61^{+0.53}_{-0.77}$	$0.03^{+0.32}_{-0.27}$	-	-	0.7	37.3
14	≤16.4	-	-	-	-	-	-	-	-	-	-	-	2.3	≤37.4
15	≤10.0	-	-	-	-	-	-	-	-	-	-	-	0.8	≤37.1
16	25.3±6.6	11.3±4.6	7.3±4.1	18.5±5.7	6.7±4.1	16.5±5.3	6.2±4.1	$-0.53^{+0.19}_{-0.21}$	$0.29^{+0.22}_{-0.21}$	$0.05^{+0.30}_{-0.24}$	N	N	0.5	37.5
17	11.1±5.1	1.8±2.9	5.5±3.8	7.4±4.3	3.7±3.6	6.4±4.0	4.4±3.8	$-0.32^{+0.36}_{-0.35}$	$-0.27^{+0.46}_{-0.56}$	$0.19^{+0.43}_{-0.38}$	-	-	0.7	37.2
18	59.1±9.1	3.9±3.4	35.5±7.1	39.4±7.5	19.7±5.8	29.7±6.6	29.0±6.7	$-0.12^{+0.14}_{-0.12}$	$-0.78^{+0.26}_{-0.27}$	$0.31^{+0.13}_{-0.12}$	N	N	0.4	37.9
19	≤2.2	-	-	-	-	-	-	-	-	-	-	-	0.2	≤36.5
20	≤9.6	-	-	-	-	-	-	-	-	-	-	-	2.2	≤37.2
21	26.2±6.5	-0.6±1.9	7.3±4.0	6.6±4.0	19.5±5.7	3.3±3.2	23.3±6.1	$0.71^{+0.17}_{-0.14}$	$-1.07^{+0.61}_{-0.92}$	$-0.38^{+0.19}_{-0.18}$	N	N	0.2	37.7
22	≤5.5	-	-	-	-	-	-	-	-	-	-	-	0.6	≤36.9
23	12.9±5.2	1.0±2.7	1.9±2.9	2.9±3.4	10.0±4.6	2.9±3.2	10.6±4.7	$0.52^{+0.30}_{-0.26}$	$0.00^{+0.69}_{-0.92}$	$-0.56^{+0.37}_{-0.54}$	-	-	0.3	37.2
24	≤8.1	-	-	-	-	-	-	-	-	-	-	-	1.5	≤37.0
25	24.2±7.7	6.7±4.0	18.5±5.6	25.2±6.4	0.1±2.9	23.3±6.1	0.6±3.2	$-0.96^{+0.05}_{-0.04}$	$-0.32^{+0.19}_{-0.22}$	$1.15^{+0.84}_{-0.46}$	N	N	8.6	37.5
26	≤3.3	-	-	-	-	-	-	-	-	-	-	-	0.9	≤36.6
27	69.3±9.7	27.4±6.4	30.5±6.7	57.9±8.8	11.5±4.8	50.5±8.3	12.1±5.0	$-0.66^{+0.09}_{-0.11}$	$0.06^{+0.13}_{-0.10}$	$0.45^{+0.17}_{-0.15}$	N	N	5.2	38.0
28	21.2±7.4	1.6±2.9	16.3±5.3	17.9±5.7	4.0±3.8	16.1±5.3	5.4±4.1	$-0.58^{+0.21}_{-0.22}$	$-0.75^{+0.37}_{-0.62}$	$0.59^{+0.40}_{-0.30}$	N	N	0.5	37.4
29	15.5±5.6	5.1±3.6	7.9±4.1	13.0±5.0	2.5±3.4	10.9±4.6	4.2±3.8	$-0.55^{+0.25}_{-0.26}$	$-0.05^{+0.24}_{-0.30}$	$0.43^{+0.56}_{-0.38}$	-	-	0.3	37.3
30	36.8±7.6	6.8±4.0	25.5±6.3	32.4±7.0	4.5±3.8	28.6±6.5	7.9±4.4	$-0.62^{+0.13}_{-0.16}$	$-0.43^{+0.16}_{-0.21}$	$0.72^{+0.35}_{-0.24}$	N	N	1.2	37.7
31	≤9.3	-	-	-	-	-	-	-	-	-	-	-	1.5	≤37.1
32	≤3.2	-	-	-	-	-	-	-	-	-	-	-	1.8	≤36.6
33	7.6±4.6	3.3±3.2	5.6±3.8	8.9±4.4	-1.3±2.3	6.7±4.0	-0.8±2.7	$-0.94^{+0.11}_{-0.06}$	$-0.08^{+0.32}_{-0.38}$	$0.92^{+0.99}_{-0.54}$	-	-	0.3	37.0

Table 9—Continued

MID	Net Counts							HR	C21	C32	Variability			Log L_X
	B-band	S1-band	S2-band	S-band	H-band	Sc-band	Hc-band				BB	k-S	signif.	(erg s^{-1})
(1)	(2)	(3)	(4)	(5)	(6)	(7)	(8)	(9)	(10)	(11)	(12)	(13)	(14)	(15)
34	≤3.4	-	-	-	-	-	-	-	-	-	-	-	0.3	≤36.6
35	7.5±4.7	5.2±3.6	2.7±3.2	7.9±4.3	-0.4±2.9	7.7±4.1	0.2±3.2	$-0.89^{+0.14}_{-0.11}$	$0.35^{+0.48}_{-0.38}$	$0.38^{+1.07}_{-0.61}$	-	-	0.7	37.0
36	10.5±5.5	8.7±4.4	2.2±3.4	10.9±5.1	-0.4±2.9	5.0±4.1	0.1±3.2	$-0.80^{+0.22}_{-0.20}$	$0.59^{+0.62}_{-0.40}$	$0.38^{+1.07}_{-0.84}$	-	-	0.3	37.1
37	24.1±6.7	6.4±4.0	9.9±4.6	16.2±5.6	7.9±4.4	11.2±4.8	10.7±4.8	$-0.10^{+0.24}_{-0.24}$	$-0.08^{+0.24}_{-0.24}$	$0.13^{+0.25}_{-0.24}$	N	N	0.3	37.5
38	≤2.5	-	-	-	-	-	-	-	-	-	-	-	0.4	≤36.5
39	≤2.4	-	-	-	-	-	-	-	-	-	-	-	1.3	≤36.5
40	≤17.4	-	-	-	-	-	-	-	-	-	-	-	2.7	≤37.3
41	150.0±13.6	48.2±8.1	88.3±10.6	136.5±12.9	13.5±5.2	109.4±11.7	25.2±6.5	$-0.67^{+0.06}_{-0.07}$	$-0.13^{+0.06}_{-0.09}$	$0.83^{+0.14}_{-0.14}$	N	N	1.0	38.3
42	512.8±23.8	93.6±10.8	302.5±18.5	396.1±21.0	116.8±11.9	337.1±19.4	163.3±13.9	$-0.42^{+0.04}_{-0.04}$	$-0.38^{+0.03}_{-0.07}$	$0.45^{+0.05}_{-0.05}$	N	N	5.5	38.8
43	≤11.8	-	-	-	-	-	-	-	-	-	-	-	1.8	≤37.2
44	7.4±4.7	1.4±2.9	2.6±3.2	4.0±3.8	3.5±3.6	2.9±3.4	3.3±3.6	$-0.03^{+0.51}_{-0.53}$	$-0.08^{+0.69}_{-0.76}$	$-0.08^{+0.59}_{-0.56}$	-	-	1.0	37.0
45	22.8±6.5	3.5±3.4	13.4±5.0	16.9±5.6	5.9±4.1	15.8±5.3	6.8±4.3	$-0.48^{+0.21}_{-0.22}$	$-0.43^{+0.30}_{-0.35}$	$0.35^{+0.29}_{-0.24}$	N	N	2.6	37.5
46	≤5.6	-	-	-	-	-	-	-	-	-	-	-	0.9	≤36.8
47	72.1±10.0	20.4±5.8	38.8±7.5	59.2±9.0	12.9±5.1	47.0±8.1	19.5±5.9	$-0.48^{+0.11}_{-0.11}$	$-0.16^{+0.12}_{-0.12}$	$0.50^{+0.17}_{-0.14}$	V	N	1.4	38.0
48	11.5±5.4	2.1±3.2	6.0±4.0	8.1±4.6	3.4±3.6	6.0±4.1	5.0±4.0	$-0.18^{+0.38}_{-0.40}$	$-0.24^{+0.43}_{-0.62}$	$0.24^{+0.48}_{-0.40}$	-	-	1.3	37.2
49	≤1.1	-	-	-	-	-	-	-	-	-	-	-	1.6	≤36.1
50	≤3.3	-	-	-	-	-	-	-	-	-	-	-	0.2	≤36.6
51	≤6.7	-	-	-	-	-	-	-	-	-	-	-	0.0	≤36.9
52	10.0±6.1	3.6±3.4	6.1±4.0	9.7±4.7	0.3±2.9	6.8±4.1	0.0±2.9	$-0.89^{+0.14}_{-0.11}$	$-0.11^{+0.38}_{-0.37}$	$0.61^{+0.92}_{-0.46}$	-	-	1.6	37.1
53	37.2±9.6	7.8±4.3	27.1±6.5	34.9±7.4	2.8±3.6	30.5±6.9	7.0±4.4	$-0.68^{+0.13}_{-0.15}$	$-0.40^{+0.16}_{-0.22}$	$0.91^{+0.54}_{-0.32}$	N	N	1.0	37.7
54	14.6±5.9	3.4±3.6	5.9±4.1	9.3±5.0	5.3±4.0	8.2±4.6	5.7±4.1	$-0.28^{+0.33}_{-0.34}$	$-0.08^{+0.43}_{-0.51}$	$0.08^{+0.38}_{-0.35}$	-	-	0.7	37.3
55	48.9±8.5	18.4±5.6	28.5±6.5	46.9±8.1	2.0±3.4	35.8±7.2	5.8±4.1	$-0.77^{+0.11}_{-0.12}$	$-0.06^{+0.12}_{-0.15}$	$1.01^{+0.63}_{-0.37}$	N	N	0.8	37.8
56	11.8±5.5	5.1±3.8	4.0±3.8	9.1±4.8	2.7±3.4	4.7±4.0	3.9±3.8	$-0.18^{+0.43}_{-0.50}$	$0.19^{+0.45}_{-0.40}$	$0.16^{+0.64}_{-0.56}$	-	-	0.1	37.2
57	16.1±7.6	8.4±4.4	6.3±4.3	14.6±5.7	1.3±3.2	12.6±5.2	0.4±3.2	$-0.93^{+0.09}_{-0.07}$	$0.21^{+0.33}_{-0.29}$	$0.51^{+0.78}_{-0.54}$	N	N	2.1	37.3
58	19.6±7.3	9.3±4.4	7.4±4.1	16.7±5.6	2.6±3.4	15.0±5.2	2.2±3.4	$-0.84^{+0.10}_{-0.16}$	$0.21^{+0.22}_{-0.24}$	$0.40^{+0.57}_{-0.37}$	N	N	0.7	37.4
59	12.5±5.8	4.0±3.8	5.6±4.1	9.6±5.1	2.9±3.6	8.0±4.7	3.3±3.8	$-0.55^{+0.19}_{-0.32}$	$-0.03^{+0.43}_{-0.48}$	$0.27^{+0.59}_{-0.48}$	-	-	0.2	37.2
60	42.2±8.2	9.0±4.4	24.9±6.4	33.9±7.3	8.3±4.4	24.3±6.4	16.9±5.6	$-0.25^{+0.13}_{-0.19}$	$-0.32^{+0.19}_{-0.19}$	$0.48^{+0.22}_{-0.19}$	N	N	0.5	37.7
61	≤1.5	-	-	-	-	-	-	-	-	-	-	-	0.5	≤36.3
62	28.8±7.2	4.4±3.8	16.3±5.4	20.7±6.2	8.1±4.4	18.5±5.8	7.4±4.4	$-0.51^{+0.19}_{-0.20}$	$-0.40^{+0.27}_{-0.35}$	$0.32^{+0.24}_{-0.21}$	N	N	2.5	37.6
63	7.8±4.7	0.7±2.7	6.0±3.8	6.7±4.1	1.1±3.2	5.7±3.8	2.9±3.6	$-0.48^{+0.27}_{-0.34}$	$-0.53^{+0.53}_{-0.77}$	$0.51^{+0.78}_{-0.48}$	-	-	0.8	37.0
64	67.4±9.7	14.3±5.1	35.0±7.1	49.3±8.3	18.1±5.7	43.3±7.8	21.7±6.1	$-0.40^{+0.11}_{-0.12}$	$-0.25^{+0.14}_{-0.15}$	$0.32^{+0.13}_{-0.13}$	N	N	1.0	37.9
65	≤3.1	-	-	-	-	-	-	-	-	-	-	-	0.8	≤36.6
66	43.7±8.3	4.6±3.8	25.4±6.4	29.9±7.0	13.7±5.2	26.9±6.6	17.3±5.7	$-0.29^{+0.14}_{-0.17}$	$-0.61^{+0.27}_{-0.31}$	$0.28^{+0.18}_{-0.14}$	N	N	0.6	37.7

Table 9—Continued

MID	Net Counts							HR	C21	C32	Variability			Log L_X
	B-band	S1-band	S2-band	S-band	H-band	Sc-band	Hc-band				BB	k-S	signif.	(erg s^{-1})
(1)	(2)	(3)	(4)	(5)	(6)	(7)	(8)	(9)	(10)	(11)	(12)	(13)	(14)	(15)
67	243.2±16.9	49.7±8.4	143.4±13.2	193.1±15.3	46.3±8.1	170.0±14.3	66.7±9.5	$-0.50^{+0.06}_{-0.05}$	$-0.33^{+0.06}_{-0.08}$	$0.52^{+0.07}_{-0.07}$	N	N	0.7	38.5
68	≤5.8	-	-	-	-	-	-	-	-	-	-	-	2.2	≤36.9
69	≤4.3	-	-	-	-	-	-	-	-	-	-	-	0.1	≤36.7
70	1479.2±39.7	424.8±21.8	858.6±30.5	1283.4±37.0	192.2±15.0	1113.6±34.6	290.3±18.2	$-0.64^{+0.02}_{-0.02}$	$-0.20^{+0.03}_{-0.02}$	$0.68^{+0.04}_{-0.03}$	N	N	5.3	39.3
71	≤13.0	-	-	-	-	-	-	-	-	-	-	-	2.7	≤37.2
72	23.4±7.0	8.2±4.6	12.5±5.1	20.7±6.4	2.8±3.6	16.7±5.8	5.0±4.1	$-0.64^{+0.21}_{-0.21}$	$-0.05^{+0.21}_{-0.27}$	$0.59^{+0.56}_{-0.38}$	-	-	1.2	37.5
73	≤8.6	-	-	-	-	-	-	-	-	-	-	-	1.8	≤37.0
74	158.2±14.0	45.7±8.3	75.8±10.2	121.5±12.7	29.1±6.8	103.3±11.7	38.4±7.6	$-0.52^{+0.07}_{-0.07}$	$-0.12^{+0.11}_{-0.06}$	$0.45^{+0.10}_{-0.09}$	N	N	0.8	38.3
75	122.5±12.6	40.3±7.9	68.6±9.7	108.8±12.1	7.2±4.5	101.1±11.5	12.5±5.2	$-0.79^{+0.05}_{-0.07}$	$-0.09^{+0.07}_{-0.10}$	$0.92^{+0.18}_{-0.17}$	N	N	3.1	38.2
76	≤2.4	-	-	-	-	-	-	-	-	-	-	-	0.1	≤36.5
77	92.0±11.3	18.7±6.2	51.7±8.8	70.5±10.3	14.9±5.4	62.7±9.7	21.8±6.2	$-0.54^{+0.08}_{-0.10}$	$-0.27^{+0.11}_{-0.13}$	$0.59^{+0.11}_{-0.15}$	N	N	0.9	38.1
78	≤66.0	-	-	-	-	-	-	-	-	-	-	-	3.9	≤37.9
79	10.2±5.0	3.8±3.4	4.4±3.6	8.1±4.4	2.1±3.2	7.0±4.1	3.7±3.6	$-0.42^{+0.32}_{-0.34}$	$0.05^{+0.38}_{-0.40}$	$0.27^{+0.64}_{-0.48}$	-	-	1.8	37.1
80	23.7±6.4	8.4±4.3	13.0±5.0	21.4±6.1	1.9±2.9	19.9±5.9	2.6±3.2	$-0.82^{+0.10}_{-0.14}$	$-0.08^{+0.21}_{-0.19}$	$0.75^{+0.51}_{-0.35}$	N	N	0.7	37.5
81	208.5±15.8	69.6±9.6	111.1±11.8	180.7±14.7	26.2±6.5	161.0±14.0	34.8±7.2	$-0.69^{+0.05}_{-0.05}$	$-0.07^{+0.05}_{-0.09}$	$0.65^{+0.10}_{-0.09}$	N	N	1.4	38.4
82	170.9±14.4	33.5±7.2	90.9±10.7	124.4±12.5	44.7±7.8	108.8±11.7	59.1±8.9	$-0.37^{+0.06}_{-0.07}$	$-0.29^{+0.07}_{-0.11}$	$0.33^{+0.10}_{-0.06}$	N	N	3.1	38.3
83	38.1±7.5	7.0±4.1	22.7±6.1	29.6±6.9	5.5±3.8	23.4±6.3	9.1±4.4	$-0.49^{+0.13}_{-0.15}$	$-0.35^{+0.16}_{-0.19}$	$0.59^{+0.21}_{-0.19}$	N	N	0.5	37.7
84	14.5±5.8	5.5±4.0	6.9±4.1	12.4±5.2	2.1±3.4	9.0±4.6	1.5±3.4	$-0.82^{+0.16}_{-0.18}$	$0.03^{+0.29}_{-0.32}$	$0.43^{+0.67}_{-0.43}$	-	-	0.3	37.3
85	≤1.6	-	-	-	-	-	-	-	-	-	-	-	4.7	≤36.3
86	620.4±26.2	126.3±12.5	367.5±20.3	493.8±23.5	126.6±12.4	404.4±21.3	189.6±14.9	$-0.43^{+0.04}_{-0.04}$	$-0.34^{+0.03}_{-0.06}$	$0.50^{+0.04}_{-0.05}$	N	N	5.0	38.9
87	50.3±9.8	13.3±5.4	26.5±6.7	39.8±8.1	9.3±4.9	36.9±7.7	11.6±5.3	$-0.58^{+0.14}_{-0.13}$	$-0.19^{+0.19}_{-0.16}$	$0.48^{+0.22}_{-0.22}$	N	N	0.1	37.8
88	23.0±6.6	3.2±3.4	19.5±5.8	22.7±6.3	0.3±2.9	22.0±6.1	1.7±3.4	$-0.92^{+0.07}_{-0.08}$	$-0.62^{+0.30}_{-0.40}$	$1.15^{+0.84}_{-0.46}$	N	N	0.1	37.5
89	≤1.7	-	-	-	-	-	-	-	-	-	-	-	0.2	≤36.3
90	93.2±11.0	19.7±5.7	53.8±8.5	73.5±9.8	19.7±5.9	62.4±9.0	27.5±6.6	$-0.45^{+0.09}_{-0.09}$	$-0.31^{+0.11}_{-0.12}$	$0.46^{+0.14}_{-0.10}$	N	N	0.4	38.1
91	≤0.9	-	-	-	-	-	-	-	-	-	-	-	0.4	≤36.1
92	≤10.6	-	-	-	-	-	-	-	-	-	-	-	1.1	≤37.1
93	36.7±7.8	12.8±5.0	16.9±5.6	29.7±7.0	7.0±4.3	25.2±6.5	8.4±4.6	$-0.57^{+0.16}_{-0.17}$	$-0.01^{+0.17}_{-0.18}$	$0.40^{+0.24}_{-0.21}$	N	N	1.9	37.7
94	≤7.1	-	-	-	-	-	-	-	-	-	-	-	0.1	≤36.9
95	10.4±5.5	2.2±3.2	9.1±4.6	11.3±5.1	-0.9±2.9	9.9±4.7	-0.5±3.2	$-0.94^{+0.10}_{-0.06}$	$-0.40^{+0.40}_{-0.57}$	$0.92^{+0.91}_{-0.54}$	-	-	0.2	37.1
96	14.8±5.9	5.5±3.8	10.5±4.7	16.0±5.6	-1.2±2.9	10.3±4.7	2.4±3.8	$-0.75^{+0.16}_{-0.25}$	$-0.16^{+0.24}_{-0.27}$	$0.99^{+1.00}_{-0.46}$	-	-	1.6	37.3
97	≤4.7	-	-	-	-	-	-	-	-	-	-	-	1.1	≤36.8
98	21.9±6.3	3.8±3.4	11.8±4.7	15.6±5.3	6.3±4.1	10.7±4.6	10.0±4.7	$-0.11^{+0.24}_{-0.24}$	$-0.35^{+0.27}_{-0.32}$	$0.27^{+0.29}_{-0.22}$	N	N	0.2	37.5
99	27.8±6.8	7.4±4.1	19.7±5.7	27.1±6.5	0.7±2.9	24.0±6.2	1.3±3.2	$-0.95^{+0.07}_{-0.05}$	$-0.29^{+0.18}_{-0.22}$	$1.07^{+0.84}_{-0.38}$	N	N	0.4	37.6

Table 9—Continued

MID	Net Counts							HR	C21	C32	Variability			Log L_X
	B-band	S1-band	S2-band	S-band	H-band	Sc-band	Hc-band				BB	k-S	signif.	(erg s^{-1})
(1)	(2)	(3)	(4)	(5)	(6)	(7)	(8)	(9)	(10)	(11)	(12)	(13)	(14)	(15)
100	≤1.5	-	-	-	-	-	-	-	-	-	-	-	2.9	≤36.3
101	≤17.1	-	-	-	-	-	-	-	-	-	-	-	1.2	≤37.3
102	288.3±18.2	101.2±11.2	148.1±13.3	249.3±16.9	39.0±7.6	207.2±15.5	54.8±8.7	$-0.63^{+0.04}_{-0.05}$	$-0.07^{+0.07}_{-0.04}$	$0.62^{+0.07}_{-0.09}$	N	N	3.7	38.6
103	170.7±15.1	39.2±7.5	94.2±10.8	133.4±12.7	36.6±7.4	114.3±11.9	51.4±8.5	$-0.45^{+0.07}_{-0.07}$	$-0.25^{+0.08}_{-0.09}$	$0.44^{+0.10}_{-0.08}$	N	N	0.5	38.3
104	10.8±5.2	-0.4±2.3	7.3±4.1	6.9±4.3	4.0±3.8	5.2±3.8	5.3±4.1	$-0.10^{+0.41}_{-0.40}$	$-0.84^{+0.53}_{-0.92}$	$0.27^{+0.43}_{-0.35}$	-	-	0.2	37.1
105	≤4.5	-	-	-	-	-	-	-	-	-	-	-	2.3	≤36.8
106	44.7±8.6	13.6±5.0	30.6±6.7	44.1±7.9	0.4±2.9	36.7±7.3	2.2±3.4	$-0.94^{+0.06}_{-0.06}$	$-0.23^{+0.13}_{-0.16}$	$1.30^{+0.84}_{-0.38}$	N	N	1.1	37.8
107	≤1.1	-	-	-	-	-	-	-	-	-	-	-	0.4	≤36.2
108	≤10.8	-	-	-	-	-	-	-	-	-	-	-	0.4	≤37.1
109	7.2±4.9	0.6±2.7	4.5±3.6	5.1±4.0	2.1±3.6	5.0±3.8	2.7±3.8	$-0.47^{+0.25}_{-0.29}$	$-0.38^{+0.53}_{-0.84}$	$0.24^{+0.73}_{-0.51}$	-	-	2.1	37.0
110	22.0±6.4	3.0±3.4	11.8±4.7	14.8±5.3	7.2±4.3	12.0±4.8	8.8±4.6	$-0.24^{+0.24}_{-0.24}$	$-0.40^{+0.32}_{-0.46}$	$0.24^{+0.24}_{-0.24}$	N	N	0.3	37.4
111	≤12.3	-	-	-	-	-	-	-	-	-	-	-	0.6	≤37.2
112	8.6±4.9	1.5±2.9	5.6±3.8	7.2±4.3	1.4±3.2	5.0±3.8	1.3±3.2	$-0.70^{+0.23}_{-0.30}$	$-0.32^{+0.45}_{-0.67}$	$0.46^{+0.72}_{-0.49}$	-	-	0.3	37.0
113	7.0±4.7	3.4±3.4	3.6±3.4	6.9±4.3	0.0±2.9	7.0±4.1	-0.4±2.9	$-0.91^{+0.13}_{-0.09}$	$0.08^{+0.48}_{-0.46}$	$0.46^{+0.99}_{-0.54}$	-	-	0.3	36.9
114	≤4.4	-	-	-	-	-	-	-	-	-	-	-	0.8	≤36.7
115	≤1.4	-	-	-	-	-	-	-	-	-	-	-	0.1	≤36.2
116	36.7±7.6	15.1±5.1	19.3±5.7	34.4±7.1	2.4±3.4	28.6±6.5	5.8±4.1	$-0.72^{+0.13}_{-0.15}$	$0.00^{+0.15}_{-0.16}$	$0.81^{+0.61}_{-0.34}$	N	N	1.4	37.7
117	3.8±4.3	1.9±2.9	5.6±3.8	7.5±4.3	-3.7±1.9	6.3±4.0	-4.0±1.9	$-0.98^{+0.07}_{-0.02}$	$-0.27^{+0.43}_{-0.56}$	$1.07^{+1.07}_{-0.54}$	-	-	1.3	36.7
118	≤5.7	-	-	-	-	-	-	-	-	-	-	-	0.5	≤36.9
119	34.7±7.4	14.1±5.0	17.4±5.4	31.5±6.9	3.2±3.6	27.2±6.5	3.9±3.8	$-0.81^{+0.10}_{-0.13}$	$0.02^{+0.16}_{-0.15}$	$0.67^{+0.48}_{-0.29}$	N	N	0.3	37.6
120	114.7±12.2	66.9±9.4	48.1±8.2	115.0±12.0	-0.3±3.2	104.5±11.4	-1.2±3.2	$-0.99^{+0.01}_{-0.01}$	$0.26^{+0.09}_{-0.08}$	$1.83^{+0.59}_{-0.77}$	N	N	0.4	38.2
121	47.3±8.4	14.2±5.1	26.3±6.4	40.5±7.7	6.8±4.3	30.2±6.7	12.3±5.1	$-0.49^{+0.15}_{-0.13}$	$-0.22^{+0.22}_{-0.08}$	$0.57^{+0.27}_{-0.19}$	N	N	2.2	37.8
122	≤6.8	-	-	-	-	-	-	-	-	-	-	-	0.6	≤36.9
123	≤4.6	-	-	-	-	-	-	-	-	-	-	-	0.6	≤36.8
124	≤11.9	-	-	-	-	-	-	-	-	-	-	-	0.9	≤37.2
125	45.1±8.2	7.7±4.1	17.3±5.4	25.0±6.4	20.2±5.9	16.9±5.4	25.0±6.4	$0.13^{+0.15}_{-0.17}$	$-0.28^{+0.25}_{-0.16}$	$-0.07^{+0.19}_{-0.11}$	N	N	0.1	37.8
126	≤6.3	-	-	-	-	-	-	-	-	-	-	-	0.7	≤36.9
127	10.2±5.1	4.9±3.6	4.3±3.6	9.2±4.6	1.0±3.2	8.1±4.3	2.7±3.6	$-0.64^{+0.18}_{-0.20}$	$0.16^{+0.38}_{-0.35}$	$0.40^{+0.86}_{-0.53}$	-	-	0.6	37.1
128	≤7.9	-	-	-	-	-	-	-	-	-	-	-	1.2	≤37.0
129	5.8±4.9	-0.2±2.7	5.8±4.0	5.6±4.3	0.2±3.2	3.8±3.6	2.7±3.8	$-0.34^{+0.28}_{-0.41}$	$-0.53^{+0.53}_{-1.00}$	$0.61^{+0.84}_{-0.53}$	-	-	1.4	36.9
130	37.4±7.8	15.0±5.2	17.8±5.6	32.8±7.1	4.5±4.0	24.6±6.3	6.8±4.4	$-0.64^{+0.16}_{-0.17}$	$0.08^{+0.17}_{-0.16}$	$0.58^{+0.38}_{-0.28}$	N	N	0.6	37.7
131	15.4±5.7	7.5±4.1	6.5±4.0	14.0±5.2	1.3±3.2	12.4±4.8	1.8±3.4	$-0.85^{+0.13}_{-0.15}$	$0.19^{+0.24}_{-0.27}$	$0.51^{+0.75}_{-0.46}$	-	-	2.2	37.3
132	30.5±7.1	7.7±4.1	19.9±5.7	27.5±6.5	2.9±3.6	24.6±6.2	4.7±4.0	$-0.76^{+0.14}_{-0.14}$	$-0.21^{+0.16}_{-0.22}$	$0.78^{+0.51}_{-0.32}$	N	N	1.9	37.6

Table 9—Continued

MID	Net Counts							HR	C21	C32	Variability			Log L_X
	B-band	S1-band	S2-band	S-band	H-band	Sc-band	Hc-band				BB	k-S	signif.	(erg s^{-1})
(1)	(2)	(3)	(4)	(5)	(6)	(7)	(8)	(9)	(10)	(11)	(12)	(13)	(14)	(15)

Note. — Col. (1): Master ID, cols. (2)−(8): net counts, in each of the 7 energy bands (see Table 3 for definitions of these bands), col. (9): hardness ratio, cols. (10) and (11) color values, errors are given as 1σ, cols. (12) and (13): short-term variability, where (BB) indicate Bayesian block analysis and (K-S) indicates the Kolmogorov-Smirnov test, in both columns symbols indicate - (N) non-variable in all observations, (V) variable in at least one observation, (P) possible variability in at least one observation, col. (14): the significance of the change in L_X between the previous observation and the current observation respectively (equation 2), col. (15): log L_X (0.3−8.0 keV). Upper limit values of net B and L_X are at the 68% confidence level.

Table 10. Source counts, hardness ratios, color-color values and variability: Observation 5

MID	Net Counts							HR	C21	C32	Variability			Log L_X
	B-band	S1-band	S2-band	S-band	H-band	Sc-band	Hc-band				BB	k-S	signif.	(erg s^{-1})
(1)	(2)	(3)	(4)	(5)	(6)	(7)	(8)	(9)	(10)	(11)	(12)	(13)	(14)	(15)
1	≤16.3	-	-	-	-	-	-	-	-	-	-	-	0.3	≤37.5
2	11.7±5.2	0.9±2.7	8.3±4.3	9.2±4.6	2.5±3.4	9.6±4.4	3.0±3.6	$-0.66^{+0.15}_{-0.24}$	$-0.53^{+0.38}_{-0.77}$	$0.46^{+0.56}_{-0.38}$	-	-	0.5	37.3
3	≤10.1	-	-	-	-	-	-	-	-	-	-	-	0.0	≤37.2
4	≤2.0	-	-	-	-	-	-	-	-	-	-	-	0.6	≤36.5
5	≤1.7	-	-	-	-	-	-	-	-	-	-	-	0.2	≤36.4
6	≤5.4	-	-	-	-	-	-	-	-	-	-	-	0.5	≤36.9
7	≤8.0	-	-	-	-	-	-	-	-	-	-	-	0.2	≤37.1
8	≤14.7	-	-	-	-	-	-	-	-	-	-	-	3.2	≤37.3
9	302.9±18.8	83.9±10.4	182.5±14.6	266.5±17.5	36.5±7.5	237.5±16.5	54.7±8.9	$-0.68^{+0.03}_{-0.05}$	$-0.15^{+0.05}_{-0.07}$	$0.75^{+0.06}_{-0.10}$	N	N	2.9	38.7
10	≤3.0	-	-	-	-	-	-	-	-	-	-	-	2.4	≤36.7
11	34.4±7.3	10.1±4.4	20.7±5.8	30.8±6.8	3.6±3.6	27.7±6.5	6.2±4.1	$-0.69^{+0.13}_{-0.15}$	$-0.19^{+0.16}_{-0.16}$	$0.72^{+0.41}_{-0.26}$	N	N	0.2	37.7
12	≤13.7	-	-	-	-	-	-	-	-	-	-	-	1.3	≤37.4
13	≤11.4	-	-	-	-	-	-	-	-	-	-	-	0.2	≤37.2
14	≤13.3	-	-	-	-	-	-	-	-	-	-	-	0.2	≤37.3
15	≤5.1	-	-	-	-	-	-	-	-	-	-	-	0.6	≤36.9
16	≤13.5	-	-	-	-	-	-	-	-	-	-	-	1.1	≤37.3
17	14.9±5.6	3.8±3.4	6.0±3.8	9.8±4.6	5.1±4.0	6.8±4.0	5.9±4.1	$-0.17^{+0.33}_{-0.32}$	$-0.05^{+0.32}_{-0.35}$	$0.08^{+0.38}_{-0.29}$	-	-	0.6	37.3
18	60.1±9.4	9.3±4.6	37.6±7.4	46.8±8.3	13.2±5.3	38.4±7.5	18.3±6.0	$-0.42^{+0.12}_{-0.14}$	$-0.45^{+0.16}_{-0.20}$	$0.47^{+0.17}_{-0.14}$	N	N	0.7	38.0
19	≤1.5	-	-	-	-	-	-	-	-	-	-	-	0.2	≤36.3
20	≤4.6	-	-	-	-	-	-	-	-	-	-	-	0.8	≤36.8
21	40.1±8.2	2.7±3.4	19.3±5.7	21.9±6.2	18.2±6.0	15.0±5.2	24.7±6.6	$0.17^{+0.17}_{-0.17}$	$-0.65^{+0.34}_{-0.50}$	$0.04^{+0.15}_{-0.17}$	N	N	0.5	37.8
22	12.6±5.6	-0.8±2.3	4.0±3.6	3.1±3.8	9.5±4.7	4.6±3.8	9.1±4.7	$0.29^{+0.33}_{-0.35}$	$-0.61^{+0.61}_{-1.07}$	$-0.32^{+0.32}_{-0.38}$	-	-	1.1	37.3
23	9.0±5.4	3.0±3.4	1.2±2.9	4.2±4.0	4.8±4.3	2.1±3.2	4.2±4.3	$0.25^{+0.55}_{-0.25}$	$0.35^{+0.88}_{-0.64}$	$-0.38^{+0.62}_{-0.85}$	-	-	0.3	37.1
24	≤1.5	-	-	-	-	-	-	-	-	-	-	-	1.5	≤36.4
25	≤0.8	-	-	-	-	-	-	-	-	-	-	-	3.0	≤36.1
26	≤14.1	-	-	-	-	-	-	-	-	-	-	-	2.2	≤37.3
27	19.8±6.2	5.8±3.8	10.1±4.6	15.9±5.4	3.8±3.8	15.8±5.3	3.5±3.8	$-0.74^{+0.12}_{-0.19}$	$-0.11^{+0.22}_{-0.27}$	$0.40^{+0.43}_{-0.32}$	-	-	3.8	37.5
28	25.8±6.7	2.8±3.2	12.7±4.8	15.5±5.3	10.4±4.7	14.6±5.1	11.0±4.8	$-0.22^{+0.20}_{-0.22}$	$-0.48^{+0.32}_{-0.41}$	$0.12^{+0.20}_{-0.20}$	N	N	0.8	37.6
29	24.4±6.5	6.1±3.8	16.0±5.2	22.1±6.0	2.3±3.4	19.7±5.7	2.0±3.4	$-0.89^{+0.08}_{-0.11}$	$-0.29^{+0.21}_{-0.22}$	$0.75^{+0.59}_{-0.35}$	N	N	1.2	37.6
30	33.9±7.3	10.8±4.6	18.7±5.6	29.5±6.7	4.3±3.8	25.4±6.3	6.9±4.3	$-0.64^{+0.15}_{-0.16}$	$-0.12^{+0.18}_{-0.18}$	$0.62^{+0.35}_{-0.27}$	N	N	0.2	37.7
31	≤6.3	-	-	-	-	-	-	-	-	-	-	-	0.4	≤37.0
32	10.1±5.1	4.4±3.6	6.5±4.0	10.9±4.8	-0.9±2.7	10.1±4.6	0.8±3.2	$-0.89^{+0.12}_{-0.11}$	$-0.05^{+0.32}_{-0.33}$	$0.84^{+0.99}_{-0.46}$	-	-	1.3	37.2
33	≤3.6	-	-	-	-	-	-	-	-	-	-	-	0.5	≤36.7

Table 10—Continued

MID				Net Counts				HR	C21	C32	Variability			Log L_X
	B-band	S1-band	S2-band	S-band	H-band	Sc-band	Hc-band				BB	k-S	signif.	(erg s^{-1})
(1)	(2)	(3)	(4)	(5)	(6)	(7)	(8)	(9)	(10)	(11)	(12)	(13)	(14)	(15)
34	≤1.6	-	-	-	-	-	-	-	-	-	-	-	0.4	≤36.4
35	≤4.0	-	-	-	-	-	-	-	-	-	-	-	0.4	≤36.8
36	≤6.4	-	-	-	-	-	-	-	-	-	-	-	0.5	≤37.0
37	≤2.6	-	-	-	-	-	-	-	-	-	-	-	2.9	≤36.6
38	≤2.0	-	-	-	-	-	-	-	-	-	-	-	0.0	≤36.5
39	5.1±4.3	3.9±3.4	1.8±2.9	5.7±4.0	-0.6±2.7	5.5±3.8	-1.0±2.7	$-0.92^{+0.12}_{-0.08}$	$0.38^{+0.61}_{-0.51}$	$0.38^{+1.07}_{-0.76}$	-	-	0.6	36.9
40	6.2±4.6	1.4±2.9	4.2±3.6	5.6±4.1	0.6±2.9	4.5±3.8	1.3±3.2	$-0.65^{+0.25}_{-0.35}$	$-0.23^{+0.54}_{-0.69}$	$0.46^{+0.92}_{-0.54}$	-	-	1.5	37.0
41	200.0±15.4	67.2±9.4	109.1±11.6	176.4±14.4	23.6±6.2	149.4±13.4	33.4±7.1	$-0.68^{+0.04}_{-0.06}$	$-0.13^{+0.11}_{-0.03}$	$0.68^{+0.13}_{-0.08}$	N	N	3.6	38.5
42	331.5±19.4	74.0±9.7	196.1±15.1	270.1±17.5	61.4±9.0	235.3±16.4	88.8±10.6	$-0.51^{+0.04}_{-0.05}$	$-0.30^{+0.05}_{-0.07}$	$0.54^{+0.05}_{-0.07}$	N	N	3.8	38.7
43	≤1.6	-	-	-	-	-	-	-	-	-	-	-	2.2	≤36.4
44	9.9±5.1	3.5±3.4	4.4±3.6	8.0±4.4	1.9±3.4	5.8±4.0	2.7±3.6	$-0.53^{+0.22}_{-0.29}$	$0.03^{+0.40}_{-0.43}$	$0.27^{+0.72}_{-0.51}$	-	-	0.5	37.2
45	≤9.6	-	-	-	-	-	-	-	-	-	-	-	1.4	≤37.2
46	≤1.9	-	-	-	-	-	-	-	-	-	-	-	1.1	≤36.4
47	66.7±9.6	17.3±5.4	41.3±7.6	58.6±8.9	8.1±4.4	52.8±8.5	12.8±5.1	$-0.66^{+0.09}_{-0.10}$	$-0.22^{+0.11}_{-0.15}$	$0.72^{+0.21}_{-0.18}$	N	N	0.3	38.0
48	≤3.8	-	-	-	-	-	-	-	-	-	-	-	1.0	≤36.8
49	≤2.9	-	-	-	-	-	-	-	-	-	-	-	0.7	≤36.6
50	≤2.1	-	-	-	-	-	-	-	-	-	-	-	0.2	≤36.5
51	6.8±4.9	1.7±3.2	4.7±3.8	6.4±4.4	0.4±2.9	7.7±4.4	0.1±2.9	$-0.90^{+0.13}_{-0.10}$	$-0.19^{+0.51}_{-0.75}$	$0.53^{+0.92}_{-0.53}$	-	-	0.2	37.0
52	20.8±7.3	4.4±3.6	13.2±5.0	17.7±5.7	2.1±3.4	18.8±5.7	2.8±3.6	$-0.83^{+0.10}_{-0.07}$	$-0.32^{+0.24}_{-0.32}$	$0.70^{+0.64}_{-0.38}$	N	N	1.4	37.5
53	≤1.6	-	-	-	-	-	-	-	-	-	-	-	3.6	≤36.4
54	≤12.2	-	-	-	-	-	-	-	-	-	-	-	0.1	≤37.3
55	49.8±8.4	15.4±5.1	26.6±6.4	42.0±7.7	7.7±4.3	34.6±7.1	10.4±4.7	$-0.60^{+0.12}_{-0.13}$	$-0.10^{+0.12}_{-0.16}$	$0.58^{+0.18}_{-0.22}$	N	N	0.6	37.9
56	≤2.7	-	-	-	-	-	-	-	-	-	-	-	1.4	≤36.6
57	≤2.2	-	-	-	-	-	-	-	-	-	-	-	1.7	≤36.5
58	8.9±5.7	4.6±3.6	2.4±3.2	7.0±4.3	1.7±3.2	7.1±4.1	1.4±3.2	$-0.78^{+0.18}_{-0.22}$	$0.35^{+0.54}_{-0.46}$	$0.11^{+0.83}_{-0.70}$	-	-	0.9	37.1
59	25.4±6.9	4.6±3.8	15.1±5.3	19.7±6.1	5.7±4.1	16.8±5.7	6.3±4.3	$-0.54^{+0.21}_{-0.22}$	$-0.38^{+0.27}_{-0.32}$	$0.43^{+0.29}_{-0.27}$	N	V	1.7	37.6
60	26.8±7.2	6.2±4.1	16.3±5.6	22.5±6.5	4.3±4.0	18.0±5.9	7.8±4.6	$-0.48^{+0.21}_{-0.21}$	$-0.27^{+0.22}_{-0.29}$	$0.56^{+0.41}_{-0.29}$	N	N	1.0	37.6
61	≤4.1	-	-	-	-	-	-	-	-	-	-	-	0.7	≤36.8
62	36.8±7.8	6.9±4.1	23.5±6.2	30.4±7.0	6.3±4.3	28.7±6.7	7.9±4.6	$-0.63^{+0.14}_{-0.16}$	$-0.40^{+0.21}_{-0.22}$	$0.56^{+0.30}_{-0.21}$	N	P	1.2	37.7
63	≤4.0	-	-	-	-	-	-	-	-	-	-	-	0.5	≤36.8
64	34.9±7.4	8.6±4.3	18.5±5.6	27.1±6.5	7.8±4.3	23.1±6.1	9.5±4.6	$-0.48^{+0.15}_{-0.17}$	$-0.21^{+0.18}_{-0.19}$	$0.40^{+0.22}_{-0.19}$	N	N	1.8	37.7
65	≤3.3	-	-	-	-	-	-	-	-	-	-	-	0.1	≤36.7
66	26.1±7.0	8.7±4.4	14.7±5.3	23.4±6.5	2.7±3.6	18.4±5.9	7.3±4.4	$-0.51^{+0.19}_{-0.21}$	$-0.11^{+0.19}_{-0.21}$	$0.67^{+0.54}_{-0.38}$	N	N	1.2	37.6

Table 10—Continued

MID	Net Counts							HR	C21	C32	Variability			Log L_X
	B-band	S1-band	S2-band	S-band	H-band	Sc-band	Hc-band				BB	k-S	signif.	(erg s^{-1})
(1)	(2)	(3)	(4)	(5)	(6)	(7)	(8)	(9)	(10)	(11)	(12)	(13)	(14)	(15)
67	198.7±20.9	28.7±6.9	110.5±11.9	139.2±13.4	60.5±9.1	126.5±12.7	68.7±9.7	$-0.37^{+0.07}_{-0.07}$	$-0.46^{+0.09}_{-0.10}$	$0.28^{+0.09}_{-0.05}$	N	N	0.4	38.5
68	≤17.6	-	-	-	-	-	-	-	-	-	-	-	1.8	≤37.4
69	≤12.9	-	-	-	-	-	-	-	-	-	-	-	1.5	≤37.3
70	1053.9±33.7	292.6±18.3	596.5±25.7	889.1±31.1	156.7±13.7	776.7±29.1	221.5±16.1	$-0.61^{+0.02}_{-0.02}$	$-0.21^{+0.04}_{-0.02}$	$0.61^{+0.04}_{-0.03}$	N	N	4.6	39.2
71	≤14.6	-	-	-	-	-	-	-	-	-	-	-	0.6	≤37.3
72	≤20.5	-	-	-	-	-	-	-	-	-	-	-	0.0	≤37.5
73	≤10.9	-	-	-	-	-	-	-	-	-	-	-	0.4	≤37.2
74	580.7±25.5	170.5±14.3	343.4±19.8	513.9±24.0	62.8±9.2	453.6±22.6	99.6±11.3	$-0.68^{+0.03}_{-0.03}$	$-0.20^{+0.05}_{-0.03}$	$0.79^{+0.04}_{-0.08}$	N	N	15.7	38.9
75	46.0±8.2	17.7±6.1	16.7±6.0	34.5±8.1	-2.7±2.7	33.7±7.8	-4.0±2.7	$-0.99^{+0.02}_{-0.01}$	$0.13^{+0.14}_{-0.13}$	$1.18^{+0.77}_{-0.42}$	N	N	4.4	37.8
76	≤5.2	-	-	-	-	-	-	-	-	-	-	-	0.6	≤36.9
77	71.7±10.1	14.8±5.6	30.5±7.3	45.4±8.7	19.4±5.9	40.7±8.3	21.0±6.1	$-0.40^{+0.10}_{-0.13}$	$-0.16^{+0.11}_{-0.17}$	$0.25^{+0.12}_{-0.14}$	N	N	0.5	38.0
78	≤32.7	-	-	-	-	-	-	-	-	-	-	-	2.5	≤37.7
79	≤1.1	-	-	-	-	-	-	-	-	-	-	-	1.8	≤36.2
80	≤14.8	-	-	-	-	-	-	-	-	-	-	-	0.8	≤37.3
81	177.5±14.6	55.4±8.7	95.9±11.0	151.3±13.6	20.8±6.0	140.6±13.2	24.4±6.4	$-0.73^{+0.04}_{-0.06}$	$-0.09^{+0.05}_{-0.09}$	$0.69^{+0.09}_{-0.12}$	N	N	0.1	38.4
82	151.9±13.6	36.5±7.3	85.3±10.4	121.8±12.3	28.1±6.6	108.3±11.7	39.1±7.5	$-0.53^{+0.06}_{-0.07}$	$-0.24^{+0.09}_{-0.09}$	$0.53^{+0.09}_{-0.10}$	N	N	0.3	38.3
83	43.1±8.1	9.9±4.6	27.1±6.5	36.9±7.5	6.3±4.0	32.3±7.1	9.3±4.4	$-0.61^{+0.12}_{-0.13}$	$-0.32^{+0.16}_{-0.19}$	$0.64^{+0.22}_{-0.21}$	N	N	1.0	37.8
84	17.6±6.1	1.8±3.2	16.0±5.3	17.8±5.8	-0.2±2.9	16.9±5.6	1.4±3.4	$-0.91^{+0.09}_{-0.09}$	$-0.67^{+0.38}_{-0.62}$	$1.07^{+0.92}_{-0.38}$	-	-	0.7	37.4
85	≤1.6	-	-	-	-	-	-	-	-	-	-	-	0.1	≤36.4
86	352.4±20.2	81.6±10.3	205.0±15.5	286.6±18.2	65.8±9.5	247.4±17.0	97.8±11.2	$-0.50^{+0.05}_{-0.05}$	$-0.27^{+0.04}_{-0.07}$	$0.54^{+0.06}_{-0.07}$	N	N	6.0	38.7
87	43.7±8.0	12.4±5.0	23.5±6.2	35.9±7.5	4.5±3.8	34.4±7.2	7.4±4.3	$-0.66^{+0.10}_{-0.13}$	$-0.14^{+0.14}_{-0.16}$	$0.64^{+0.25}_{-0.21}$	N	N	0.0	37.8
88	17.5±6.0	11.1±4.7	7.0±4.1	18.1±5.8	-0.7±2.7	17.2±5.6	-1.0±2.7	$-0.98^{+0.04}_{-0.02}$	$0.29^{+0.25}_{-0.21}$	$0.84^{+0.99}_{-0.46}$	-	-	0.3	37.4
89	97.6±12.8	27.1±6.5	47.2±8.1	74.3±10.0	23.7±6.3	57.7±8.9	27.4±6.6	$-0.42^{+0.09}_{-0.11}$	$-0.11^{+0.10}_{-0.12}$	$0.32^{+0.14}_{-0.09}$	N	N	7.4	38.2
90	71.2±9.7	13.4±4.8	38.6±7.4	52.0±8.4	19.3±5.7	42.8±7.7	24.8±6.3	$-0.34^{+0.10}_{-0.13}$	$-0.32^{+0.11}_{-0.17}$	$0.30^{+0.17}_{-0.08}$	N	N	0.4	38.0
91	≤0.8	-	-	-	-	-	-	-	-	-	-	-	0.0	≤36.1
92	≤1.3	-	-	-	-	-	-	-	-	-	-	-	1.9	≤36.3
93	26.6±7.0	6.2±4.1	12.4±5.0	18.7±6.0	7.9±4.4	16.1±5.6	9.5±4.7	$-0.34^{+0.20}_{-0.22}$	$-0.16^{+0.24}_{-0.27}$	$0.21^{+0.25}_{-0.21}$	N	N	0.5	37.6
94	≤4.0	-	-	-	-	-	-	-	-	-	-	-	0.3	≤36.8
95	40.5±7.9	6.3±4.0	26.5±6.4	32.8±7.1	7.7±4.3	27.4±6.5	10.6±4.7	$-0.51^{+0.14}_{-0.15}$	$-0.48^{+0.19}_{-0.24}$	$0.54^{+0.24}_{-0.16}$	N	N	3.4	37.8
96	19.9±6.2	10.3±4.6	9.3±4.4	19.6±5.9	0.3±2.9	17.5±5.6	-0.1±2.9	$-0.97^{+0.05}_{-0.03}$	$0.16^{+0.22}_{-0.21}$	$0.84^{+0.84}_{-0.46}$	-	-	0.9	37.5
97	≤2.8	-	-	-	-	-	-	-	-	-	-	-	0.2	≤36.6
98	11.9±5.1	0.3±2.3	8.7±4.3	8.9±4.4	3.0±3.4	7.8±4.1	4.7±3.8	$-0.36^{+0.31}_{-0.31}$	$-0.84^{+0.53}_{-0.76}$	$0.43^{+0.46}_{-0.35}$	-	-	1.0	37.2
99	47.8±8.4	10.2±4.4	31.5±6.8	41.7±7.7	6.1±4.1	33.5±7.0	12.8±5.1	$-0.51^{+0.12}_{-0.14}$	$-0.38^{+0.17}_{-0.16}$	$0.70^{+0.27}_{-0.19}$	N	N	2.2	37.8

Table 10—Continued

MID				Net Counts				HR	C21	C32	Variability			Log L_X
	B-band	S1-band	S2-band	S-band	H-band	Sc-band	Hc-band				BB	k-S	signif.	(erg s^{-1})
(1)	(2)	(3)	(4)	(5)	(6)	(7)	(8)	(9)	(10)	(11)	(12)	(13)	(14)	(15)
100	≤1.4	-	-	-	-	-	-	-	-	-	-	-	0.1	≤36.3
101	18.0±6.0	1.6±2.9	8.0±4.3	9.6±4.7	8.4±4.4	6.5±4.1	12.1±5.0	$0.24^{+0.27}_{-0.28}$	$-0.46^{+0.43}_{-0.61}$	$0.03^{+0.24}_{-0.24}$	-	-	0.5	37.4
102	140.2±13.2	38.3±7.4	81.7±10.2	120.0±12.2	20.2±5.9	102.2±11.3	27.6±6.6	$-0.63^{+0.07}_{-0.07}$	$-0.20^{+0.07}_{-0.10}$	$0.62^{+0.14}_{-0.09}$	N	N	5.2	38.3
103	143.1±14.1	19.6±5.7	86.1±10.4	105.7±11.5	36.4±7.3	94.9±10.9	44.0±7.9	$-0.43^{+0.06}_{-0.09}$	$-0.52^{+0.11}_{-0.12}$	$0.40^{+0.10}_{-0.08}$	N	N	0.1	38.3
104	≤1.6	-	-	-	-	-	-	-	-	-	-	-	1.5	≤36.4
105	≤11.7	-	-	-	-	-	-	-	-	-	-	-	1.4	≤37.2
106	29.5±7.5	11.0±4.6	16.6±5.3	27.5±6.5	1.2±3.2	27.3±6.5	0.9±3.2	$-0.97^{+0.05}_{-0.03}$	$-0.07^{+0.18}_{-0.16}$	$0.91^{+0.75}_{-0.40}$	N	N	1.0	37.6
107	≤1.2	-	-	-	-	-	-	-	-	-	-	-	0.1	≤36.2
108	≤9.2	-	-	-	-	-	-	-	-	-	-	-	0.0	≤37.1
109	8.7±4.7	0.2±2.3	1.7±2.9	1.9±3.2	6.8±4.1	-0.4±2.3	9.4±4.6	$0.95^{+0.05}_{-0.09}$	$-0.23^{+0.84}_{-0.99}$	$-0.46^{+0.46}_{-0.61}$	-	-	0.4	37.1
110	35.8±7.6	3.2±3.4	19.3±5.7	22.5±6.2	13.3±5.2	18.2±5.6	15.7±5.6	$-0.15^{+0.18}_{-0.18}$	$-0.58^{+0.28}_{-0.44}$	$0.19^{+0.16}_{-0.17}$	N	N	1.8	37.7
111	6.6±4.6	1.5±2.9	2.7±3.2	4.3±3.8	2.4±3.4	3.5±3.4	1.9±3.4	$-0.44^{+0.28}_{-0.56}$	$-0.05^{+0.61}_{-0.78}$	$0.05^{+0.73}_{-0.59}$	-	-	0.7	37.0
112	8.8±4.9	1.9±2.9	6.1±3.8	7.9±4.3	0.8±3.2	8.9±4.3	0.5±3.2	$-0.90^{+0.13}_{-0.10}$	$-0.29^{+0.40}_{-0.57}$	$0.53^{+0.85}_{-0.45}$	-	-	0.3	37.2
113	≤1.7	-	-	-	-	-	-	-	-	-	-	-	1.0	≤36.4
114	≤5.4	-	-	-	-	-	-	-	-	-	-	-	0.3	≤36.9
115	≤3.9	-	-	-	-	-	-	-	-	-	-	-	0.7	≤36.8
116	51.5±8.6	16.0±5.2	37.4±7.3	53.4±8.5	-1.9±2.3	49.5±8.2	-0.4±2.9	$-1.00^{+0.02}_{-0.00}$	$-0.28^{+0.16}_{-0.10}$	$1.84^{+0.86}_{-0.62}$	N	N	1.9	37.9
117	≤1.3	-	-	-	-	-	-	-	-	-	-	-	0.5	≤36.3
118	≤2.0	-	-	-	-	-	-	-	-	-	-	-	0.5	≤36.5
119	27.8±6.7	6.2±3.8	17.9±5.4	24.1±6.2	3.8±3.6	19.7±5.7	7.5±4.3	$-0.52^{+0.17}_{-0.19}$	$-0.32^{+0.19}_{-0.22}$	$0.64^{+0.41}_{-0.26}$	N	N	0.2	37.6
120	148.4±13.4	81.1±10.1	66.7±9.3	147.7±13.3	0.6±2.9	135.9±12.7	1.1±3.2	$-0.99^{+0.01}_{-0.01}$	$0.22^{+0.08}_{-0.06}$	$1.60^{+0.82}_{-0.40}$	V	V	3.0	38.4
121	49.0±8.4	19.9±5.7	18.9±5.6	38.8±7.5	10.2±4.7	32.8±6.9	12.7±5.1	$-0.51^{+0.12}_{-0.14}$	$0.13^{+0.16}_{-0.12}$	$0.30^{+0.19}_{-0.18}$	N	N	0.9	37.9
122	≤17.7	-	-	-	-	-	-	-	-	-	-	-	2.2	≤37.4
123	≤6.0	-	-	-	-	-	-	-	-	-	-	-	0.4	≤37.0
124	≤6.2	-	-	-	-	-	-	-	-	-	-	-	1.1	≤37.0
125	25.7±6.8	4.4±3.6	13.1±5.0	17.5±5.7	8.2±4.6	15.9±5.3	10.6±5.0	$-0.28^{+0.20}_{-0.22}$	$-0.32^{+0.27}_{-0.30}$	$0.21^{+0.25}_{-0.21}$	N	N	1.3	37.6
126	≤11.1	-	-	-	-	-	-	-	-	-	-	-	0.9	≤37.3
127	≤2.8	-	-	-	-	-	-	-	-	-	-	-	1.1	≤36.6
128	≤7.2	-	-	-	-	-	-	-	-	-	-	-	0.2	≤37.0
129	≤8.4	-	-	-	-	-	-	-	-	-	-	-	0.6	≤37.2
130	18.3±5.9	3.1±3.2	12.7±4.8	15.8±5.3	2.5±3.4	10.3±4.6	6.2±4.1	$-0.40^{+0.25}_{-0.26}$	$-0.35^{+0.30}_{-0.35}$	$0.67^{+0.54}_{-0.38}$	-	-	1.4	37.5
131	20.2±6.4	6.6±4.0	6.8±4.1	13.4±5.2	6.8±4.4	10.7±4.7	8.1±4.7	$-0.27^{+0.27}_{-0.27}$	$0.13^{+0.27}_{-0.26}$	$0.05^{+0.33}_{-0.29}$	N	N	1.0	37.5
132	31.4±7.3	5.5±3.8	19.4±5.7	24.8±6.4	6.6±4.4	24.3±6.2	7.1±4.6	$-0.67^{+0.15}_{-0.16}$	$-0.27^{+0.22}_{-0.24}$	$0.51^{+0.27}_{-0.24}$	N	N	1.3	37.8

Table 10—Continued

MID	Net Counts							HR	C21	C32	Variability			Log L_X
	B-band	S1-band	S2-band	S-band	H-band	Sc-band	Hc-band				BB	k-S	signif.	(erg s^{-1})
(1)	(2)	(3)	(4)	(5)	(6)	(7)	(8)	(9)	(10)	(11)	(12)	(13)	(14)	(15)

Note. — Col. (1): Master ID, cols. (2)−(8): net counts, in each of the 7 energy bands (see Table 3 for definitions of these bands), col. (9): hardness ratio, cols. (10) and (11) color values, errors are given as 1σ, cols. (12) and (13): short-term variability, where (BB) indicate Bayesian block analysis and (K-S) indicates the Kolmogorov-Smirnov test, in both columns symbols indicate - (N) non-variable in all observations, (V) variable in at least one observation, (P) possible variability in at least one observation, col. (14): the significance of the change in L_X between the previous observation and the current observation respectively (equation 2), col. (15): log L_X (0.3−8.0 keV). Upper limit values of net B and L_X are at the 68% confidence level.

Table 11. Properties of optical sources that are correlated with an X-ray point source

Masterid	V	I	V−I	B−V	V−R	B−R	Radial Velocity	GC separation (arcsec)	Ratio	Reference
(1)	(2)	(3)	(4)	(5)	(6)	(7)	(8)	(9)	(10)	(11)
41	21.148±0.008	20.297±0.010	0.851±0.013	-	-	-	-	0.307	1.31	4
42	21.880±0.011	20.753±0.012	1.127±0.016	1.074	0.519	1.590	889±7	0.448	1.84	1,4,6
50	22.569±0.022	21.307±0.021	1.262±0.030	-	-	-	-	0.410	1.23	4
55	20.059±0.004	19.007±0.004	1.052±0.006	-	-	1.240	776±4	0.380	1.59	1,4
61	22.923±0.032	22.094±0.043	0.829±0.054	-	-	-	-	0.219	0.32	4
62	21.006±0.010	19.877±0.012	1.129±0.016	-	-	1.260	1071±18	0.146	0.54	3,4
66	21.517±0.013	20.334±0.013	1.183±0.018	-	-	1.310	1258±38	0.174	0.67	2,4
67	21.567±0.025	20.702±0.038	0.865±0.045	-	-	-	-	0.141	0.61	4
79	21.796±0.013	20.765±0.015	1.031±0.020	-	-	1.260	546±45	0.373	0.38	3,4
119	21.180	-	-	0.988	0.560	1.550	1048±4	0.380	1.07	1,6
31	22.322±0.060	21.751±0.087	0.571±0.106	-	-	-	-	0.516	0.69	5
43	25.396±0.457	23.902±0.388	1.494±0.599	-	-	-	-	0.366	0.71	5
68	24.068±0.274	22.775±0.269	1.293±0.384	-	-	-	-	0.310	0.94	5
85	23.482±0.129	21.969±0.107	1.513±0.168	-	-	-	-	0.478	0.92	5

Note. — The sources in the top section of the table, denoted by the horizontal line, have been confirmed as globular clusters, while those in the bottom section of the table have all been identified as background objects.

References. — 1. Bergond et al. 2006, 2. Puzia et al. 2004, 3. Pierce et al. 2006, 4. Kundu & Whitmore (2001), confirmed GCs, 5. Kundu & Whitmore (2001), background objects, 6. Rhode & Zepf, 2004.

Table 12. Properties of optical sources that have been classified as 'excluded matches'; sources detected between 0.6″ and 3″ of an X-ray point source

Masterid	V	I	V−I	B−V	V−R	B−R	Radial Velocity	GC separation (arcsec)	Ratio	Reference
(1)	(2)	(3)	(4)	(5)	(6)	(7)	(8)	(9)	(10)	(11)
28	23.213±0.030	21.984±6	1.229±0.042	-	-	-	-	1.555	5.55	4
34	22.041±0.014	20.931±6	1.110±0.020	-	-	1.220	790±41	1.088	2.05	3,4
40	25.379±0.450	24.040±6	1.339±0.567	-	-	-	-	1.341	2.95	4
46	21.573±0.012	20.474±6	1.099±0.019	-	-	1.280	1080±32	2.197	4.53	2,4
49	23.782±0.063	22.629±6	1.153±0.099	-	-	-	-	2.971	6.66	4
51	23.226±0.050	22.105±6	1.121±0.076	-	-	-	-	2.101	5.27	4
58	24.061±0.068	23.545±6	0.516±0.130	-	-	-	-	2.405	5.97	4
70	22.319±0.077	21.253±6	1.066±0.118	-	-	-	-	1.352	6.30	4
71	21.102±0.039	19.939±6	1.163±0.060	-	-	-	-	1.115	3.67	4
76	22.066±0.027	21.336±6	0.730±0.046	-	-	-	-	2.173	2.50	4
25	25.714±0.384	23.482±6	2.232±0.416	-	-	-	-	2.596	10.16	5
29	25.389±0.324	24.637±6	0.752±0.606	-	-	-	-	2.790	9.55	5
44	25.060±0.289	23.191±6	1.869±0.335	-	-	-	-	2.228	5.07	5
45	24.790±0.264	23.367±6	1.423±0.351	-	-	-	-	2.740	7.60	5
53	24.132±0.271	22.981±6	1.151±0.388	-	-	-	-	2.413	9.15	5
54	24.652±0.472	23.622±6	1.030±0.704	-	-	-	-	0.988	2.52	5
56	24.742±0.332	23.314±6	1.428±0.428	-	-	-	-	1.332	3.15	5
59	24.571±0.373	23.416±6	1.155±0.520	-	-	-	-	2.924	9.64	5
65	24.382±0.259	22.841±6	1.541±0.346	-	-	-	-	2.695	4.84	5
69	25.931±0.933	25.401±6	0.530±1.854	-	-	-	-	2.810	5.73	5
72	24.419±0.323	22.953±6	1.466±0.413	-	-	-	-	2.417	6.45	5
89	25.969±1.380	22.659±6	3.310±1.396	-	-	-	-	1.192	3.86	5
93	25.756±0.899	23.636±6	2.120±0.968	-	-	-	-	0.911	3.39	5

Note. — The sources in the top section of the table, denoted by the horizontal line, have been confirmed as globular clusters, while those in the bottom section of the table have all been identified as background objects.

References. — 1. Bergond et al. 2006, 2. Puzia et al. 2004, 3. Pierce et al. 2006, 4. Kundu & Whitmore (2001), confirmed GCs, 5. Kundu & Whitmore (2001), background objects, 6. Rhode & Zepf, 2004.

Table 13. Ratio Values of Potential Transient Candidates

Masterid	Mode Ratio	Lower Bound Ratio	Variability
25	161.39	43.48	TC
50	6.83	5.87	PTC
53	11.40	4.20	V
85	30.19	9.00	PTC
89	18.39	16.42	TC
91	8.49	4.75	V
92	7.44	3.15	V
94	19.21	13.18	TC
100	20.21	14.05	TC
115	12.88	6.84	PTC
128	85.09	50.69	TC

Note. — The 11 sources that were identified as potential transients candidates. Mode ratios and lower bound ratios were derived from Bayesian modeling, see §2.4 for more details. Sources were determined to be transient candidates (TC) if the lower bound >10, possible transient candidates (PTC) if the lower bound >5 and variable (V), if lower than 5.

Table 14. Summary of Long-Term and Short-Term Source Variability

Short-Term Variability	Long-Term Variability N	V	TC	PTC	-	Total
N	2 **(2)**	8 **(7)**	0 **(0)**	0 **(0)**	0 **(0)**	10 **(9)**
V	2 **(2)**	3 **(2)**	2 **(1)**	0 **(0)**	0 **(0)**	7 **(5)**
P	3 **(3)**	4 **(4)**	0 **(0)**	0 **(0)**	0 **(0)**	7 **(7)**
-	37 **(27)**	41 **(30)**	3 **(3)**	3 **(3)**	24 **(14)**	108 **(77)**
Total	44 **(34)**	56 **(43)**	5 **(4)**	3 **(3)**	24 **(14)**	132 **(98)**

Note. — The long-term variability definitions: N-non-variable, V-variable, TC-transient candidate, PTC-possible transient candidate and - unable to determine variability as all individual observations were upper limits. Short-term variability definitions: N-non-variable in all five observation, V-variable in a least one observation, P-possible variability in at least one observation (see §2.4 for full definition), - too few counts in all five observations to determine variability. Bold values in brackets indicate the number of sources within the D_{25} ellipse.

Table 15. Raw source and background counts from the co-added observation

Masterid	Net B Counts	Raw Counts													
		B-band		S1-band		S2-band		H-band		Bc-band		Sc-band		Hc-band	
		(Src)	(Bkg)	(Src)	(Bkg)	(Src)	(Bkg)	(Src)	(Bkg)	(Src)	(Bkg)	(Src)	(Bkg)	(Src)	(Bkg)
(1)	(2)	(3)	(4)	(5)	(6)	(7)	(8)	(9)	(10)	(11)	(12)	(13)	(14)	(15)	(16)
1	58.9	82	23.1	20	5.8	42	5.6	20	11.7	77	19.4	52	6.3	25	13.1
2	36.2	57	20.8	6	4.5	29	6.0	22	10.3	56	17.9	31	6.2	25	11.6
3	28.9	52	23.1	13	5.7	21	5.9	18	11.5	45	19.3	23	6.5	22	12.9
4	1.8	6	4.2	1	1.1	1	1.1	4	2.0	6	3.5	2	1.2	4	2.3
5	4.6	6	1.4	0	0.3	3	0.4	3	0.7	6	1.2	2	0.4	4	0.8
6	-	-	-	-	-	-	-	-	-	-	-	-	-	-	-
7	38.7	59	20.3	12	5.0	29	5.1	18	10.2	55	17.4	29	5.9	26	11.5
8	24.7	47	22.3	13	4.4	21	5.6	13	12.3	40	19.9	23	5.8	17	14.0
9	997.6	1036	38.4	281	9.6	577	9.7	178	19.0	982	31.9	736	10.3	246	21.6
10	27.9	49	21.1	7	5.5	9	5.5	33	10.1	45	17.6	8	6.3	37	11.4
11	165.6	187	21.4	48	4.7	102	6.2	37	10.6	179	19.4	131	7.1	48	12.3
12	32.8	53	20.2	13	4.8	24	5.8	16	9.6	48	17.0	26	6.0	22	11.0
13	40.2	60	19.8	4	4.4	26	5.4	30	9.9	59	17.1	24	5.8	35	11.4
14	38.4	85	46.6	17	12.0	29	11.4	39	23.2	76	38.0	28	12.0	48	26.0
15	18.7	38	19.3	10	4.1	12	5.5	16	9.7	34	17.2	17	5.9	17	11.3
16	76.8	99	22.2	28	5.1	40	5.8	31	11.3	92	20.1	59	6.9	33	13.2
17	66.9	87	20.1	18	4.2	38	4.6	31	11.3	82	17.5	46	5.2	36	12.3
18	195.7	234	38.3	24	9.7	131	9.1	79	19.5	225	32.8	122	10.7	103	22.1
19	-	-	-	-	-	-	-	-	-	-	-	-	-	-	-
20	19.8	42	22.2	12	4.8	15	5.2	15	12.2	35	19.6	19	5.7	16	13.9
21	127.2	167	39.8	10	9.9	61	9.2	96	20.7	164	33.7	46	10.3	118	23.4
22	-	-	-	-	-	-	-	-	-	-	-	-	-	-	-
23	44.9	80	35.1	13	8.4	18	8.3	49	18.4	73	29.8	21	9.5	52	20.3
24	21.0	43	22.0	8	5.3	13	5.1	22	11.6	40	19.0	15	6.3	25	12.8
25	195.3	216	21.2	67	4.9	124	5.7	25	10.5	200	18.6	170	6.5	30	12.1
26	18.5	39	20.5	9	3.6	16	5.7	14	11.2	36	18.2	22	5.8	14	12.4
27	525.7	552	26.3	200	4.7	258	7.8	94	13.8	506	24.1	390	8.3	116	15.8
28	109.9	132	22.1	18	5.2	74	5.9	40	11.0	128	19.5	82	6.9	46	12.6
29	78.9	99	20.1	25	4.1	50	4.8	24	11.3	92	18.2	64	5.8	28	12.4
30	171.9	193	21.1	51	4.7	113	5.5	29	10.9	184	18.8	136	6.4	48	12.4
31	18.7	44	25.3	8	5.6	14	6.8	22	12.9	40	22.6	14	7.9	26	14.7
32	32.6	59	26.4	21	6.1	30	7.2	8	13.0	58	23.2	47	8.9	11	14.4

Table 15—Continued

Masterid	Net B Counts	Raw Counts													
		B-band		S1-band		S2-band		H-band		Bc-band		Sc-band		Hc-band	
		(Src)	(Bkg)	(Src)	(Bkg)	(Src)	(Bkg)	(Src)	(Bkg)	(Src)	(Bkg)	(Src)	(Bkg)	(Src)	(Bkg)
(1)	(2)	(3)	(4)	(5)	(6)	(7)	(8)	(9)	(10)	(11)	(12)	(13)	(14)	(15)	(16)
33	24.7	46	21.3	11	3.9	18	6.3	17	11.1	41	19.3	20	6.9	21	12.4
34	8.9	36	27.1	10	7.0	13	6.9	13	13.2	33	23.9	18	9.4	15	14.5
35	31.1	53	21.9	18	4.5	19	5.3	16	12.1	50	19.5	31	5.9	19	13.5
36	22.5	49	26.5	22	7.5	14	6.4	13	12.6	41	23.9	27	10.1	14	13.8
37	66.2	89	22.8	24	6.0	40	6.3	25	10.5	85	20.0	50	8.5	35	11.5
38	11.8	35	23.2	5	5.2	20	5.6	10	12.4	31	20.5	16	6.5	15	14.1
39	26.6	49	22.4	20	5.4	15	5.7	14	11.4	43	19.9	27	7.3	16	12.6
40	28.3	54	25.7	12	7.6	24	6.7	18	11.5	50	22.2	30	9.4	20	12.8
41	718.7	747	28.3	269	7.7	370	8.0	108	12.7	681	24.8	536	10.9	145	14.0
42	1741.8	1764	22.2	355	4.8	1057	5.5	352	11.9	1709	19.8	1213	6.0	496	13.7
43	14.9	42	27.1	8	6.9	14	7.5	20	12.8	39	23.9	16	9.8	23	14.1
44	37.0	61	24.0	21	6.1	22	6.4	18	11.5	52	21.5	30	8.9	22	12.6
45	41.8	69	27.2	15	7.4	32	7.4	22	12.3	65	23.2	42	9.5	23	13.7
46	20.4	49	28.3	18	7.5	17	7.8	14	13.0	41	25.1	26	10.4	15	14.7
47	278.0	304	26.4	86	6.7	150	7.6	68	12.1	287	23.6	197	10.1	90	13.5
48	31.0	58	26.5	10	7.5	33	7.9	15	11.1	57	23.5	39	10.6	18	12.8
49	12.8	40	25.9	13	6.5	9	7.6	18	11.8	34	22.6	16	9.3	18	13.4
50	49.5	70	20.5	14	5.4	34	5.7	22	9.5	64	17.7	30	7.2	34	10.4
51	23.7	54	30.3	21	8.1	22	11.1	11	11.1	48	26.9	33	13.6	15	13.3
52	52.1	78	25.0	19	6.7	39	6.6	20	11.7	70	21.5	45	8.8	25	12.7
53	152.9	185	32.1	63	9.1	89	11.4	33	11.6	173	28.2	129	14.2	44	14.0
54	41.7	75	33.3	32	9.8	27	11.4	16	12.2	66	29.2	47	14.9	19	14.3
55	240.0	261	21.0	84	3.9	151	6.3	26	10.8	241	19.3	194	7.2	47	12.1
56	31.0	61	30.0	12	8.2	36	10.1	13	11.7	57	26.2	40	12.6	17	13.7
57	-	-	-	-	-	-	-	-	-	-	-	-	-	-	-
58	64.7	88	23.1	27	6.8	40	5.8	21	10.5	83	19.4	60	7.6	23	11.7
59	72.2	109	36.8	27	10.7	56	12.9	26	13.1	100	33.0	68	18.1	32	15.0
60	159.9	198	38.1	53	12.0	103	12.8	42	13.3	187	32.9	123	17.8	64	15.1
61	11.3	38	26.7	10	7.5	12	7.7	16	11.5	32	23.5	14	10.7	18	12.7
62	169.8	203	32.9	40	9.7	114	9.6	49	13.7	191	28.8	130	12.9	61	16.0
63	27.7	56	28.3	11	6.4	24	6.3	21	15.5	52	24.6	25	7.7	27	17.0
64	201.2	225	23.8	54	6.6	112	7.4	59	9.8	214	20.8	138	9.5	76	11.2

Table 15—Continued

Masterid	Net B Counts	Raw Counts													
		B-band		S1-band		S2-band		H-band		Bc-band		Sc-band		Hc-band	
		(Src)	(Bkg)	(Src)	(Bkg)	(Src)	(Bkg)	(Src)	(Bkg)	(Src)	(Bkg)	(Src)	(Bkg)	(Src)	(Bkg)
(1)	(2)	(3)	(4)	(5)	(6)	(7)	(8)	(9)	(10)	(11)	(12)	(13)	(14)	(15)	(16)
65	16.3	48	32.6	16	9.2	16	9.5	16	13.9	43	28.5	24	12.6	19	16.0
66	164.5	200	35.5	41	10.6	109	12.9	50	12.0	195	32.4	130	18.6	65	13.8
67	1008.9	1042	33.1	211	10.9	596	13.7	235	8.5	1012	30.2	690	19.9	322	10.4
68	71.8	83	11.2	20	3.7	44	4.2	19	3.3	82	10.0	61	6.0	21	3.9
69	21.4	52	30.6	12	9.6	17	9.9	23	11.1	51	27.3	24	14.5	27	12.8
70	7222.3	7266	43.7	1833	13.8	4143	18.5	1290	11.4	6949	40.8	5158	26.8	1791	14.0
71	91.5	110	18.5	41	6.2	54	7.8	15	4.6	99	17.1	83	11.1	16	6.0
72	111.0	150	39.0	52	12.5	66	12.9	32	13.6	134	35.2	88	19.1	46	16.2
73	-	-	-	-	-	-	-	-	-	-	-	-	-	-	-
74	1165.4	1211	45.6	373	16.5	672	18.9	166	10.2	1144	40.8	902	27.5	242	13.3
75	373.6	433	59.4	183	23.1	211	23.8	39	12.5	405	51.6	353	35.8	52	15.8
76	-	-	-	-	-	-	-	-	-	-	-	-	-	-	-
77	414.4	452	37.6	125	15.7	239	14.7	88	7.3	431	33.2	320	24.1	111	9.2
78	174.9	190	15.1	51	5.5	98	5.5	41	4.1	181	13.5	127	8.7	54	4.7
79	5.1	28	22.9	5	5.2	12	7.0	11	10.8	28	20.3	16	8.4	12	11.9
80	77.9	94	16.1	20	4.9	58	7.0	16	4.2	90	15.0	67	10.1	23	4.9
81	858.2	891	32.8	305	11.5	472	12.3	114	9.0	835	29.4	685	19.0	150	10.4
82	661.8	690	28.2	167	9.9	373	11.5	150	6.8	664	25.4	468	17.5	196	7.9
83	177.3	198	20.7	58	6.6	111	8.7	29	5.4	189	19.2	143	12.9	46	6.3
84	55.0	63	8.0	16	2.5	38	2.2	9	3.3	58	7.0	46	3.2	12	3.8
85	27.7	31	3.3	8	1.0	16	1.0	7	1.3	28	2.9	20	1.4	8	1.5
86	2114.3	2170	55.7	489	22.2	1217	18.0	464	15.4	2093	47.7	1444	30.5	649	17.2
87	213.6	248	34.4	74	13.7	132	11.9	42	8.9	237	29.3	180	18.9	57	10.4
88	115.8	145	29.2	38	8.1	89	9.3	18	11.8	140	26.5	110	12.6	30	13.9
89	101.8	138	36.6	30	11.2	65	11.2	43	14.2	126	32.9	75	16.6	51	16.3
90	377.8	399	21.2	83	5.2	223	5.5	93	10.5	379	18.7	259	6.9	120	11.8
91	5.1	33	27.9	12	7.8	12	7.8	9	12.3	30	24.6	19	10.4	11	14.2
92	25.6	50	24.4	14	5.9	18	5.4	18	13.0	43	21.3	22	7.3	21	14.0
93	138.4	173	34.6	45	10.8	84	10.7	44	13.1	163	30.9	110	15.9	53	15.0
94	83.6	114	30.4	46	8.1	53	8.9	15	13.4	102	27.1	84	11.8	18	15.3
95	81.6	111	29.4	26	8.0	61	8.8	24	12.6	101	26.5	71	12.2	30	14.3
96	53.2	82	28.8	32	7.6	32	7.7	18	13.5	71	25.5	48	10.3	23	15.3

Table 15—Continued

Masterid	Net B Counts	Raw Counts													
		B-band		S1-band		S2-band		H-band		Bc-band		Sc-band		Hc-band	
		(Src)	(Bkg)	(Src)	(Bkg)	(Src)	(Bkg)	(Src)	(Bkg)	(Src)	(Bkg)	(Src)	(Bkg)	(Src)	(Bkg)
(1)	(2)	(3)	(4)	(5)	(6)	(7)	(8)	(9)	(10)	(11)	(12)	(13)	(14)	(15)	(16)
97	20.3	46	25.7	9	6.3	22	7.2	15	12.2	43	23.2	25	9.2	18	14.0
98	107.0	126	19.0	32	3.8	60	5.2	34	9.9	117	16.9	70	5.5	47	11.4
99	185.1	209	23.9	48	6.0	124	6.6	37	11.3	198	21.1	146	8.3	52	12.8
100	75.6	103	27.4	88	6.9	7	8.0	8	12.5	68	24.4	60	9.8	8	14.6
101	61.3	87	25.7	7	6.7	27	7.7	53	11.4	86	22.6	19	9.8	67	12.8
102	1389.0	1416	27.0	563	6.3	663	7.5	190	13.2	1272	24.2	1010	9.0	262	15.2
103	636.9	652	15.1	153	3.8	367	4.1	132	7.2	625	13.6	450	5.4	175	8.1
104	29.3	52	22.7	8	5.6	20	5.6	24	11.5	48	20.0	19	6.8	29	13.1
105	40.4	67	26.2	14	6.7	35	7.2	18	12.3	65	23.1	42	9.3	23	13.7
106	261.1	285	23.4	91	5.2	169	6.4	25	11.8	266	21.2	227	8.1	39	13.1
107	-	-	-	-	-	-	-	-	-	-	-	-	-	-	-
108	28.9	55	26.1	9	6.3	25	7.3	21	12.5	53	23.4	29	9.2	24	14.3
109	46.5	68	21.5	5	4.9	26	5.6	37	11.1	67	19.5	22	7.0	45	12.5
110	113.9	143	29.1	24	7.6	66	7.2	53	14.4	134	25.6	70	8.9	64	16.7
111	39.8	64	24.2	13	6.4	24	5.8	27	12.1	59	20.8	27	7.4	32	13.5
112	44.2	65	20.8	17	4.6	31	4.7	17	11.5	60	18.8	43	6.0	17	12.8
113	32.0	55	23.0	18	5.3	20	5.9	17	11.9	50	20.6	29	7.2	21	13.4
114	41.4	64	22.6	22	5.5	30	5.9	12	11.2	56	20.0	41	7.4	15	12.6
115	17.2	41	23.8	12	6.3	14	6.3	15	11.2	39	20.7	22	8.1	17	12.6
116	140.2	166	25.8	58	5.3	94	7.3	14	13.2	156	22.5	133	6.9	23	15.6
117	12.0	33	21.0	13	4.7	11	4.6	9	11.7	28	18.7	18	5.9	10	12.8
118	15.4	38	22.6	7	5.9	16	6.0	15	10.6	36	19.6	19	7.6	17	12.0
119	136.9	158	21.1	46	3.6	78	6.0	34	11.5	147	19.6	100	6.8	47	12.8
120	643.2	664	20.8	378	4.8	264	6.1	22	9.8	599	17.8	576	5.9	23	11.9
121	258.4	280	21.6	86	5.7	126	5.6	68	10.3	259	18.1	172	6.4	87	11.8
122	34.9	57	22.1	11	5.8	28	6.0	18	10.3	53	19.1	29	7.2	24	11.9
123	21.1	42	20.9	6	4.8	22	5.7	14	10.5	39	18.4	19	6.7	20	11.7
124	18.0	41	23.0	9	5.8	12	5.0	20	12.1	39	19.7	13	6.4	26	13.3
125	153.6	182	28.4	35	6.1	91	8.1	56	14.2	173	25.1	98	9.3	75	15.8
126	23.3	43	19.7	7	4.2	13	5.6	23	9.9	38	16.9	11	5.4	27	11.5
127	35.5	63	27.5	19	6.0	23	6.8	21	14.7	57	24.6	33	8.0	24	16.6
128	567.7	598	30.3	127	6.7	280	7.2	191	16.4	567	26.9	334	8.5	233	18.4

Table 15—Continued

Masterid	Net B Counts	Raw Counts													
		B-band		S1-band		S2-band		H-band		Bc-band		Sc-band		Hc-band	
		(Src)	(Bkg)	(Src)	(Bkg)	(Src)	(Bkg)	(Src)	(Bkg)	(Src)	(Bkg)	(Src)	(Bkg)	(Src)	(Bkg)
(1)	(2)	(3)	(4)	(5)	(6)	(7)	(8)	(9)	(10)	(11)	(12)	(13)	(14)	(15)	(16)
129	48.0	68	20.0	9	4.0	38	5.8	21	10.2	66	17.4	37	6.1	29	11.3
130	146.7	168	21.3	49	4.6	87	5.5	32	11.2	155	19.0	113	6.3	42	12.6
131	114.4	149	34.6	43	7.3	61	8.7	45	18.6	140	30.5	85	9.4	55	21.2
132	152.9	189	36.1	43	7.8	100	8.9	46	19.4	179	31.6	123	10.3	56	21.3

Note. — Col. (1): Master ID, cols. (2): net broad-band counts. Cols. (3), (5), (7), (9), (11), (13) and (15): raw source counts in each of the 7 energy bands (see Table 3 for definitions of these bands), cols. (4), (6), (8), (10), (12), (14) and (16): background counts in each of the 7 energy bands. In some instances background counts are very low. For these sources standard aperture photometry results in negative net counts, so, instead, the source cell determined by *wavdetect* has been used. This results in a large area ratio between the background and source regions and therefore a low background count value is derived.

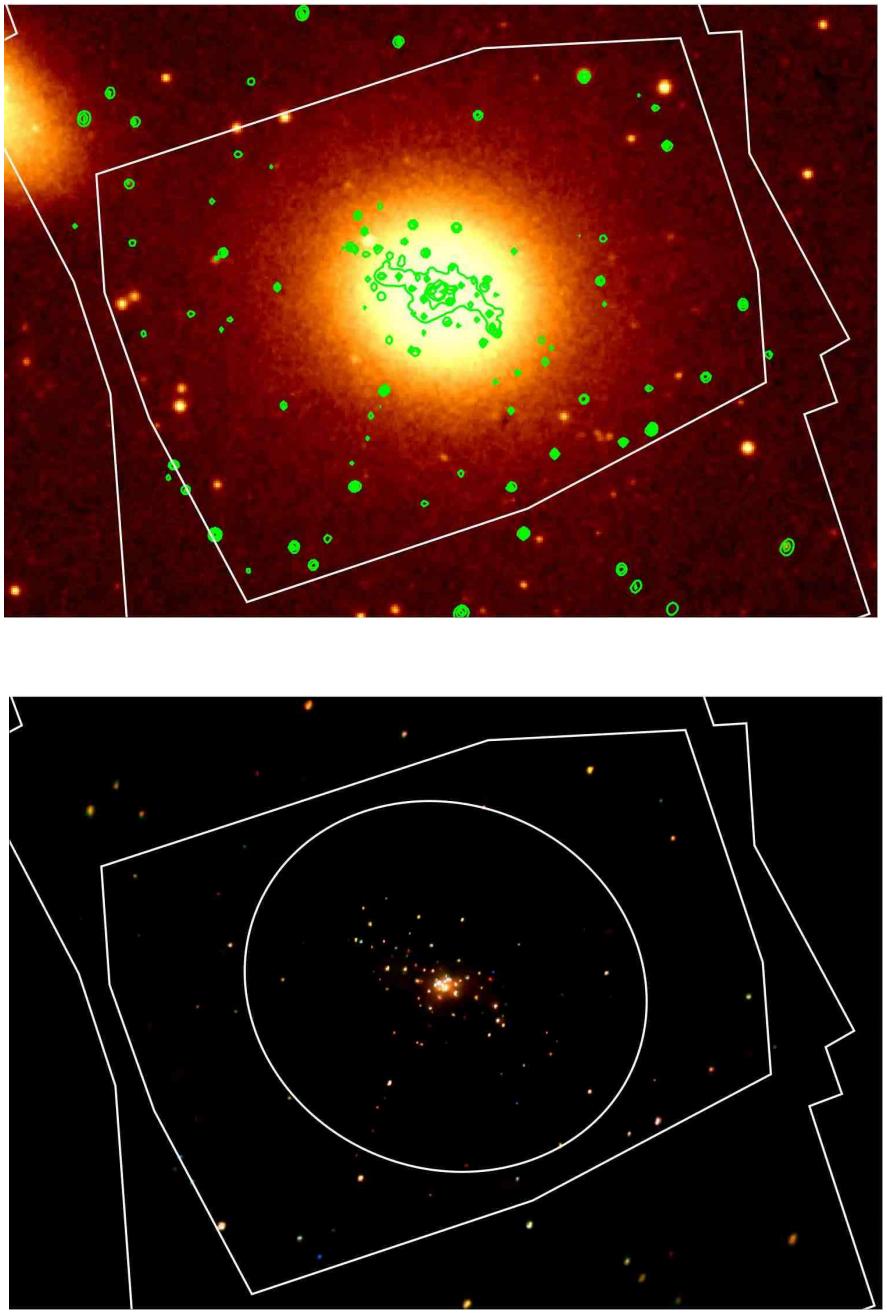

Fig. 1.— Top: An optical image of NGC 3379, with full band, adaptively smoothed, X-ray contours overlaid. Also shown is the outline of the total area covered by the ACIS-S3 chips, from the five separate observations, and the smaller region overlapped by all five of the pointings. Bottom: A 'true color' image of the galaxy, where red corresponds to 0.3−0.8 keV, green to 0.8−2.5 keV and blue to 2.5−8.0 keV. The D_{25} ellipse of this galaxy, the coverage from all observations and the overlapping region are also shown.

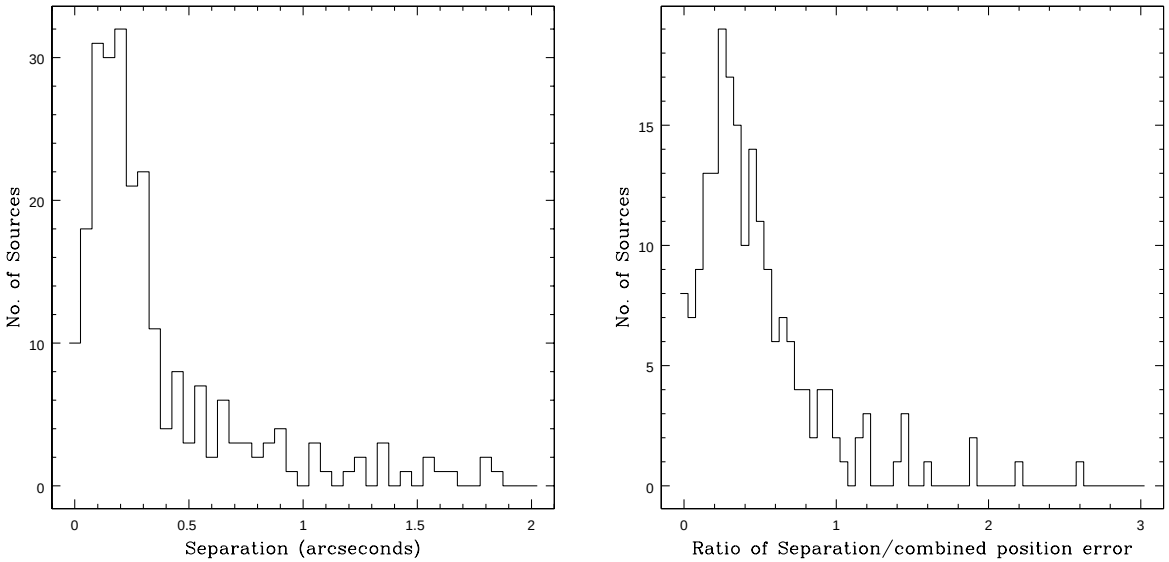

Fig. 2.— Left: Histogram of the separation between sources detected in the co-added observation and sources detected in single observations. Right: Histogram of the ratio of separation between sources detected in the co-added observation and sources detected in single observations, divided by the combined position uncertainty of these sources.

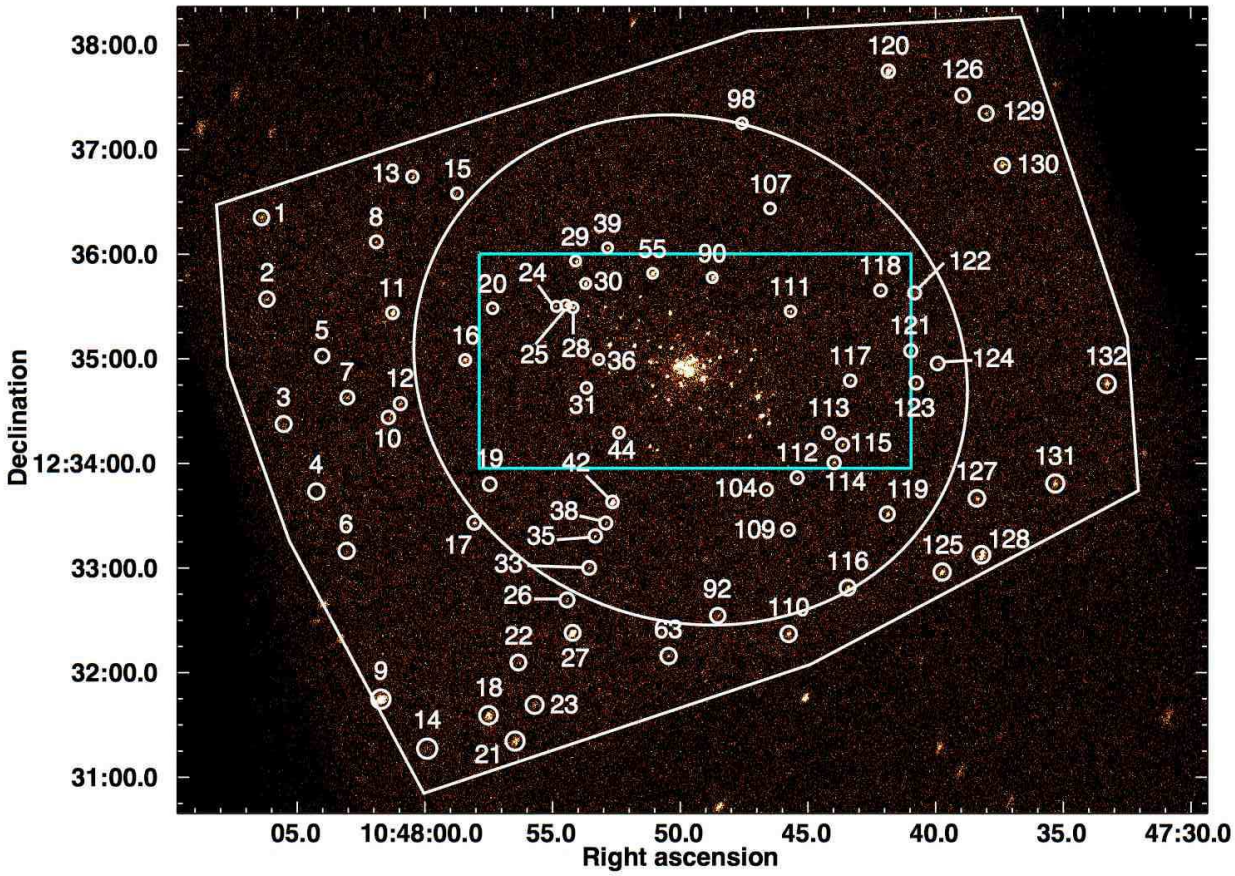

Fig. 3.— The main image, presents a full band, raw (unsmoothed, with no exposure correction) image from the co-added observation of NGC 3379, with the D_{25} ellipse and the region overlapped by all five observations overlaid. Source region numbering corresponds to the naming convention in Table 4 and regions represent the 95% encircled energy radius at 1.5 keV. The cyan box in the central region indicates the area shown in the next image, the central region of the galaxy, with sources labeled with the same convention as in the main image. The cyan box shown here encloses the nuclear region of the galaxy, where there is a dense population of sources. This is presented in the final image, where these individual sources can be more clearly seen.

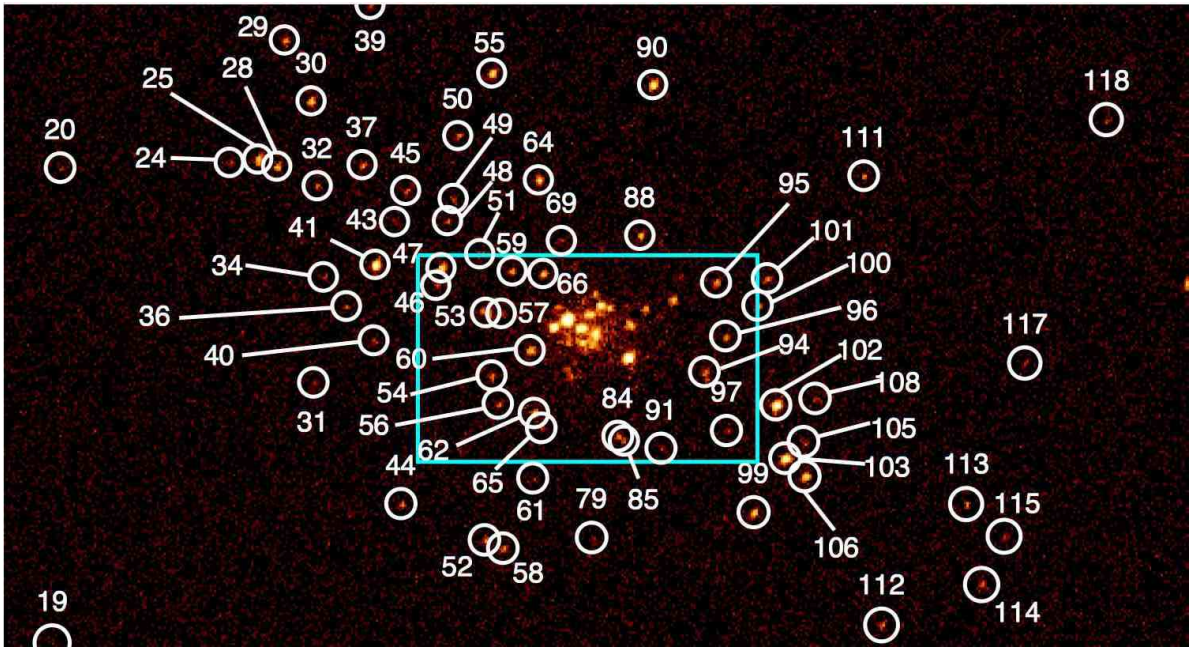
29
39
55
90
118
25
28
30
50
20
37
49
64
111
24
32
45
48
95
51
69
88
41
43
101
47
59
100
34
66
46
53
57
96
36
117
40
60
94
102
54
97
108
84
91
31
56
105
62
44
65
99
103
113
61
79
85
115
106
52
58
112
19
114

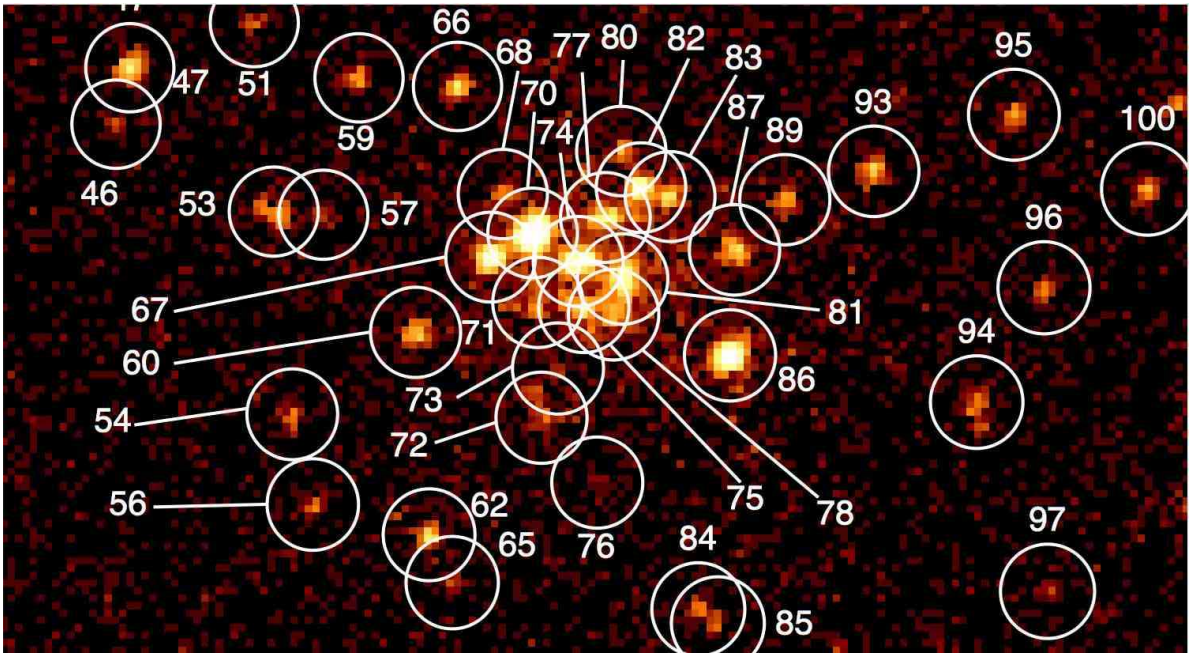
66
68
77
80
82
83
95
47
51
70
87
93
100
74
89
59
46
53
57
96
67
81
71
94
60
86
73
54
72
75
78
56
62
97
65
76
84
85

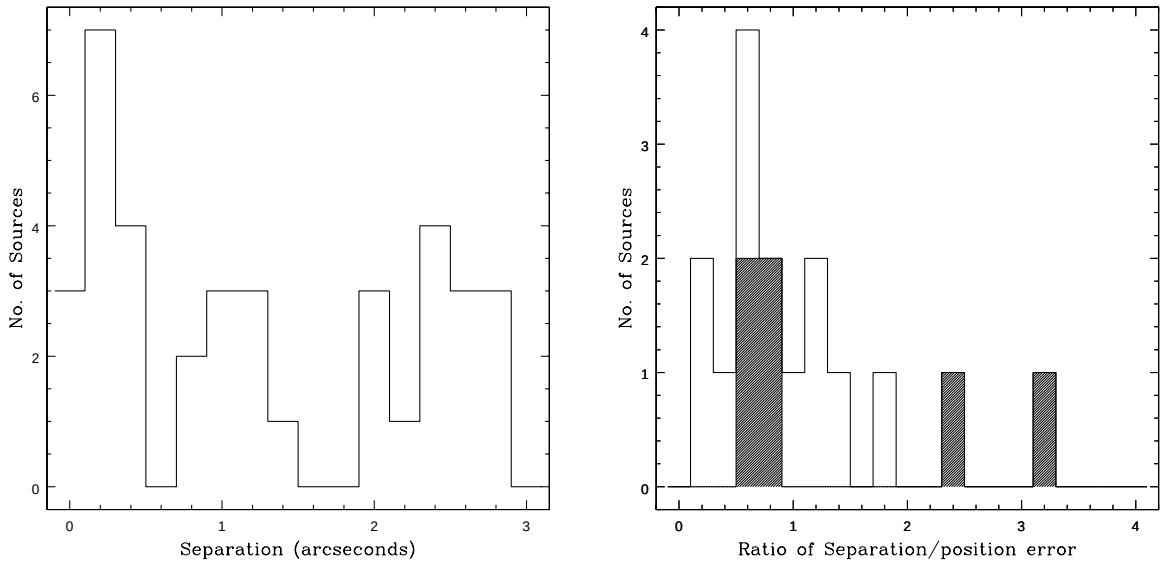

Fig. 4.— Left:A histogram of the separation between the co-added X-ray source position and the optical counterpart. Right: Histogram of the ratio of separation divided by the position uncertainty from the X-ray point source for all optical-X-ray correlations with separations smaller than 1″. Shaded regions indicate correlations with optical objects that have been classified as background sources (details of this classification are given in the text).

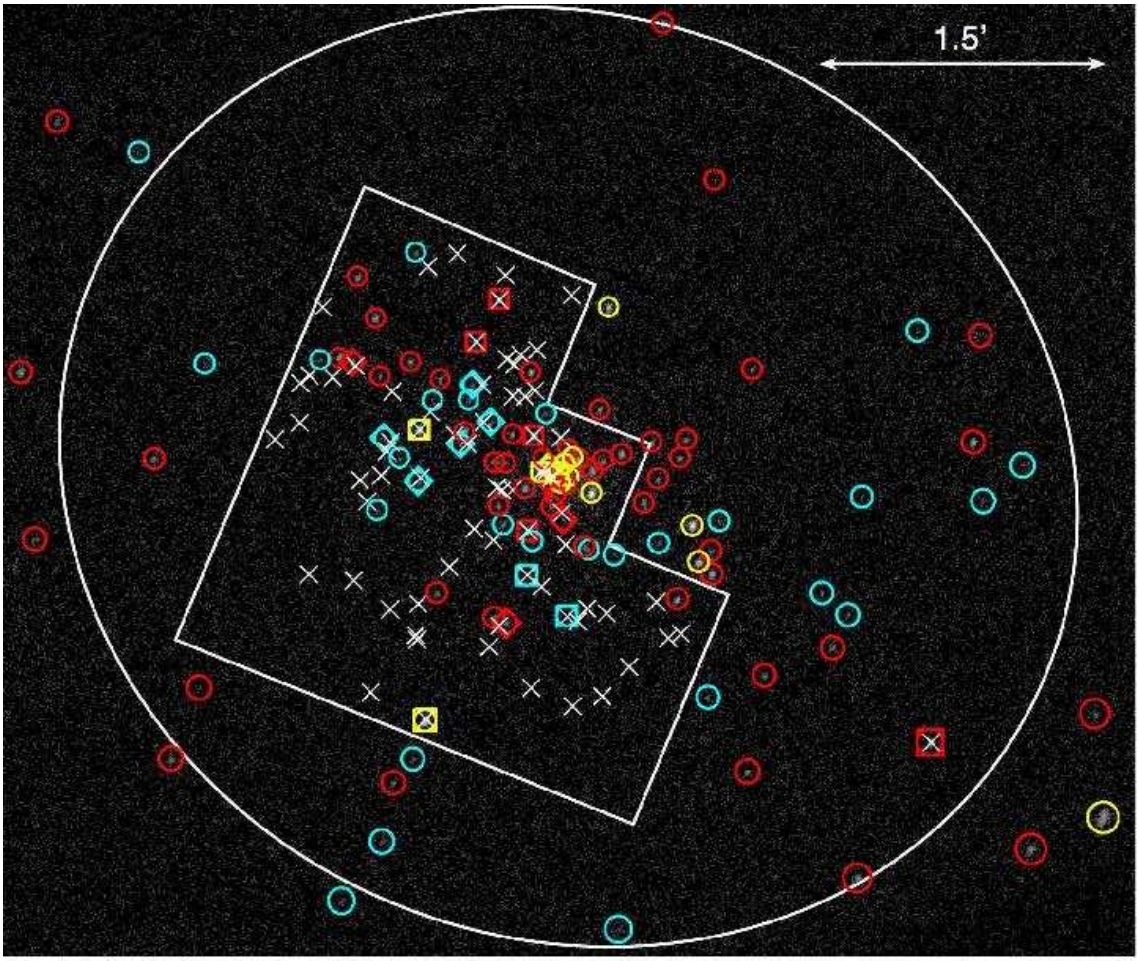

Fig. 5.— A full band X-ray image from the co-added observation of NGC 3379, with confirmed GCs from the *HST* observation indicated by white 'X' marks (with the GC position of the additional LMXB-GC match, external to the *HST* Field of View, also shown). X-ray sources that have correlated GCs are indicated by box regions, sources that are 'excluded matches' are indicated with a diamond region and X-ray sources without a GC counterpart are shown by circular regions. X-ray regions are colored to indicate the 0.3−8.0 keV luminosity of the source from the co-added observation; yellow regions indicate $L_{\rm X}\geq 1\times10^{38}$erg s^{-1}, red regions have $1\times10^{38}\ \geq L_{\rm X}\geq 1\times10^{37}$erg s^{-1}, and cyan regions show sources with $L_{\rm X}\leq 1\times10^{37}$erg s^{-1}. Also shown are the D_{25} ellipse and the *HST* FOV. The GC X-ray correlation shown external to the *HST* FOV was detected in two other independent GC studies (see text for more details).

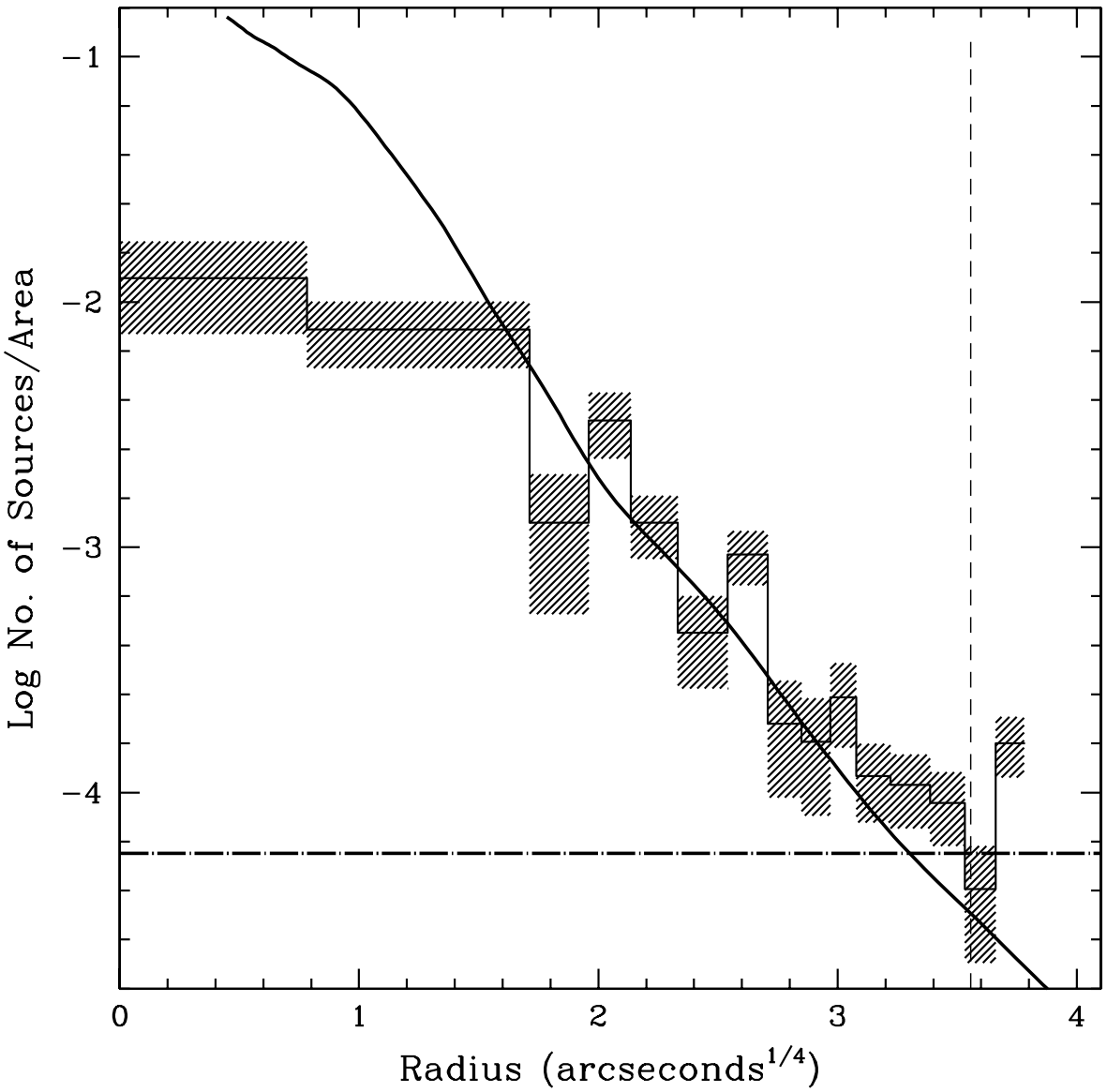

Fig. 6.— X-ray source density profile compared to the optical profile. The histogram indicates the X-ray data and the thick black line is the I-band surface brightness best fit of Cappellari *et al.* (2006). The vertical dashed line is the D_{25} ellipse and the horizontal dot-dashed line indicates the expected number of background sources.

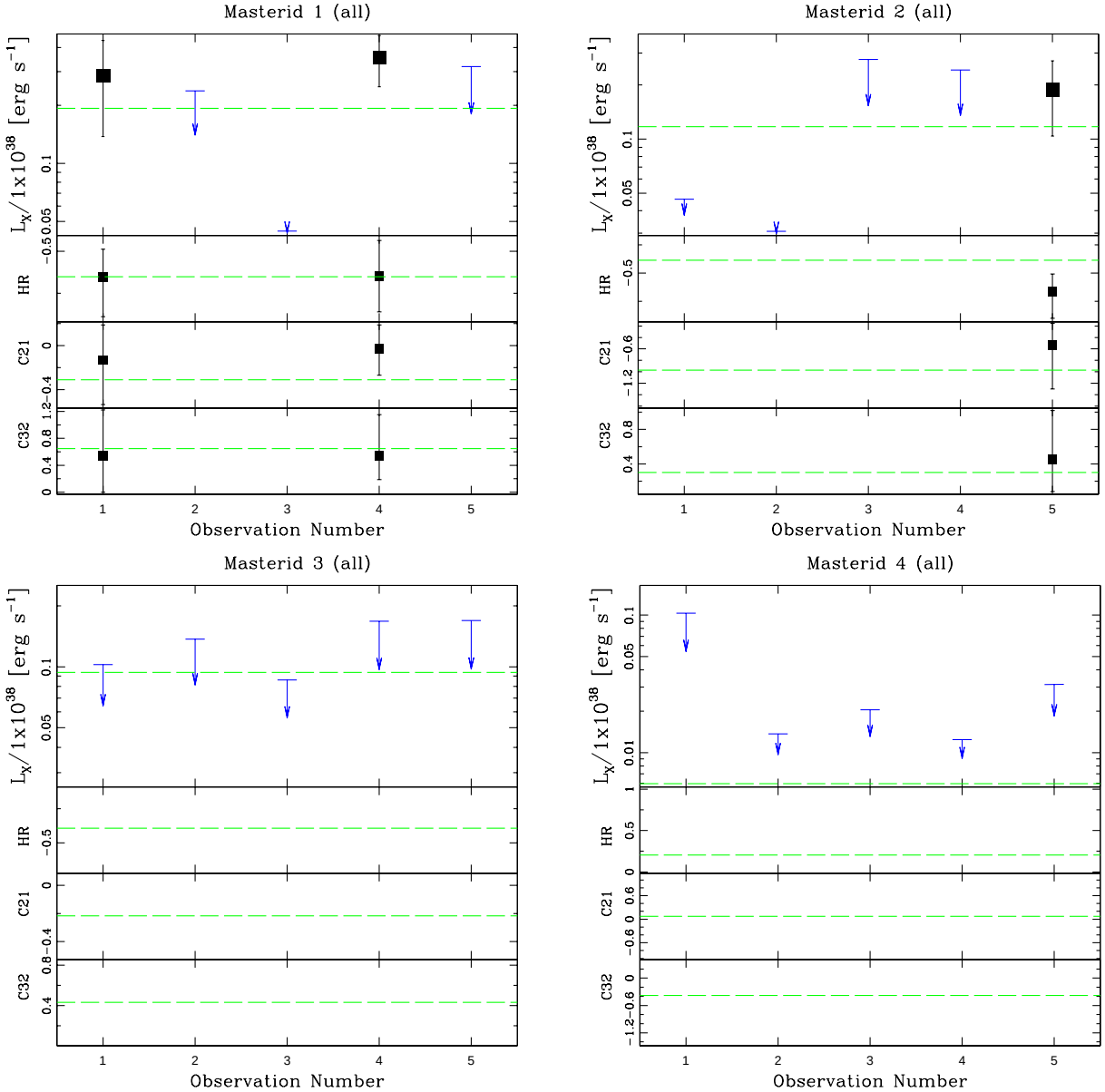

Fig. 7.— Plots of the the 132 detected sources, summarizing the variations in properties of each source between each observation. In the main panel the long-term light curves are shown. In the second panel down, the hardness ratios are indicated. These are defined to be HR = H−S / H+S, where H is the number of counts in the hard band (2.0−8.0 keV) and S is the number of counts in the soft band (0.5−2.0 keV). In the third and fourth panels the color ratios; C21 and C32, are plotted, where C21=*log*S2+*log*S1 and C32=−*log*H+*log*S2. For the color ratios the bandwidths are defined to be S1=0.3−0.9 keV, S2=0.9−2.5 keV and H=2.5−8.0 keV. In cases where a source was not detected in a single observation, an upper limit of the X-ray luminosity has been calculated, details of which are discussed in section 2.1. In all of the panels, the green horizontal line indicates the value derived from the co-added observation. In cases where the source was not detected in the co-added observation, a blue horizontal line indicates the upper luminosity calculated for that source.

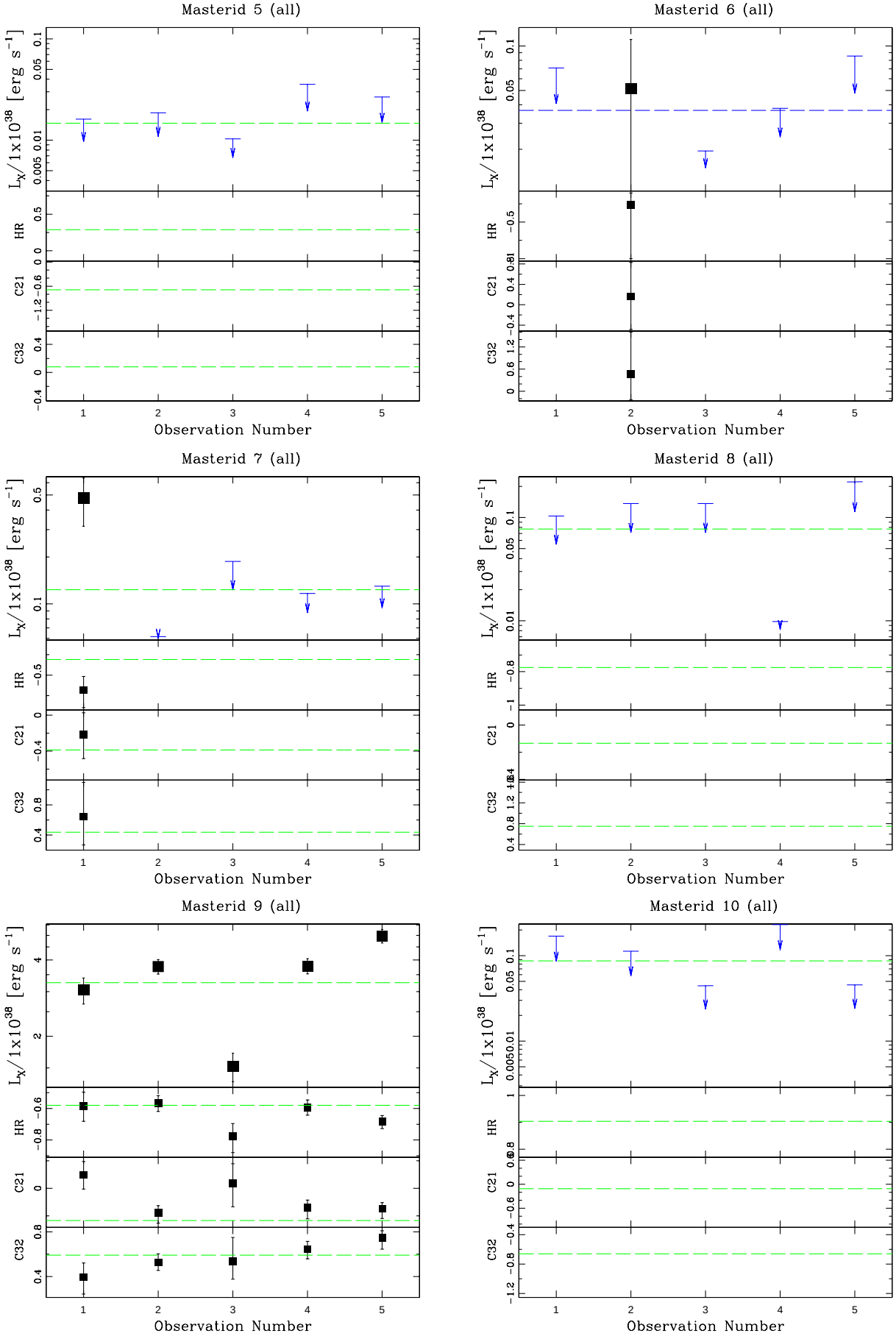
Masterid 5 (all)
Masterid 6 (all)
Masterid 7 (all)
Masterid 8 (all)
Masterid 9 (all)
Masterid 10 (all)
$L_X/1x10^{38}$ [erg s^{-1}]
HR
C21
C32
Observation Number

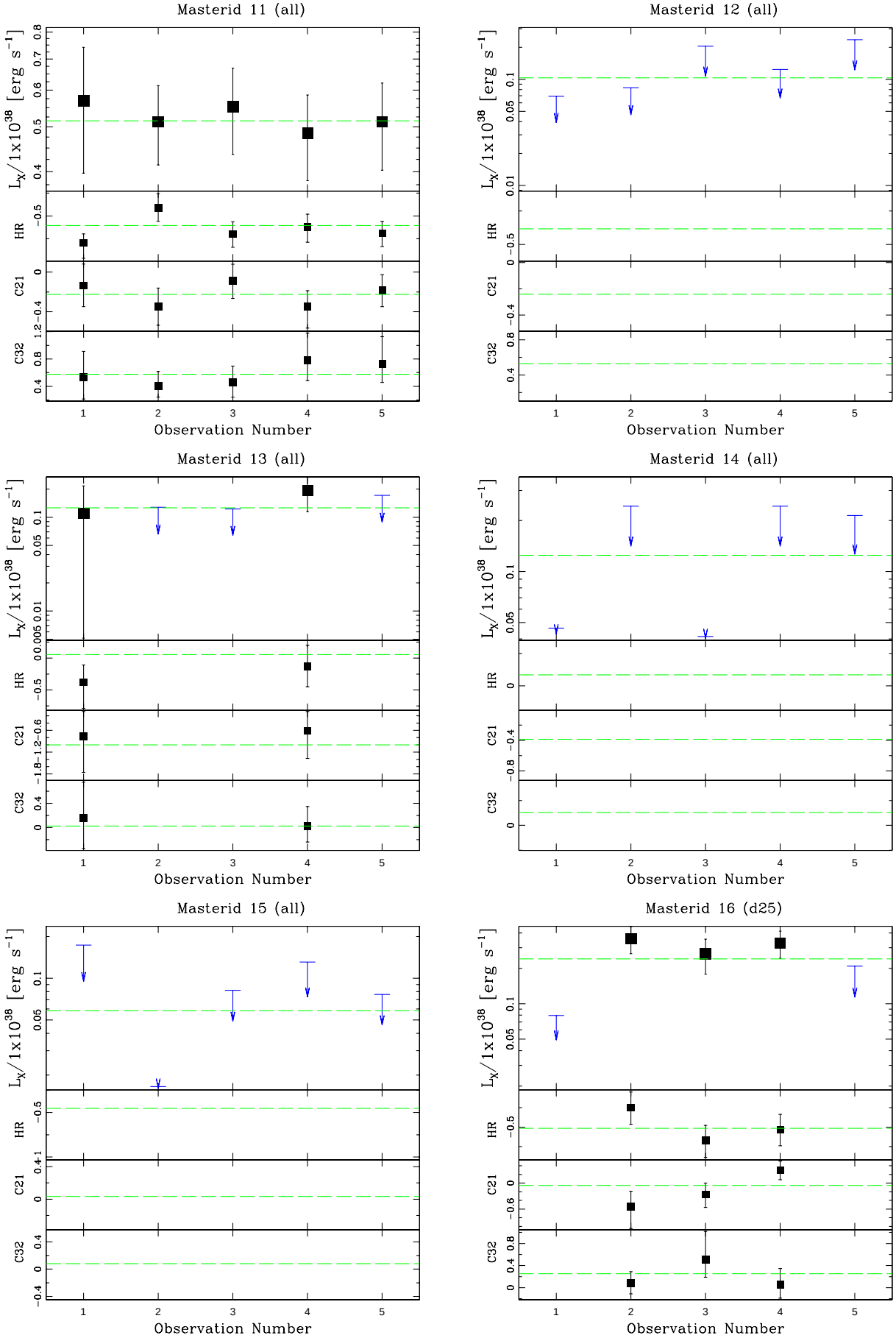
Masterid 11 (all)
Masterid 12 (all)
Masterid 13 (all)
Masterid 14 (all)
Masterid 15 (all)
Masterid 16 (d25)
$L_X/1x10^{38}$ [erg s^{-1}]
HR
C21
C32
Observation Number

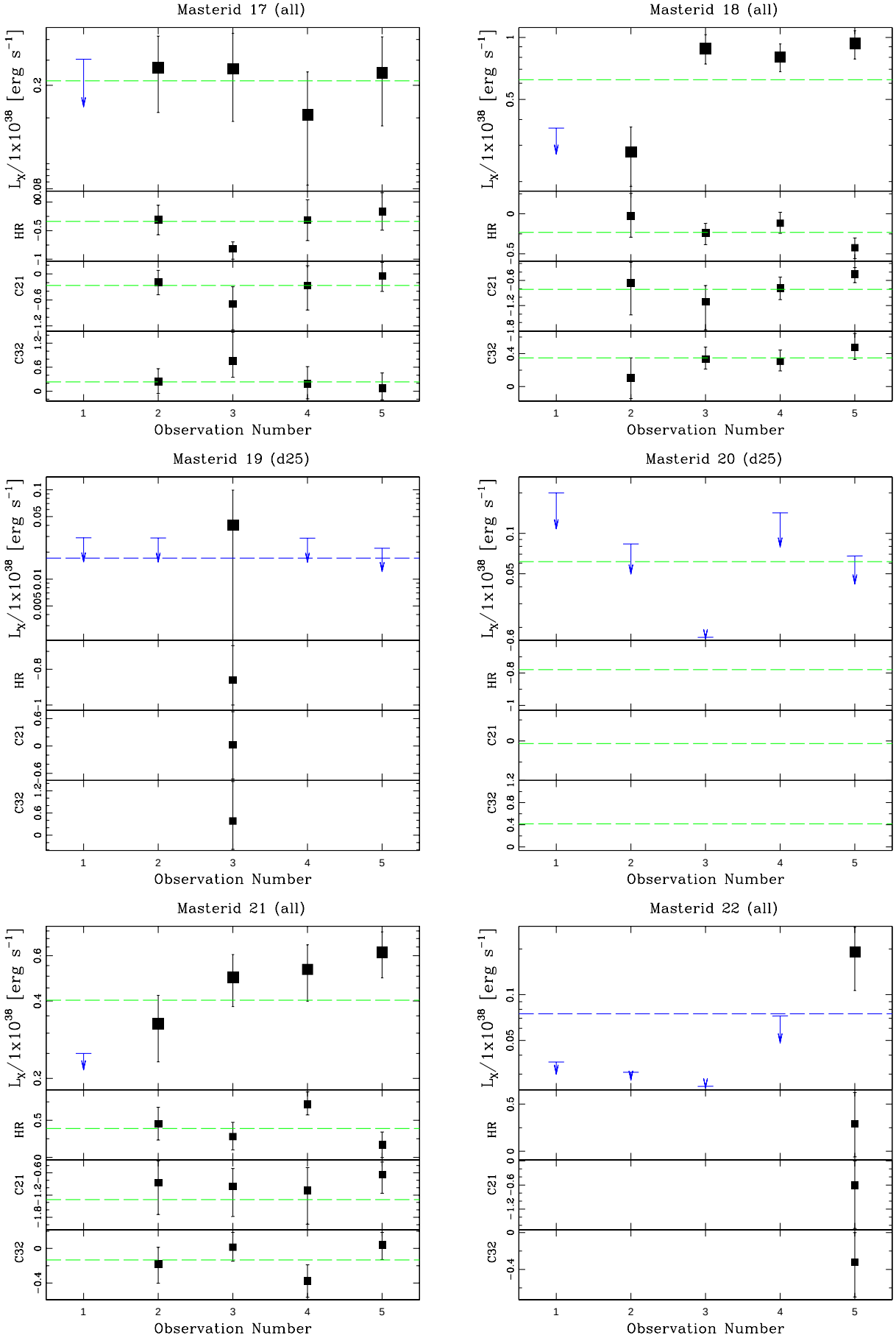
Masterid 17 (all)
Masterid 18 (all)
Masterid 19 (d25)
Masterid 20 (d25)
Masterid 21 (all)
Masterid 22 (all)
$L_X/1x10^{38}$ [erg s^{-1}]
HR
C21
C32
Observation Number

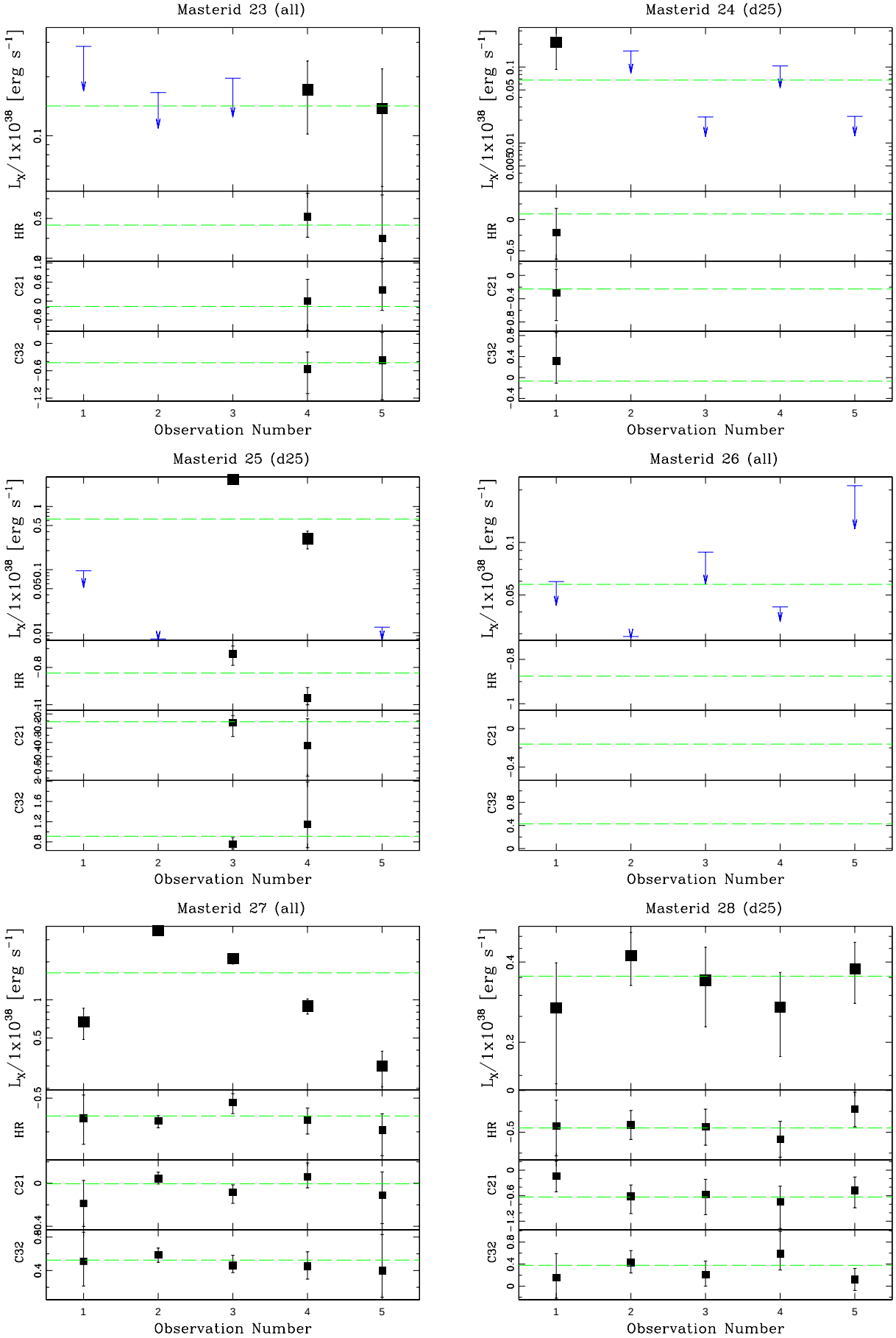
Masterid 23 (all)
Masterid 24 (d25)
Masterid 25 (d25)
Masterid 26 (all)
Masterid 27 (all)
Masterid 28 (d25)
$L_X/1x10^{38}$ [erg s^{-1}]
HR
C21
C32
Observation Number

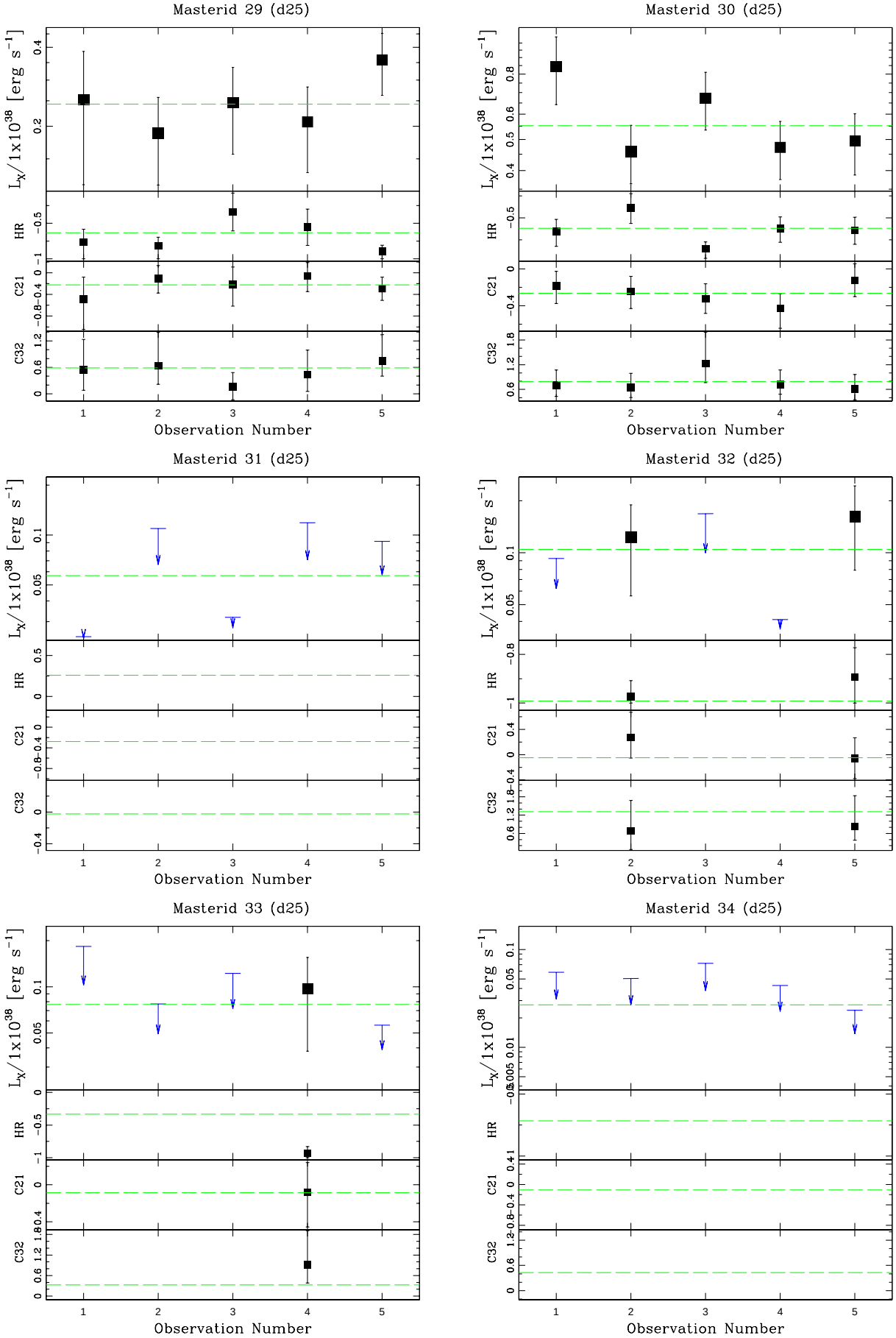
Masterid 29 (d25)
Masterid 30 (d25)
Masterid 31 (d25)
Masterid 32 (d25)
Masterid 33 (d25)
Masterid 34 (d25)
$L_X/1x10^{38}$ [erg s^{-1}]
HR
C21
C32
Observation Number

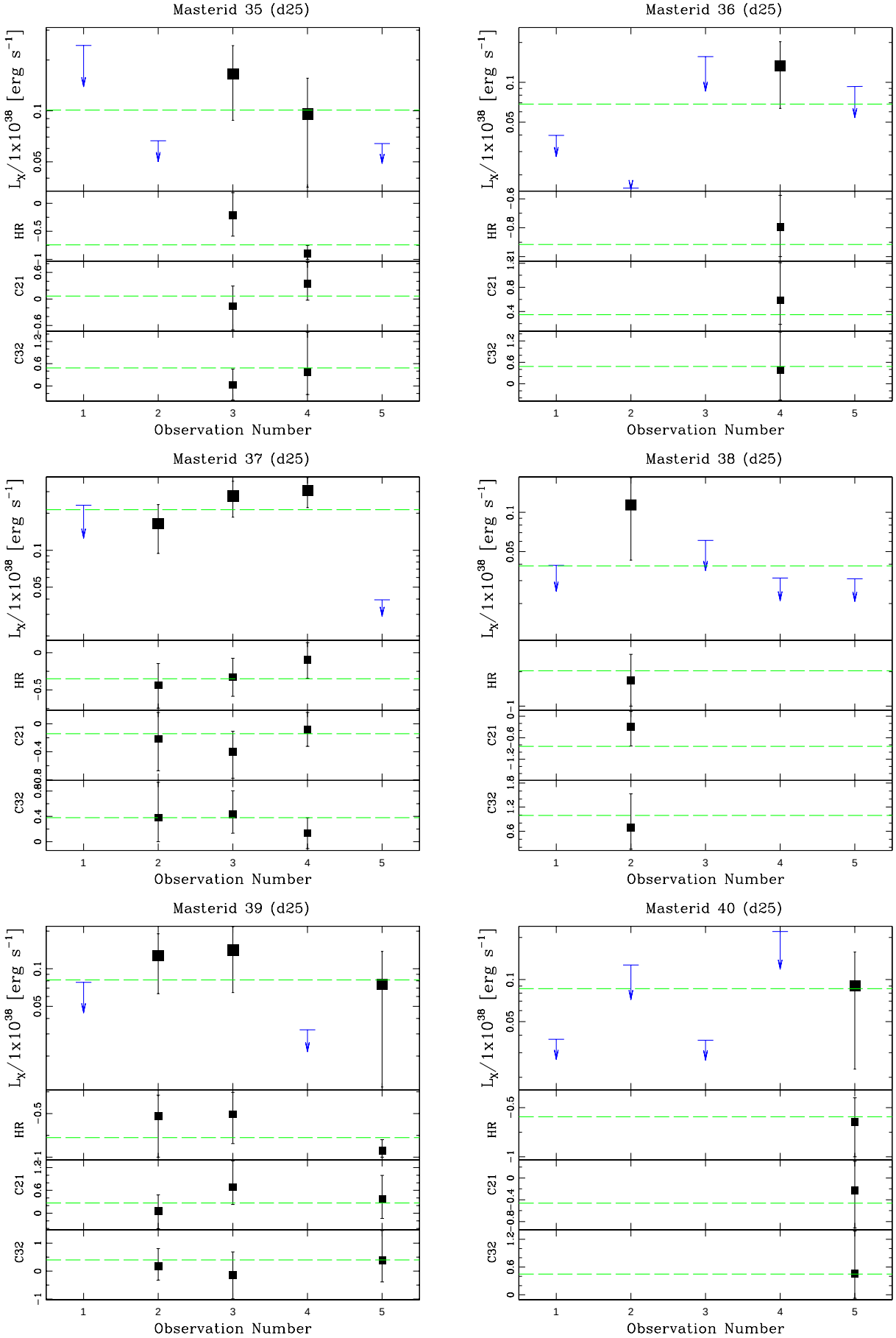
Masterid 35 (d25)
Masterid 36 (d25)
Masterid 37 (d25)
Masterid 38 (d25)
Masterid 39 (d25)
Masterid 40 (d25)
$L_X/1x10^{38}$ [erg s^{-1}]
HR
C21
C32
Observation Number

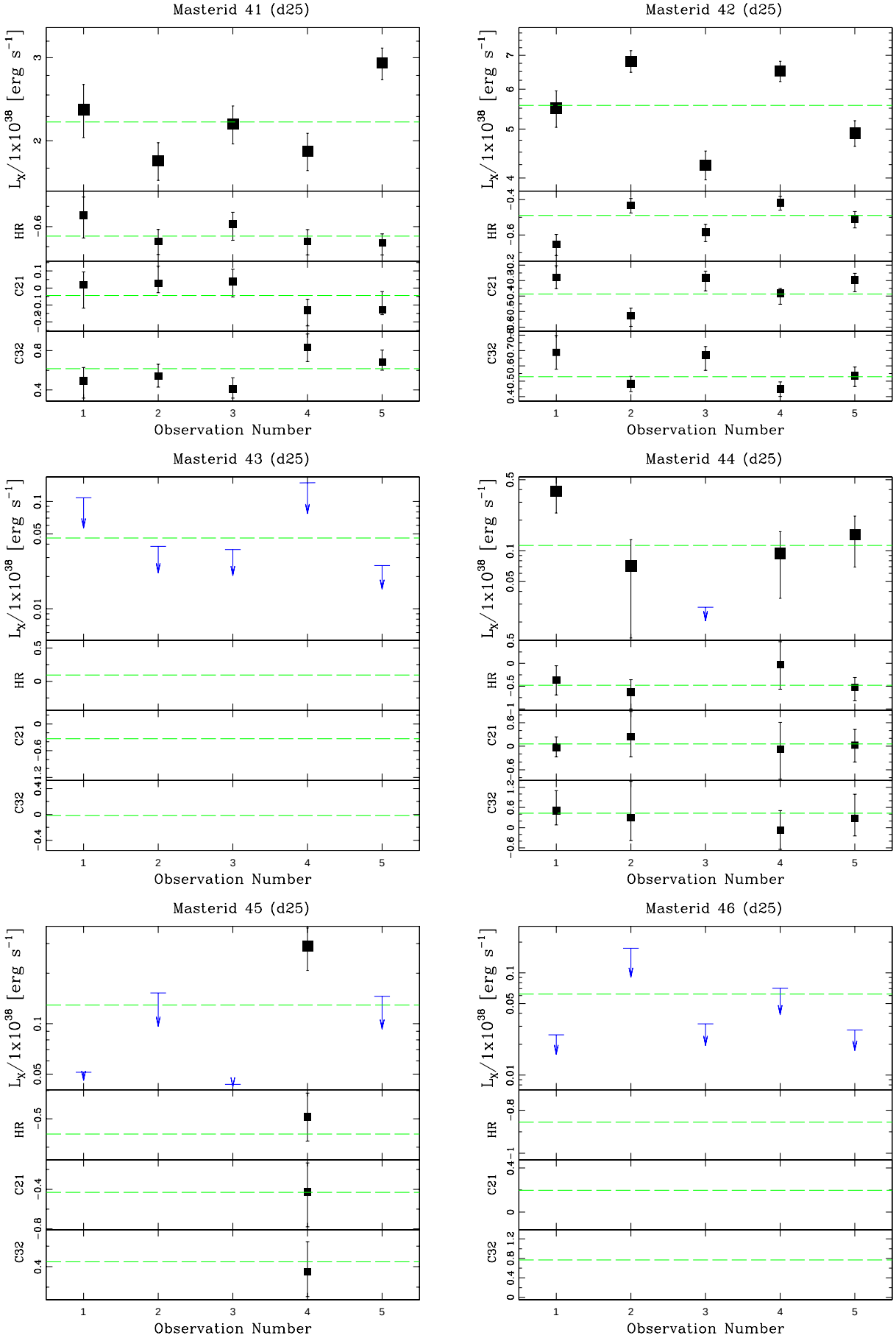
Masterid 41 (d25)
Masterid 42 (d25)
Masterid 43 (d25)
Masterid 44 (d25)
Masterid 45 (d25)
Masterid 46 (d25)
$L_X/1x10^{38}$ [erg s^{-1}]
HR
C21
C32
Observation Number

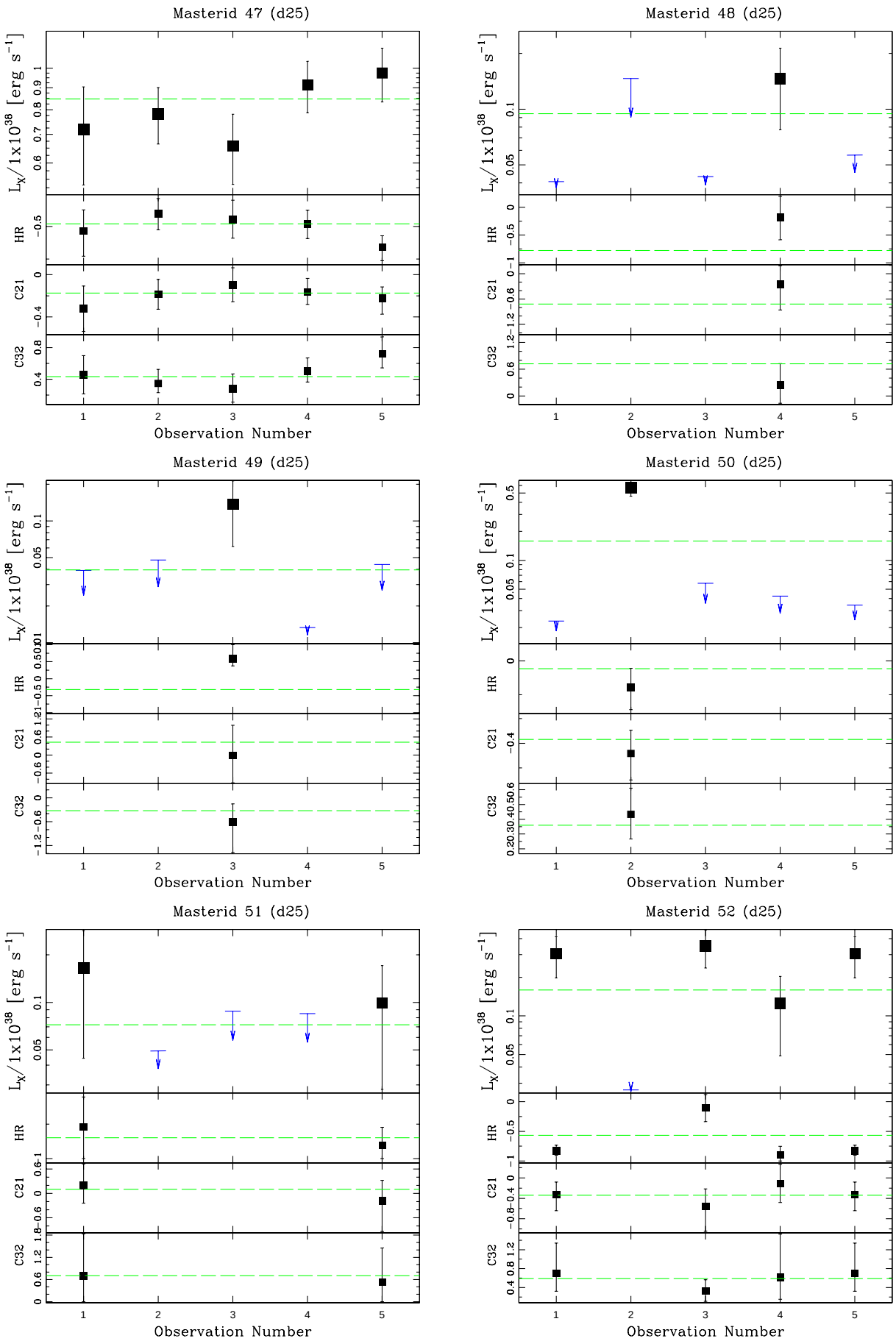
Masterid 47 (d25)
Masterid 48 (d25)
Masterid 49 (d25)
Masterid 50 (d25)
Masterid 51 (d25)
Masterid 52 (d25)
$L_X/1x10^{38}$ [erg s^{-1}]
HR
C21
C32
Observation Number

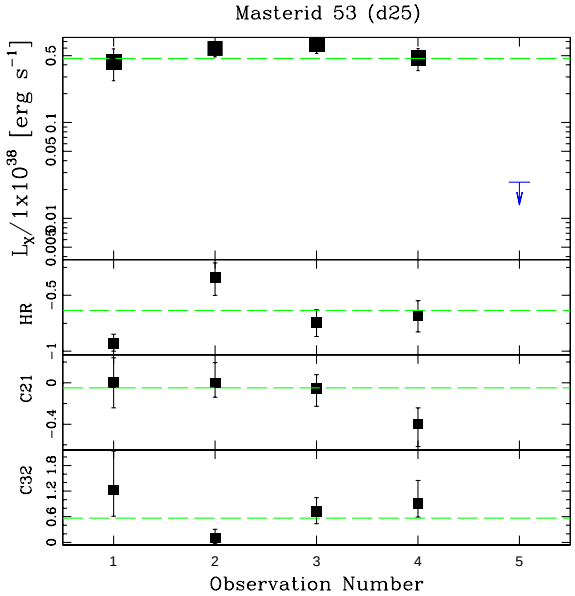
Masterid 53 (d25)
$L_X/1x10^{38}$ [erg s^{-1}]
HR
C21
C32
Observation Number

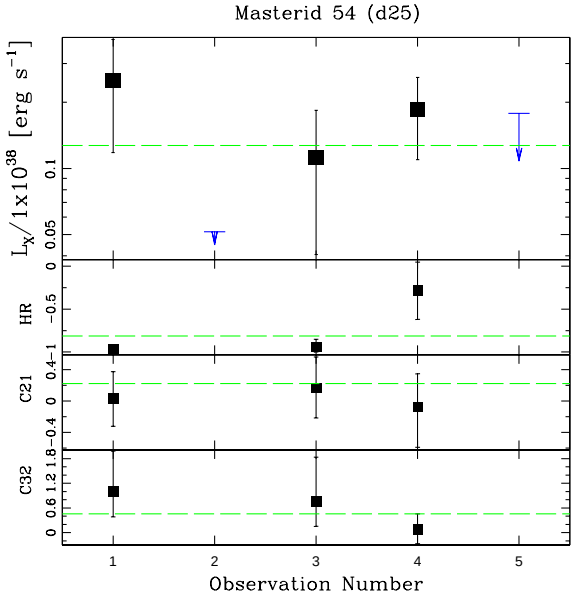
Masterid 54 (d25)
$L_X/1x10^{38}$ [erg s^{-1}]
HR
C21
C32
Observation Number

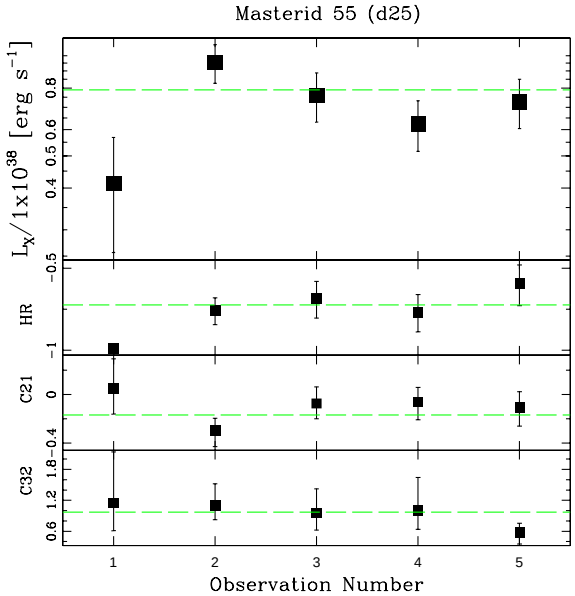
Masterid 55 (d25)
$L_X/1x10^{38}$ [erg s^{-1}]
HR
C21
C32
Observation Number

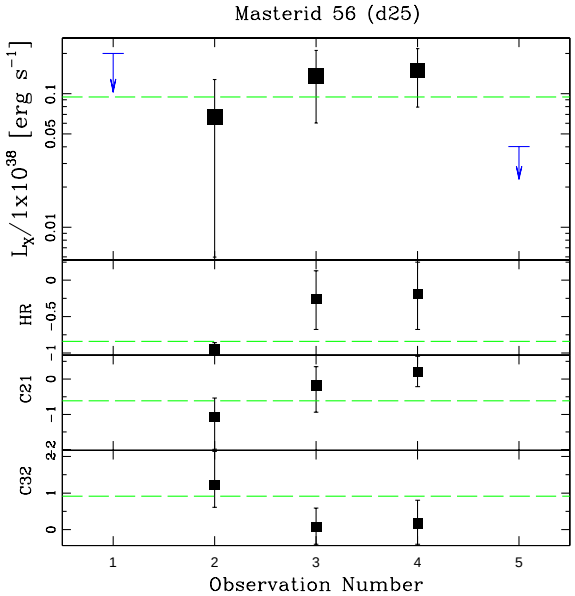
Masterid 56 (d25)
$L_X/1x10^{38}$ [erg s^{-1}]
HR
C21
C32
Observation Number

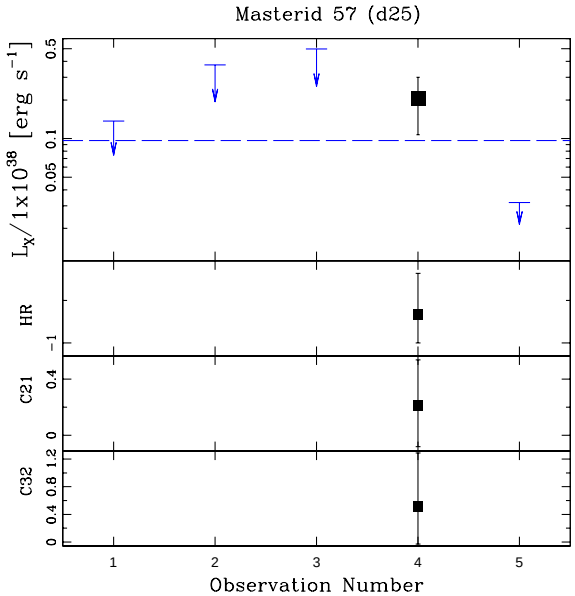
Masterid 57 (d25)
$L_X/1x10^{38}$ [erg s^{-1}]
HR
C21
C32
Observation Number

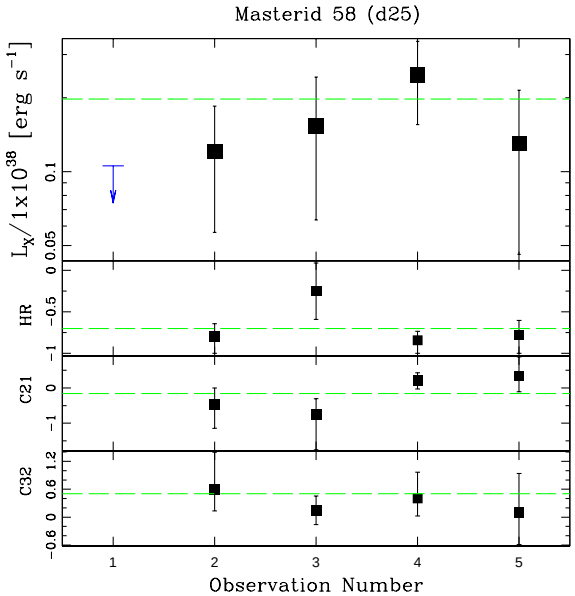
Masterid 58 (d25)
$L_X/1x10^{38}$ [erg s^{-1}]
HR
C21
C32
Observation Number

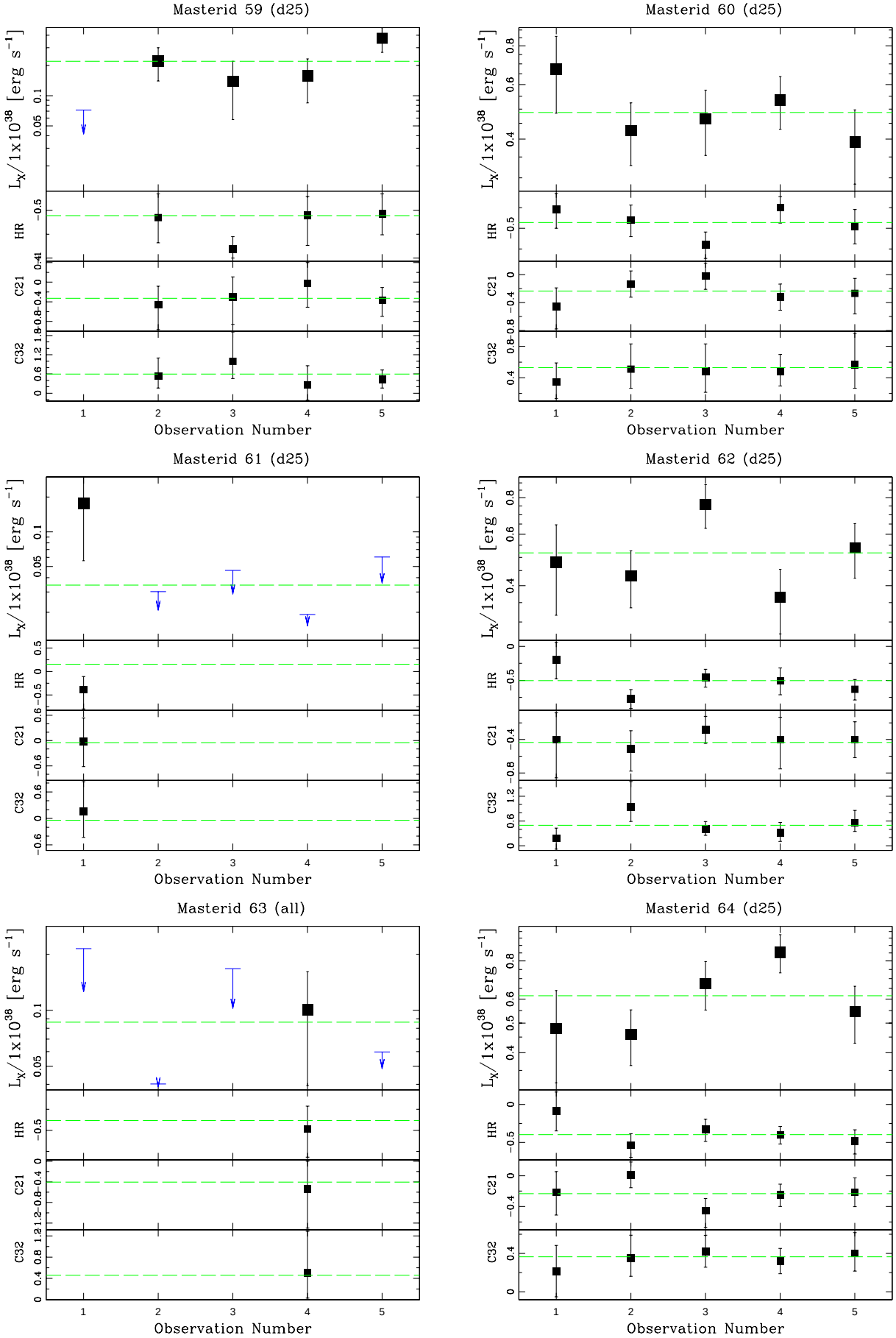
Masterid 59 (d25)
Masterid 60 (d25)
Masterid 61 (d25)
Masterid 62 (d25)
Masterid 63 (all)
Masterid 64 (d25)
$L_X/1x10^{38}$ [erg s^{-1}]
HR
C21
C32
Observation Number

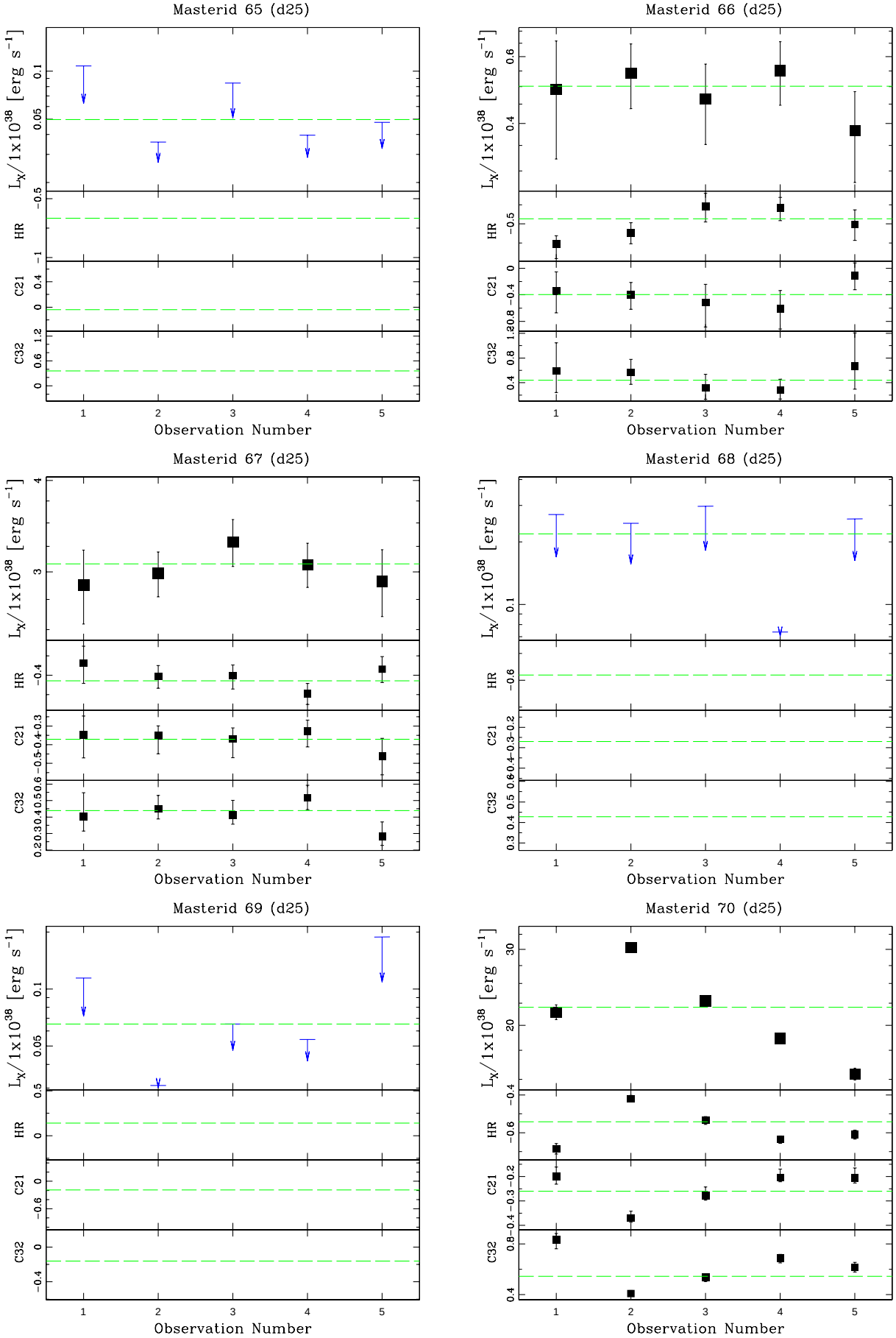
Masterid 65 (d25)
Masterid 66 (d25)
Masterid 67 (d25)
Masterid 68 (d25)
Masterid 69 (d25)
Masterid 70 (d25)
$L_X/1x10^{38}$ [erg s^{-1}]
HR
C21
C32
Observation Number

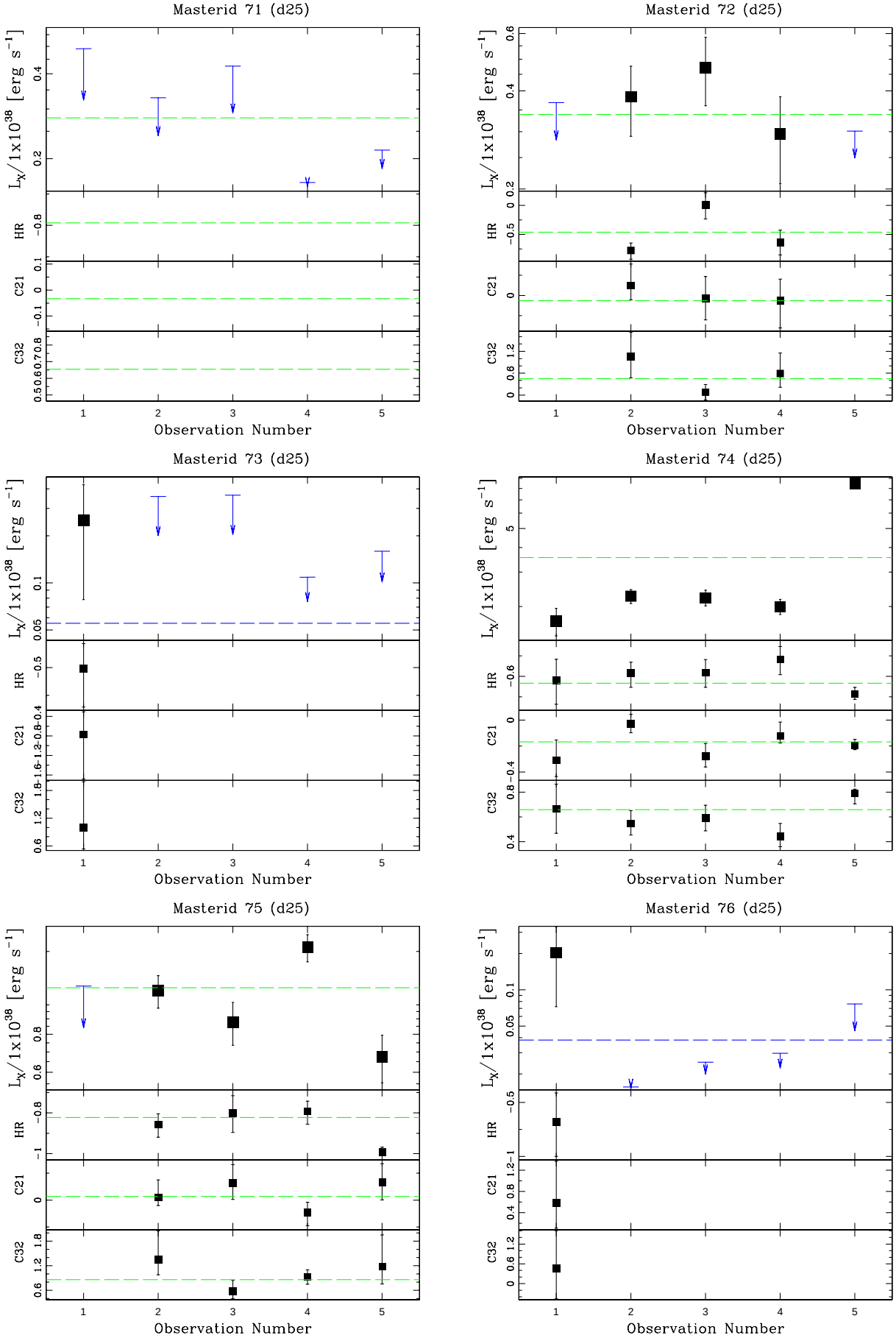
Masterid 71 (d25)
Masterid 72 (d25)
Masterid 73 (d25)
Masterid 74 (d25)
Masterid 75 (d25)
Masterid 76 (d25)
$L_X/1x10^{38}$ [erg s^{-1}]
HR
C21
C32
Observation Number

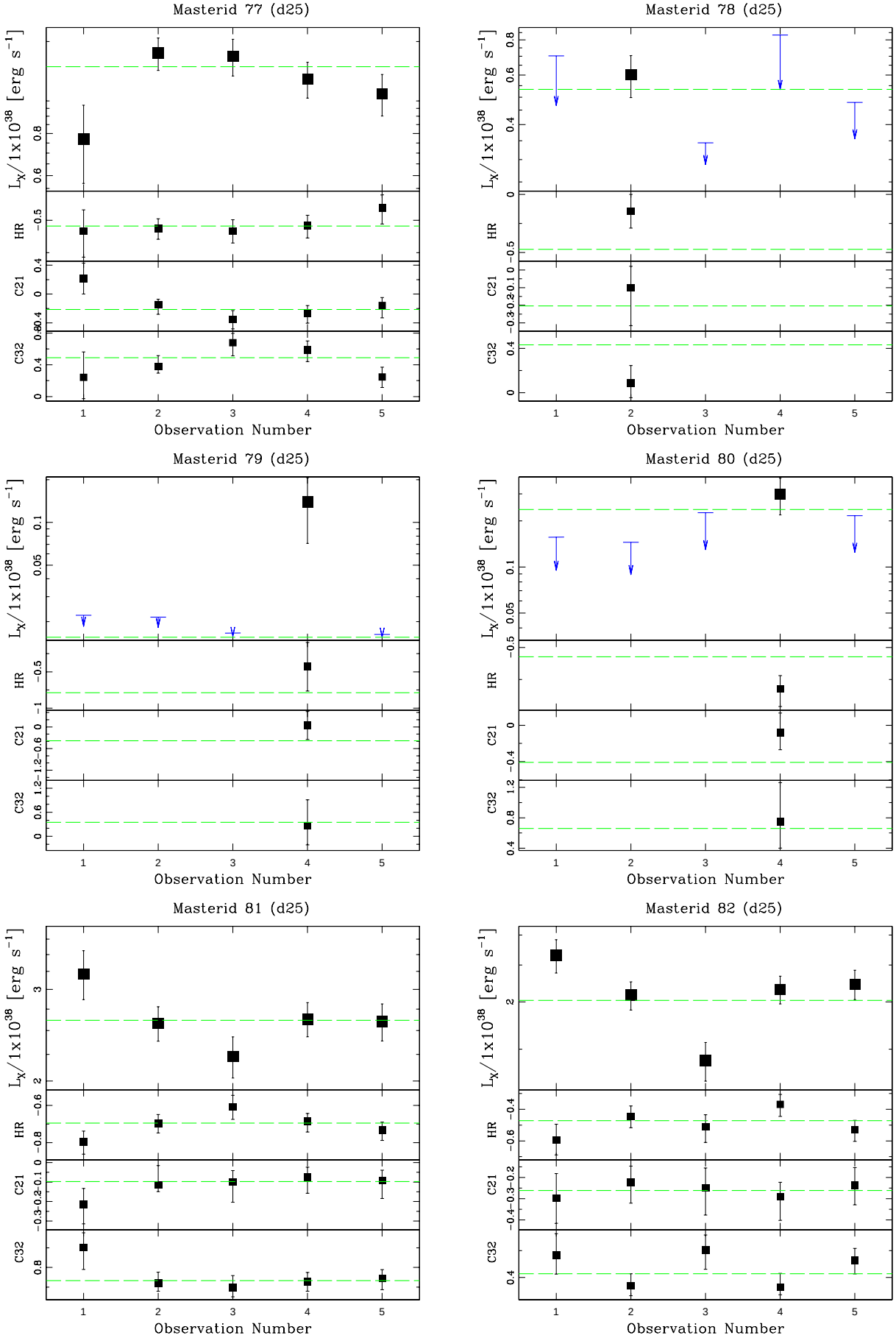
Masterid 77 (d25)
Masterid 78 (d25)
Masterid 79 (d25)
Masterid 80 (d25)
Masterid 81 (d25)
Masterid 82 (d25)
$L_X/1x10^{38}$ [erg s^{-1}]
HR
C21
C32
Observation Number

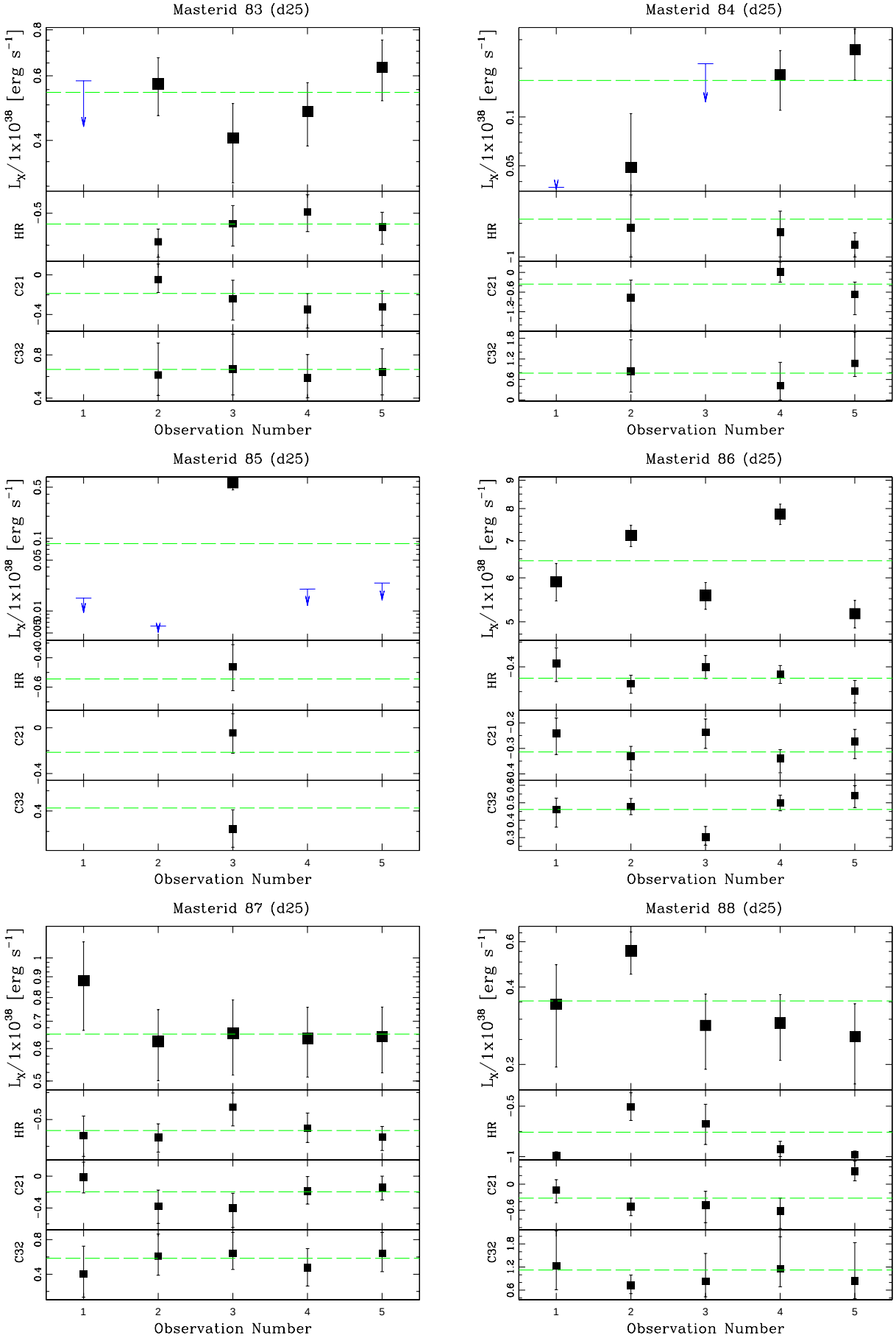
Masterid 83 (d25)
Masterid 84 (d25)
Masterid 85 (d25)
Masterid 86 (d25)
Masterid 87 (d25)
Masterid 88 (d25)
$L_X/1x10^{38}$ [erg s^{-1}]
HR
C21
C32
Observation Number

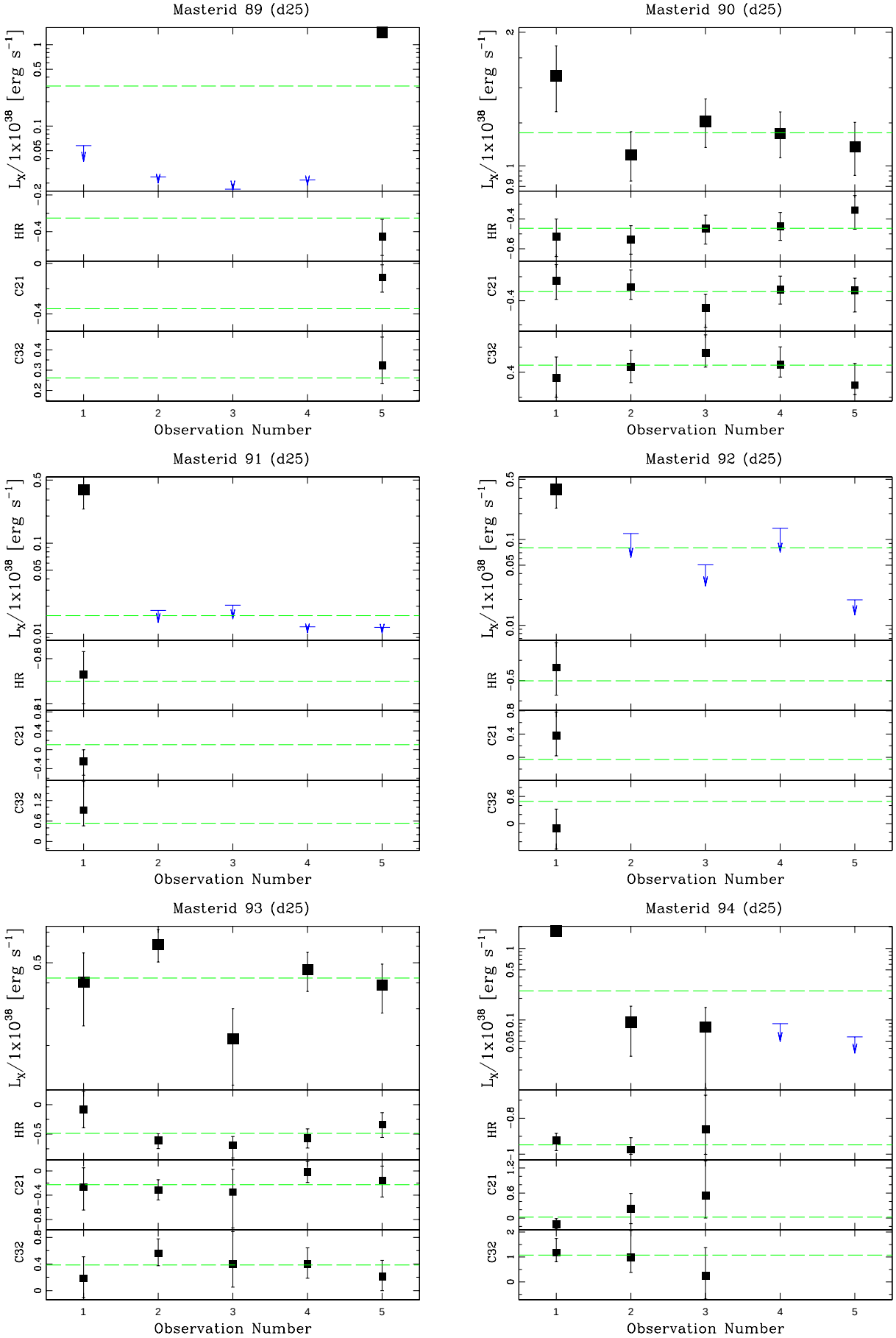
Masterid 89 (d25)
Masterid 90 (d25)
Masterid 91 (d25)
Masterid 92 (d25)
Masterid 93 (d25)
Masterid 94 (d25)
$L_X/1x10^{38}$ [erg s^{-1}]
HR
C21
C32
Observation Number

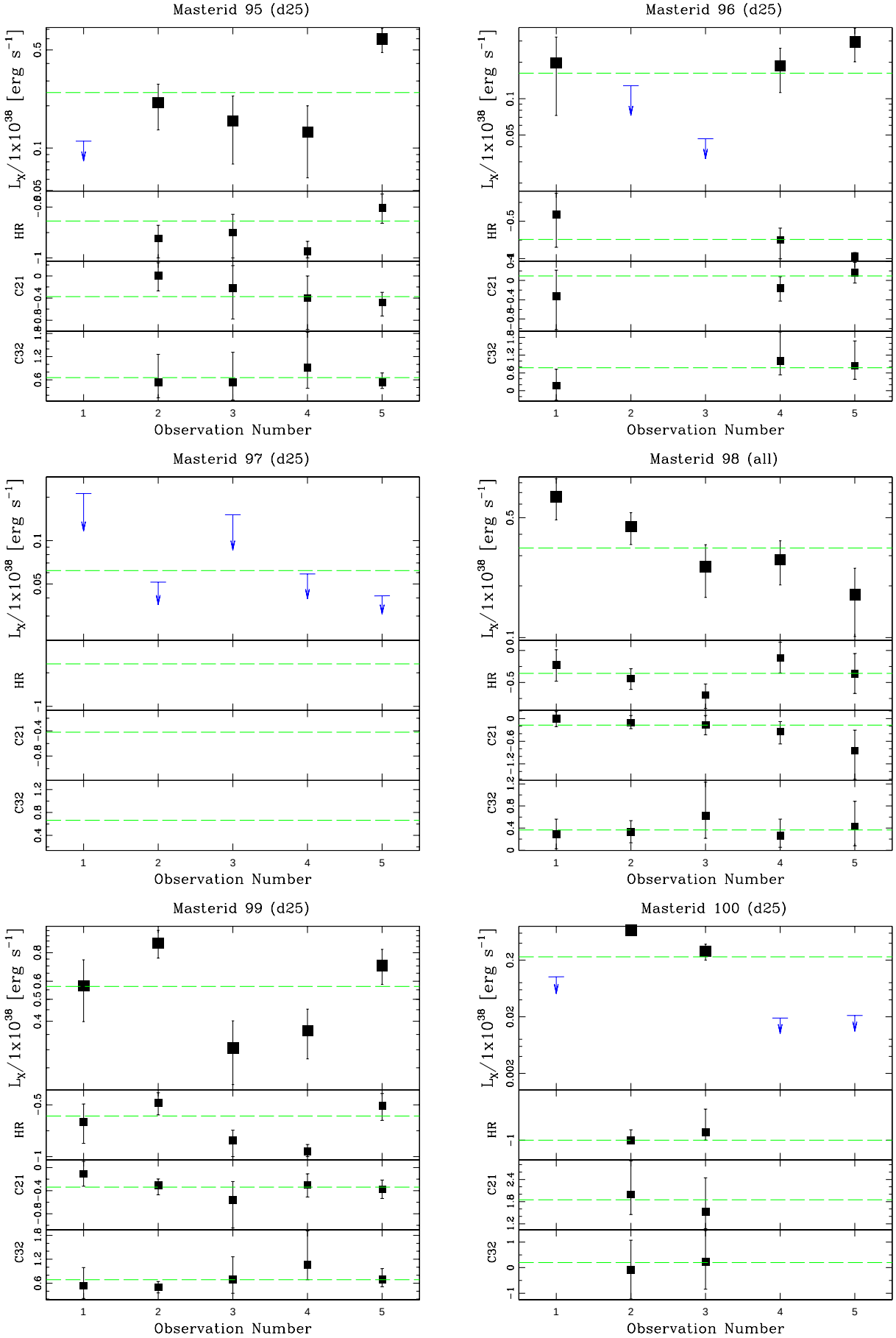
Masterid 95 (d25)
Masterid 96 (d25)
Masterid 97 (d25)
Masterid 98 (all)
Masterid 99 (d25)
Masterid 100 (d25)
$L_X/1x10^{38}$ [erg s^{-1}]
HR
C21
C32
Observation Number

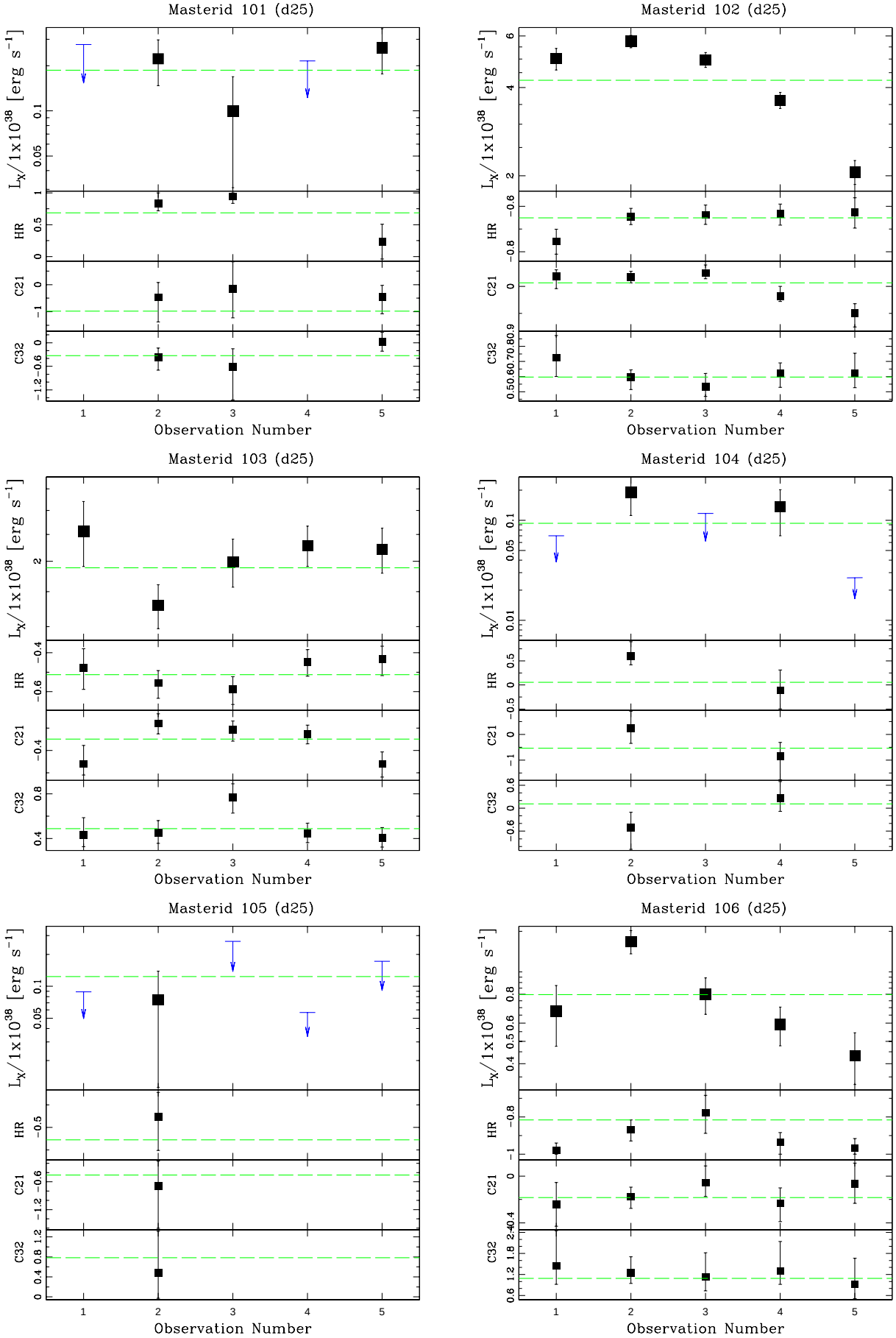
Masterid 101 (d25)
Masterid 102 (d25)
Masterid 103 (d25)
Masterid 104 (d25)
Masterid 105 (d25)
Masterid 106 (d25)
$L_X/1x10^{38}$ [erg s^{-1}]
HR
C21
C32
Observation Number

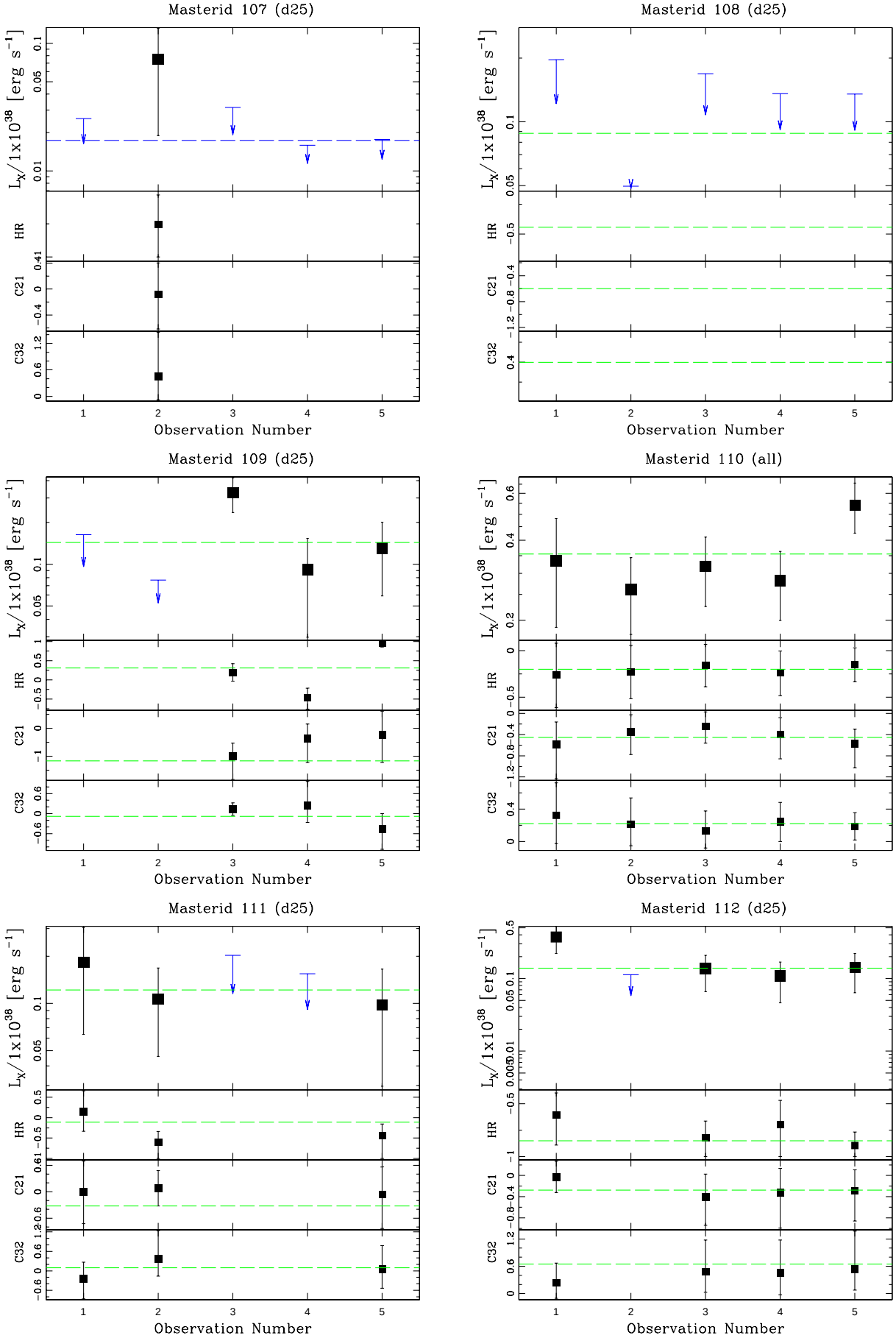
Masterid 107 (d25)
Masterid 108 (d25)
Masterid 109 (d25)
Masterid 110 (all)
Masterid 111 (d25)
Masterid 112 (d25)
$L_X/1x10^{38}$ [erg s^{-1}]
HR
C21
C32
Observation Number

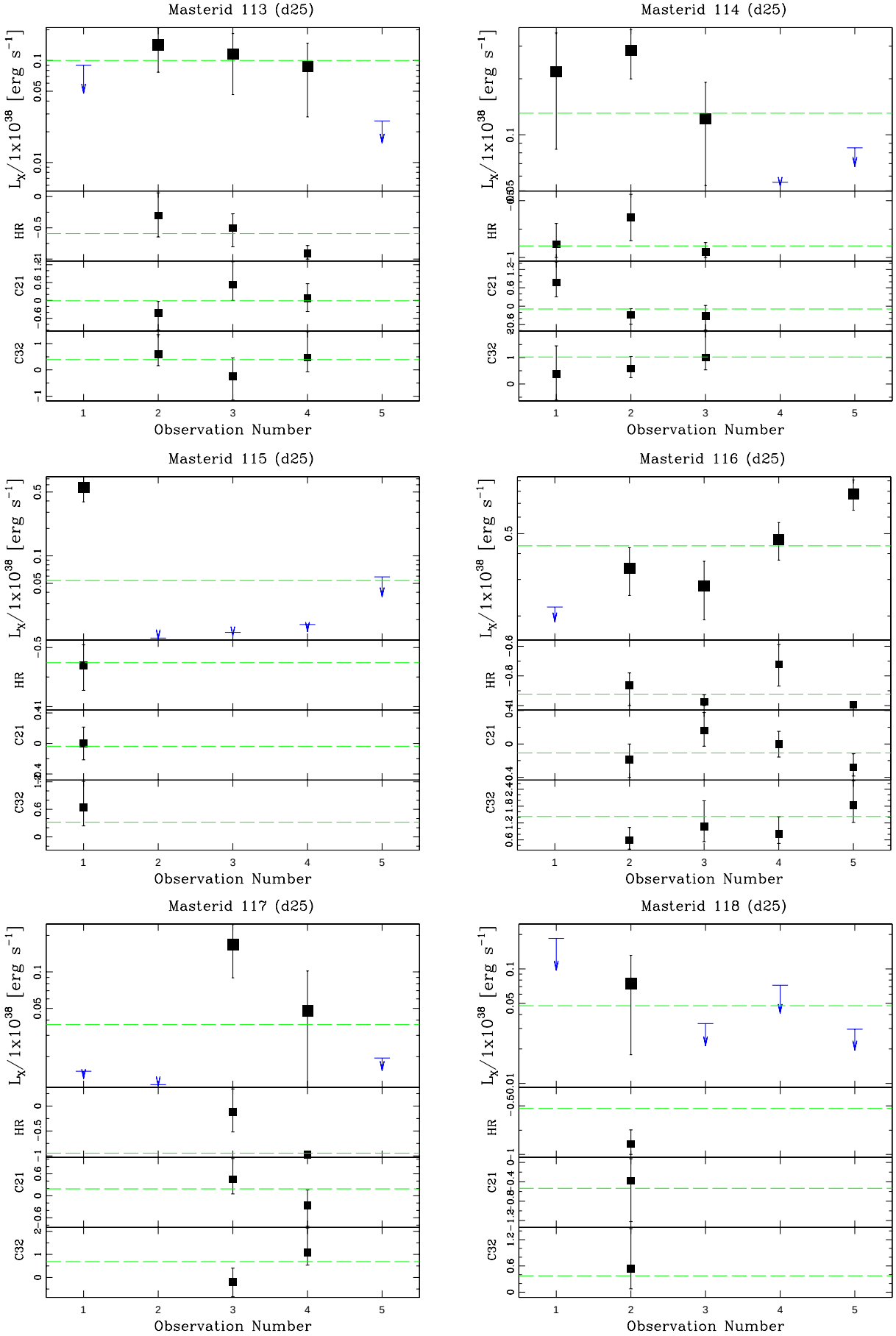
Masterid 113 (d25)
Masterid 114 (d25)
Masterid 115 (d25)
Masterid 116 (d25)
Masterid 117 (d25)
Masterid 118 (d25)
$L_X/1x10^{38}$ [erg s^{-1}]
HR
C21
C32
Observation Number

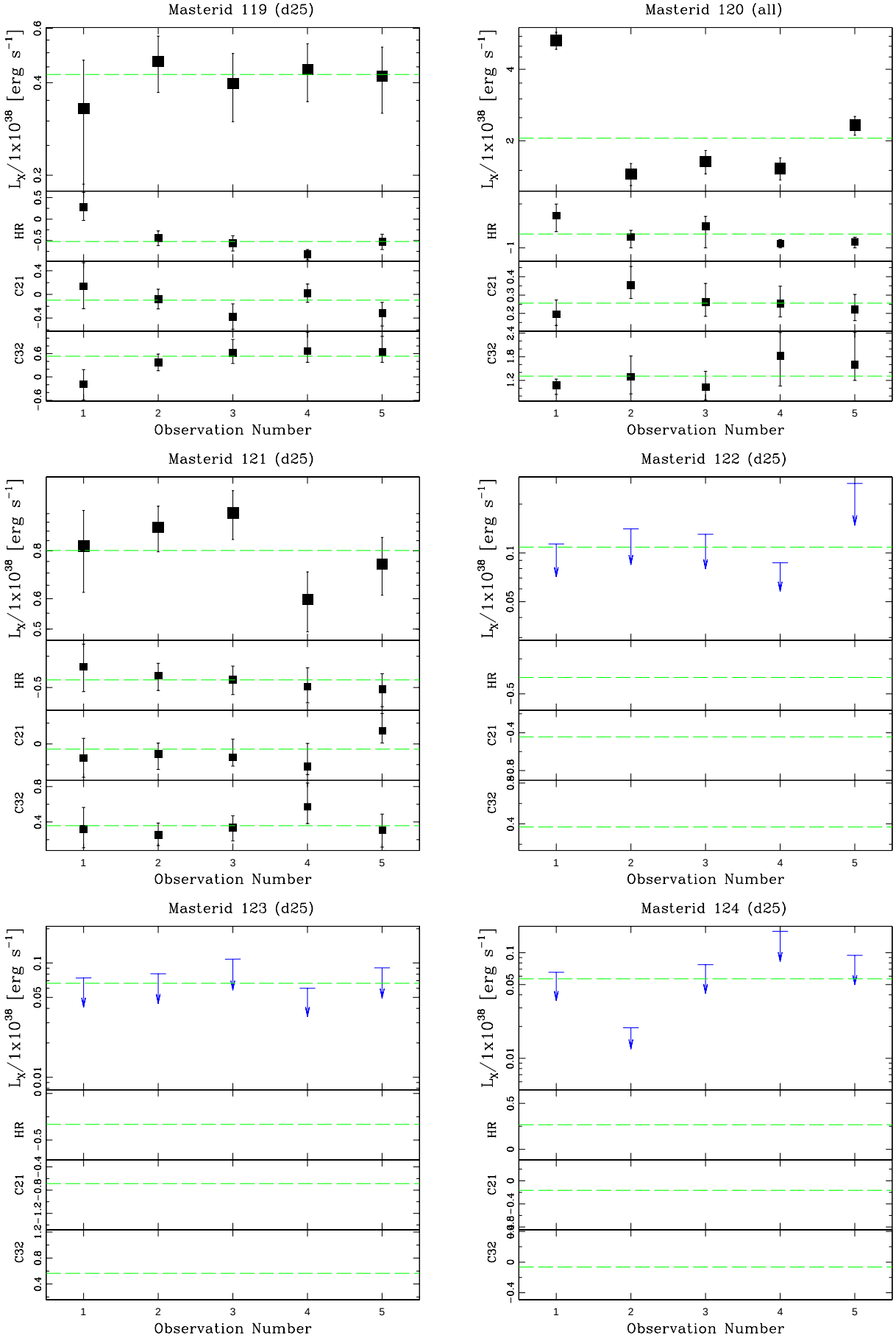
Masterid 119 (d25)
Masterid 120 (all)
Masterid 121 (d25)
Masterid 122 (d25)
Masterid 123 (d25)
Masterid 124 (d25)
$L_X/1x10^{38}$ [erg s^{-1}]
HR
C21
C32
Observation Number

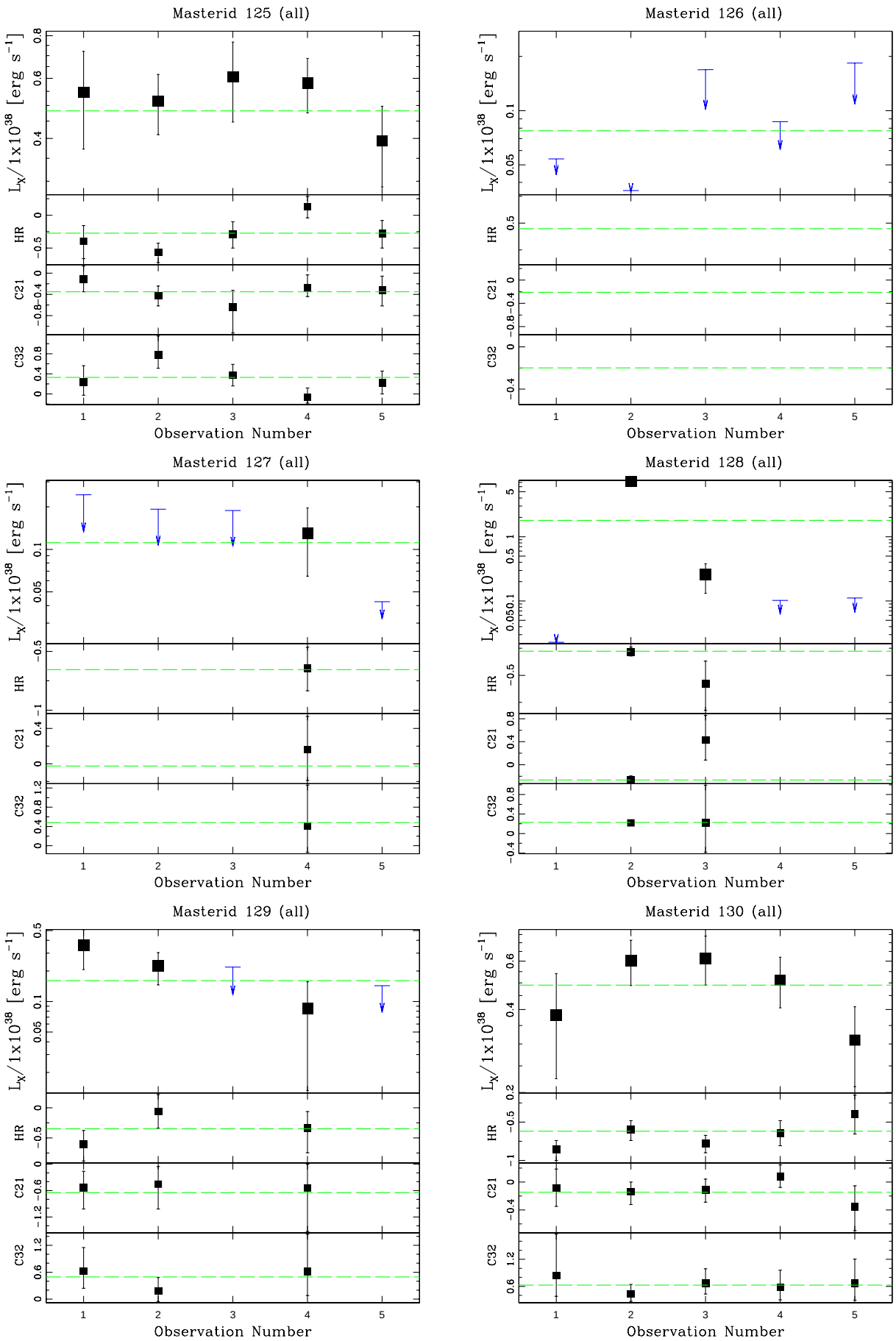
Masterid 125 (all)
Masterid 126 (all)
Masterid 127 (all)
Masterid 128 (all)
Masterid 129 (all)
Masterid 130 (all)
$L_X/1x10^{38}$ [erg s^{-1}]
HR
C21
C32
Observation Number

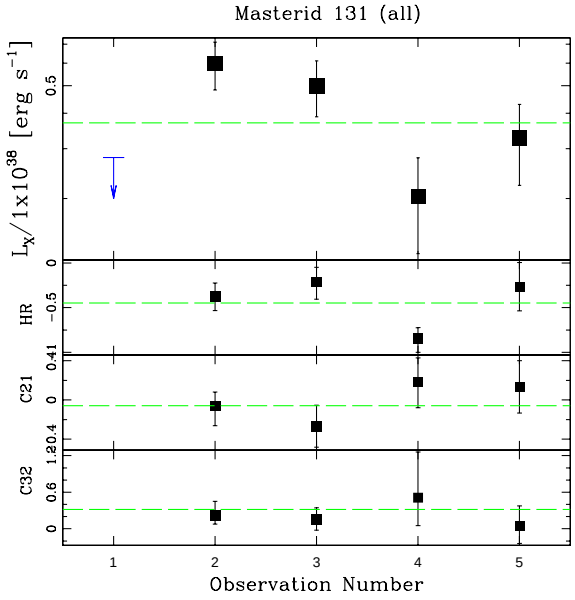
Masterid 131 (all)
$L_X/1x10^{38}$ [erg s^{-1}]
HR
C21
C32
Observation Number

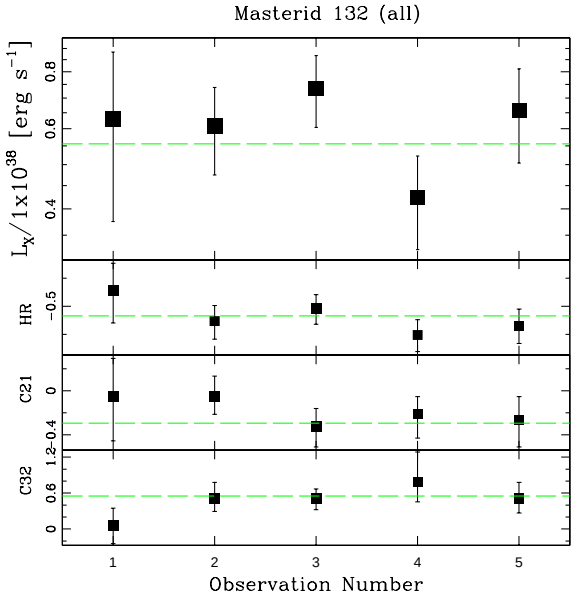
Masterid 132 (all)
$L_X/1x10^{38}$ [erg s^{-1}]
HR
C21
C32
Observation Number

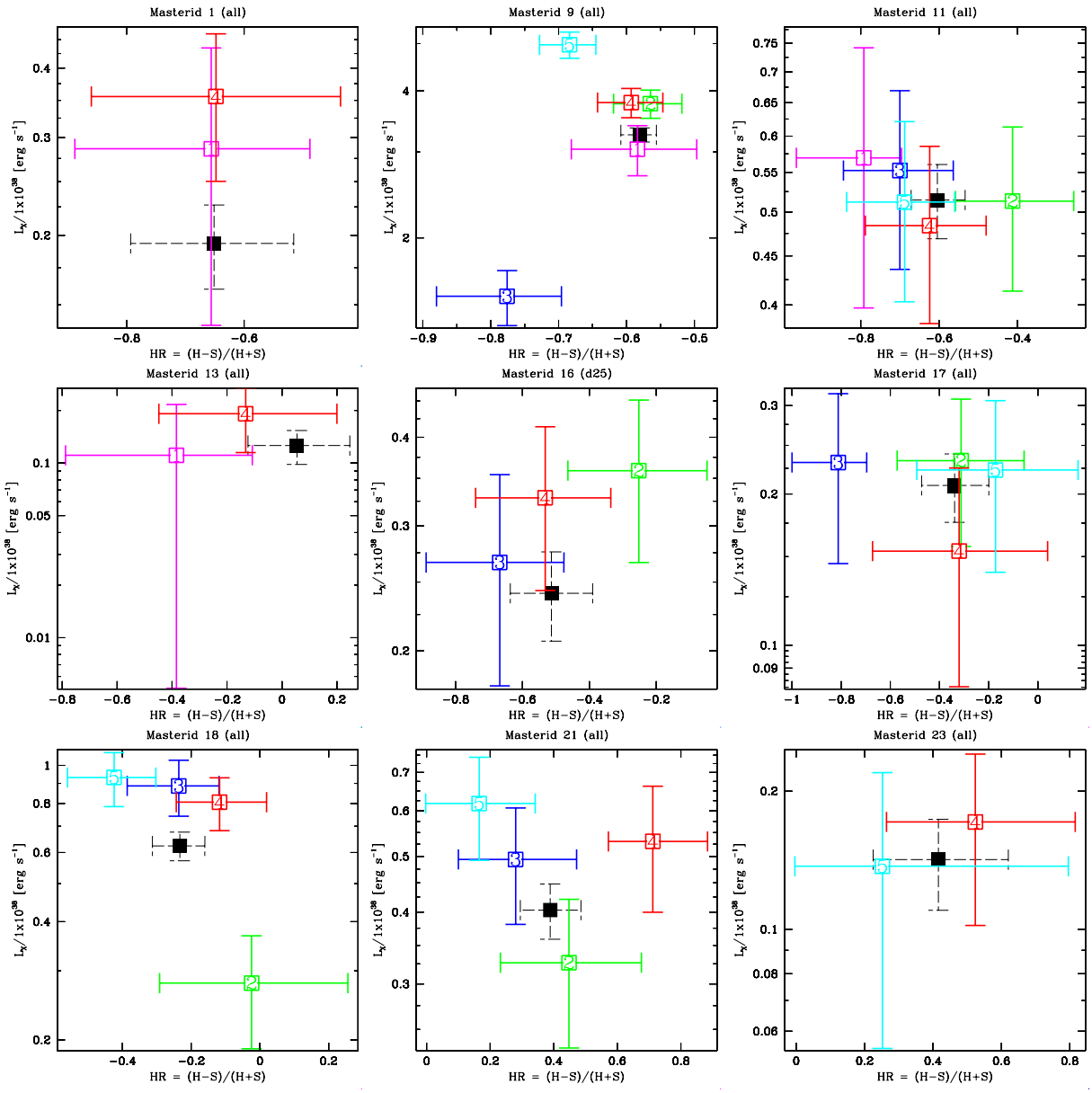

Fig. 8.— HR−L_X plots for each source detected in more that one individual observation, with each observation plotted in a different color; observation 1 is magenta, observation 2 is green, observation 3 blue, observation 4 red and observation 5 is cyan. The HR and L_X values for the combined observation are also shown, plotted in black. The hardness ratios are defined to be HR = H−S / H+S, where H is the number of counts in the hard band (2.0−8.0 keV) and S is the number of counts in the soft band (0.5−2.0 keV).

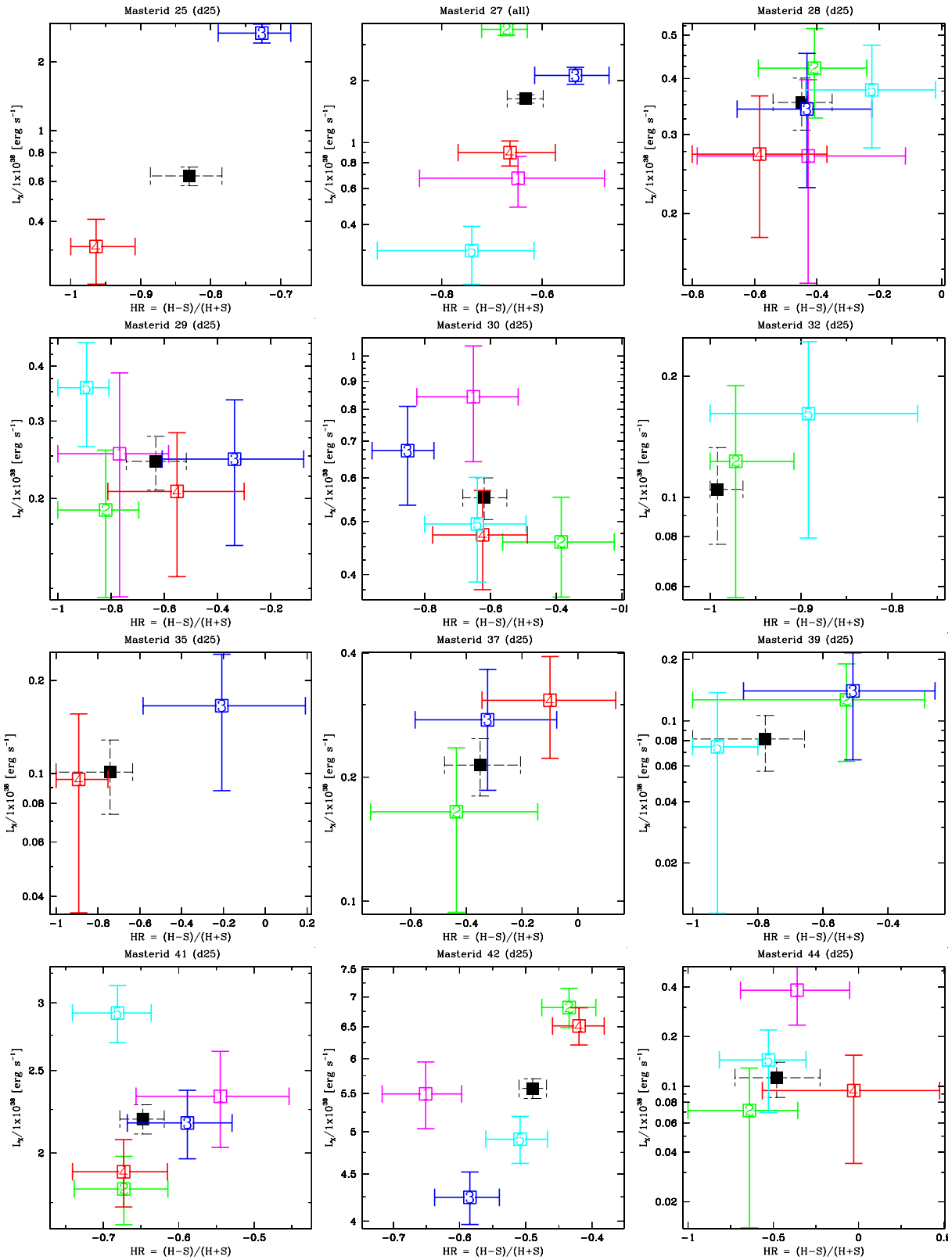
Masterid 25 (d25)
Masterid 27 (all)
Masterid 28 (d25)
Masterid 29 (d25)
Masterid 30 (d25)
Masterid 32 (d25)
Masterid 35 (d25)
Masterid 37 (d25)
Masterid 39 (d25)
Masterid 41 (d25)
Masterid 42 (d25)
Masterid 44 (d25)
$L_X/1x10^{38}$ [erg s^{-1}]
HR = (H−S)/(H+S)

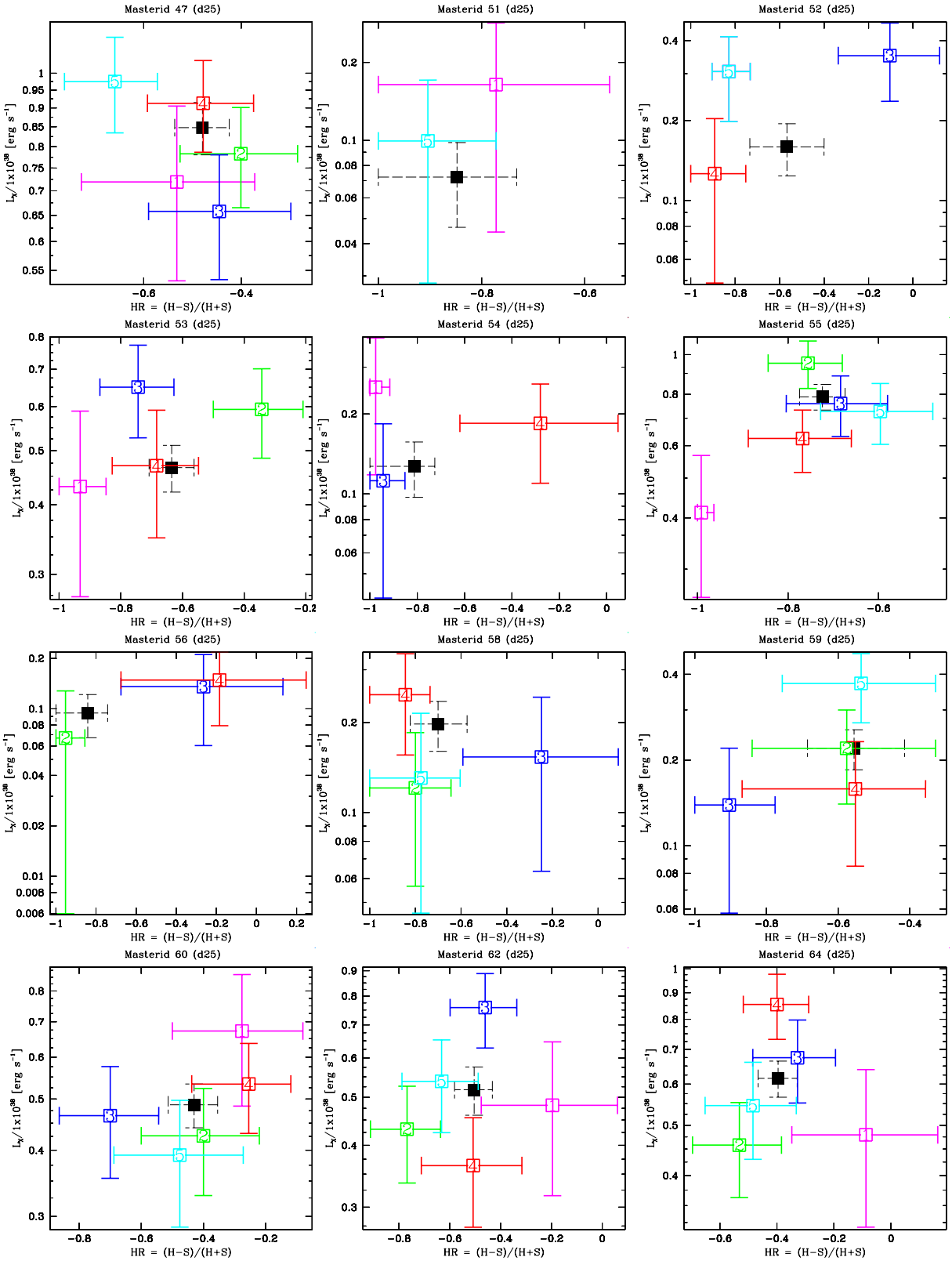
Masterid 47 (d25)
Masterid 51 (d25)
Masterid 52 (d25)
Masterid 53 (d25)
Masterid 54 (d25)
Masterid 55 (d25)
Masterid 56 (d25)
Masterid 58 (d25)
Masterid 59 (d25)
Masterid 60 (d25)
Masterid 62 (d25)
Masterid 64 (d25)
$L_X/1x10^{38}$ [erg s^{-1}]
HR = (H−S)/(H+S)

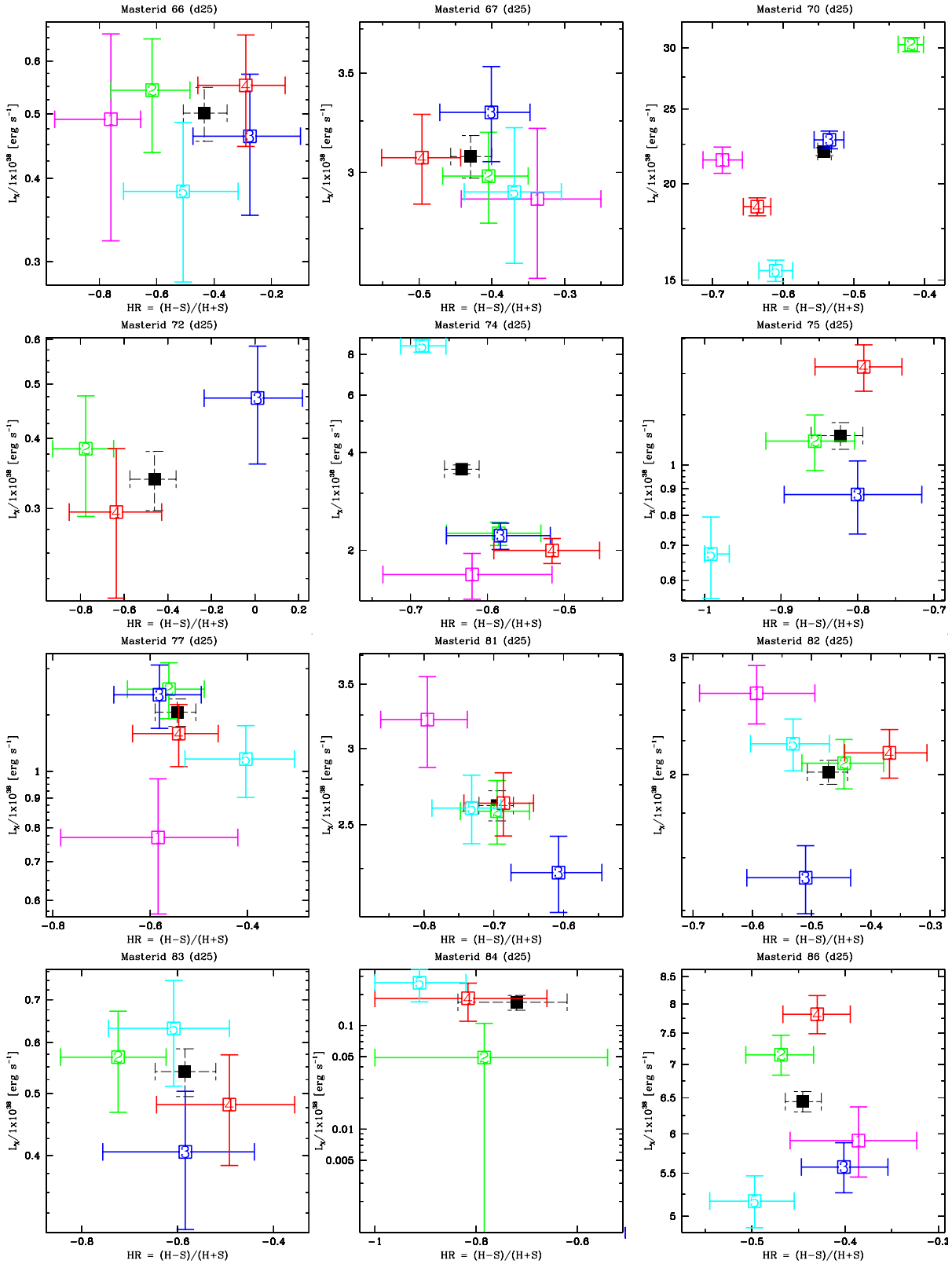
Masterid 66 (d25)
Masterid 67 (d25)
Masterid 70 (d25)
Masterid 72 (d25)
Masterid 74 (d25)
Masterid 75 (d25)
Masterid 77 (d25)
Masterid 81 (d25)
Masterid 82 (d25)
Masterid 83 (d25)
Masterid 84 (d25)
Masterid 86 (d25)
$L_X/1x10^{38}$ [erg s^{-1}]
HR = (H−S)/(H+S)

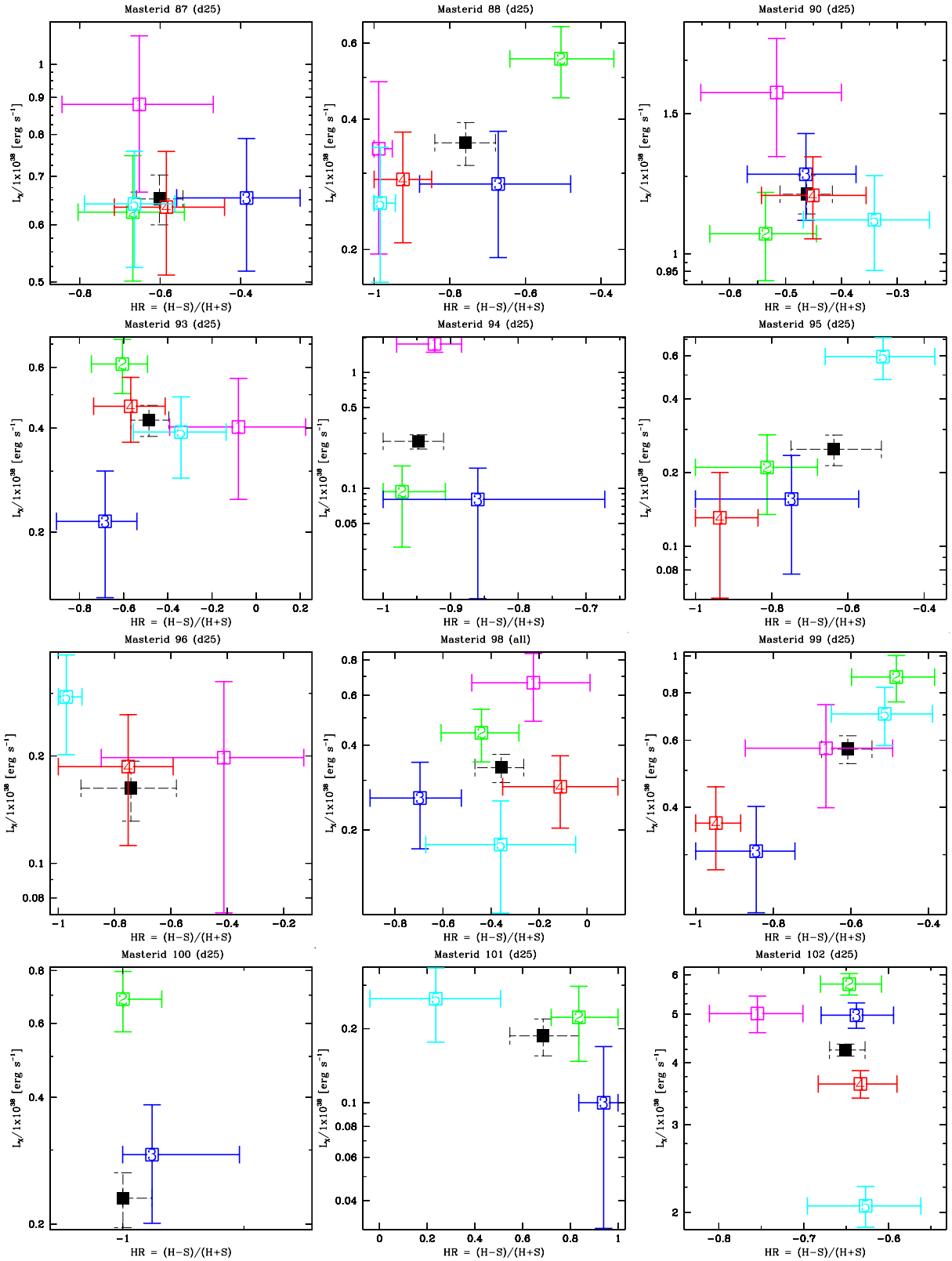
Masterid 87 (d25)
Masterid 88 (d25)
Masterid 90 (d25)
Masterid 93 (d25)
Masterid 94 (d25)
Masterid 95 (d25)
Masterid 96 (d25)
Masterid 98 (all)
Masterid 99 (d25)
Masterid 100 (d25)
Masterid 101 (d25)
Masterid 102 (d25)
$L_X/1x10^{38}$ [erg s^{-1}]
HR = (H−S)/(H+S)

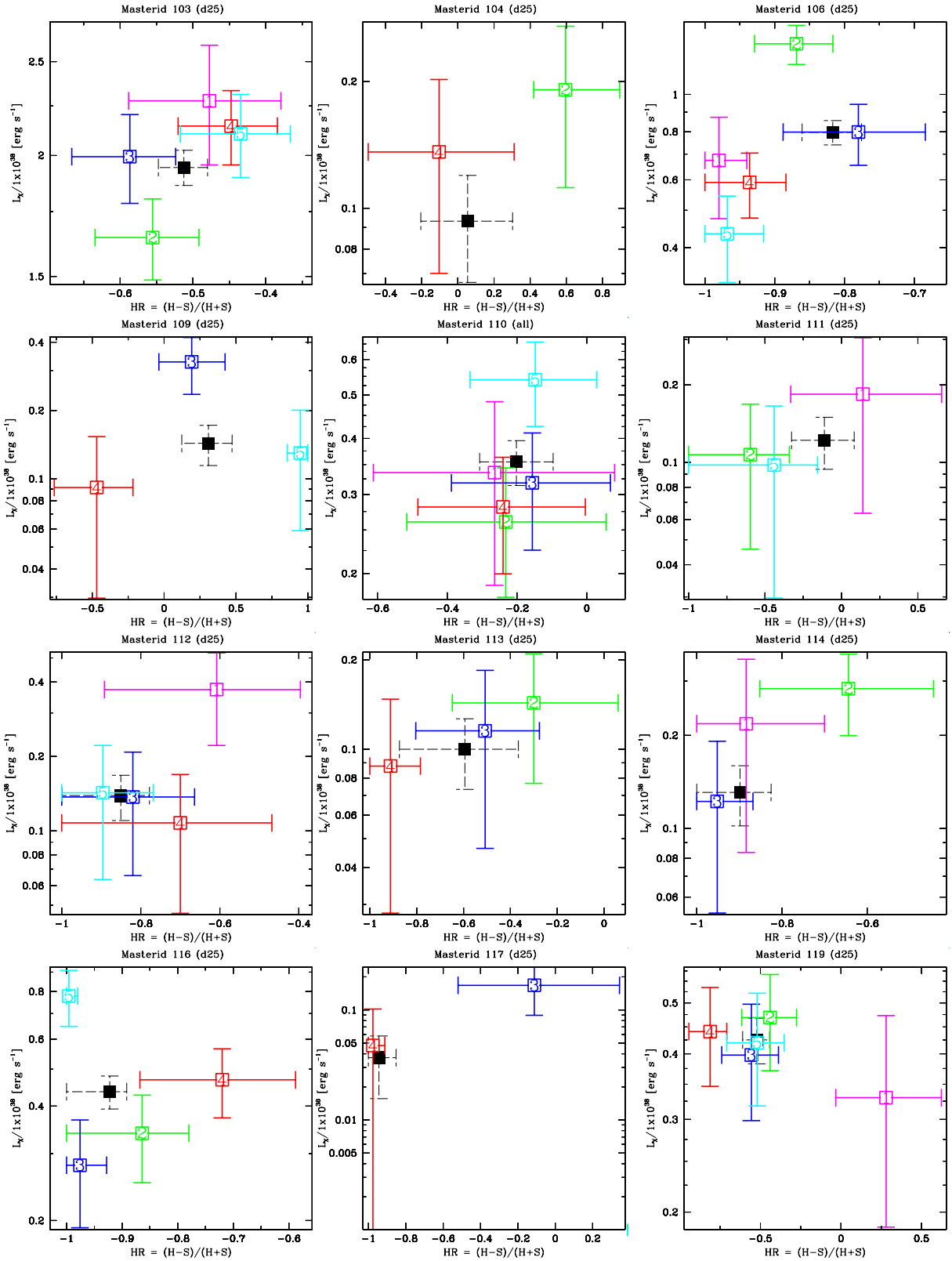
Masterid 103 (d25)
Masterid 104 (d25)
Masterid 106 (d25)
Masterid 109 (d25)
Masterid 110 (all)
Masterid 111 (d25)
Masterid 112 (d25)
Masterid 113 (d25)
Masterid 114 (d25)
Masterid 116 (d25)
Masterid 117 (d25)
Masterid 119 (d25)
$L_X/1x10^{38}$ [erg s^{-1}]
HR = (H−S)/(H+S)

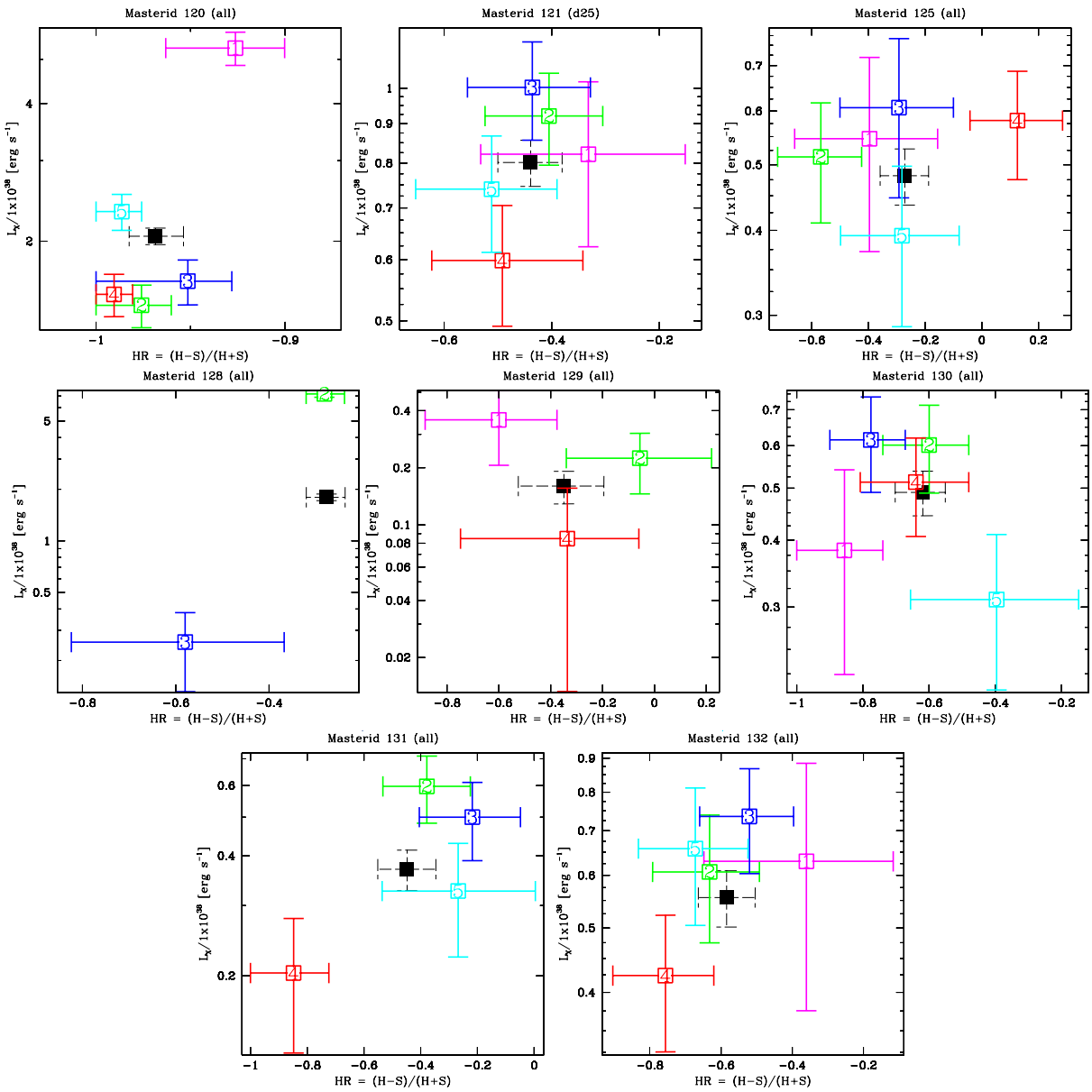
Masterid 120 (all)
Masterid 121 (d25)
Masterid 125 (all)
Masterid 128 (all)
Masterid 129 (all)
Masterid 130 (all)
Masterid 131 (all)
Masterid 132 (all)
$L_X/1x10^{38}$ [erg s^{-1}]
HR = (H−S)/(H+S)

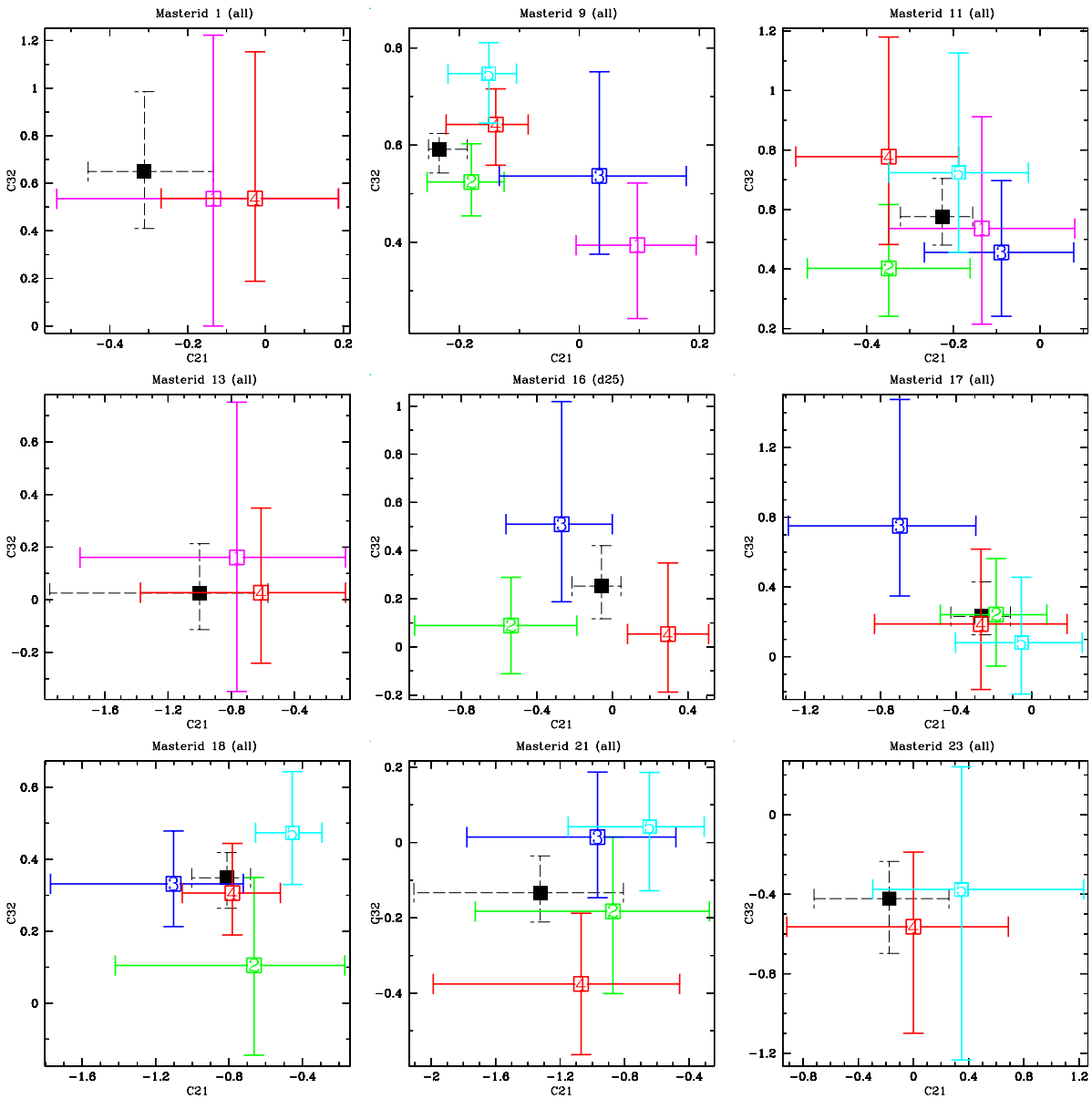

Fig. 9.— Color-color plots for each source that has been detected in more that one individual observation, with each observation plotted in a different color; observation 1 is magenta, observation 2 is green, observation 3 blue, observation 4 red and observation 5 is cyan. The combined observation is also plotted in black. The color ratios; C21 and C32, are plotted, where C21=logS2+logS1 and C32=$-log$H+logS2. For the color ratios the bandwidths are defined to be S1=0.3−0.9 keV, S2=0.9−2.5 keV and H=2.5−8.0 keV.

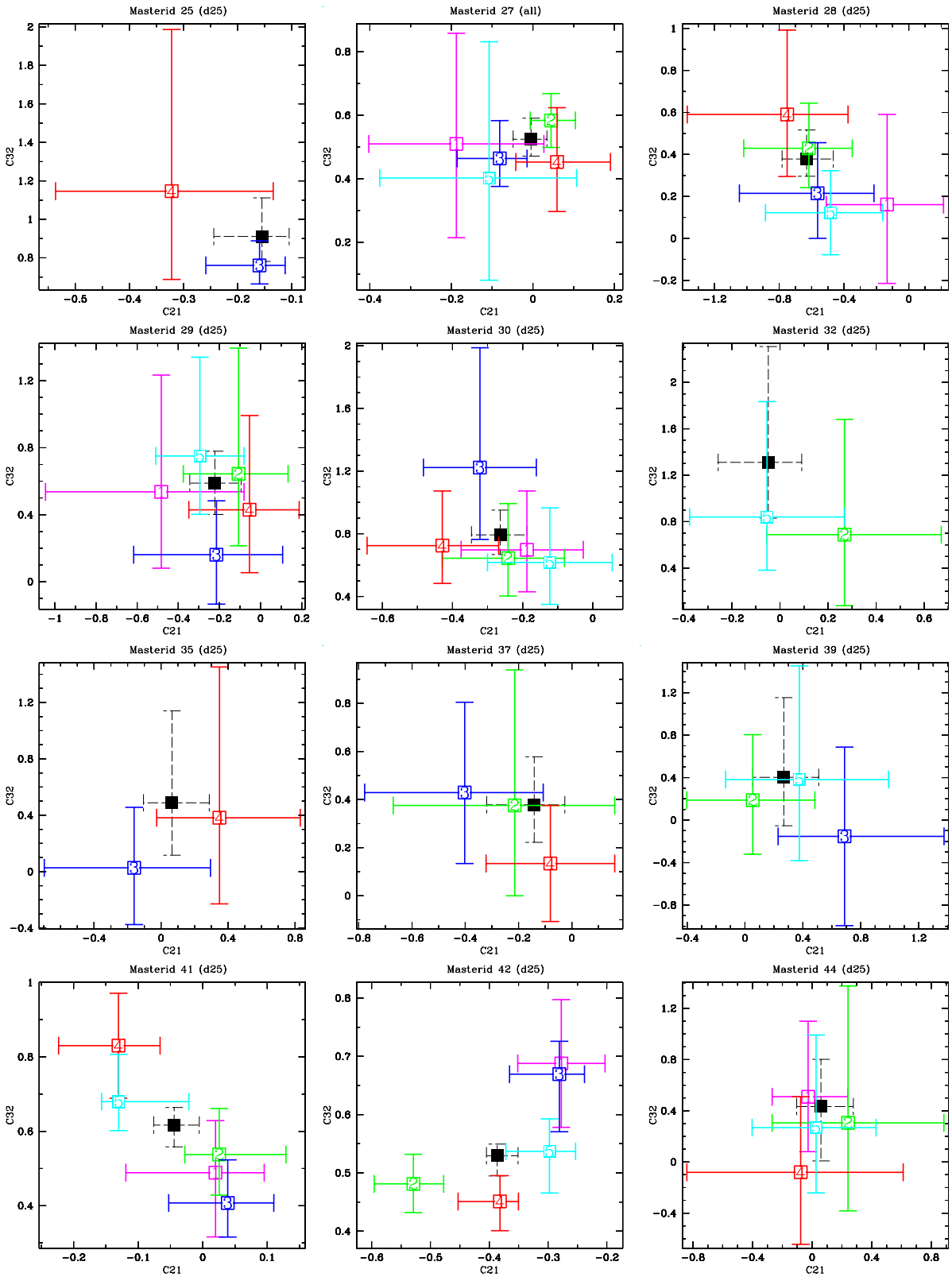
Masterid 25 (d25)
Masterid 27 (all)
Masterid 28 (d25)
Masterid 29 (d25)
Masterid 30 (d25)
Masterid 32 (d25)
Masterid 35 (d25)
Masterid 37 (d25)
Masterid 39 (d25)
Masterid 41 (d25)
Masterid 42 (d25)
Masterid 44 (d25)
C21
C32

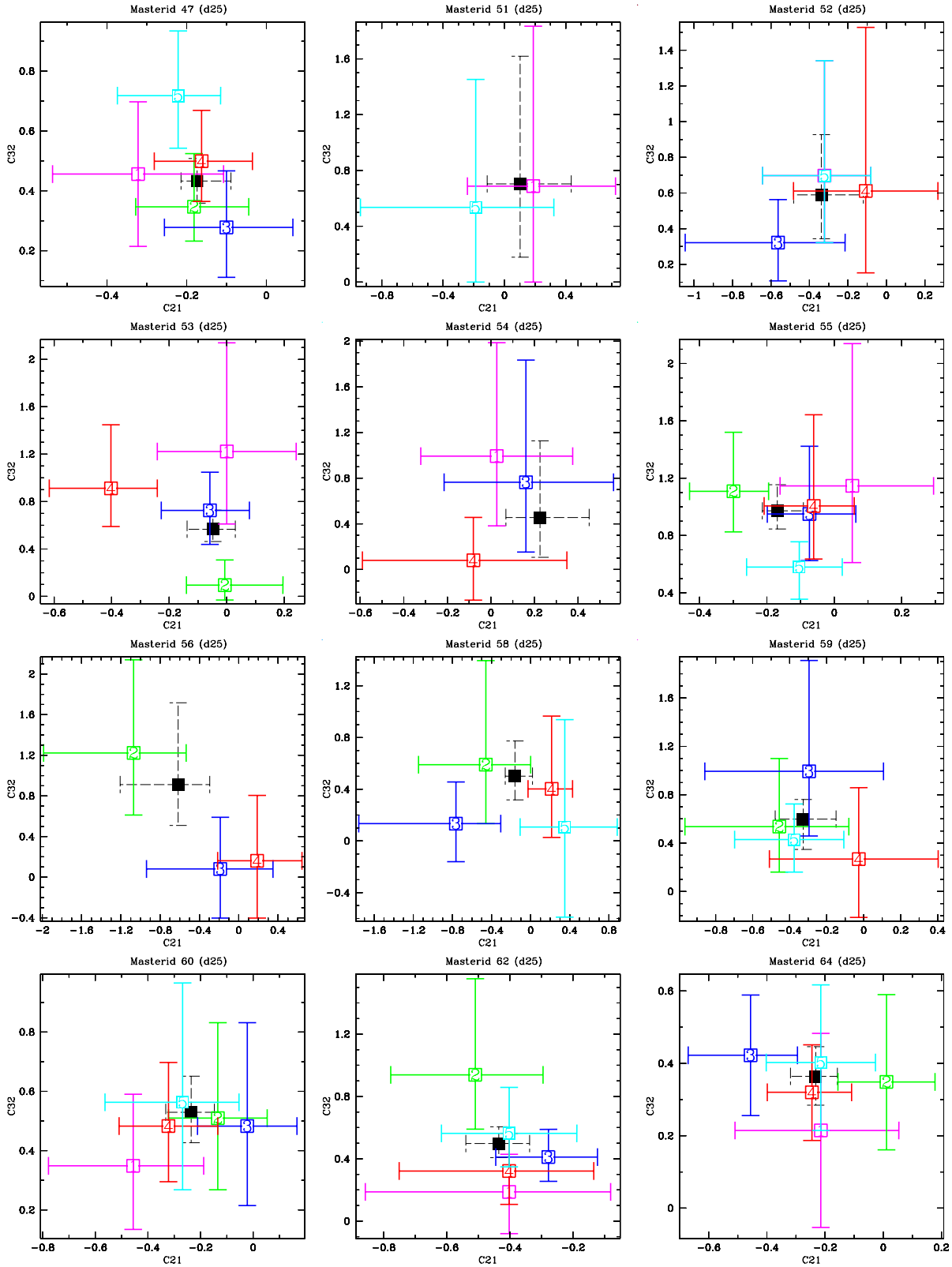
Masterid 47 (d25)
Masterid 51 (d25)
Masterid 52 (d25)
Masterid 53 (d25)
Masterid 54 (d25)
Masterid 55 (d25)
Masterid 56 (d25)
Masterid 58 (d25)
Masterid 59 (d25)
Masterid 60 (d25)
Masterid 62 (d25)
Masterid 64 (d25)
C21
C32

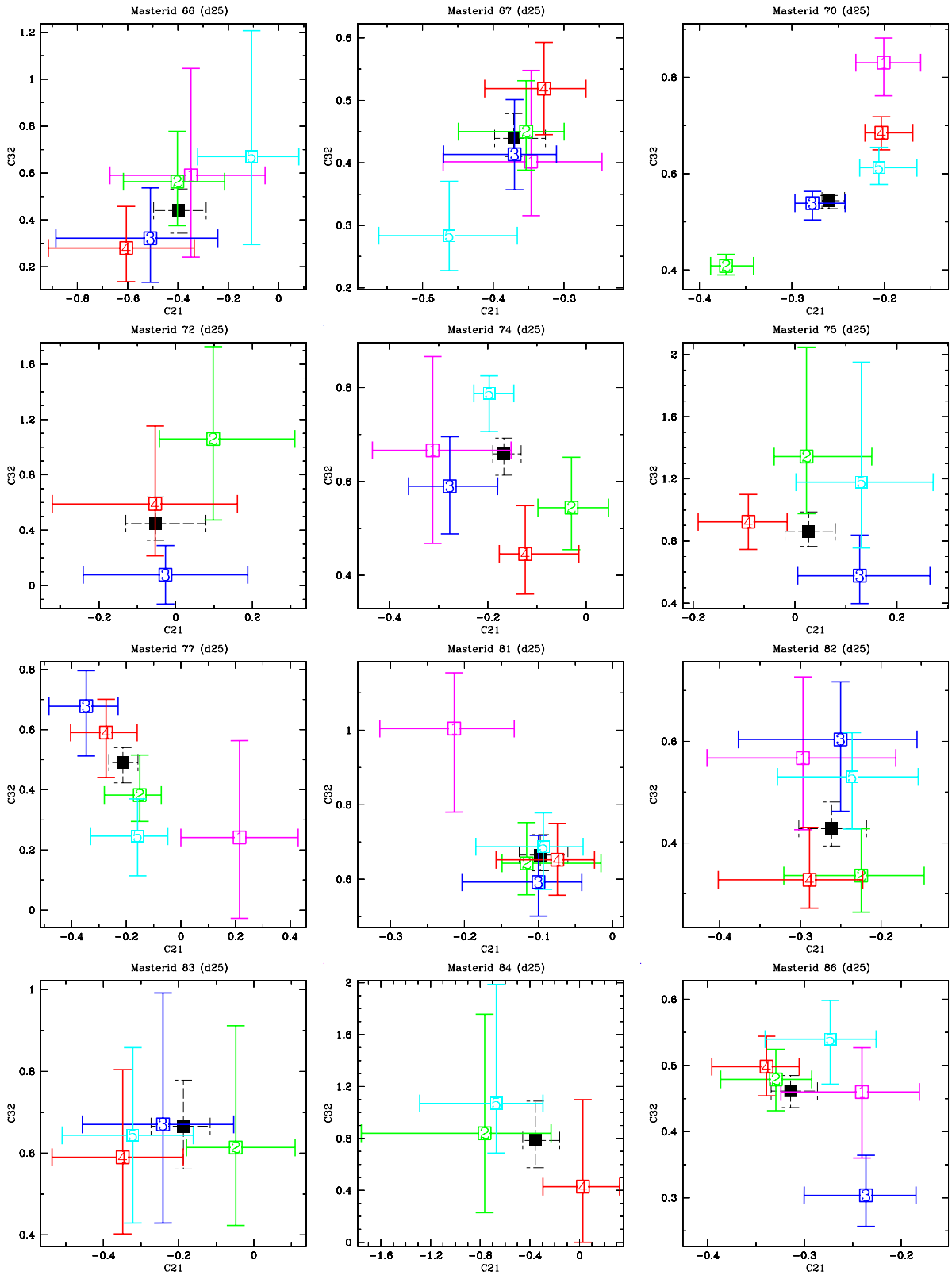
Masterid 66 (d25)
Masterid 67 (d25)
Masterid 70 (d25)
Masterid 72 (d25)
Masterid 74 (d25)
Masterid 75 (d25)
Masterid 77 (d25)
Masterid 81 (d25)
Masterid 82 (d25)
Masterid 83 (d25)
Masterid 84 (d25)
Masterid 86 (d25)
C21
C32

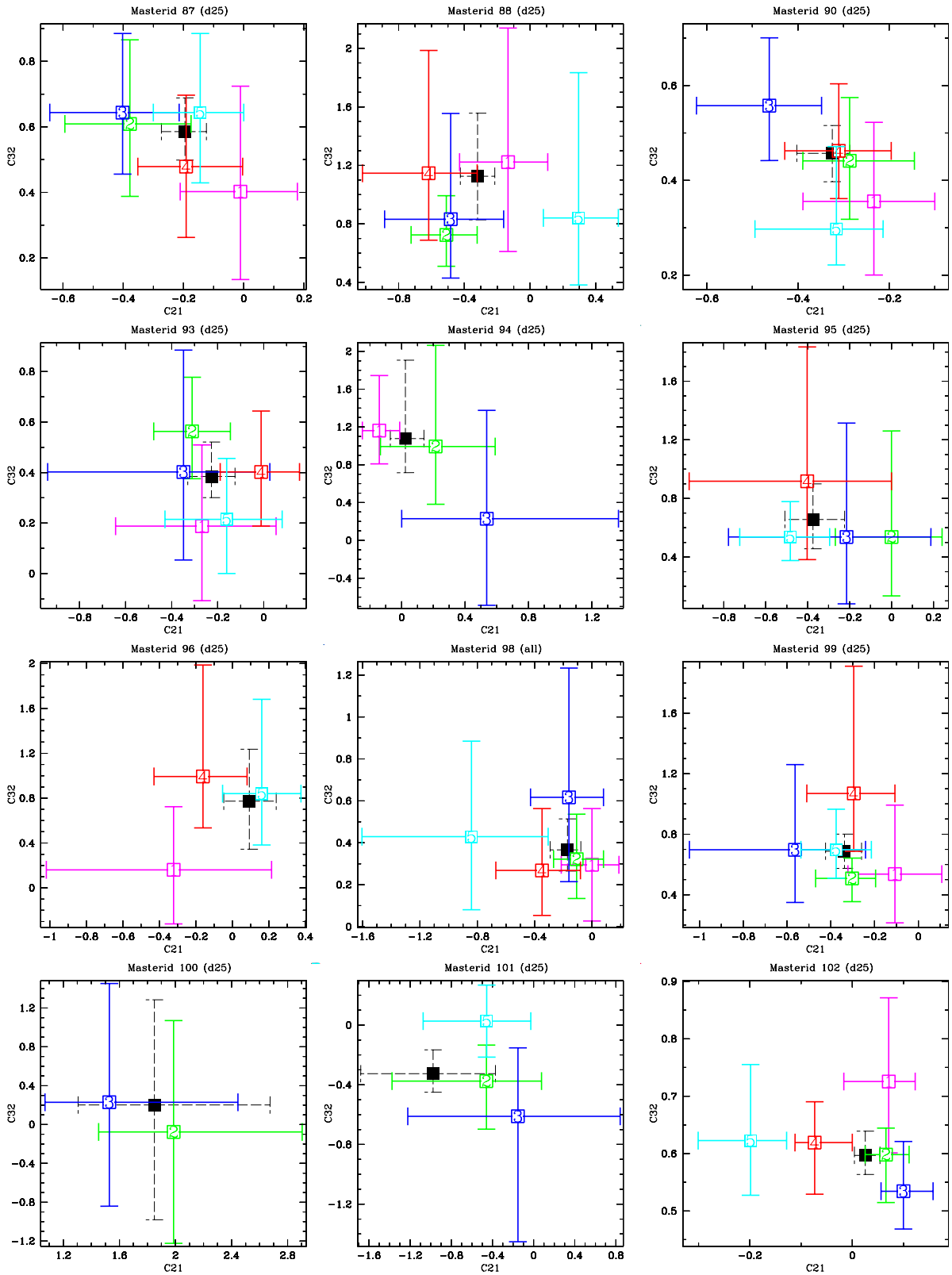
Masterid 87 (d25)
Masterid 88 (d25)
Masterid 90 (d25)
Masterid 93 (d25)
Masterid 94 (d25)
Masterid 95 (d25)
Masterid 96 (d25)
Masterid 98 (all)
Masterid 99 (d25)
Masterid 100 (d25)
Masterid 101 (d25)
Masterid 102 (d25)
C21
C32

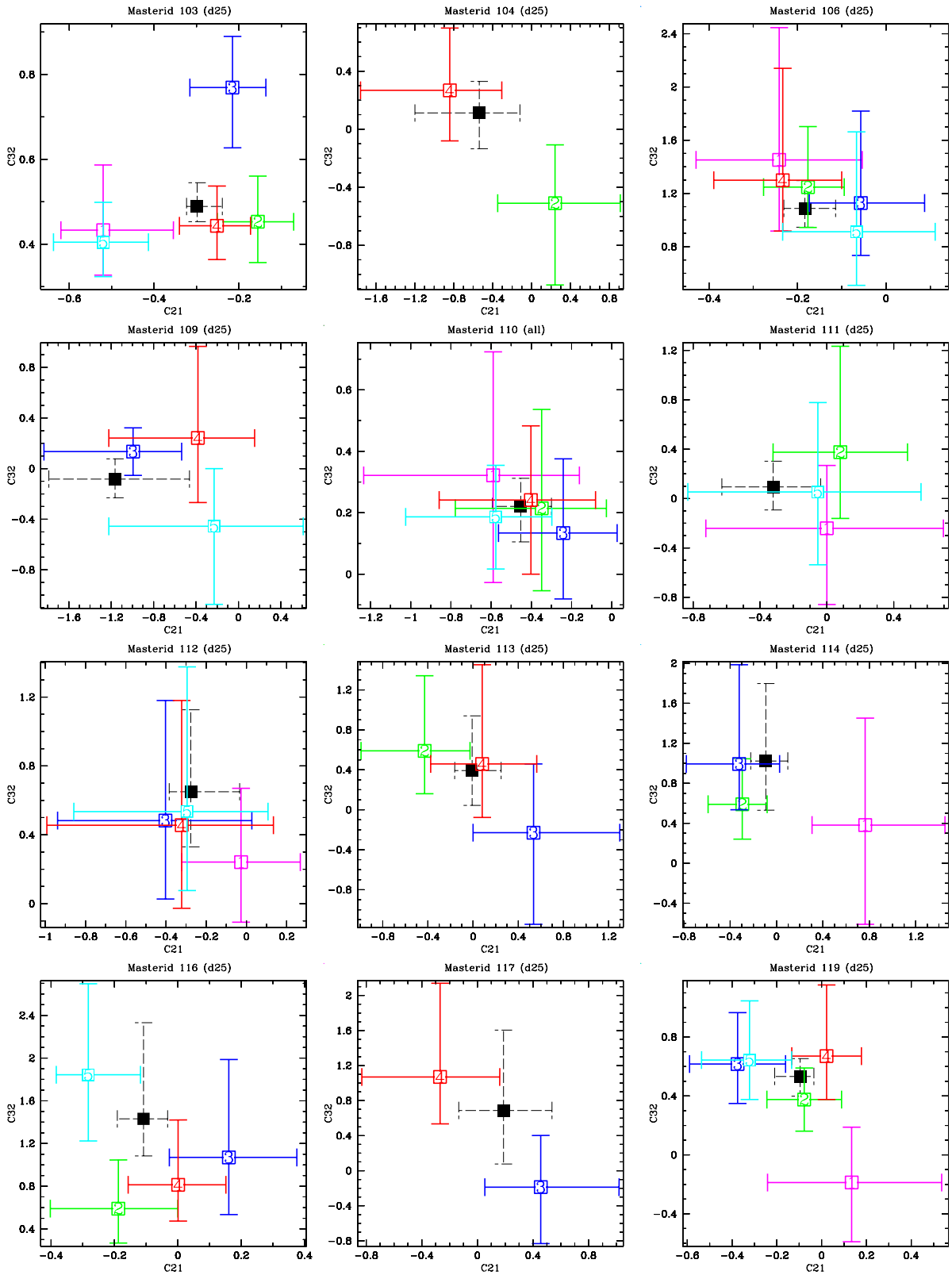
Masterid 103 (d25)
Masterid 104 (d25)
Masterid 106 (d25)
Masterid 109 (d25)
Masterid 110 (all)
Masterid 111 (d25)
Masterid 112 (d25)
Masterid 113 (d25)
Masterid 114 (d25)
Masterid 116 (d25)
Masterid 117 (d25)
Masterid 119 (d25)
C21
C32

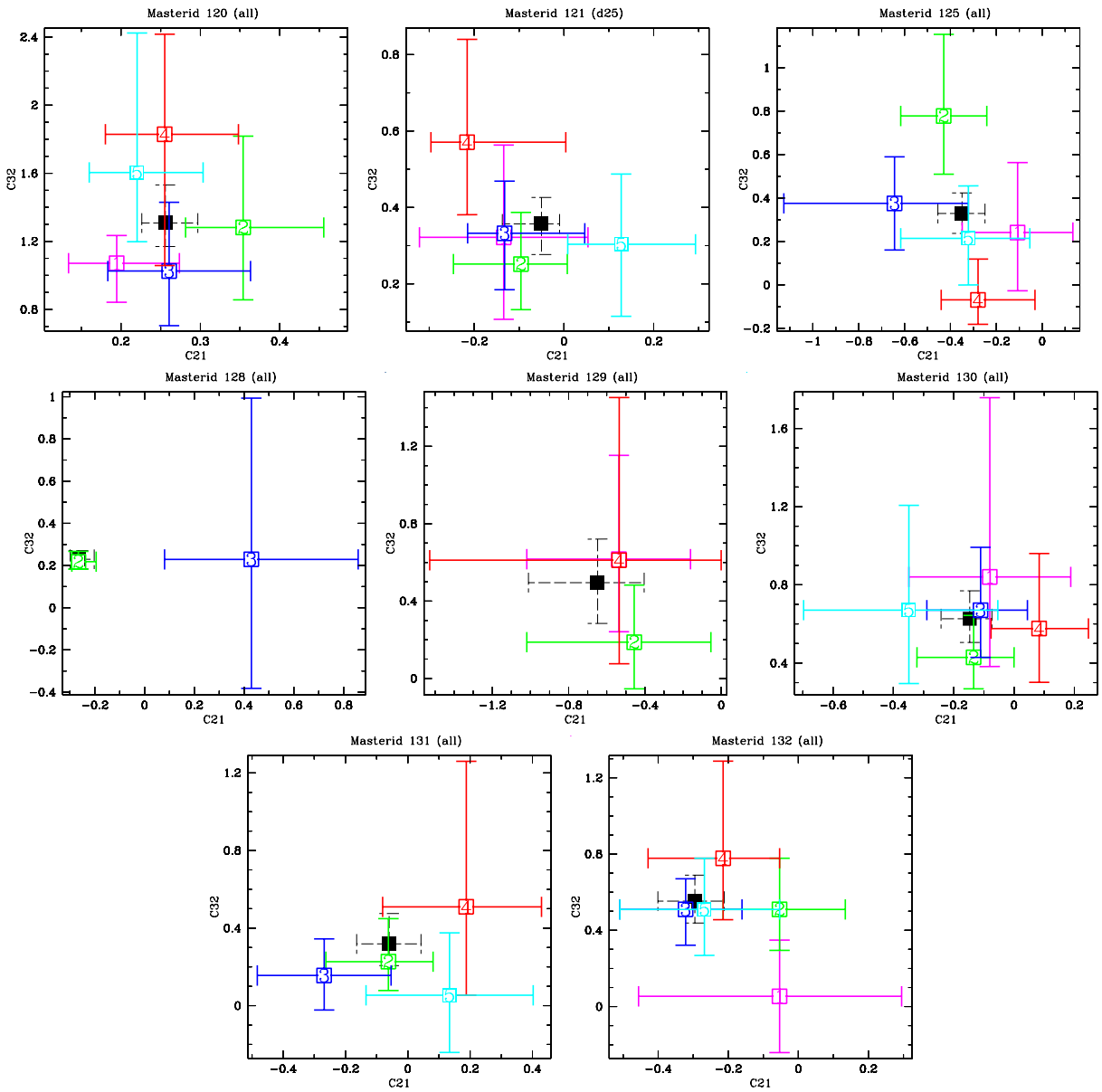
Masterid 120 (all)
Masterid 121 (d25)
Masterid 125 (all)
Masterid 128 (all)
Masterid 129 (all)
Masterid 130 (all)
Masterid 131 (all)
Masterid 132 (all)
C21
C32

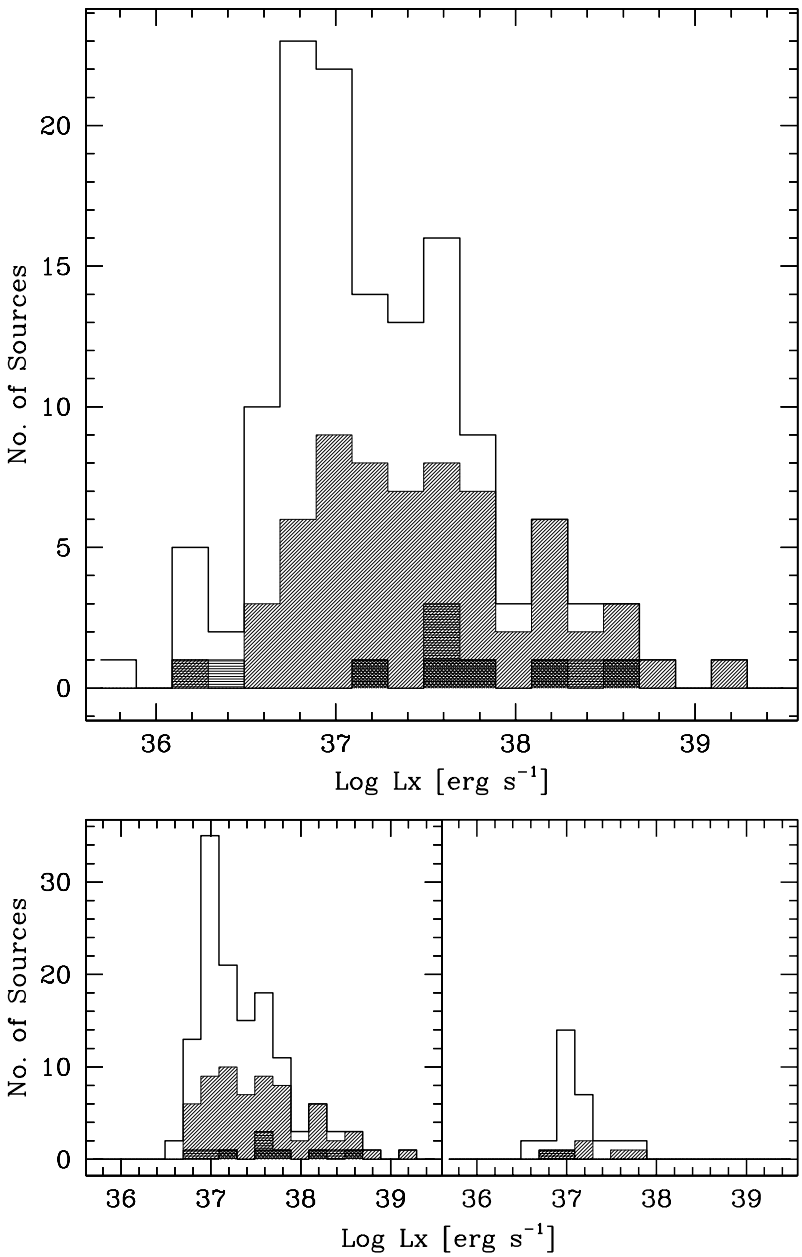

Fig. 10.— The top figure presents the $L_{\rm X}$ distribution of the 132 sources detected within the overlapping region, covered by all five *Chandra* pointings. The unshaded histogram indicates sources that have been determined to be non-variable sources (or we are not able to determine variability), with no GC counterpart. The lightly shaded region shows variable sources (including both transient classes) that have no GC counterpart. The darker histogram indicates non-varying sources associated with a GC and the darkest histogram shows varying sources that have a confirmed GC counterpart. The bottom left image indicates the same 132 sources, but for those with SNR<3, 3σ upper limit values have been used in place of $L_{\rm X}$. The bottom right image presents these upper limit values only. The shading for these two figures are the same as described for the main histogram.

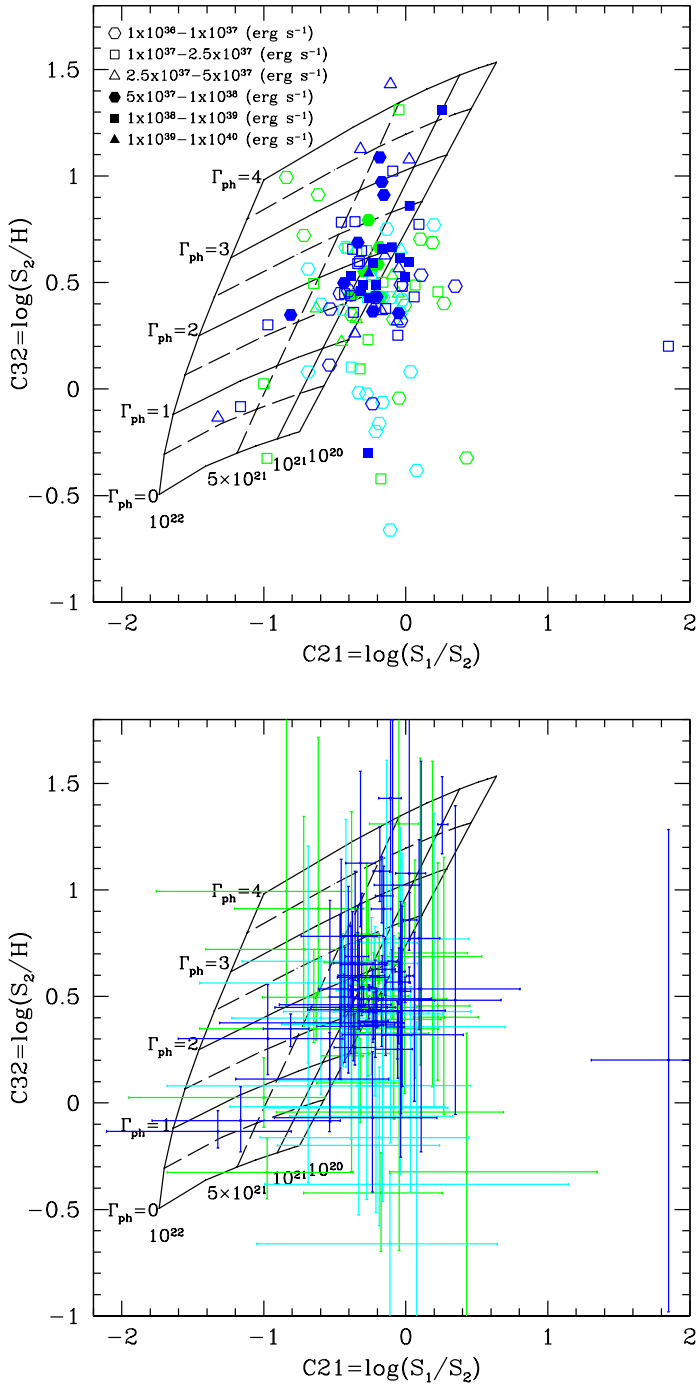

Fig. 11.— The color-color diagram of the X-ray point sources detected in the co-added observation. In the top panel color-color values are plotted, with the sources divided into luminosity bins, with symbols of each bin indicated by the labeling in the panel. Variability is also indicated, where variable sources are shown in blue, non-variable source are indicated in green and sources that do not have determined variability are shown in cyan. In the lower panel the error values for each of the sources are presented. In both of the panels, the grid indicates the predicted locations of the sources at redshift z=0 with various photon indices ($0 \leq \Gamma_{ph} \leq 4$, from top to bottom.) and absorption column densities ($10^{20} \leq N_{\rm H} \leq 10^{22}$ cm^2, from right to left).

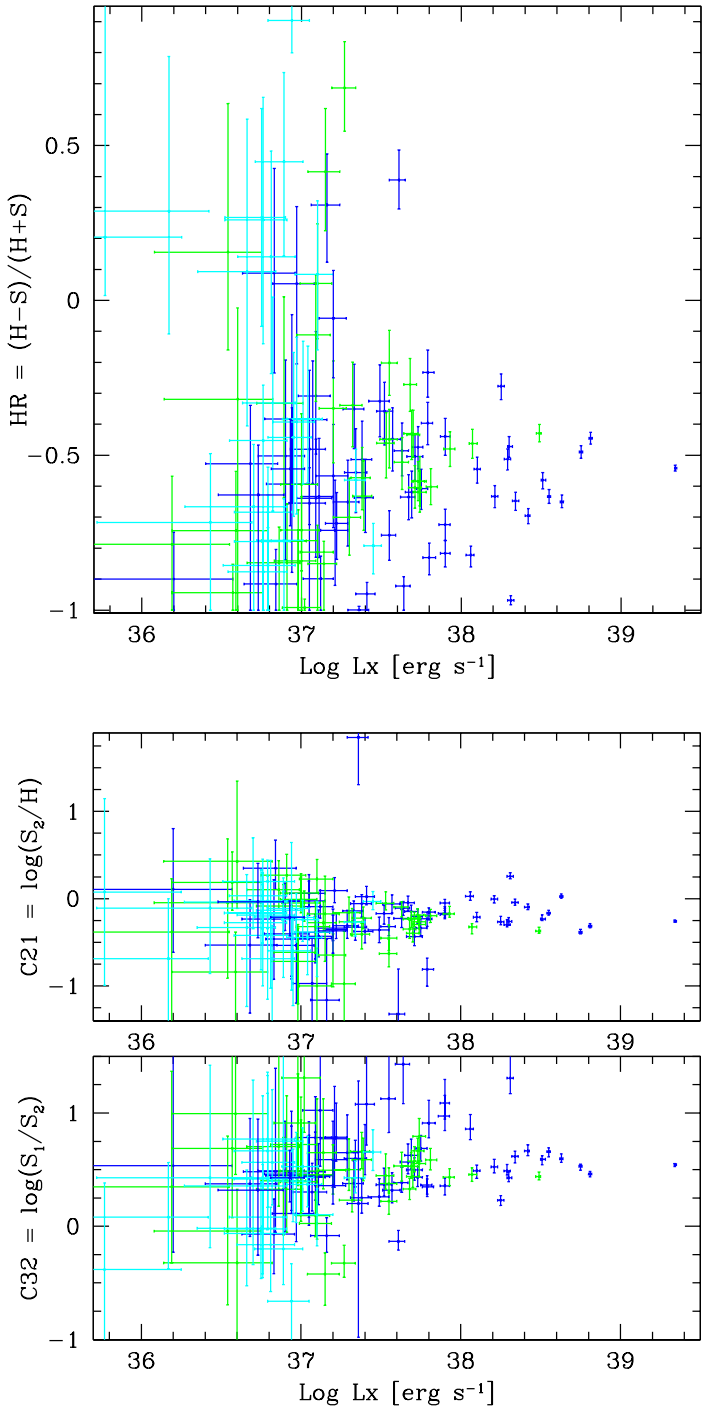

Fig. 12.— The top panel presents the L_X-HR diagram of the X-ray point sources detected in the co-added observation. The second panel shows the L_X-C21 plot for this population and the bottom panel shows the L_X-C32 values. In all three panels the variable sources are plotted in blue, non-variable sources are plotted in green and the cyan points indicate sources that do not have enough information to classify their variability.

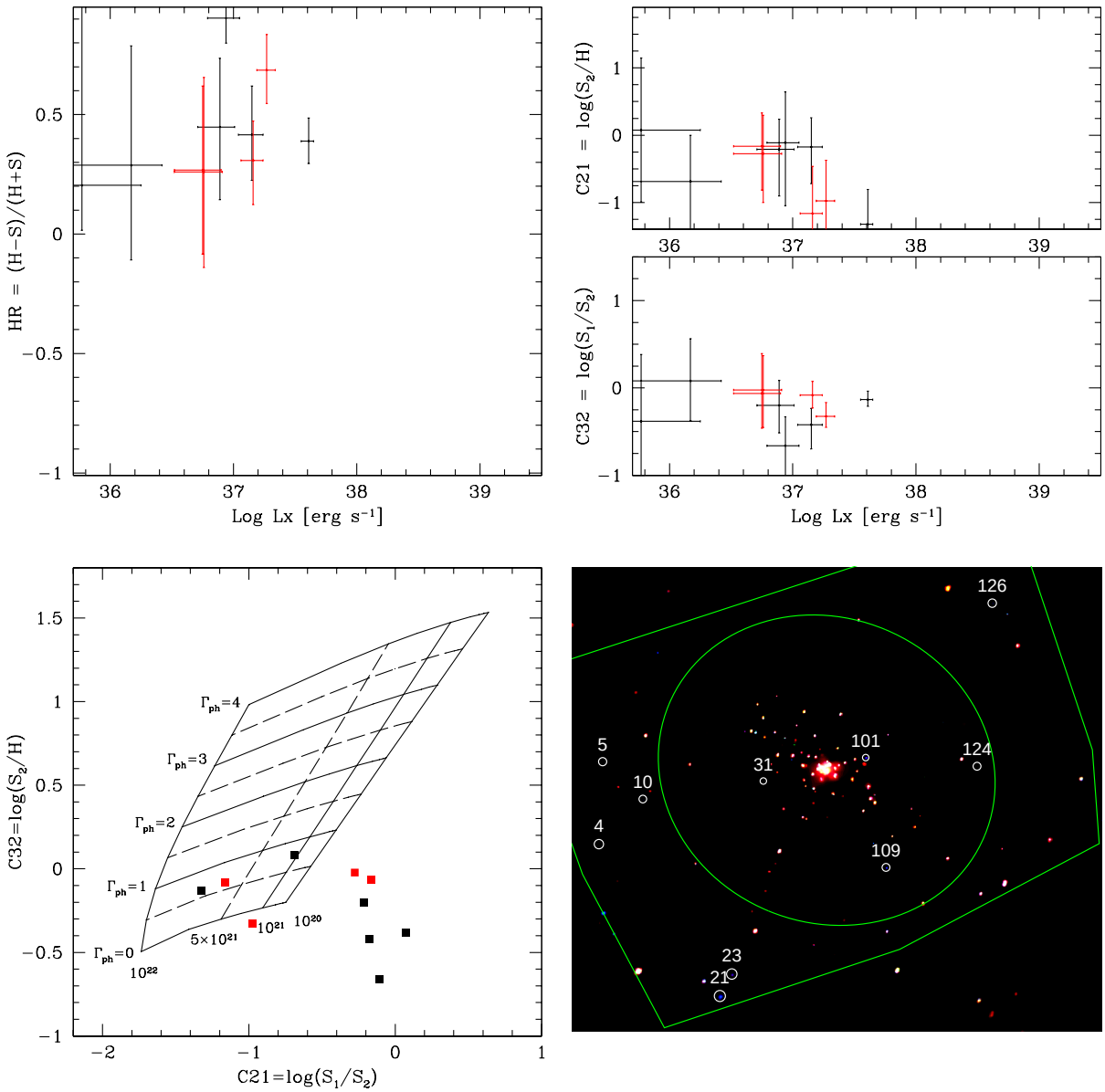

Fig. 13.— Hardness ratio and color values of the 10 sources that have been found to exhibit HR values >0.2. In the top left panel the $L_{\rm X}$-HR values of these sources are presented. The top right panel shows the $L_{\rm X}$-C21 and $L_{\rm X}$-C32 plots for these sources, while the bottom left panel presents the color-color diagram. In all three of these panels, sources within the D_{25} ellipse are plotted in red, whilst those external to this region are shown in black. In the bottom right panel of the figure the 'true color' image of the galaxy is shown, with the D_{25} ellipse and overlapping region covered in all five pointings overlaid in green. Also indicated in this image are the 10 X-ray sources, shown in white.

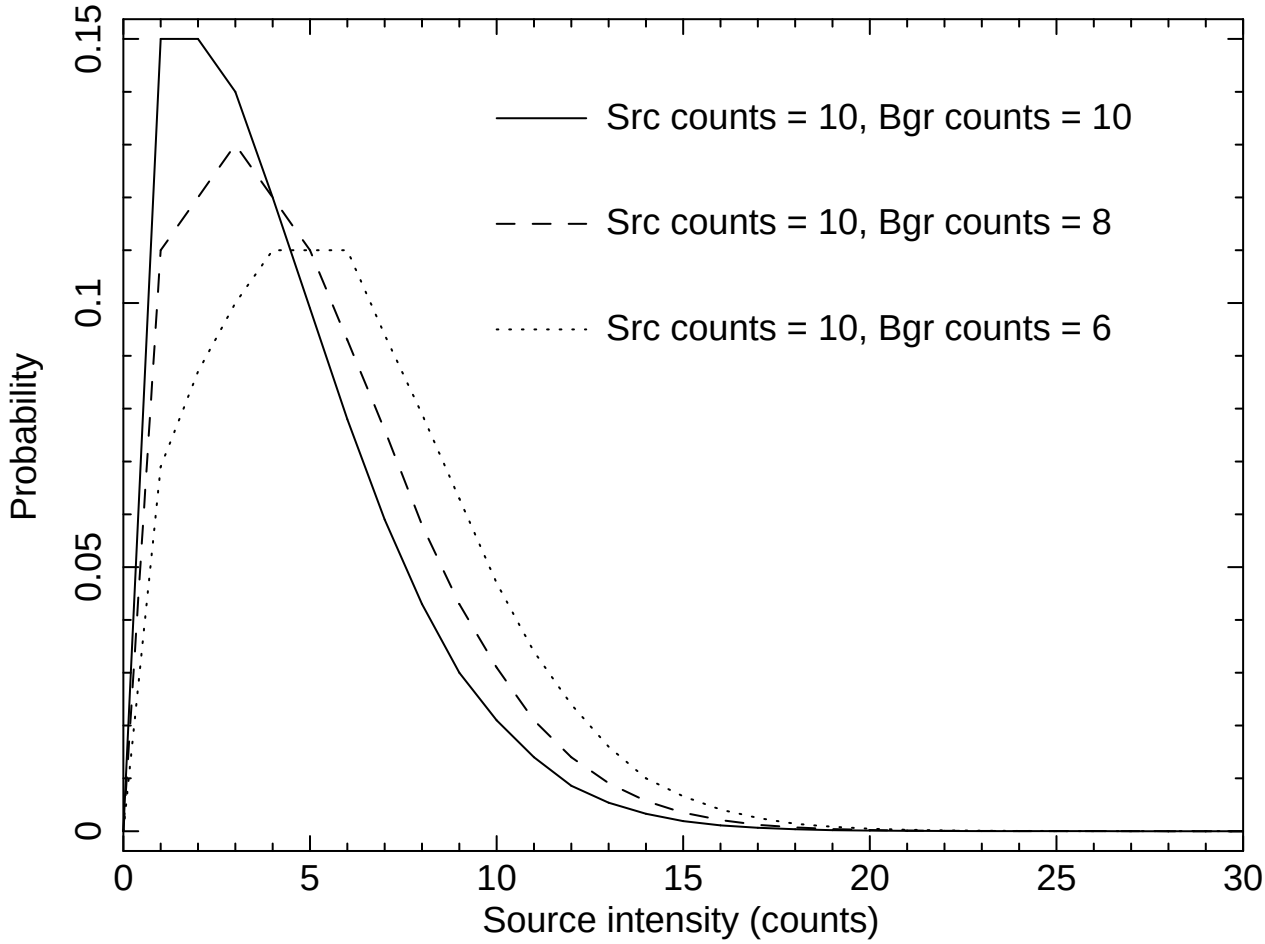

Fig. 14.— The posterior probability distributions for hypothetical sources with 10 observed counts and background counts of 6, 8 and 10. Based on Bayesian estimations of the 'real' sources intensity.